Combined Space-Time Diversity and Interference Cancellation for MIMO Wireless Systems

Jiann-An Tsai

Dissertation submitted to the Faculty of the

Virginia Polytechnic Institute and State University

in partial fulfillment of the requirements for the degree of

Doctor of Philosophy

in

Electrical and Computer Engineering

Brian D. Woerner, Co-Chair

R. Michael Buehrer, Co-Chair

Jeffrey H. Reed

J. Ken Shaw

Warren L. Stutzman

May, 2002

Blacksburg, Virginia

Keywords: Wireless Communications, Space-Time Diversity, Interference Cancellation,

MIMO, Adaptive Antenna Arrays

Combined Space-Time Diversity and Interference Cancellation for MIMO Wireless Systems

Jiann-An Tsai

(ABSTRACT)

There is increasing interest in the exploitation of multiple-input and multiple-output (MIMO) channels to enhance the capacity of wireless systems. In this study, we develop and evaluate a channel model, evaluate the corresponding channel capacity, and design and analyze a simple orthogonal transmit waveform for MIMO channels in mobile radio environments. We also evaluate the system performance of various interference cancellation techniques when employing multiple-receive antenna in interference-limited systems.

The first part of this dissertation presents two major contributions to MIMO systems. The analytical expression for space-time MIMO channel correlation is derived for a Rayleigh fading channel. The information-theoretic channel capacity based on this correlation is also evaluated for a wide variety of mobile radio channels.

The second part of this dissertation presents two major contributions to the area of orthogonal waveform design. We analyze the bit-error-rate (BER) performance of a proposed space-time orthogonal waveform for MIMO mobile radio communications. The application of the proposed space-time orthogonal waveform to a conventional cellular system is also evaluated and briefly discussed.

Finally, this dissertation investigates a number of interference cancellation techniques for multiple-receive antenna systems. Both adaptive beamforming and multiuser detection are evaluated for various signal waveforms over a variety of mobile radio channels.

Acknowledgments

This work has been made possible by the generous support from many people. First of all, I would like to express my thanks to the Lord for providing me with the spiritual support to complete this project. Next, I would like to thank my advisor Dr. Brian D. Woerner for his invaluable advice, encouragement, and financial support throughout my doctoral studies. His insight, kindness, and genuine concern for his students made working with him a memorable experience. I also would like to thank my co-chair Dr. R. Michael Buehrer for his technical and spiritual support during the course of this study. I sincerely appreciate the time and effort he had spent in providing me valuable guidance and suggestions. I am also very grateful to my committee members for their time and counsel. The MPRG staff also deserves acknowledgment for their invaluable assistance and support.

This research could not have been completed without the valuable help of several students at the MPRG. Listing them here does not begin to express my thanks. James Hicks, Ran Gozali, and Fakhrul Alam provided valuable discussions on a variety of technical issues with regard to my research. Patrick Chang and R. Venkatasubramanian have made invaluable contribution for validating the simulation tool used in the research. I am also grateful to all my other friends and colleagues at the MPRG and Virginia Tech. Your compassion has made the journey of my research a wonderful memory. Thanks also go the MPRG Industrial Affiliates Foundation and the Defense Advanced Research Projects Agency (DARPA) for providing me the financial support throughout my study.

Last but not least, I would like to express my gratitude to my wife Kathy for all her love and understanding. Thanks for always being so thoughtful. Finally, I would like to thank my grandparents, my parents for their endless love and encouragement throughout my life.

Contents

List of Figures

List of Tables

Abbreviations

AOA	angle-of-arrival
AOD	angle-of-departure
AWGN	additive white Gaussian noise
BER	bit error rate
CDMA	code-division multiple access
CE	cross entropy
BPSK	binary phase shift keying
DAB	digital audio broadcasting)
DSP	digital signal processing
DVB	digital video broadcasting)
FER	frame error rate
ICI	inter-carrier interference
ISI	inter-symbol interference
MAI	multiple access interference
MIMO	multiple-transmit antenna and multiple-receive antenna
MMSE	minimum mean square error
MMSE-SIC	mmse beamforming with successive interference cancelation
MMSE-PIC	mmse beamforming with parallel interference cancelation
MRC	maximal-ratio-combining
MUD	multiuser detection
OFDM	orthogonal-frequency division multiplexing
OFDM-CDMA	OFDM code-division multiple access
pdf	probability density function
PCS	personal communication systems

PIC	parallel interference cancellation
RF	radio frequency
SIR	signal-to-interference ratio
SIC	successive interference cancelation
SISO	soft-input soft-output
SNR	signal-to-noise ratio
SRSJD	spatially reduced search joint detection
STS	space-time spreading
ST-OTW	space-time orthogonal transmit waveform
TDMA	time-division multiple access
UCA	uniform circular array
ULA	uniform linear array

Chapter 1

Introduction

In the past two decades, wireless communications has grown with unprecedented speed from early radio paging, cordless telephone, and cellular telephony to today's personal communication and computing devices. These commercial wireless applications have had a profound impact on today's business world and people's daily lives. The growth and demand for wireless services will play a significant role in the evolution of Internet service from the current landline system to wireless systems. This evolution will almost certainly fuel further growth in wireless communications. This has motivated research investigating methods of increasing wireless system capacity.

1.1 Limits in Wireless Systems

The system performance of current wireless communication systems are limited by three major channel impairments. They are signal fading, Inter-Symbol Interference (ISI), and cochannel interference. Signal fading and ISI arise from multipath propagation while interference is generally caused by cochannel users or unknown jammers in the system. To mitigate signal fading, diversity schemes such as spatial diversity, polarization diversity, frequency diversity, and time diversity can be used. Spatial diversity and polarization diversity are achieved by using antenna arrays while frequency diversity and time diversity can be exploited from time-varying multipath channels. To remedy ISI, channel equalization techniques such as adaptive equalizers or RAKE receivers can be used to equalize the multipath channels. An adaptive equalizer is typically used for narrowband signals such as those used in Time-Division Multiple Access (TDMA) systems while a RAKE receiver is primarily used for Code-Division Multiple Access (CDMA) systems. To alleviate cochannel interference, interference cancellation techniques such as adaptive beamforming or multiuser detection can be used to reject the interference. Adaptive beamforming is generally used when information about the interference is not avaliable while multiuser detection is only possible when some information about the interference is known to the receiver. The combination of adaptive beamforming with multiuser detection can provide further performance improvement at the expense of system complexity.

1.2 Overview of Research

The main focus of this research is to design a new signal waveform that can more fully exploit the space and time diversity of radio channels for use in future wireless systems. The proposed signal waveform is based on Direct-Sequence CDMA (DS-CDMA) waveforms . This waveform is designed using orthogonal spreading codes and transmit antenna arrays. The proposed transmit signal waveform can provide orthogonality over the space and time domains of the radio channels while obtaining spatial and temporal diversity. The proposed space-time orthogonal waveform is well-suited for multiple-input and multiple-output (MIMO) wireless systems. The efforts in this area of research are to determine the statistical properties of the MIMO channel, to evaluate the information-theoretic MIMO channel capacity, and analyze the space-time characteristics of MIMO channels. Lastly, the performance of the space-time orthogonal waveform for the MIMO channels is evaluated from a communication perspective.

The second focus of this research is to evaluate the system performance of various interference cancellation techniques for multiple-receive antenna systems. These interference cancellation techniques include adaptive beamforming, multiuser detection, as well as combined adaptive beamforming and multiuser detection techniques. In the area of adaptive beamforming, we focus on Minimum Mean Square Error (MMSE) beamforming. In the area of multiuser detection, we focus on both Successsive Interference Cancellation (SIC) and Parallel Interference Cancellation (PIC). Several signal waveforms are also considered in this area of the study. They include generic narrowband signals, generic wideband signals, Orthogonal-Frequency Division Multiplexing (OFDM) signals, as well as the hybrid signal waveform of OFDM and CDMA known as MC-CDMA signals.

In the next several sections, we briefly discuss the subjects of MIMO systems, signal waveforms, and interference cancellation techniques.

1.2.1 MIMO Systems

Antenna arrays have been widely used for several decades to provide spatial diversity and thus improve the received signal quality [1][2]. However, antenna arrays have been primarily used in the uplink channel (the link from a mobile station to a base station) in wireless communications. With the anticipated emergence of data-dominated wireless systems in the future, the capacity requirement for the downlink channel (the link from a base station to a mobile station) has become critically important. This motivates research on improving the system performance of the downlink channel. Several approaches such as open-loop transmit diversity and closed-loop transmit beamforming have been proposed to provide diversity, average power improvement and possibly some degree of interference rejection [3][4][5]. Other approaches such as space-time coding (*i.e., space-time trellis codes and space-time block codes*) have also been proposed to provide transmit diversity gains as well as some degree of coding gain. These works combined with information theoretic studies have generated much interest in general multiple-transmit and multiple-receive antenna systems for future wireless systems. It has been shown that MIMO systems are a viable approach to provide significant capacity improvement over conventional wireless antenna systems [6][7]. MIMO-based signal processing techniques such as the Bell Labs Layered Space-Time architecture (BLAST) have been proposed and examined for practical communication applications [6]. Others like space-time trellis codes and space-time block codes have also been proposed and evaluated for future wireless applications [4][8][9]. In this research, we design a simple space-time orthogonal transmit waveform and analyze the system performance of this orthogonal transmit waveform for MIMO channels from a communication perspective.

1.2.2 Signal Waveforms

In this section, we briefly discuss three major signal waveforms used in this research. They are DS-CDMA, OFDM, and MC-CDMA signal waveforms.

Spread spectrum technology was developed in 1950's for military applications [10][11][12] and has become quite common for use in military systems in the past several decades. However, there has also been strong interest in using spread-spectrum techniques for commercial applications. Although there are several methods for generating spread-spectrum signals, currently DS-SS-CDMA (or DS-CDMA) appears to be the most popular. This is particularly true in cellular and personal communication systems (PCS). The reason is that for moderate processing gain and good power control DS-CDMA systems can provide significant interference suppression capability for multipath resistance and multiple access interference (MAI) reduction. Furthermore, the wide bandwidth can be used to mitigate the effects of multipath fading channels. It also has been shown that DS-CDMA can significantly enhance the system capacity for conventional cellular systems [13]. Many of the benefits of DS-CDMA systems for commercial applications have been discussed in [14][15][16][13].

Orthogonal-Frequency Division Multiplexing (OFDM) is a favorable transmission technique for time dispersive channels. It has been adopted as a modulation scheme for the European terrestrial transmission of DAB (Digital Audio Broadcasting) and DVB (Digital Video Broadcasting) [17][18]. The significance of OFDM is its capability to mitigate the distortion due to multipath propagation in wireless communications [19][20][21]. The principle of OFDM waveforms is to divide the entire channel into many narrow orthogonal subchannels, thereby increasing the OFDM symbol duration and eliminating the ISI due to multipath channels. The ISI is eliminated by inserting a guard interval in every OFDM symbol. When cyclic prefixing is implemented for every OFDM symbol, both ISI and ICI (inter-carrier interference) can completely eliminated provided channel is essentially static over a OFDM symbol duration . This eliminates the need for using elaborate equalization techniques while obtaining high data rate[22].

The hybrid of a DS-CDMA signal waveform and an OFDM signal waveform, known as MC-CDMA (or OFDM-CDMA), has recently been proposed and examined for mobile radio communications [23][24][25]. In time-dispersive channels, MC-CDMA not only can exploit the frequency diversity as DS-SS-CDMA signals, but can also eliminate the ISI as OFDM signals do. Performance comparisons between DS-CDMA and OFDM-CDMA have been studied for mobile radio environments [26][27].

1.2.3 Interference Cancellation

In recent years, there have been two active ongoing research areas in the area of interference suppression or interference cancellation in wireless communications, namely *adaptive beamforming* and *multiuser detection* (MUD). Adaptive beamforming techniques in conjunction with antenna arrays, known as smart antenna systems, enable the receiver to provide interference suppression, thus enhancing system capacity [28][29][30]. Multiuser detection receivers, on the other hand, generally improve the system performance by eliminating or cancelling the interference in the system without the need for adaptive antennas. In this section, we briefly describe these two signal processing techniques. In Chapter 8, we will present a comprehensive survey of these two techniques.

Communication receivers can be divided into two major classes. One is a conventional single-user receiver. The other is a multiuser detection receiver. A conventional single-user receiver only utilizes the decision statistics of the desired user for signal detection while multiuser detection receivers not only exploit the decision statistics of the desired user, but also those of the interfering signals. Note that these interfering signals are also considered to be the "desired signals" from a multiuser detection point of view. The basic ideal of multiuser detection is to make use of the information avaliable about the interference to reduce its effects. This can be accomplished by joint detection techniques, adaptive interference suppression techniques, or subtractive interference cancellation techniques [31][32][33]. Although in principle multiuser detection can be applied to both CDMA (wideband signal) systems as well as TDMA (narrowband signal) systems, most of work in the past decade has primarily focused on CDMA systems. This is because wireless CDMA capacity significantly suffers from the near-far problem due to imperfect power control, and multiuser detection techniques can provide near-far resistance to enhance system capacity [34][35].

Adaptive beamforming is based on the principle of *adaptive spatial filtering*. One can think of adaptive beamforming as the application of adaptive filter theory in the spatial domain, while adaptive channel equalization is the application in the temporal domain. The basic principle of adaptive spatial filtering is to combine individual weighted antenna outputs to form an optimized estimate of the transmitted signal. The optimization criterion of the adaptive weights is dependent on signal waveforms, the characteristics of the channel, as well as the array architecture. In fading channels, adaptive beamforming systems with large antenna element spacing not only provide spatial diversity to mitigate the effects of fading channels, but also can eliminate the effects of the interference. It should be noted that the adaptive beamforming system is generally effective in suppressing the interference when the number of antenna elements is greater than the number of interferers in the system. In addition, the spatial diversity provided by adaptive beamforming systems is more robust and reliable than the path diversity provided by frequency-selective fading channel. This is because in reality multiple resolvable paths may not exist at all times in time-varying wireless channels.

Some forms of jointly combining the adaptive beamforming systems with MUD receivers for CDMA have been proposed to provide a better solution for minimizing the three aforementioned impairments [36][37][38]. However, the explosive increase in complexity due to signal synchronization and acquisition in the proposed joint systems may not be feasible for commercial applications.

In this research, we focus on evaluating the system performance of adaptive beamforming techniques for various signal waveforms and antenna configurations over a wide variety of radio environments. We also examine the combination of the adaptive beamforming systems and multiuser detection receivers for an overloaded array system with reasonable complexity [39]. Note that by overloaded array system, we mean the number of active users in the system is much greater than the number of antenna elements.

1.3 Outline of Dissertation

Based on the above discussion, we have focused in this research on three major areas.

The first part of this research makes contributions to the area of MIMO antenna systems. From a channel modeling perspective, we develop a space-time channel model for MIMO channels in mobile radio environments. We derive an analytical expression for the space-time MIMO channel correlation for Rayleigh fading channels assuming specific statistics for the physical environment. Using these results, we evaluate the information-theoretic channel capacity of MIMO channels for various antenna configurations. Two types of antenna arrays are considered in this study: the *uniform circular array* (UCA) and the *uniform linear array* (ULA). Note that by uniform we refer to the antenna element spacing. From a receive antenna perspective, we compare the BER performance of the uniform circular array and the uniform linear array in a Rayleigh fading channel. From a transmit antenna perspective, we compare the BER performance of the open-loop transmit diversity scheme and the closed-loop transmit beamforming over Rayleigh and Ricean fading channels.

The second part of this research makes two contributions to the area of orthogonal waveform design. We propose a simple space-time orthogonal waveform design for MIMO-based wireless communication systems. From a communications perspective, we analyze the BER performance of the space-time orthogonal waveform for MIMO mobile radio environments. It is found that the system performance of the space-time orthogonal waveform significantly outperforms other proposed orthogonal diversity waveforms. From an application perspective, we apply the proposed space-time orthogonal waveform to a conventional cellular system. We find that the performance of the proposed space-time orthogonal transmit waveform (ST-OTW) is superior to the existing space-time spreading (STS) waveform for high mobility cellular CDMA systems [40].

Finally, the third part of this research makes two contributions to the area of interference cancellation techniques for multiple-receive antenna systems. For the case when the number of receive antennas is greater than or equal to the number of users in the system, we evaluate the BER performance of adaptive beamforming techniques for various signal waveforms over both additive white Gaussian noise (AWGN) channels and Rayleigh fading channels. For the case where the number of users exceeds the number of receive antennas, known as overloaded array systems, we propose a new signal extraction method that combines adaptive beamforming with multiuser detection for both interference cancellation and suppression [39]. There have been few contributions geared specifically towards signal extraction in an overloaded array environment [41][42]. As compared to [41][42], the complexity and performance of the proposed signal extraction method is significantly lower than the previous signal extraction method.

This dissertation is organized as follows.

In Chapter 2, we first characterize the wireless propagation environment and develop a statistical and time-varying wireless vector channel model for systems using various antenna arrays. We compare the characteristics of a statistical-based time-variant vector channel model with a geometrically-based vector channel model. We then develop a statistical-based time-varying MIMO channel model for mobile radio environment.

In Chapter 3, we derive an analytical expression for the space-time fading correlation function for MIMO channels using the previously developed model. The space-time fading correlation is dependent on the temporal fading correlation and the spatial fading correlation. The temporal fading correlation is a function of the Doppler spread and time delay while the spatial fading correlation is a function of the angle spread and distance between elements (the latter being dependent on the array geometry). Comparative results on the fading correlation function for both the ULA and the UCA are given. Computer simulations are carried out to verify the analytical results.

In Chapter 4, we evaluate the information-theoretic channel capacity of the MIMO channel using the developed channel model with various antenna configurations. Both uniform linear array (ULA) and circular array (UCA) geometries are considered in mobile cellular environments. The prefered choice for MIMO antenna configurations in mobile environments is suggested.

In Chapter 5, we examine the transmission side of MIMO systems. Two transmit antenna schemes are evaluated and compared: *open-loop transmit diversity methods* and *closed-loop transmit beamforming methods*. We evaluate the BER performance of these two transmit antenna schemes for MIMO systems over Rayleigh and Ricean fading channels. The effects of channel estimation and feedback robustness are considered for these transmit antenna schemes.

In Chapter 6, we examine the reception side of MIMO systems. We compare the diversity performance of a uniform circular array and a uniform linear array using maximal-ratio-combining (MRC) in mobile radio communications. Diversity performance is evaluated based on BER results. The analytical BER is derived as function of spatial fading antenna correlation for both types of antenna arrays. A truncated Gaussian angle-of-arrival (AOA) distribution and Rayleigh fading are assumed in this study. Simulations are carried out to verify the analytical BER results.

In Chapter 7, we propose and evaluate a simple space-time orthogonal transmit waveform in a MIMO cellular environment. The performance of the ST-OTW waveform in a MIMO system is evaluated based on the BER performance for both uplink and downlink communications in a flat Rayleigh fading channel. An analytical BER formula for the ST-OTW waveform is derived as a function of the eigenvalues of the space-time channel covariance matrix. The effects of angle spread and Doppler frequency of a mobile channel on the BER performance of the ST-OTW waveform are also evaluated. The application of ST-OTW waveform to a conventional cellular CDMA scenario is also evaluated as a special case of MIMO systems.

In Chapter 8, we present a survey of adaptive beamforming and multiuser detection for wireless communications. Starting with the principles and fundamentals of signal detection techniques for various MUD receivers, we discuss the features of both optimum MUD receivers and various suboptimum MUD receivers. Later, we review the various optimization criterion for calculating the adaptive weights needed for smart antenna systems. The practical issues on the implementation of adaptive algorithms are also discussed.

In Chapter 9, we evaluate the performance of MMSE beamforming for DS-CDMA and OFDM systems in AWGN and Rayleigh fading channels. The performance of MMSE beamforming is evaluated based on BER simulations. The effects of angle spread and user location as well as practical implementation issues are considered. The comparative BER performance of MMSE beamforming and Max SNR beamforming are also evaluated.

In Chapter 10, we propose a signal extraction method that combines MMSE beamforming with successive interference cancellation. The combination of MMSE beamforming with successive interference cancellation (MMSE-SIC) is proposed for overloaded airborne communications using narrowband TDMA signal formats.

Finally in Chapter 11, a summary of the results is presented, concluding remarks are given, and possible areas for future work to extend this research are outlined.

1.4 Contributions of this Work

The work presented here makes a number of novel contributions to the field. Some of the significant contributions of this report include:

- A statistical-based multipath MIMO channel model developed for mobile radio environment.
- A derivation of the first analytical result on the space-time fading correlation for MIMO channels.
- An information-theoretic channel capacity of the MIMO channels is evaluated for UCA and ULA based on the above statistical MIMO channel model.
- The BER performance of UCA and ULA is evaluated for mobile cellular environments based the analytical spatial correlation derived above.
- The BER performance of open-loop transmit diversity and closed-loop transmit beamforming are evaluated and compared for both Rayleigh and Ricean fading channels.

- A simple open-loop space-time orthogonal transmit waveform design is proposed for MIMO-based wireless communications systems.
- The analytical BER expression for the space-time orthogonal waveform in MIMO systems is derived.
- The application of the space-time orthogonal waveform to a conventional cellular system is evaluated.
- The system performance of MMSE beamforming for DS-CDMA and OFDM systems is evaluated for both UCA and ULA.
- A novel MMSE-SIC signal extraction method is proposed for an overloaded antenna array system.

Chapter 2

MIMO Channel Model

In this chapter, we characterize the wireless propagation environment and develop a statistical and time-varying wireless MIMO channel model for systems using antenna arrays. We begin with the description of fundamental radio propagation mechanisms in Section 2.1. We describe the characteristics of the multipath scalar channel model in Section 2.2 and those of the multipath vector channel model in Section 2.3. A brief discussion of two classes of multipath vector channel models, the geometrically-based vector channel model and the statistical-based vector channel model, is given in Section 2.4 and Section 2.5. Based on the above vector channel model, we develop the statistical time-varying MIMO channel model for multiple-transmit and multiple receive antenna systems in Section 2.6. Finally, a brief summary is given in Section 2.7.

2.1 Fundamentals of Radio Propagation

In wireless communications, the radio waves propagate through a physical medium interacting with physical objects and structures such as buildings, hills, tree, mountains, and moving vehicles is a complicated process. This process can result in a single line-of-sight

(LOS) propagation path, many non-LOS reflected propagation paths, or a combination of LOS and non-LOS propagation paths (multipath environment). The multipath propagation results from reflection, diffraction, and scattering. An illustration of wireless propagation environment is shown in Figure 2.1.

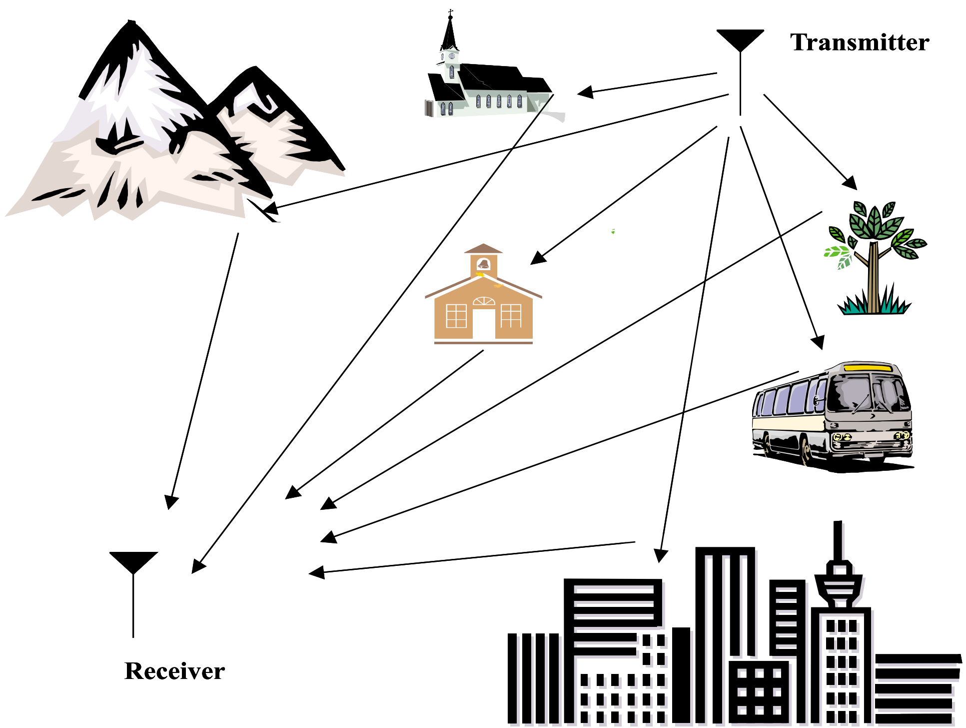

Figure 2.1: Wireless propagation

Reflection occurs when propagation waves impinging upon a physical object which has a large surface relative to the wavelength of the propagation wave. In general reflection results from the surface of the earth, mountains, or the wall of a building.

Diffraction results from the resultant bending of waves that occurs when the propagation wave is obstructed by an irregularly sharp surface or edges,

Scattering occurs when the size of the physical objects in the propagation medium are smaller than the propagation wavelength. Scattered waves generally result from foliage, street signs, or lamp posts.

In addition to reflection, diffraction, scattering, the signal strength is attenuated due to the physical separation between the transmitter and the receiver. The signal strength is also time-varying due to the mobility of the receiver or the transmitter. From an analytical point of view, we can characterize the radio propagation by two partially separable effects: *large-scale signal attenuation* and *small-scale signal distortion*. The large-scale signal attenuation is due to the path loss and shadowing between a transmitter and a receiver while the small-scale signal distortion is due to multipath propagation. We describe these two effects in the following section.

2.1.1 Radio Propagation: Large-Scale Effects

Figure 2.2 shows the large-scale effects of the signal attenuation in mobile radio propagation environment. As shown, the large-scale signal attenuation in mobile radio propagation includes path loss and shadowing (known as slow fading). *Path loss* (PL) is due to the physical separation between the transmitter and the receiver. *Shadowing* is the received power variation resulting from signal attenuation due to physical obstructions between the transmitter and the receiver.

Path loss χ_{PL} is related to the ratio of the received power to the transmitted power

$$\chi_{\mathsf{PL}} \propto \frac{P_r}{P_t}, \tag{2.1}$$

where P_r is the received power and P_t is the transmitted power. In practice, χ_{PL} can be evaluated as a function the distance between the transmitter and the receiver

$$\chi_{\mathsf{PL}} \propto \Big(\frac{1}{d_{TR}}\Big)^{n_l}, \tag{2.2}$$

where n_{l} is the path loss exponent and d_{TR} is the distance between the transmitter and the receiver. References [43][44] provide a comprehensive survey on propagation loss based on considerable measurement data. As suggested in [43], n_{l} is typically in the range from 2.5 to 4, depending on the propagation environment. For instance, in typical urban areas

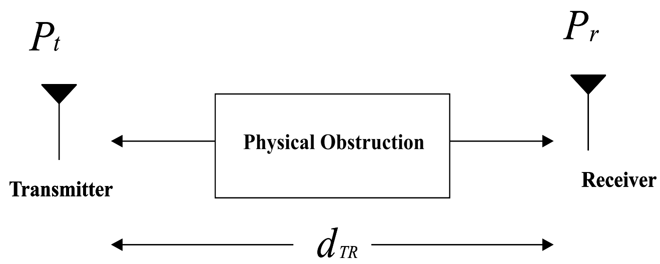

Figure 2.2: Wireless path loss and shadowing

n_l is about 3.8 to 4.5 and in rural areas n_l is about 2.5 to 3. As mentioned above, the physical obstacles between the transmitter and the receiver result in a variation around the mean received power P_r, known as shadowing. Shadowing is considered to be slow fading and is statistically characterized by a log-normal distribution (normal distribution in dB scale).

2.1.2 Radio Propagation: Small-Scale Effects

As discussed earlier, multipath propagation resulting from reflection, diffraction, and scattering gives rise to many non-LOS propagation paths. These non-LOS propagation paths arrive with displacement at the receiving antenna with respect to one another in the time and spatial domains; thus resulting in three small-scale effects due to the mobile radio channels: delay spread, angle spread, and Doppler spread. Figure 2.3 shows three small-scale effects due to non-LOS propagation paths on the mobile radio channel.

Delay spread is the measure of the relative propagation delays among the non-LOS propagation paths caused by the reflectors such as mountains or a cluster of buildings, as shown in Figure 2.3.

Angle spread is the measure of the angle displacement due to non-LOS propagation with respect to the angle of LOS propagation. Figure 2.3 shows the angle displacement caused by the non-LOS propagation paths.

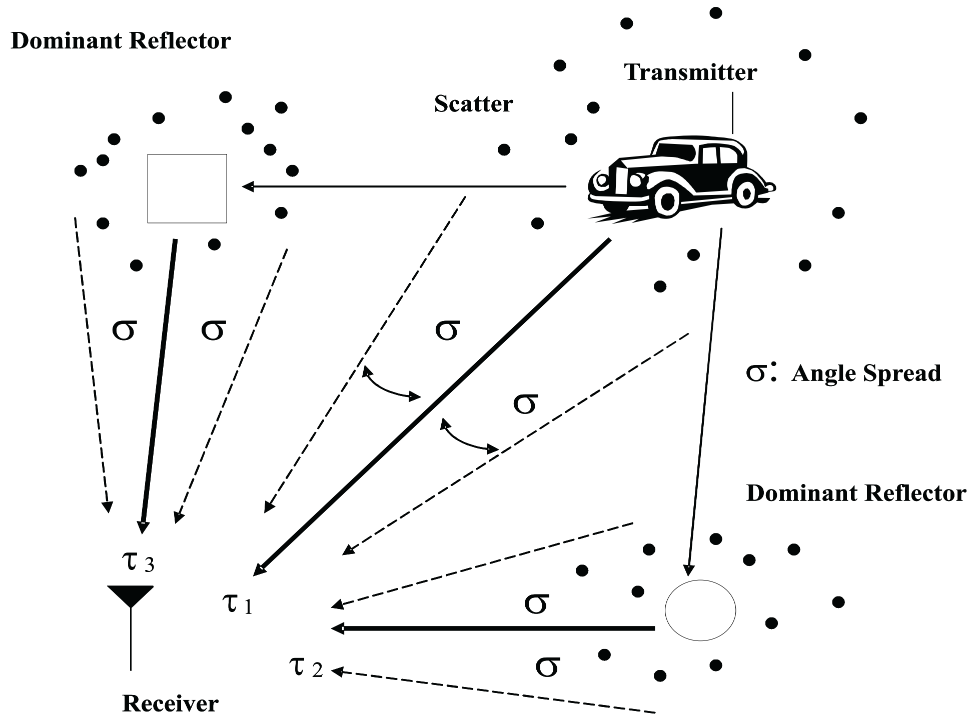

Figure 2.3: Small-scale effects in wireless channel

Doppler spread is the measure of channel variation rate caused by the movement of the transmitter and/or receiver relative to local scatterers in the multipath propagation environment.

In addition, with the composite sum of many non-LOS propagation paths, the multipath propagation results in signal fluctuation in received signal amplitude , thereby inducing signal fading and signal distortion. For our channel modeling efforts, our focus in this study is the multipath propagation effects (small-scale effects) for transmitter and/or receivers employing antenna arrays.

2.2 Multipath Scalar Channel Model

In this section, we develop a statistical multipath scalar channel model for wireless communication systems employing a single transmit antenna and a single receive antenna. As shown in Figure 2.1, the received signal is considered to be the sum of a large number of non-LOS propagation paths due to local scatterers, which is also known as Jake's model. The complex baseband received signal $x(t)$[1] based on Jake's model can be expressed as [45][1]

$$\begin{aligned} x(t) &= s(t) \star h(t,\tau) \\ &= \sum_{s=1}^{L_s} A_s s(t-\tau_s) e^{j[2\pi F_d \cos(\Psi_s)t + \phi_s]}, \end{aligned} \tag{2.3}$$

where $s(t)$ is the complex baseband model of the transmitted signal with bandwidth B, the symbol $\star$ denotes the convolution operation, τ_s is the multipath time delay, L_s is the number of scatterers used in Jake's model, ϕ_s is uniformly distributed random phases over $[0,\, 2\pi]$, Ψ_s is the random angles of arrival relative to the motion of the mobile of each scatterer, and F_d is the maximum Doppler frequency due to mobility. We assume the minimum and maximum multipath delay are τ_1 and τ_{L_s}, respectively. If the relative delay $\Delta\tau = \tau_{L_s} - \tau_1$ is much less than the inverse bandwidth of the signal ($\Delta\tau \ll \tau B^{-1}$) (i.e. a narrowband channel), then $s(t-\tau_s) \approx s(t-\tau_1)$. Then we can rewrite (2.3) as

$$\begin{aligned} x(t) &= s(t-\tau_1)\Big(\sum_{s=1}^{L_s} A_s e^{j[2\pi F_d \cos(\Psi_s)t + \phi_s]}\Big) \\ &= s(t-\tau_1)\alpha(t)e^{j\Theta(t)} \\ &= s(t-\tau_1)\beta(t), \end{aligned} \tag{2.4}$$

where

$$\beta(t) = \alpha(t)e^{j\Theta(t)} = \sum_{s=1}^{L_s} A_s e^{j[2\pi F_d \cos(\Psi_s)t + \phi_s]}. \tag{2.5}$$

If we assume that the $\{A_s\}$ are independent and identically distributed (i.i.d.) and independent of the ϕ_s, then $\beta(t)$ will essentially be a complex Gaussian random variable

[1] For simplicity, we ignore the impact of white Gaussian noise.

as the number of scatterers L_s is becomes large [46]. In such case, $\alpha(t)$ has a Rayleigh distribution [1]

$$f(\alpha) = \frac{2\alpha}{\sigma_0^2}\exp\Big(-\frac{\alpha^2}{\sigma_0^2}\Big), \tag{2.6}$$

where $\sigma_0^2 = E\{\alpha^2\}$. Based on the field measurement data, the received signal envelope exhibit a good agreement with Rayleigh distribution. If the direct LOS path is present in (2.3), then $\alpha(t)$ will have a Rician distribution [43]

$$f(\alpha) = \frac{2\alpha}{\sigma_0^2}\exp\Big(-\frac{\alpha^2+K^2}{\sigma_0^2}\Big)I_0\Big(\frac{2\alpha K}{\sigma_0^2}\Big), \tag{2.7}$$

where K is the power ratio of LOS path over non-LOS path and I_0 is the zero-order of the modified Bessel function of the first kind. By comparing the result of (2.4) with (2.3), the channel impulse response $h(t;\tau)$ can be shown to be

$$h(t;\tau) = \sum_{s=1}^{L_s} A_s e^{j[2\pi F_d\cos(\Psi_s)t+\phi_s]}\delta(\tau-\tau_s). \tag{2.8}$$

In practice, the baseband complex equivalent channel impulse response $h(t;\tau)$ generated based on a finite number of scatterers. If we assume τ_1 is the first arriving multipath path (i.e. $\tau_1 = 0$), then the normalized $h(t;\tau)$ is reduced to $h(t)$ and can be modeled as

$$\begin{aligned} h(t) &= \sum_{s=1}^{L_s}\frac{1}{\sqrt{L_s}}e^{j[2\pi F_d\cos(\Psi_s)t+\phi_s]} \\ &= \alpha(t)e^{j\Theta(t)} \\ &= \beta(t). \end{aligned} \tag{2.9}$$

As the signal bandwidth B increases such that $\Delta\tau \approx B^{-1}$ (*i.e., a wideband channel*), the received signal becomes a sum of multiple copies of the original signal, with each copy delayed by τ_l, attenuated by $\alpha_l(t)$ and phase shifted by $\Theta_l(t)$. In the wideband channel model, if the incoming paths from the same subpath cluster arrive within $1/B$ seconds, they are not *resolvable* at the receiver. Thus they are combined into a single path. If a finite number of resolvable paths is present due to multiple dominant reflectors, then the received signal can be written as

$$x(t) = \sum_{l=1}^{L} s(t-\tau_l)\alpha_l(t-\tau_l)e^{j\Theta_l(t-\tau_l)}$$

$$= \sum_{l=1}^{L} s(t-\tau_l)\beta_l(t-\tau_l), \tag{2.10}$$

where L is the number of resolvable paths, τ_l, $\alpha_l(t)$, and $\Theta_l(t)$ are the delay, amplitude, and phase for each resolvable path. The complex channel gains $\beta_l(t)$ for the L resolvable path are statistically independent. Without a direct LOS path in the received signal, the envelope $\alpha_l(t)$ and the phase $\Theta_l(t)$ for the lth resolvable path are Rayleigh distributed and uniformly distributed, respectively. If a LOS path is present, then the envelope $\alpha_l(t)$ for the lth resolvable path is Rician distributed. Comparing the result of (2.10) with (2.3), the normalized baseband equivalent channel impulse response $h(t;\tau)$ for the wideband channel can be modeled as

$$\begin{aligned} h(t;\tau) &= \sum_{l=1}^{L}\sum_{s=1}^{L_s} \frac{1}{\sqrt{L_s}} e^{j\left[2\pi F_d \cos(\Psi_{s,l})t+\phi_{s,l}\right]}\delta(\tau-\tau_1) \\ &= \sum_{l=1}^{L} \alpha_l(t)e^{j\Theta_l(t)}\delta(\tau-\tau_l) \\ &= \sum_{l=1}^{L} \beta_l(t)\delta(\tau-\tau_l). \end{aligned} \tag{2.11}$$

The channel response with the forms of (2.9) and (2.11) are characterized as flat fading and frequency-selective fading, respectively. One can think of (2.9) as a special case of (2.11) with $L = 1$.

For the interest of this research, it is important to determine the temporal correlation of $\beta_l(t)$. The temporal fading correlation ρ_t for the lth resolvable path is given by

$$\rho_t = E\{\beta_l(t)\beta_l^*(t+\nu)\}, \tag{2.12}$$

where the superscript $*$ denotes the complex conjugate, ν is a time delay. It can be shown that [30]

$$\rho_t = J_0(2\pi F_d \nu), \tag{2.13}$$

where $J_n(\cdot)$ is the Bessel function of the first kind of order n.

2.3 Multipath Vector Channel Model

In this section, we develop a statistical multipath vector channel model for systems employing receive antenna arrays. We begin with defining the array response vectors for uniform linear and uniform circular arrays. Then, a brief comment on the difference between statistical-based vector channel models and geometrically-based vector channel models is given. A justification for using statistical-based vector channel model throughout the research is given.

2.3.1 Array Response Vector

Figure 2.4 shows a wireless communication system employing a uniform circular antenna array with M evenly spaced receive elements. Following the same notation and defini-

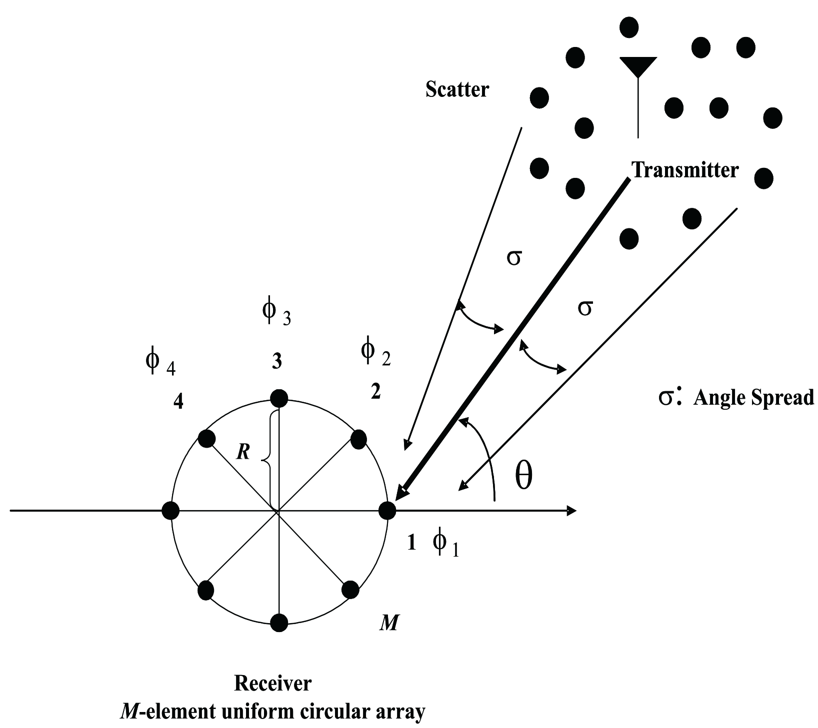

Figure 2.4: Wireless communication systems employing M-element uniform circular arrays

tions used in [30][47], the array manifold vector $\mathbf{v}(\theta)$ for a single received plane wave in a uniform circular array can be written as

$$\mathbf{v}(\theta) = \begin{bmatrix} v_1(\theta) \\ v_2(\theta) \\ \vdots \\ v_M(\theta) \end{bmatrix} = \begin{bmatrix} e^{-j2\pi\frac{R}{\lambda}\sin(\varsigma)\cos(\theta-\phi_1)} \\ e^{-j2\pi\frac{R}{\lambda}\sin(\varsigma)\cos(\theta-\phi_2)} \\ \vdots \\ e^{-j2\pi\frac{R}{\lambda}\sin(\varsigma)\cos(\theta-\phi_M)} \end{bmatrix}, \tag{2.14}$$

where R is the circular radius of the antenna array, ς is the elevation angle, and $\lambda = c/f_c$ is the wavelength. c is the speed of light and f_c is the carrier frequency. For simplicity, only azimuth angles are considered in the propagation geometry ($\varsigma = 90°$), but the results can be generalized to three dimensions. As shown in Figure 2.4, θ is the main angle of arrival (AOA) and ϕ_m is the phase excitation of mth element in azimuth plane.

Similarly, Figure 2.5 shows a wireless communications system employing a uniform linear antenna array with M evenly spaced receive elements. The array manifold vector $\mathbf{v}(\theta)$ for a specific arriving plane wave in a uniform linear array can be written as [30][47]

$$\mathbf{v}(\theta) = \begin{bmatrix} v_1(\theta) \\ v_2(\theta) \\ \vdots \\ v_M(\theta) \end{bmatrix} = \begin{bmatrix} 1 \\ e^{-j2\pi\frac{D}{\lambda}\sin(\pi/2-\theta)} \\ e^{-j2\pi\frac{2D}{\lambda}\sin(\pi/2-\theta)} \\ \vdots \\ e^{-j2\pi\frac{(M-1)D}{\lambda}\sin(\pi/2-\theta)} \end{bmatrix}, \tag{2.15}$$

where D is the antenna element spacing and θ is the AOA at received antenna array. In the next section, we extend the scalar channel model to the vector channel model. The vector channel model based on the array response vector $\mathbf{v}(\theta)$ is developed for both AWGN channel and multipath fading channel.

2.3.2 AWGN Channel

For an AWGN (Additive White Gaussian Noise) channel, θ is a constant and is equivalent to the AOA of the LOS propagation path. In this case, we use the so-called *narrowband*

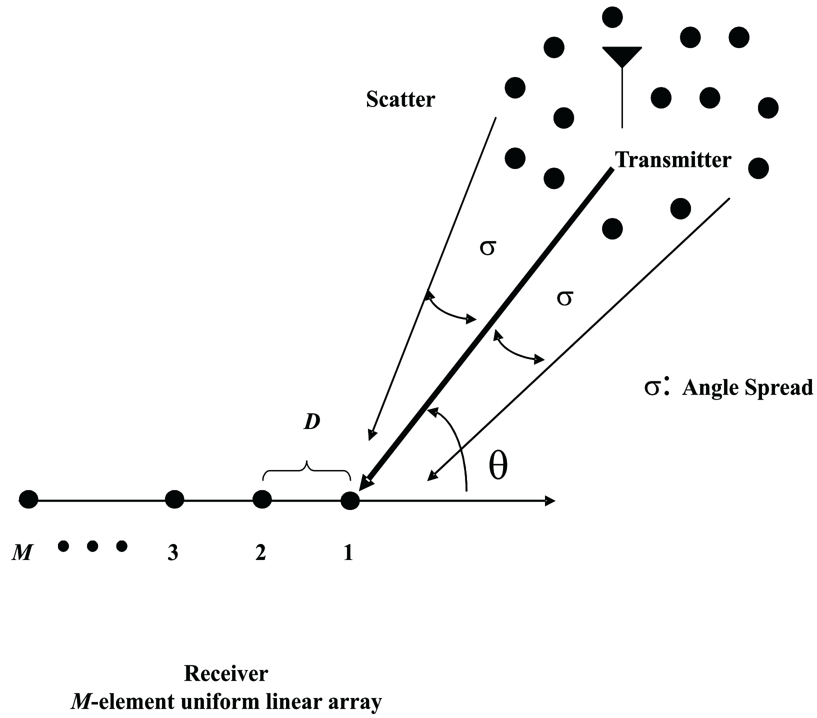

Figure 2.5: Wireless communication systems employing M-element uniform linear arrays

data model to model the received signal at the antenna arrays. The narrowband data model assumes that the envelope of the signal wavefront propagating across the antenna array essentially remains constant [48]. This model is valid when the signals or the antennas have a bandwidth that is much smaller than the carrier frequency f_c. For wideband signals such as CDMA signals, this model is also valid, provided that the propagation time across the array is small relative to the inverse of signal bandwidth B^{-1}. Under the above assumptions, the vector from of the baseband complex equivalent received signal can be written as [48][49]

$$\mathbf{x}(t) = \mathbf{v}(\theta)s(t) + \mathbf{N}_w(t), \tag{2.16}$$

where $\mathbf{N}_w(t))$ is AWGN with zero mean and two-sided power spectral density given by $No/2$. This is simply a plane-wave model. Note that boldface type is used to represent vector quantities.

2.3.3 Multipath Fading Channel

For the multipath fading channel, the received signal is the sum of a large number of non-LOS propagation paths due to local scatterers or reflectors, as shown in Figure 2.3. The vector form of the baseband complex equivalent received signal for an antenna array can be expressed as

$$\begin{aligned}\mathbf{x}(t) &= s(t) \star \mathbf{h}(t,\tau) \\ &= \sum_{s=1}^{L_s} \mathbf{v}(\theta_s) A_s e^{j[2\pi F_d \cos(\Psi_s)t + \phi_s]} s(t-\tau_s), \end{aligned} \tag{2.17}$$

where $\tau_1 < \tau_2 < \cdots < \tau_{L_s}$, $\mathbf{h}(t,\tau)$ is the multipath vector channel impulse response for received antenna arrays, and $\mathbf{v}(\theta_s)$ is the array response vector for the sth non-LOS propagation path. For a uniform circular array and a uniform linear array, $\mathbf{v}(\theta_s)$ can be expressed as (2.14) and (2.15) respectively. If $\Delta\tau = \tau_{L_s} - \tau_1$ is less than the inverse bandwidth of the signal ($\Delta\tau \ll \tau B^{-1}$), then $s(t-\tau_s) \approx s(t-\tau_1)$. In such a case, we can rewrite (2.17) as

$$\begin{aligned}\mathbf{x}(t) &= s(t)\Big(\sum_{s=1}^{L_s} \mathbf{v}(\theta_s) A_s e^{j[2\pi F_d \cos(\Psi_s)t + \phi_s]}\Big) \\ &= s(t)\boldsymbol{\alpha}(t) e^{j\boldsymbol{\Theta}(t)} \\ &= s(t)\boldsymbol{\beta}(t), \end{aligned} \tag{2.18}$$

where

$$\boldsymbol{\beta}(t) = \boldsymbol{\alpha}(t) e^{j\boldsymbol{\Theta}(t)} = \sum_{s=1}^{L_s} \mathbf{v}(\theta_s) A_s e^{j[2\pi F_d \cos(\Psi_s)t + \phi_s]}, \tag{2.19}$$

and

$$\boldsymbol{\beta}(t) = \Big[\beta_1(t) \cdots \beta_M(t)\Big], \tag{2.20}$$

$$\boldsymbol{\alpha}(t) = \Big[\alpha_1(t) \cdots \alpha_M(t)\Big]. \tag{2.21}$$

Again, if we assume that the $\{A_s\}$ are independent and identically distributed (i.i.d.) and independent of the ϕ_s, then $\beta_m(t)$ for $m = 1, 2, \cdots M$ will be a complex Gaussian random variable as the number of scatterers L_s becomes large [46]. In such a case, the envelope of the received signal $\alpha_m(t)$ for $m = 1, 2, \cdots M$ has a Rayleigh distribution [1]. For simplicity we ignore the white Gaussian noise at the receiver in the analysis.

Again, by comparing the result of (2.18) with (2.17), the normalized multipath vector channel impulse response $\mathbf{h}(t;\tau)$ can be shown as

$$\mathbf{h}(t;\tau) = \sum_{s=1}^{L_s} \mathbf{v}(\theta_s) A_s e^{j[2\pi F_d \cos(\Psi_s)t + \phi_s]} \delta(\tau - \tau_s). \tag{2.22}$$

In practice, the normalized baseband equivalent channel impulse response $\mathbf{h}(t;\tau)$ is generated based on a finite number of scatterers. If we assume τ_1 is the first arriving multipath path (*i.e.,* $\tau_1 = 0$), the normalized $\mathbf{h}(t;\tau)$ reduced to $\mathbf{h}(t)$ and can be modeled as

$$\begin{aligned} \mathbf{h}(t) &= \sum_{s=1}^{L_s} \frac{1}{\sqrt{L_s}} \mathbf{v}(\theta_s) e^{j[2\pi F_d \cos(\Psi_s)t + \phi_s]} \\ &= \boldsymbol{\alpha}(t) e^{j\boldsymbol{\Theta}(t)} \\ &= \boldsymbol{\beta}(t). \end{aligned} \tag{2.23}$$

Note that (2.23) is the flat fading vector channel response. As the signal bandwidth B increases such that $\Delta\tau \approx B^{-1}$, the vector channel impulse response (2.23) becomes a frequency-selective fading vector channel response. For multipath propagation with L resolvable paths due to L dominant reflectors, the baseband complex equivalent vector channel impulse response $\mathbf{h}(t;\tau)$ can be written as

$$\begin{aligned} \mathbf{h}(t;\tau) &= \sum_{l=1}^{L} \sum_{s=1}^{L_s} \frac{1}{\sqrt{L_s}} \mathbf{v}(\theta_{s,l}) e^{j\left[2\pi F_d \cos(\Psi_{s,l})t + \phi_{s,l}\right]} \delta(\tau - \tau_l) \\ &= \sum_{l=1}^{L} \boldsymbol{\alpha}_l(t) e^{j\boldsymbol{\Theta}_l(t)} \delta(\tau - \tau_l), \\ &= \sum_{l=1}^{L} \boldsymbol{\beta}_l(t) \delta(\tau - \tau_l), \end{aligned} \tag{2.24}$$

where L is the number of resolvable paths, τ_l, $\boldsymbol{\alpha}_l(t)$, and $\boldsymbol{\Theta}_l(t)$ are the delay, amplitude, and phase for each resolvable path. The complex channel gains $\beta_l(t)$ for L resolvable paths are statistically independent. Without a direct LOS path in the received signal, the envelope $\alpha_l(t)$ and the phase $\mathbf{\Theta}_l(t)$ for the lth resolvable path are Rayleigh distributed and uniformly distributed, respectively. If a LOS path is present, then the envelope $\alpha_l(t)$ for the lth resolvable path is Rician distributed. By comparing (2.23) with (2.24), one can think of (2.23) as a special case of (2.24) with $L = 1$.

In order to model the multipath vector channel response $\mathbf{h}(t;\tau)$ in (2.24), we need to determine the values for $\theta_{s,l}$ $\Psi_{s,l}$, and τ_l. In the literature, two main classes of multipath vector channel are developed for systems with an antenna array: *statistically-based vector channel model* and *geometrically based vector channel model.* A discussion of these two vector channel models is given the following sections.

2.4 Geometrically Based Vector Channel Models

Geometrically based vector channel models (GBVCM) rely upon the location distribution of scatterers or reflectors in the multipath propagation environment to generate the parameter distributions needed in (2.24). These parameters are $\theta_{s,l}$, $\Psi_{s,l}$, and τ_l. By generating a large number of scatterers or reflectors for a given location distribution, one can jointly generate the distribution of $\theta_{s,l}$,$\Psi_{s,l}$, and τ_l at received antenna arrays, based upon the relative positions between the scatterers and the receiver. The location distribution of scatterers or reflectors in the GBVCM is typically assumed to be circular distribution for an outdoor macrocell environment and an elliptical distribution for indoor or microcell environment [50]. Figures 2.6 and 2.7 show the circular and elliptical distributions of scatterers used in the GBVCM, respectively.

One can determine the angle spread, Doppler spread spectrum, and delay spread profile based on the distributions of $\theta_{s,l}$, $\Psi_{s,l}$, and τ_l, respectively. As shown in Figures 2.6 and 2.7, the distributions of $\theta_{s,l}$, $\Psi_{s,l}$, and τ_l are function of the distance between the transmitter and the receiver (d_{TR}) as well as the distribution of the scatterers. For example, if we change the cluster size in Figure 2.6, assuming d_{TR} is fixed, the distributions of

$\theta_{s,l}$ (*i.e.*, angle spread) will become larger. In general, the GBVCM does not provide much freedom in selecting the channel parameters independently for $\theta_{s,l}$, $\Psi_{s,l}$, and τ_l, but it does provide the relationships among these three channel parameters. In addition, it gives a direct connection between the channel parameters and the corresponding physical propagation environment.

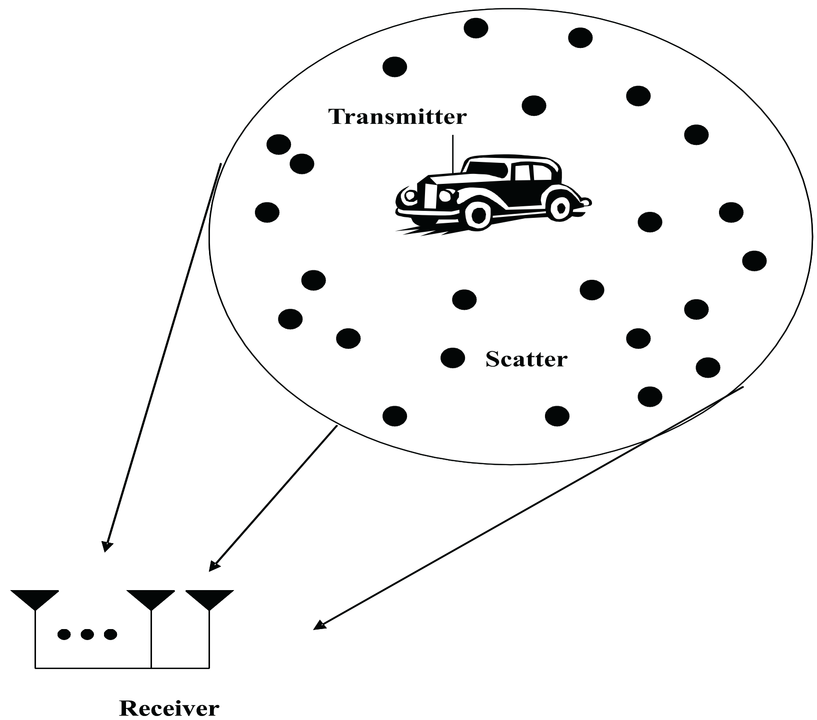

Figure 2.6: Circular distributions of scatterers used in GBVCM (macrocell model)

2.5 Statistically Based Vector Channel Model

Although the GBVCM can provide a complete description of the physical propagation channel, it also make the channel parameters a function of other parameters such as d_{TR} and the cluster size of the scatterers. From an analysis point of view, however, this model is not convenient. In addition, it is computationally intensive from a simulation point of view. Therefore, throughout this research, our focus is on statistically based

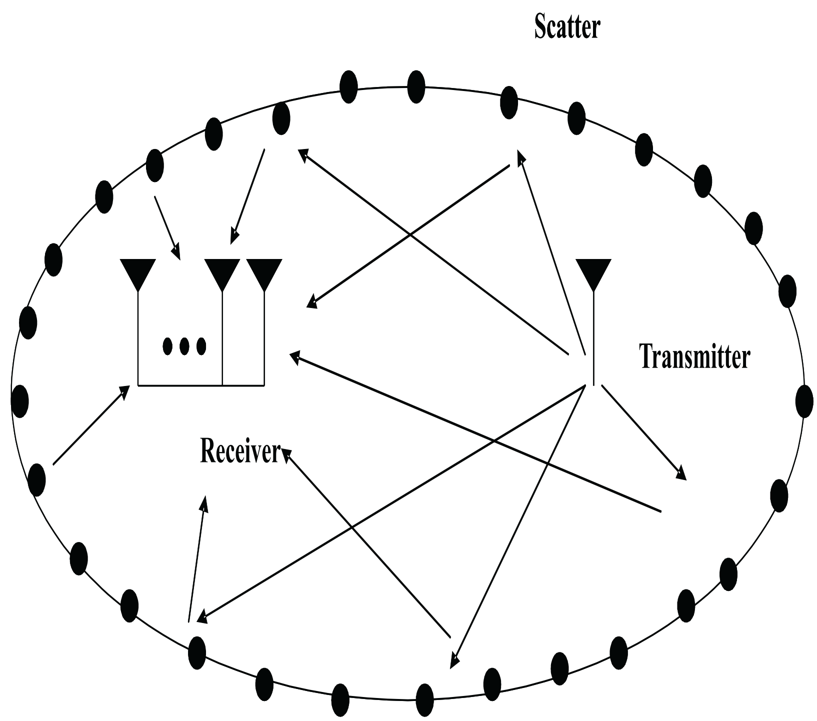

Figure 2.7: Elliptical distributions of scatterers used in GBVCM (microcell model)

vector channel models (SBVCM).

SBVCM does not rely upon the specific distribution of scatterers in the physical propagation environment. Instead, models the channel parameters directly to simulate the three small-scale effects of the physical channel: angle spread, Doppler spread, and delay spread.

For a given resolvable path l in (2.24), angle spread is characterized by the probability density function (pdf) of AOA, or $f(\theta_s)$. It is suggested that a cosine-shape or bell-shape AOA distribution at the received antenna array exhibits good agreement with measurement data [50]. In this research, three AOA distributions similar to cosine-shape or bell-shape AOA distribution are considered: uniform, truncated Gaussian, and truncated Laplacian distributions. Figure 2.8 shows the probability density function

$f(\theta_s)$ for the three AOA distributions with the same angle spread[2] variance.

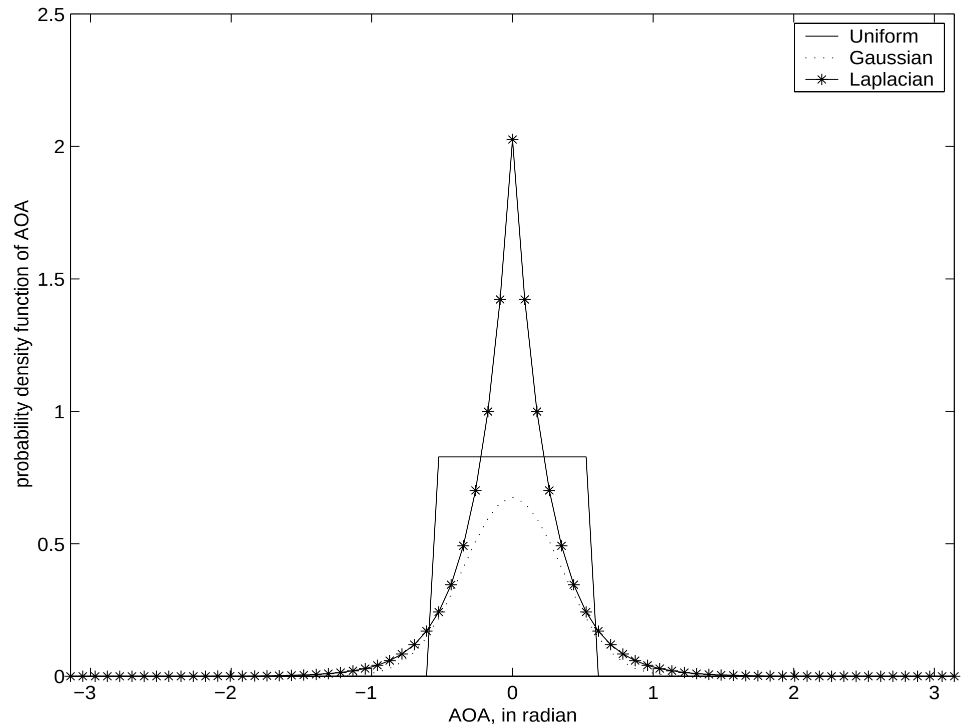

Figure 2.8: Comparisons for three AOA distributions ($\sigma = 20°$)

Similarly, for a given resolvable path l in (2.24), Doppler spectrum is determined by the probability density function of Ψ_s (or $f(\Psi_s)$) and the mobile antenna pattern. As mentioned in the previous section, Ψ_s is the random angle of arrival relative to the motion of the mobile of each scatterer. If $f(\Psi_s)$ is assumed uniformly distributed over $[0,\, 2\pi]$, and an omni-directional receive element is used, the Doppler spectrum appears to be a conventional U-shape power spectrum [51][52][53]. The shape of the Doppler spectrum determines the time domain fading waveform and the temporal correlation. As shown in [51][52], the U-shape Doppler spectrum $S_z(f)$ can be expressed as

$$S_z(f) = \frac{G_a}{\pi F_d \sqrt{1 - \left(f/F_d\right)^2}}, \tag{2.25}$$

[2]We define angle spread as the standard deviation of the AOA distribution in degrees.

where G_a is the antenna gain for a omni-directional antenna and F_d is the maximum Doppler frequency. Figure 2.9 shows a conventional U-shape Doppler spread spectrum, which is used throughout this research.

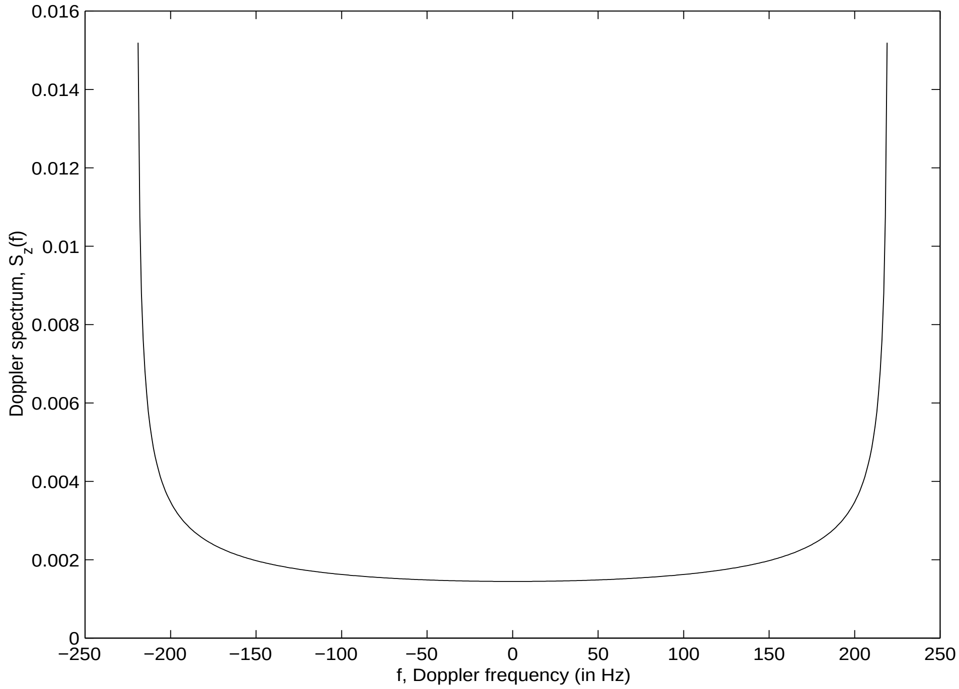

Figure 2.9: A conventional U-shape Doppler spread spectrum

The third small-scale effect is delay spread. Delay spread is determined by the distribution of τ_l. It is anticipated that as the propagation delay τ_l lengthens, the received signal strength of the delay path l becomes weaker. As the measurements suggested in [44][1], the resolvable path delay τ_l can be modeled as an exponential random variable. That is

$$f(\tau_l) = \frac{1}{\tau_m} \exp\Big(-\frac{\tau}{\tau_m}\Big), \tag{2.26}$$

where τ_m is the mean time delay. Figure 2.10 shows an probability of distribution for τ_l . However, from an analysis and simulation point of view, the number of resolvable paths L in (2.24) is generally less than 4 for most of cases of interest. Hence, in order to take the relative average power of each resolvable path into account, (2.24) can be

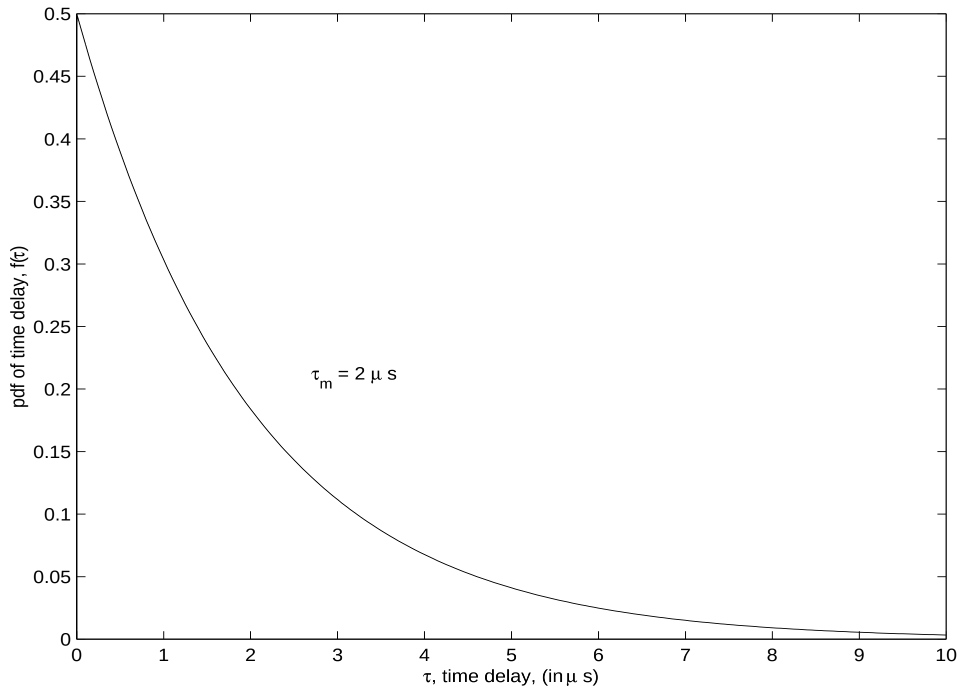

Figure 2.10: An exponentially distributed power delay profile

written as

$$\begin{aligned}\mathbf{h}(t;\tau) &= \sum_{l=1}^{L}\sum_{s=1}^{L_s}\frac{1}{\sqrt{L_s}}\sqrt{\Gamma_l}\mathbf{v}(\theta_{s,l})e^{j\left[2\pi F_d\cos(\Psi_{s,l})t+\phi_{s,l}\right]}\delta(\tau-\tau_l)\\ &= \sum_{l=1}^{L}\sqrt{\Gamma_l}\boldsymbol{\alpha}_l(t)e^{j\boldsymbol{\Theta}_l(t)}\delta(\tau-\tau_l),\\ &= \sum_{l=1}^{L}\sqrt{\Gamma_l}\boldsymbol{\beta}_l(t)\delta(\tau-\tau_l),\end{aligned} \tag{2.27}$$

where Γ_l is the relative average power of each resolvable path. The multipath profiles considered in this research are shown in Table 2.1. To be consistent with the scalar channel model in the previous section, the multipath scalar channel impulse in (2.11) is also modified by Γ_l; thus the baseband complex equivalent channel impulse response $h(t;\tau)$ for wideband signal can be modeled as

$$h(t;\tau) = \sum_{l=1}^{L}\sum_{s=1}^{L_s}\frac{1}{\sqrt{L_s}}\sqrt{\Gamma_l}e^{j\left[2\pi F_d\cos(\Psi_{s,l})t+\phi_{s,l}\right]}\delta(\tau-\tau_l)$$

Table 2.1: Various Multipath Profiles

L	Path Power (Γ_l/Γ_1)
1	0dB
2	0,-5dB
3	0,-5dB,-10dB

$$\begin{aligned} &= \sum_{l=1}^{L} \sqrt{\Gamma_l}\alpha_l(t)e^{j\Theta_l(t)}\delta(\tau-\tau_l) \\ &= \sum_{l=1}^{L} \sqrt{\Gamma_l}\beta_l(t)\delta(\tau-\tau_l). \end{aligned} \tag{2.28}$$

2.6 Statistical MIMO Channel Model

Based on the previous discussion, we extend the statistical multipath vector channel model to the statistical multipath MIMO channel model where the system employs multiple-transmit and multiple-receive antenna array systems. As a general case, we consider both the uplink and downlink channel models for MIMO systems. Figure 2.11 shows a M-element transmit-antenna array and N-element receive-antenna array denoted as a (M, N) MIMO system in a mobile radio environment.

Based on the vector channel model developed in Section 2.5, the L resolvable multipath channel impulse response for the pth transmit antenna at the mth receive antenna element for both downlink and uplink communications can be expressed as, respectively

$$h^d_{m,p}(t;\tau) = \sum_{l=1}^{L} \sqrt{\Gamma_l}h^d_{l,m,p}\delta(t-\tau_l), \tag{2.29}$$

and

$$h^u_{m,p}(t;\tau) = \sum_{l=1}^{L} \sqrt{\Gamma_l}h^u_{l,m,p}\delta(t-\tau_l), \tag{2.30}$$

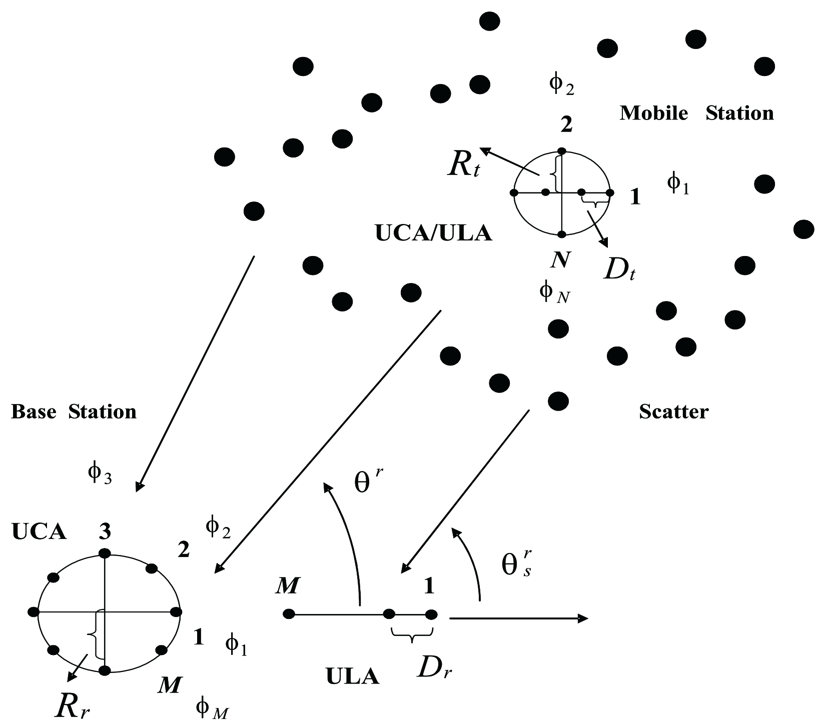

Figure 2.11: (M, N) MIMO system in mobile radio communications.

where the superscript d and u denote the downlink and uplink respectively, Γ_l is the relative average received power for lth resolvable path. Since L resolvable multipath are generally modeled as L independent paths, we can model each resolvable path independently. For simplicity, we consider the case of a flat fading channel ($L = 1$, $\Gamma_1 = 1$, and $\tau_1 = 0$). That is, $h^d_{m,p}(t;\tau)$ in (2.29) reduces to $h^d_{m,p}(t)$, which can be expressed as a function of antenna spacing, Doppler frequency, and angle-of-arrival as

$$h^d_{m,p}(t) = \sum_{s=1}^{L_s} \frac{1}{\sqrt{L_s}} v^r_p(\theta^r_s) v^t_m(\theta^t_s) e^{j\left[2\pi F_d \cos(\Psi^d_s)t + \phi_s\right]}, \tag{2.31}$$

where L_s is the number of scatterer, ϕ_s is uniformly distributed random phases over [0, 2π], F_d is the maximum Doppler frequency due to mobility, $v^r_p(\theta^r_s)$ is the array response for pth transmitting antenna and sth scatterer path at a base station, $v^t_m(\theta^t_s)$ is the array response for mth receiving antenna and sth scatterer path at a mobile station, Ψ^d_s are random angles-of-arrival relative to the motion of the mobile and is determined by θ^t_s. $h^d_{m,p}(t)$ becomes a complex Gaussian random process as the number of scatterers L_s is becomes large. Note that the superscript r denote the base station while the superscript t denote the base station. Both $v_p^r(\theta_s^r)$ and $v_m^t(\theta_s^t)$ for ULA can be expressed as follows

$$v_p^r(\theta_s^r) = e^{-j2\pi\frac{D_r}{\lambda}(p-1)\sin(\pi/2-\theta_s^r)}, \tag{2.32}$$

$$v_m^t(\theta_s^t) = e^{-j2\pi\frac{D_t}{\lambda}(m-1)\sin(\pi/2-\theta_s^t)}, \tag{2.33}$$

where D_r and D_t is the antenna element spacing between two elements at a base station and a mobile station, respectively. For a UCA, $v_p^r(\theta_s^r)$ and $v_m^t(\theta_s^t)$ can be expressed as follows

$$v_p^r(\theta_s^r) = e^{-j2\pi\frac{R_r}{\lambda}\sin(\varsigma)\cos(\theta_s^r-\phi_p)}, \tag{2.34}$$

$$v_m^t(\theta_s^t) = e^{-j2\pi\frac{R_t}{\lambda}\sin(\varsigma)\cos(\theta_s^t-\phi_m)}, \tag{2.35}$$

where R_r and R_t are the circular radius of the antenna array for a base station and a mobile station, respectively. ς is the elevation angle, and λ is the wavelength of carrier. For simplicity, only azimuth angles are considered in the propagation geometry ($\varsigma = 90°$), but the results can be generalized to three dimensions. ϕ_m is the phase excitation of mth element in azimuth plane, as shown in Figure 2.11. For the sth scatterering path on the downlink, θ_s^r is the angle-of-departure (AOD) at a mobile access point (base station) and θ_s^t is the angle-of-arrival (AOA) at a mobile station. Both θ_s^t and θ_s^r are random variables. θ_s^t is assumed uniformly distributed over $[0,\ 2\pi]$. A uniform distribution for θ_s^t is expressed as

$$f(\theta_s^t) = \begin{cases} \frac{1}{2\pi} & : \quad -\pi \leq \theta_s^t \leq \pi \\ 0 & : \quad \text{otherwise}\ , \end{cases} \tag{2.36}$$

and three θ_s^r (AOA) distributions are considered: uniform, truncated Gaussian, and truncated Laplacian. A uniform AOA distribution for θ_s^r is expressed as

$$f(\theta_s^r) = \begin{cases} \frac{1}{2\Delta} & : \quad -\Delta + \theta^r \leq \theta_s^r \leq \Delta + \theta^r \\ 0 & : \quad \text{otherwise}\ , \end{cases} \tag{2.37}$$

where 2Δ is the range of the angle distribution. θ_r is the central AOD for the downlink and the central AOA for the uplink. A truncated Gaussian distribution for θ_s^r is expressed as

$$f(\theta_s^r) = C_g e^{-\frac{(\theta_s^r - \theta^r)^2}{2\sigma_a}} \quad , \quad -\pi + \theta^r \leq \theta_s^r \leq \pi + \theta^r, \tag{2.38}$$

where C_g is a normalizing constant chosen to make $f(\theta_s^r)$ a density function and can be shown to be

$$C_g = \frac{1}{\sqrt{2\pi}\sigma_a \operatorname{erf}\left(\frac{\pi}{\sqrt{2}\sigma_a}\right)}, \tag{2.39}$$

where erf(x) is the error function and is defined as

$$\operatorname{erf}(x) = \int_0^x e^{-t^2}\, dt, \tag{2.40}$$

and σ_a is a parameter of the distribution closely related to angle spread. A truncated Laplacian AOA distribution is also considered in this paper and is given by

$$f(\theta_s^r) = C_l e^{-a|\theta_s^r - \theta^r|} \quad , \quad -\pi + \theta^r \leq \theta_s^r \leq \pi + \theta^r \ , \tag{2.41}$$

where C_l is a normalizing constant chosen to make $f(\theta_s^r)$ a density function and can be shown to be

$$C_l = \frac{a}{2(1 - e^{-a\pi})}, \tag{2.42}$$

and a is a positive decaying factor which is related to the angle spread. Specifically, as a increases, the angle spread decreases. Note that the angle spread σ is the standard deviation of each of the distributions and is defined as $\sigma = \left\{\frac{\Delta}{\sqrt{3}}, \sigma_g C_g, \frac{2}{a^2} - \frac{2ae^{-a\pi}}{1-e^{-a\pi}}\left(\frac{\pi^2 a + 2\pi}{a^2}\right)\right\}$ for a uniform, truncated Gaussian, and truncated Laplacian distribution respectively.

Similarly, for uplink communication, $h_{p,m}^u(t)$ can be expressed as

$$h_{m,p}^u(t) = \sum_{s=1}^{L_s} \frac{1}{\sqrt{L_s}} v_p^t(\theta_s^r) v_m^r(\theta_s^t) e^{j(2\pi F_d \cos(\Psi_s^u)t + \phi_s)}, \tag{2.43}$$

where $v_p^t(\theta_s^t)$ is the array response for pth transmitting antenna and the sth scatterer path at a mobile station and $v_m^r(\theta_s^r)$ is the array response for mth receiving antenna and sth scatterer at a mobile access point. For a ULA both $v_p^r(\theta_s^r)$ and $v_m^t(\theta_s^t)$ can be expressed as

$$v_p^t(\theta_s^t) = e^{-j2\pi\frac{D_t}{\lambda}(p-1)\sin(\pi/2 - \theta_s^t)}, \tag{2.44}$$

$$v_m^r(\theta_s^r) = e^{-j2\pi \frac{D_r}{\lambda}(m-1)\sin(\pi/2-\theta_s^r)}, \tag{2.45}$$

where D_r and D_t are the antenna element spacing between two elements at the base station and the mobile station, respectively. For a UCA, $v_p^t(\theta_s^r)$ and $v_m^r(\theta_s^t)$ can be expressed as

$$v_p^t(\theta_s^t) = e^{-j2\pi \frac{R_t}{\lambda}\sin(\varsigma)\cos(\theta_s^t-\phi_p)}, \tag{2.46}$$

$$v_m^r(\theta_s^r) = e^{-j2\pi \frac{R_r}{\lambda}\sin(\varsigma)\cos(\theta_s^r-\phi_m)}. \tag{2.47}$$

For the sth scatterer path on uplink communications, θ_s^t is the angle-of-departure (AOD) at the mobile station and θ_s^r is the angle-of-arrival (AOA) at a base station. Note that Ψ_s^u is the random angle of departure relative to the motion of the mobile for each scatterer and is determined by θ_s^t.

2.7 Summary

In this chapter, we reviewed the characteristics of multipath channel models for wireless environments. We compared geometrically based vector channel models with statistically based vector channel models. We described a statistical-based vector channel model for uniform linear arrays and uniform circular arrays. Finally, we developed the statistical multipath MIMO channel model to be used in our research.

Chapter 3

Space-Time Fading Correlation of MIMO Channels

In this chapter, we derive an analytical expression for the space-time fading correlation function of a MIMO (multiple transmit and multiple receive antennas) channel in a mobile cellular environment. Specifically, we find the space-time correlation between any two links, where a link is defined as a transmit-receive antenna pair. The space-time fading correlation is dependent on the temporal fading correlation and the spatial fading correlation. The temporal fading correlation is a function of the Doppler spread and time delay while the spatial fading correlation is a function of the angle spread and distance between elements (the latter being dependent on the array geometry). This chapter is organized as follows. In Section 3.1, we briefly discuss the usefulness of space-time fading correlation to the analysis of wireless communications. In Section 3.2, we review a statistical channel model for a (4,4) MIMO antenna array system. In Section 3.3, we derive an expression for the space-time fading correlation function for a MIMO system using both UCA and ULA antenna arrays. In Section 3.4, we evaluate the impact of AOA energy distribution on the spatial fading correlation function for both UCA and ULA systems. In Section 3.5, we plot the space-time fading as a function of the

Doppler spread, angle spread, antenna element spacing for a typical scenario. Computer simulations are carried out to verify the analytical results. Finally, concluding remarks are given in Section 3.6.

3.1 Introduction

To assess the performance of space-time processing algorithms, it is important to understand space-time correlation. In this chapter, we derive an analytical space-time fading correlation for the MIMO channel as function of antenna spacing, angle spread, and Doppler spread. Both the UCA and ULA are considered for MIMO systems. The analytical space-time fading function derived here can be used for diversity combining analysis as well as for estimating the information-theoretic channel capacity of MIMO systems. The information-theoretic channel capacity of MIMO systems will be discussed in Chapter 4 and the diversity combining analysis of MIMO systems will be evaluated in Chapter 7.

3.2 Space-Time MIMO Channel Model

We assume a 4-element transmit and receive array in a mobile cellular environment, as shown in Figure 3.1. For simplicity, we consider the case of a flat fading channel. Based on the MIMO channel model developed in Section 2.6, the multipath channel impulse response for the pth transmit antenna at the mth receive antenna element can be expressed as a function of antenna element spacing, Doppler frequency, and angle-of-arrival (AOA). The multipath MIMO channel impulse response for the downlink and uplink channels can be expressed as (2.31) and (2.43) respectively. The array responses used in (2.31) and (2.43) for a ULA and a UCA are also defined in Section 2.6. In the temporal domain of the MIMO channel model, a conventional U-shape Doppler

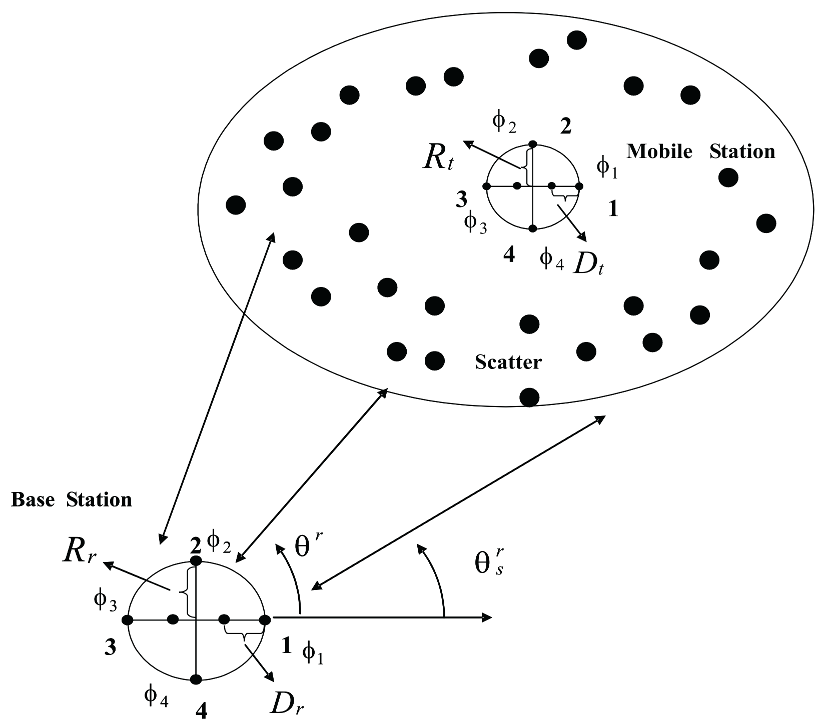

Figure 3.1: 4-element UCA-ULA MIMO system in mobile radio communications.

spectrum is observed at the mobile station based on the MIMO channel model developed in Chapter 2. In the spatial domain of the MIMO channel model, we consider three different AOA distributions at the base station antenna array for the spatial fading correlation: uniform, truncated Gaussian, and truncated Laplacian distributions. The probability density function these three distributions are described in Chapter 2.

3.3 Space-Time Fading Correlation

The space-time fading correlation consists of the temporal fading correlation and the spatial fading correlation. The space-time correlation function $\rho_{st}(\nu, mp, m'p')$ between two channels $h_{m,p}$ and $h_{m',p'}$ for a MIMO channel can be defined as

$$\rho_{st}(\nu, mp, m'p') = E\{h_{m,p}(t)h^*_{m',p'}(t+\nu)\}, \tag{3.1}$$

where $h_{m,p}(t)$ is the multipath channel impulse response for the pth transmit antenna at the mth receive antenna element, as defined in Section 2.6. Since $h_{m,p}(t)$ is function of angle spread (spatial domain) and Doppler spread (temporal domain), we can further express $\rho_{st}(\nu, mp, m'p')$ as

$$\begin{aligned}\rho_{st}(\nu, mp, m'p') &= E\{\beta(t)\beta(t+\nu)^*\}E\{v_p(\zeta^p)v_m(\zeta^m)v_{p'}^*(\zeta^p)v_{m'}(\zeta^m)^*\} \\ &= \mathrm{R}_t(\nu)\mathrm{R}_s(mp, m'p'), \end{aligned} \tag{3.2}$$

where the superscript $(\cdot)^*$ denotes the complex conjugate, ζ^p is the angle of departure, ζ^m is the angle-of-arrival,

$$\beta(t) = \sum_{s=1}^{L_s} \frac{1}{\sqrt{L_s}} e^{j(2\pi F_d \cos(\Psi_s)t + \phi_s)}, \tag{3.3}$$

$\mathrm{R}_t(\nu)$ is the temporal fading correlation for delay ν, and $\mathrm{R}_s(mp, m'p')$ is the spatial fading correlation. $\mathrm{R}_t(\nu)$ is defined as

$$\mathrm{R}_t(\nu) = E\{\beta(t)\beta(t+\nu)^*\} \tag{3.4}$$

When L_s is large, $\mathrm{R}_t(\nu)$ can be expressed as

$$\mathrm{R}_t(\nu) = \frac{1}{2\pi}\int_0^{2\pi} e^{j[2\pi F_d \cos(\Psi)\nu]}\, d\Psi \tag{3.5}$$

It is shown in [1][30], $\mathrm{R}_t(\nu)$ can be expressed as

$$\mathrm{R}_t(\nu) = J_0(2\pi F_d\, \nu), \tag{3.6}$$

where $J_n(\cdot)$ is a Bessel function of the first kind of order n. Thus, the space-time correlation $\rho_{st}(\nu)$ can be rewritten as

$$\rho_{st}(\nu, mp, m'p') = J_0(2\pi F_d\, \nu)\mathrm{R}_s(mp, m'p'), \tag{3.7}$$

where $\mathrm{R}_s(mp, m'p')$ is the spatial correlation between two channels $h_{m,p}$ and $h_{m',p'}$ and is defined as

$$\begin{aligned}\mathrm{R}_s(mp, m'p') &= E\{v_p(\zeta^p)v_m(\zeta^m)v_{p'}^*(\zeta^p)v_{m'}(\zeta^m)^*\} \\ &= \int_{\zeta^p}\int_{\zeta^m} v_p(\zeta^p)v_m(\zeta^m)v_{p'}^*(\zeta^p)v_{m'}^*(\zeta^m)f(\zeta^p, \zeta^m)d\,\zeta^m d\,\zeta^p, \end{aligned} \tag{3.8}$$

where $f(\zeta^p, \zeta^m)$ is the joint probability density function of AOD and AOA. Since ζ^p and ζ^m are statistically independent, we can rewrite (3.8) as

$$\begin{aligned}\mathrm{R}_s(mp, m'p') &= \int_{\zeta^p} v_p(\zeta^p) v^*_{p'}(\zeta^p) f(\zeta^p) d\,\zeta^p \int_{\zeta^m} v_m(\zeta^m) v^*_{m'}(\zeta^m) f(\zeta^m) d\,\zeta^m, \\ &= \mathrm{R}_s(p, p')\mathrm{R}_s(m, m'), \end{aligned} \tag{3.9}$$

where $f(\zeta^p)$ is the probability density function of AOD and $f(\zeta^m)$ is the probability density function of AOA. $\mathrm{R}_s(p, p')$ is the spatial correlation due to the transmit antennas and is expressed as

$$\mathrm{R}_s(p, p') = \int_{\zeta^p} v_p(\zeta^p) v^*_{p'}(\zeta^p) f(\zeta^p) d\,\zeta^p \tag{3.10}$$

and $\mathrm{R}_s(m, m')$ is the spatial correlation due to the receive antennas and is expressed as

$$\mathrm{R}_s(m, m') = \int_{\zeta^m} v_m(\zeta^m) v^*_{m'}(\zeta^m) f(\zeta^m) d\,\zeta^m \tag{3.11}$$

In the following sections, we derive the space-time correlation functions for downlink and uplink MIMO channels assuming both a ULA and a UCA.

3.3.1 Downlink Spatial Correlation

Using (3.7), (3.10), and (3.11) the space-time correlation $\rho_{st}(\nu, mp, m'p')$ for downlink communications can be written as

$$\rho_{st}(\nu, mp, m'p')^d = J_0(2\pi F_d\, \nu)\mathrm{R}_s(mp, m'p')^d. \tag{3.12}$$

where

$$\mathrm{R}_s(mp, m'p')^d = \mathrm{R}_s(p, p')^d \mathrm{R}_s(m, m')^d, \tag{3.13}$$

where

$$\mathrm{R}_s(p, p')^d = \int_{\zeta^r} v^r_p(\zeta^r) v^{r,*}_{p'}(\zeta^r) f(\zeta^r) d\,\zeta^r \tag{3.14}$$

$$\mathrm{R}_s(m, m')^d = \int_{\zeta^t} v^t_m(\zeta^t) v^{t,*}_{m'}(\zeta^t) f(\zeta^t) d\,\zeta^t, \tag{3.15}$$

where $v_p^r(\zeta^r)$, $v_m^t(\zeta^t)$, $f(\zeta^r)$, and $f(\zeta^t)$ are defined in Section 2.6. In Appendix A, it is shown that the real and imaginary parts of $\mathrm{R}_s(p,p')^d$ for a UCA with θ_s^r uniformly distributed can be expressed as

$$\mathrm{Re}\{\mathrm{R}_s(p,p')^d\} = J_0(Z_c^r) + 2\sum_{k=1}^{\infty} J_{2k}(Z_c^r)\cos(2k(\theta^r+\alpha^r))\mathrm{sinc}(2k\Delta), \tag{3.16}$$

$$\mathrm{Im}\{\mathrm{R}_s(p,p')^d\} = 2\sum_{k=0}^{\infty} J_{2k+1}(Z_c^r)\sin((2k+1)(\theta^r+\alpha^r))\mathrm{sinc}((2k+1)\Delta), \tag{3.17}$$

where $\mathrm{sinc}(x)$ is defined as

$$\mathrm{sinc}(x) = \frac{\sin(x)}{x}. \tag{3.18}$$

In Appendix B, it is shown that the real and imaginary parts of $\mathrm{R}_s(p,p')^d$ for a UCA with θ_s^r truncated Gaussian distributed can be expressed as

$$\mathrm{Re}\{\mathrm{R}_s(p,p')^d\} = J_0(Z_c^r) + 2\sqrt{2\pi}C_g\sigma_a\sum_{k=1}^{\infty} e^{-2k^2\sigma_a^2} J_{2k}(Z_c^r)\cos[2k(\theta^r+\alpha^r)], \tag{3.19}$$

$$\mathrm{Im}\{\mathrm{R}_s(p,p')^d\} = 2\sqrt{2\pi}C_g\sigma_a\sum_{k=0}^{\infty} e^{\frac{-(2k+1)^2\sigma_a^2}{2}} J_{2k+1}(Z_c^r)\sin[(2k+1)(\theta^r+\alpha^r)]. \tag{3.20}$$

In Appendix C, it is shown that the real and imaginary parts of $\mathrm{R}_s(p,p')^d$ for a UCA with θ_s^r truncated Laplacian distributed can be expressed as

$$\mathrm{Re}\{\mathrm{R}_s(p,p')^d\} = J_0(Z_c^r) + 4C_l\sum_{k=1}^{\infty} \frac{a^2(1-e^{-a\pi})}{a^2+4k^2} J_{2k}(Z_c^r)\cos[2k(\theta^r+\alpha^r)], \tag{3.21}$$

$$\mathrm{Im}\{\mathrm{R}_s(p,p')^d\} = 4C_l\sum_{k=0}^{\infty} \frac{a(1+e^{-a\pi})}{a^2+(2k+1)^2} J_{2k+1}(Z_c^r)\sin[(2k+1)(\theta^r+\alpha^r)], \tag{3.22}$$

where Z_c^r is related to the antenna spacing and α^r is the relative angle between the pth and p'th antenna element, as defined in the appendix. $J_n(x)$ is an nth order Bessel function of the first kind. C_g, C_l, a, and σ_a are related to angle spread, as defined in Chapter 2.

In [54], it is shown that the real and imaginary parts of $\mathrm{R}_s(p,p')^d$ for a ULA with θ_s^r uniformly distributed can be expressed as

$$\mathrm{Re}\{\mathrm{R}_s(p,p')^d\} = J_0(Z_l^r) + 2\sum_{k=1}^{\infty} J_{2k}(Z_l^r)\cos(2k(\theta^r))\mathrm{sinc}(2k\Delta), \tag{3.23}$$

$$\mathrm{Im}\{\mathrm{R}_s(p,p')^d\} = 2\sum_{k=0}^{\infty} J_{2k+1}(Z_l^r)\sin((2k+1)(\theta^r))\mathrm{sinc}((2k+1)\Delta). \tag{3.24}$$

In Appendix D, it is shown that the real and imaginary parts of $\mathrm{R}_s(p,p')^d$ for a ULA with θ_s^r truncated Gaussian distributed can be expressed as

$$\mathrm{Re}\{\mathrm{R}_s(p,p')^d\} = J_0(Z_l^r) + 2\sqrt{2\pi}C_g\sigma_a\sum_{k=1}^{\infty} e^{-2k^2\sigma_a^2} J_{2k}(Z_l^r)\cos[2k(\theta^r)], \tag{3.25}$$

$$\mathrm{Im}\{\mathrm{R}_s(p,p')^d\} = 2\sqrt{2\pi}C_g\sigma_a\sum_{k=0}^{\infty} e^{\frac{-(2k+1)^2\sigma_a^2}{2}} J_{2k+1}(Z_l^r)\sin[(2k+1)(\theta^r)]. \tag{3.26}$$

In Appendix E, it is shown that the real and imaginary parts of $\mathrm{R}_s(p,p')^d$ for a ULA with θ_s^r truncated Laplacian distributed can be expressed as

$$\mathrm{Re}\{\mathrm{R}_s(p,p')^d\} = J_0(Z_l^r) + 4C_l\sum_{k=1}^{\infty}\frac{a^2(1-e^{-a\pi})}{a^2+4k^2} J_{2k}(Z_l^r)\cos[2k(\theta^r)], \tag{3.27}$$

$$\mathrm{Im}\{\mathrm{R}_s(p,p')^d\} = 4C_l\sum_{k=0}^{\infty}\frac{a(1+e^{-a\pi})}{a^2+(2k+1)^2} J_{2k+1}(Z_l^r)\sin[(2k+1)(\theta^r)], \tag{3.28}$$

where Z_l^r is a function of D_r and λ as shown in the Appendix D.

In [55], it is shown that $\mathrm{R}_s(m,m')^d$ with θ_s^t uniformly distributed over $[0, 2\pi]$ for a UCA can be expressed as

$$\mathrm{R}_s(m,m')^d = J_0(Z_c^t), \tag{3.29}$$

where

$$Z_c^t = \sqrt{K_{1,t}^2 + K_{2,t}^2}, \tag{3.30}$$

and

$$K_{1,t} = 2\pi\frac{R_t}{\lambda}[cos(\phi_m) - \cos(\phi_{m'})], \tag{3.31}$$

$$K_{2,t} = 2\pi\frac{R_t}{\lambda}[sin(\phi_m) - \sin(\phi_{m'})]. \tag{3.32}$$

In [54], it is shown that $\mathrm{R}_s(m,m')^d$ with θ_s^t uniformly distributed over $[0, 2\pi]$ for a ULA can be expressed as

$$\mathrm{R}_s(m,m')^d = J_0(Z_l^t), \tag{3.33}$$

where

$$Z_l^t = 2\pi\frac{(m-m')D_t}{\lambda}. \tag{3.34}$$

3.3.2 Uplink Spatial Correlation

Using (3.7), (3.10), and (3.11) the space-time correlation $\rho_{st}(\nu, mp, m'p')$ for uplink communications can be written as

$$\rho_{st}(\nu, mp, m'p')^u = J_0(2\pi F_d \nu)\mathrm{R}_s(mp, m'p')^u, \tag{3.35}$$

where

$$\mathrm{R}_s(mp, m'p')^u = \mathrm{R}_s(p, p')^u \mathrm{R}_s(m, m')^u, \tag{3.36}$$

and

$$\mathrm{R}_s(p, p')^u = \int_{\zeta^r} v_p^t(\zeta^r) v_{p'}^{t,*}(\zeta^r) f(\zeta^r) d\,\zeta^r, \tag{3.37}$$

$$\mathrm{R}_s(m, m')^u = \int_{\zeta^t} v_m^r(\zeta^t) v_{m'}^{r,*}(\zeta^t) f(\zeta^t) d\,\zeta^t, \tag{3.38}$$

where $v_p^t(\zeta^t)$ and $v_m^r(\zeta^r)$ are defined in Section 2.6. Due to reciprocity of uplink and downlink communications, $\mathrm{R}_s(p, p')^u$ and $\mathrm{R}_s(m, m')^u$ can be expressed directly by $\mathrm{R}_s(m, m')^d$ and $\mathrm{R}_s(p, p')^d$ with exchange of p with m. That is

$$\mathrm{R}_s(p, p')^u = \mathrm{R}_s(m, m')^d, \tag{3.39}$$

$$\mathrm{R}_s(m, m')^u = \mathrm{R}_s(p, p')^d. \tag{3.40}$$

3.4 Impact of AOA Energy Distribution on Spatial Correlation

In this section, we evaluate the impact of the three AOA distributions on the spatial correlation functions for both a ULA and a UCA. Without loss of generality, we consider uplink communications only. In order to fairly compare the spatial correlation, we set the angle spread or the distribution standard deviation for three AOA distribution to be identical. Three angle spreads are evaluated: $\sigma = 1°$, $\sigma = 5°$, $\sigma = 20°$. Note that for the uniform distribution, $\sigma = \frac{\Delta}{\sqrt{3}}$, while for the truncated Gaussian distribution $\sigma = C_g \sigma_a$.

Finally, for the truncated Laplacian distribution, $\sigma = \frac{2}{a^2} - \frac{2ae^{-a\pi}}{1-e^{-a\pi}}\left(\frac{\pi^2 a+2\pi}{a^2}\right)$. The three values of angle spread ($\sigma = \{1°, 5°, 20°\}$) represent small angle spread, moderate angle spread, and large angle spread.

For a UCA, Figure 3.2 shows the spatial fading correlation for $|\mathrm{R}_s(21, 11)^u|$ with three AOA distributions at the mean AOA $\theta = 0°$ and for various σ. Note that $|\mathrm{R}_s(ab, cd)^u|$ is the uplink spatial correlation between the link from transmit antenna b to receive antenna a and the link from transmit antenna d and receive antenna c. As shown, the spatial fading correlation decreases as antenna spacing and/or the angle spread σ increases. Note that the antenna element spacing R is equal to R_r for uplink communications, as shown in Figure 3.2. Results also show that the three AOA distributions give similar spatial fading correlation for the same angle spread. The correlation at low angle spreads is identical to a radius of 5λ, while moderate and high angle spreads show similar correlation down to approximately 0.5. Below this value, the correlation functions begin to differ significantly. However, it should be noted that when considering diversity performance, there is little difference between two antennas which have a correlation of 0.5 and two antennas which have a correlation of zero. Thus, while the correlation functions differ significantly below 0.5, if we are interested in BER performance, the exact AOA distribution may not matter, as the variance will dominate performance. Also note that the Laplacian distribution provides the strongest correlation while the uniform distribution provides the weakest correlation. This makes sense since for the same variance the Laplacian distribution will have more energy concentrated about the mean AOA than a uniform distribution. For example, a Laplacian distribution with a variance of 5° will have 50% of its energy within ±2° of the center AOA. By contrast, a uniform distribution with the same variance will have 50% of its energy within ±5° of the center AOA.

To see this more clearly, let's examine the correlation functions given in equations (3.16) to (3.22). Note that there are three main components in each term of the summations. The first component is related to the angle spread. For the uniform distribution, it is the sinc$(k\Delta)$. For the Gaussian distribution it is $e^{-k\sigma_g^2}$ and for the Laplacian distribution it is the term $\frac{C_l(1-e^{-a\pi})}{a}$. In each of these instances, large angle spreads will decrease the correlation while small angle spread will increase the correlation. The second component in each summation is related to the distance between elements. In each of the three distributions, there is a term $J_{2k}(Z_c^r)$ (and $J_{2k+1}(Z_c^r)$). It can be demonstrated that Z_c^r is merely the distance between elements (see Appendix A). Thus, as Z_c^r increases the correlation decreases since $J_{2k}(Z_c^r)$ decreases. Thus, as in the case of linear arrays, correlation is inversely related to angle spread and distance. The third component of the correlation sums contains the terms $\cos 2k(\theta^r + \alpha^r)$ or $\sin{(2k+1)(\theta^r + \alpha^r)}$. These terms relate the geometry of the two elements considered to the central angle of arrival. It can be shown that $\alpha^r = \tan^{-1}\left(\frac{\Delta x}{\Delta y}\right)$, where Δx and Δy are the position differences between the two elements under consideration in cartesian co-ordinates. Thus, if two elements have the same x co-ordinate $\alpha^r = 0$ and if two elements have the same y co-ordinate $\alpha^r = \frac{\pi}{2}$. It can be shown that when $\alpha^r - \theta^r = k\pi$ for integer k the correlation is the lowest, whereas when $\alpha^r + \theta^r = k\pi + \frac{\pi}{2}$ the correlation is the highest. Thus, when the central AOA is perpendicular to the line which connects the two elements, the correlation is the lowest. By contrast when the central AOA is parallel to the line connecting the two elements the correlation is the highest.

For a ULA, Figure 3.3 shows the spatial fading correlation for $|\mathrm{R}_s(21, 11)^u|$ with three AOA distributions at the mean AOA $\theta = 90°$ and for various σ. Similar results to the case of UCA is observed. The correlation at low angle spreads is identical to a radius of 5λ, while moderate and high angle spreads show similar correlation down to approximately 0.5. Below this value, the correlation functions begin to differ significantly. Note that the antenna element spacing D is equal to D_r for uplink communications, as shown in Figure 3.3. The results suggest that from a BER performance perspective, the angle spread dominates the correlation between elements, rather than the exact AOA energy distribution.

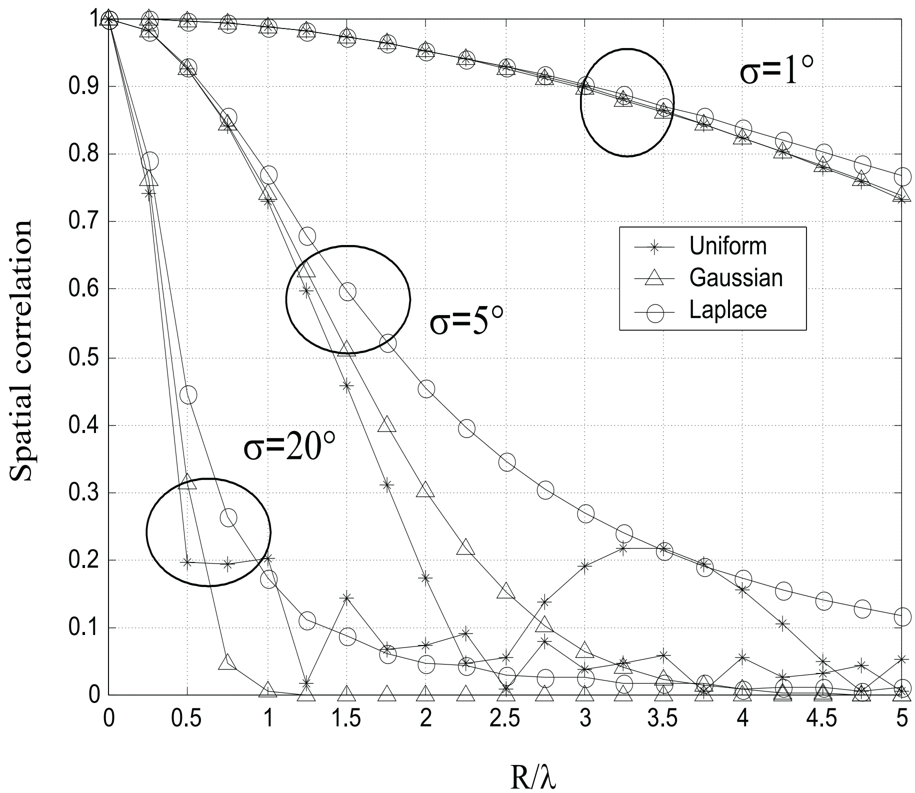

Figure 3.2: Comparative spatial fading correlation for UCA with three AOA distributions and $\theta^r = 45^\circ$ $(R = R_r)$

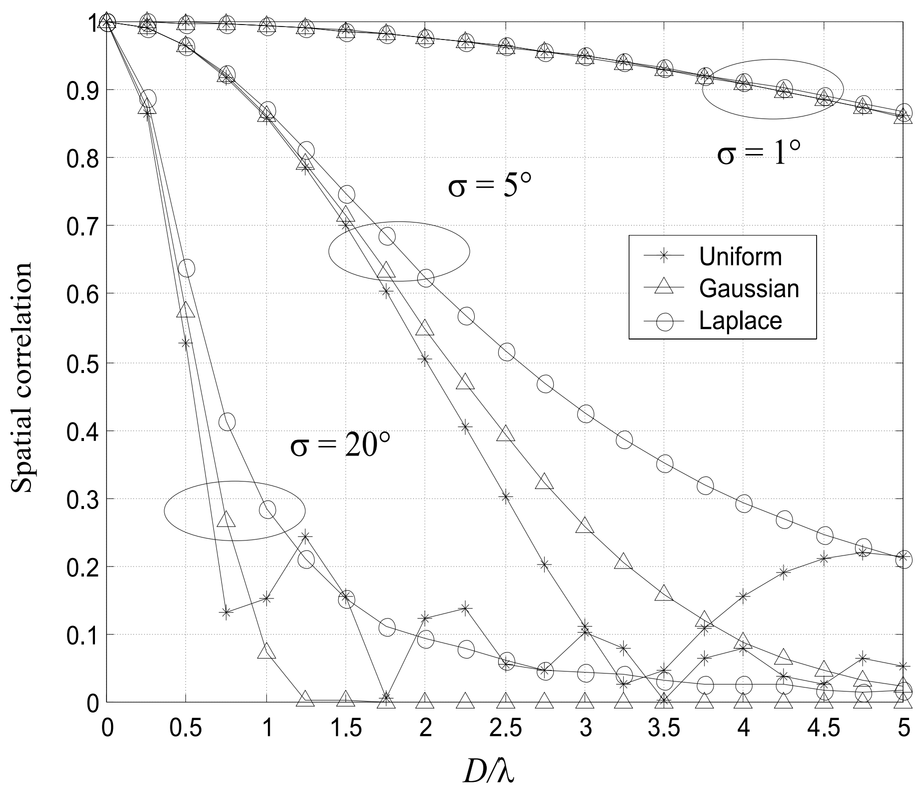

Figure 3.3: Spatial fading correlation for ULA with three AOA distributions at a mean AOA $\theta^r = 90^\circ$ and for various σ ($D = D_r$).

3.5 Results on MIMO Space-Time Correlation

In this section we present the temporal fading correlation and the analytical spatial fading correlation results based on the formulas derived in Section 3.3 and verify these analytical results through the use of computer simulations. Since it is suggested in Section 3.4 that the angle spread dominates the correlation between elements rather than the exact AOA energy distribution, we consider a truncated Gaussian AOA energy distribution for evaluating MIMO Space-Time Correlation in mobile radio channels.

3.5.1 Temporal Correlation

We first plot the temporal correlation which is consistent across all three fading distributions since it is for a single antenna. Figure 3.4 shows the temporal fading correlation as a function of delay ν for various Doppler frequencies F_d. As expected, the temporal fading correlation R_t decreases as the ν increases or as the Doppler frequency F_d increases. As a point of reference, the frame length in IS-95 based CDMA cellular systems in 20ms. Thus, for an interleaver to provide temporal diversity to the decoder, we desire the correlation to be below approximately 0.7 for a delay of about 10ms. This means that for fading rates above 100Hz, good temporal diversity is achieved through interleaving and convolutional coding.

3.5.2 Uplink Spatial Fading Correlation

For practical uplink applications, we consider an example of a ULA with two antenna elements (antennas 1 and 4 shown in Figure 3.1) at the mobile station and a UCA or a ULA with four antenna elements at the base station. Note that the numbering for ULA is from right to left. We fix the antenna spacing at the mobile station at 1.5λ and vary the antenna spacing at the base station. Figure 3.5 present the analytical

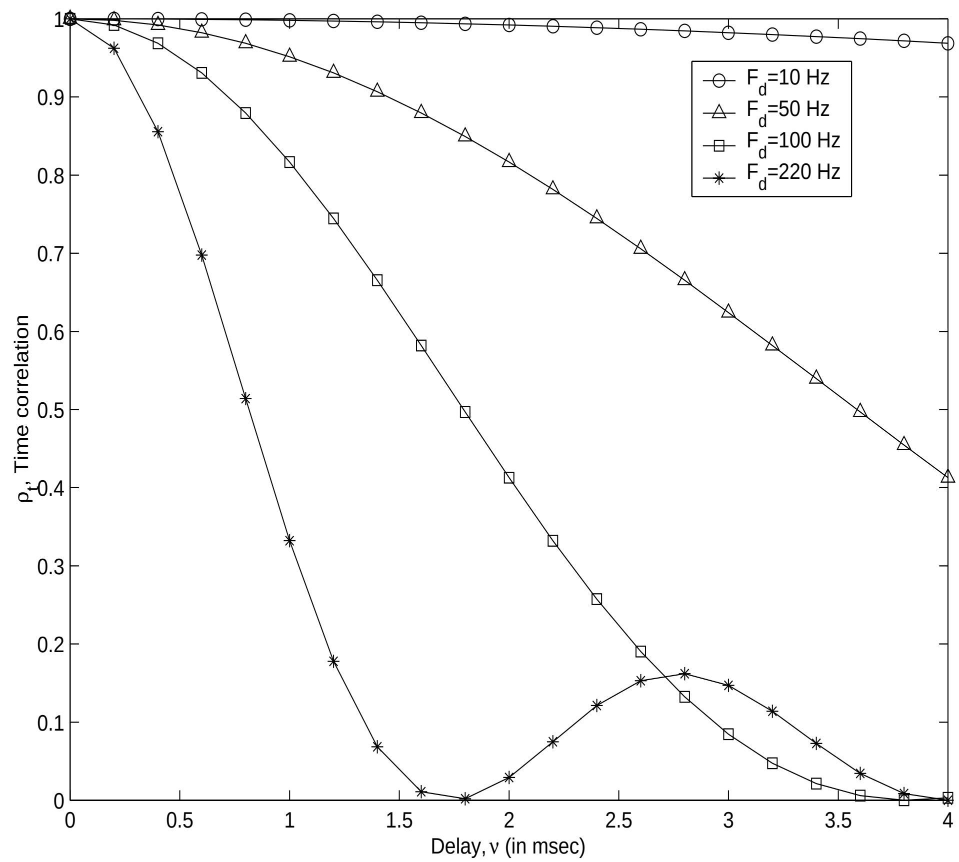

Figure 3.4: Temporal fading correlation vs. delays for various Doppler spread (F_d)

and simulation results of spatial fading correlation for $|\mathrm{R}_s(21,12)^u|$, $|\mathrm{R}_s(31,41)^u|$ and $|\mathrm{R}_s(41,32)^u|$ when the mean AOA $\theta^r = 90°$, $\sigma_a = 5°$ and a UCA is used at the access point. Again $|\mathrm{R}_s(ab,cd)^u|$ is the uplink spatial correlation between the link from transmit antenna b to receive antenna a and the link from transmit antenna d and receive antenna c. The simulation results exhibit good agreement with analytical results. Figure 3.6 presents the analytical and simulation results of spatial fading correlation for $|\mathrm{R}_s(21,12)^u|$, $|\mathrm{R}_s(31,41)^u|$ and $|\mathrm{R}_s(11,42)^u|$ when the mean AOA $\theta^r = 90°$ and $\sigma_a = 5°$ when a ULA is used at access point. As expected, the spatial correlation decreases as either R_r or D_r increase. Figures 3.7 presents analytical results for spatial fading correlation for $|\mathrm{R}_s(31,41)^u|$ for both the ULA and the UCA for various values of angle spread σ_a. It is shown that the spatial correlation decreases as σ_a increases and the ULA experiences high correlation for small values of θ^r (close to endfire), while the UCA experiences the lowest correlation at $\theta^r = 45°$ and the highest at $\theta^r = 0°$ and $\theta^r = 90°$. This is due to the fact that the correlation along lines perpendicular to the central AOA is lower than along lines parallel to the AOA. As compared to ULA, the UCA experiences lower correlation on average.

3.5.3 Downlink Spatial Fading Correlation

In this section we present the analytical spatial fading correlation results for practical downlink application. We consider an example of a ULA with two antenna elements (antenna 1 and 4 shown in Figure 3.1) at a base station and a ULA with four antenna elements at a mobile station. We fix the antenna spacing between two elements at a mobile station with 0.5λ and vary the antenna spacing at a base station. Figure 3.8 present the analytical and simulation results of spatial fading correlation for $|\mathrm{R}_s(21,12)^d|$, $|\mathrm{R}_s(31,41)^d|$ and $|\mathrm{R}_s(41,32)^d|$ when the mean AOD $\theta^r = 90°$ and $\sigma_a = 5°$. It is shown that the simulation results exhibit good agreement with analytical results.

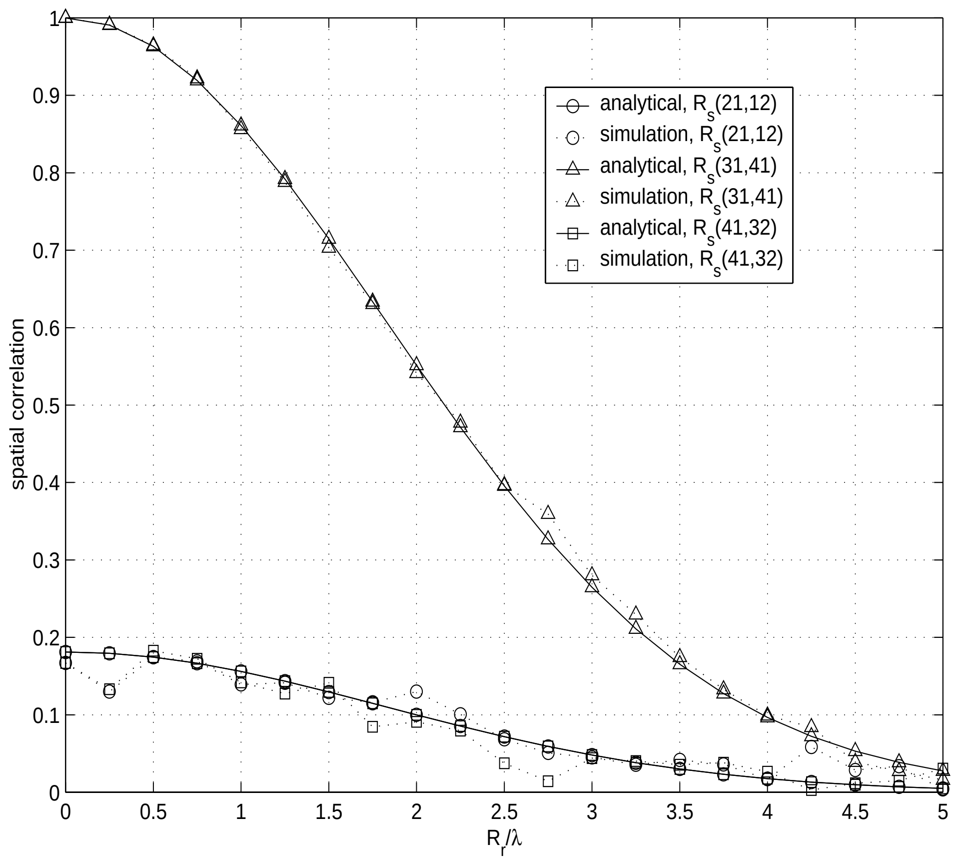

Figure 3.5: Analytical and simulation results of uplink spatial correlation for UCA used at a base station ($\theta_r = 90^\circ$ and $\sigma_a = 5^\circ$)

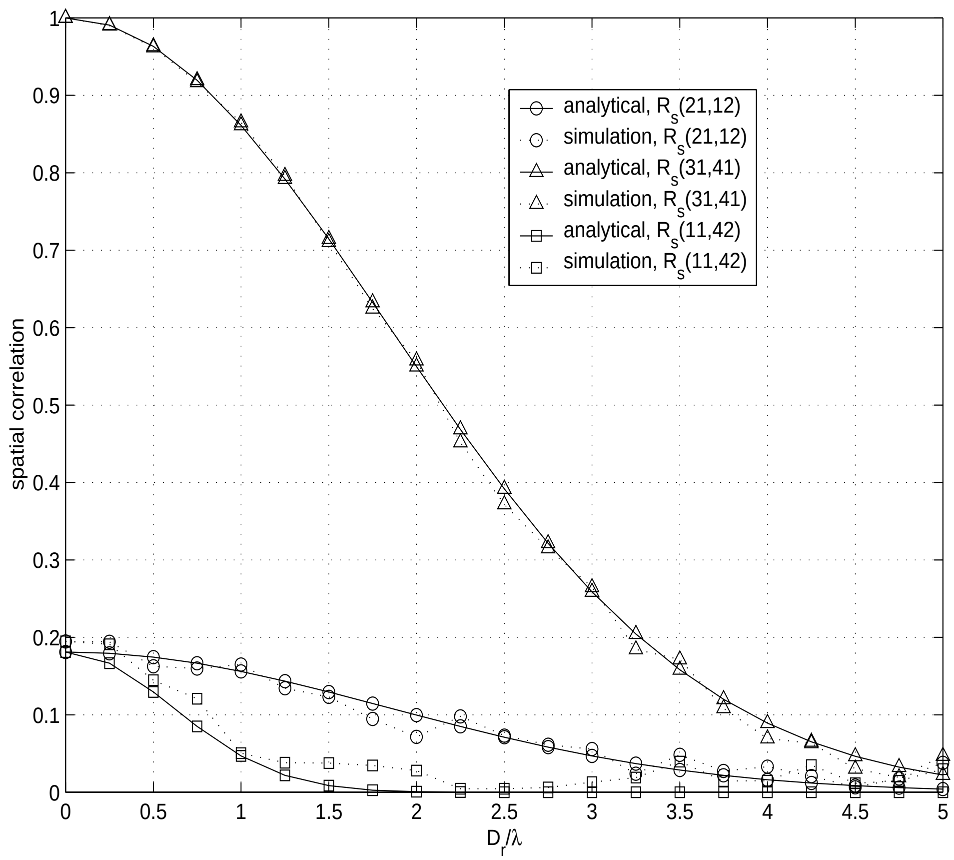

Figure 3.6: Analytical and simulation results of uplink spatial correlation for ULA used at a base station ($\theta_r = 90^\circ$ and $\sigma_a = 5^\circ$)

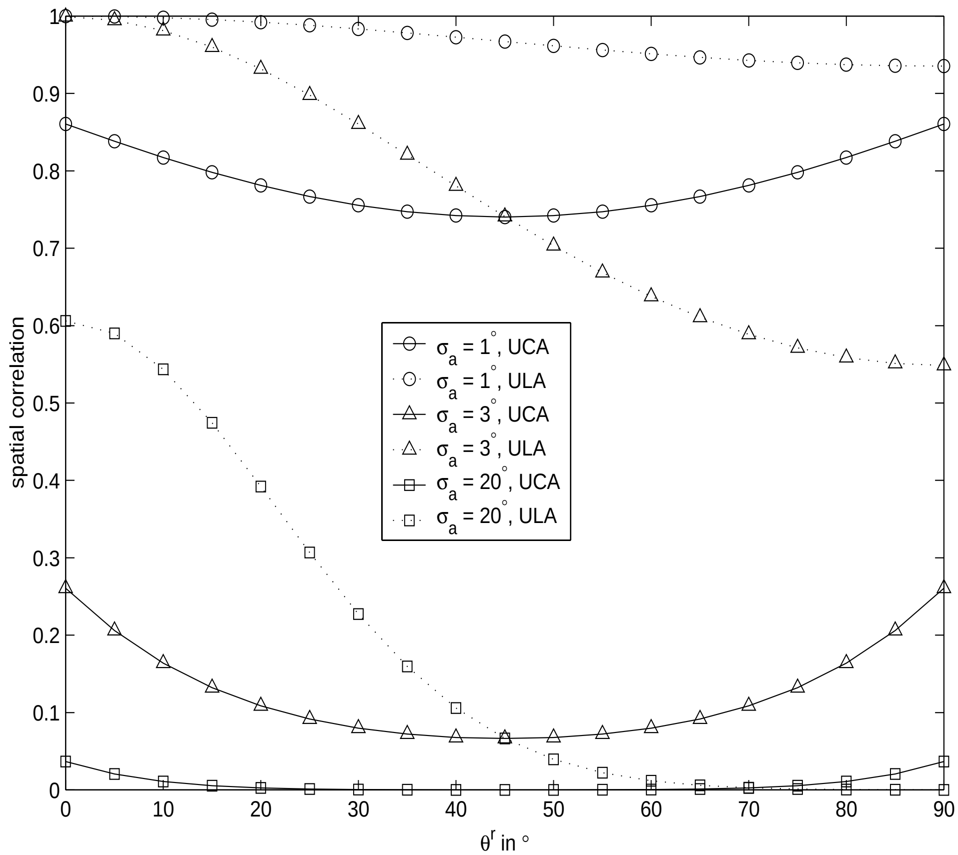

Figure 3.7: Analytical uplink spatial correlation as function of θ^r for various angle spread σ_a

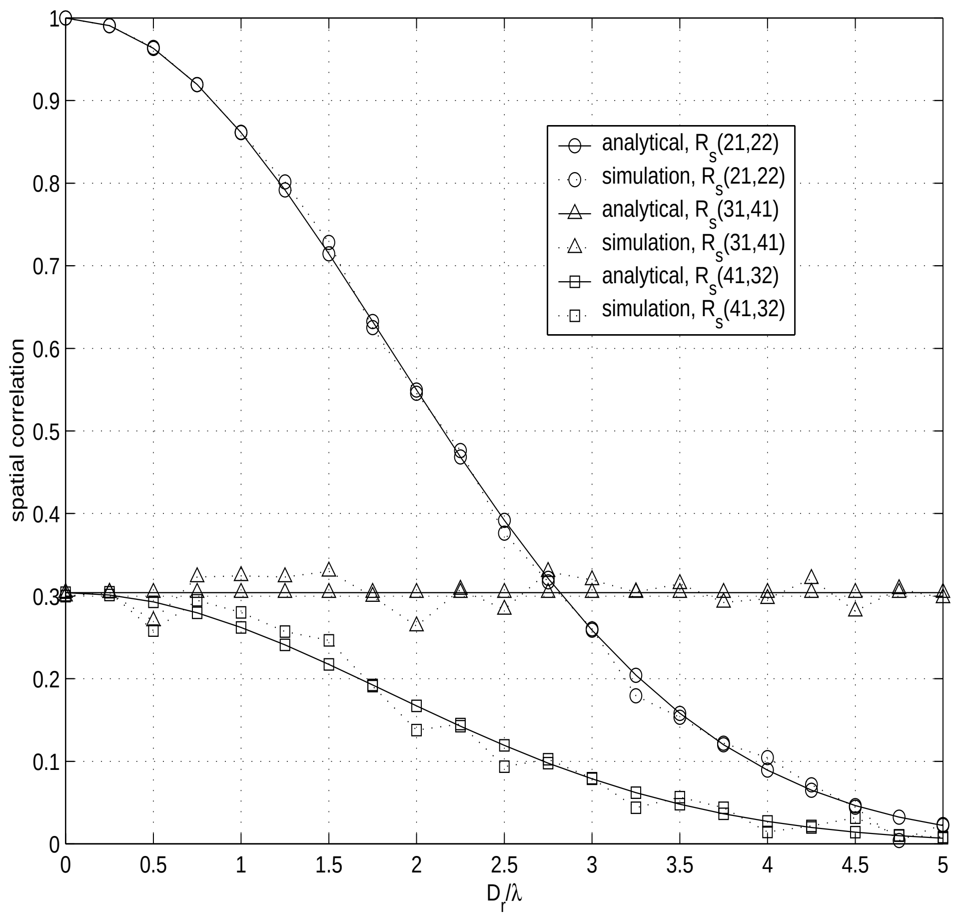

Figure 3.8: Analytical and simulation results of downlink spatial correlation for ULA used at a base station ($\theta_r = 90^\circ$ and $\sigma_a = 5^\circ$)

3.5.4 Space-Time Fading Correlation

Space-Time coding has become an very important research topic. To assess the performance of space-time processing algorithms, it is important to understand space-time correlation. For the application of most interest, we consider the example of two transmit antennas and two receive antennas. We present the downlink space-time fading correlation for various Doppler spread and angle spread. Figure 3.9 shows the space-time fading correlation as a function of Doppler spread F_d and angle spread σ_a for $\rho_{st}(\nu, 21, 12)^d$ at a mean AOA $\theta^r = 90°$. As shown, the space-time fading correlation decreases as angle spread σ_a and/or Doppler spread F_d increase.

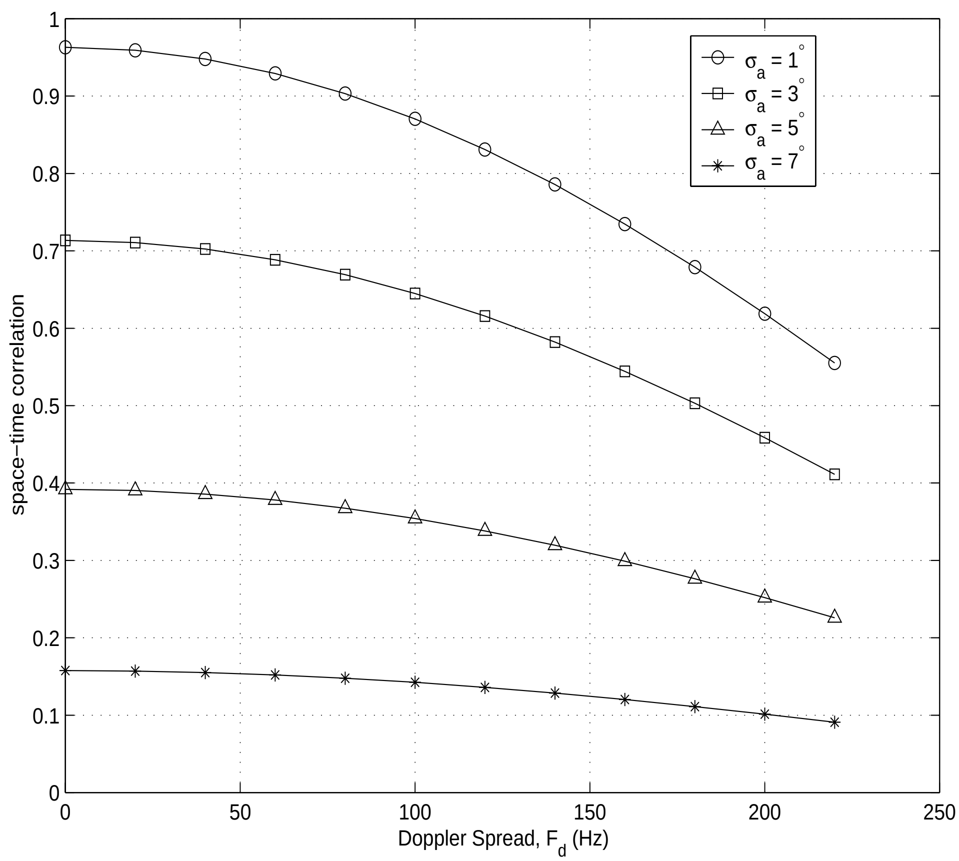

Figure 3.9: Analytical results of space-time correlation for downlink MIMO commutations ($D_r = 3.3\lambda$ and $\nu = 1\,msec$)

3.6 Summary

In this chapter, we derived an analytical expression for the MIMO channel space-time fading correlation for uniform circular array and uniform linear array in mobile radio environment. The MIMO channel space-time fading correlation are evaluated for both uplink and downlink communication. The MIMO space-time fading correlation is composed of temporal fading correlation and the spatial fading correlation. The temporal fading correlation is a function of the Doppler spread and time delay while the spatial fading correlation is a function of the angle spread and distance between elements. Results showed that the temporal fading correlation decreases as the Doppler spread and/or time delay increase and the spatial fading correlation decreases as the antenna spacing and/or angle spread increase. Three AOA distributions are considered: uniform, truncated Gaussian, and truncated Laplacian. Results show that the three AOA distributions give similar spatial fading correlation for the same angle spread, suggesting that the variance of the distribution is more important than the actual distribution. Computer simulations are carried out to verify the analytical results.

Chapter 4

Channel Capacity of MIMO Channels

In this chapter, we evaluate the information-theoretic channel capacity of the MIMO channel based on the MIMO channel model developed in Chapter 2. The information-theoretic channel capacity is evaluated for both a uniform linear array and a uniform circular array geometries in a mobile radio environment. This chapter is organized as follows. In Section 4.1, we present an overview of the information-theoretic channel capacity for the MIMO wireless communications. For practical applications, we evaluate the channel capacity of a (4,4) MIMO channel with a combination of UCA and ULA in mobile radio environment in Section 4.2. The channel capacity of the MIMO system is derived as function of the number of transmit-receive antenna elements and the eigenvalues of the spatial fading correlation matrix for the MIMO channel. For the purpose of evaluating the channel capacity, we review the statistical MIMO channel model in Section 4.3. Simulation validation methods used in this study are described in Section 4.4. The results on the channel capacity of the MIMO channel for various antenna configurations are presented in Section 4.5. Finally, concluding remarks are given in Section 4.6.

4.1 Information-Theoretic Channel Capacity

Recent research has shown that MIMO antenna array system can provide significant capacity improvement over conventional wireless antenna systems [6][7]. MIMO-based signal processing techniques such as the Bell Labs Layered Space-Time (BLAST)) architecture codes, space-time trellis codes, and space-time block codes have been proposed and examined for future wireless applications [4][8]. The system model of an n_T transmit and n_R receive MIMO antenna array system often referred to as an (n_T,n_R) system, as shown in Figure 4.1. The discrete received signal model for a (n_T,n_R) system can be

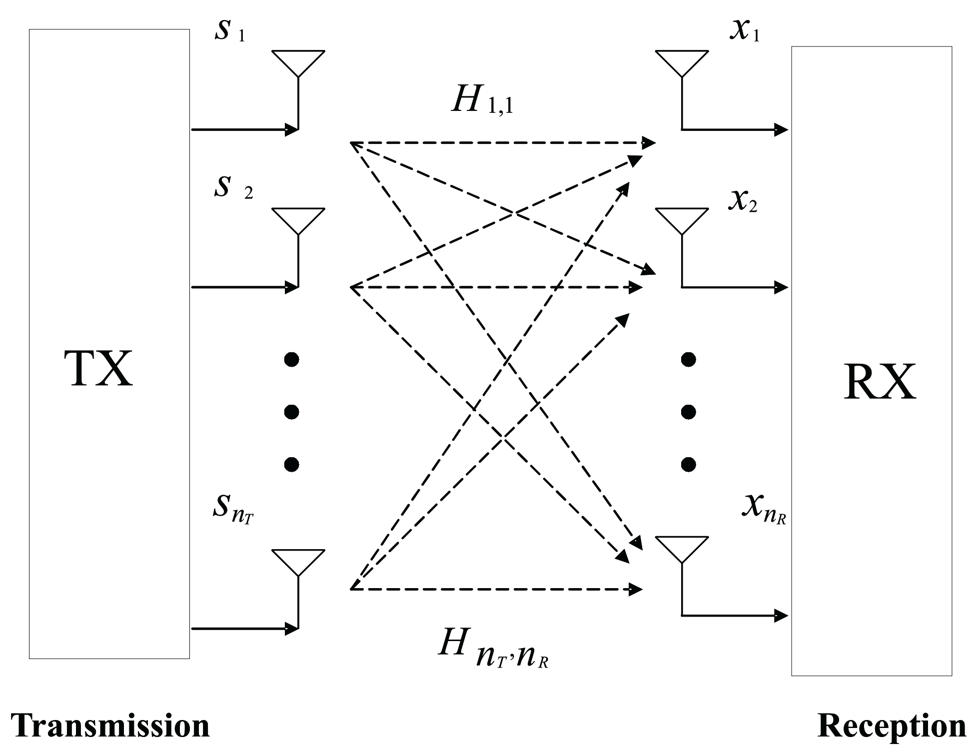

Figure 4.1: System model of of a (n_T,n_R) MIMO antenna arrays systems

expressed as

$$\mathbf{x} = H\mathbf{s} + \mathbf{n}, \tag{4.1}$$

where H is the channel matrix with the size of $n_R \times n_T$ and $\mathbf{x}$ is the received signal vector. $\mathbf{s} = [s_1\, s_2 \cdots s_{n_T}]$ is the transmit signal vector. $\mathbf{n}$ is an additive white Gaussian noise vector and each component is modeled as Gaussian random variable with zeros mean and unity variance.

In [6], it is shown that the channel capacity for a statistical (n_T,n_R) MIMO Rayleigh flat fading channel can be expressed as

$$C = \log_2 det\left(\mathbf{I}_{n_R} + \frac{\gamma}{n_T} HH^\dagger\right), \quad \text{(bits/second/Hz)} \tag{4.2}$$

where $\mathbf{I}_{n_R}$ is the $n_R \times n_R$ identity matrix, det is the determinant operation, and $\dagger$ is the Hermitian transpose. γ is the signal-to noise ratio at each receive antenna. H is the Raleigh fading channel matrix and is known to the receiver. Equation (4.2) assumes maximal-ratio combining (MRC) is employed at the receiver. For the mth receive antenna and pth transmit antenna, the channel gain $H_{m,p}$ is modeled as a complex Gaussian random variable with zero mean and unit variance, which is denoted as $\widetilde{N} \sim (0, 1)$. That is, in-phase and quadrature components of a complex Gaussian random variable are modeled as $\widetilde{N} \sim (0, 0.5)$. Note that the channel capacity C is a random variable for a statistical channel. If $H_{m,p}$ are and independent and identically distributed (i.i.d.) and $n_T = n_R$, we can further rewrite (4.2) as

$$C = \sum_{k=1}^{n_R} \log_2\left(1 + \frac{\gamma}{n_T} |H_{k,k}|^2\right), \quad \text{(bits/second/Hz)} \tag{4.3}$$

where $|H_{k,k}|^2$ is the channel power gain for the kth diagonal component of $HH^\dagger$. For the case of $\gamma \gg 1$, (4.3) can be reduced to

$$C \approx n_R \log_2 \gamma, \quad \text{(bits/second/Hz)}. \tag{4.4}$$

That is, the channel capacity increases proportionally with the number of antenna elements provided $n_T = n_R$.

For the case of H assuming deterministic channels rather than statistical channels, [56] shows that the channel capacity C is function of the number of transmit antennas, the number of receive antennas, and the number of deterministic multipath paths. For large γ, the channel capacity C for deterministic channels can be expressed as

$$C \approx \min(n_T, n_R, n_P) \log_2 \gamma, \quad \text{(bits/second/Hz)} \tag{4.5}$$

where n_P is the number of deterministic multipath and $\min(x)$ denotes choosing the minimum values out of the set of parameters x.

4.2 MIMO Channel Capacity Analysis

Although the MIMO channel can enhance the capacity of wireless systems, as shown in [6], it was assumed that all links are statistically independent (*i.e.,* The MIMO channel exhibits no spatial fading correlation). Indeed, in a practical propagation environment this assumption may not be valid due to small angle spread and/or insufficient antenna spacing. It has been observed that the channel capacity is significantly degraded when the spatial fading correlation of the MIMO channel is high [56]. It has been shown in [56] that the MIMO channel capacity can be expressed as function of the eigenvalues of cross-correlation matrix for a statistical correlated MIMO channel.

In [7], it is further shown that an (n_T,n_R) MIMO system can be transformed into an equivalent system with $n = \min(n_T, n_R)$ decoupled single-transmit, single-receive antenna (SISO) subchannels with SNR's related to the eigenvalues of cross-correlation matrix of the channel. Thus, the information-theoretical channel capacity of a (n_T,n_R) MIMO system can be expressed by the sum of the channel capacity of n SISO subchannels with power gain ε_k^2. That is

$$C = \sum_{k=1}^{n} \log_2(1 + P_k \varepsilon_k^2) \quad \text{(bits/second/Hz)}, \tag{4.6}$$

where P_k is the transmit power allocated to the kth subchannel and ε_k^2 are the eigenvalues of $HH^\dagger$. Note that (4.6) assumes a unity noise power at the receiver. The total transmit power constraint requires that $\sum_{k=1}^{n} P_k \leq P_T$, where P_T is the total transmit power. P_k can be chosen to maximize channel capacity using the "water-pouring" algorithm [57]. However, for practical applications, an equal power allocation scheme is often used [58], i.e., $P_k = P_T/n$. If we assume $n = n_T = n_R$, the channel capacity with equal transmit powers can be expressed as [56]

$$C = \sum_{k=1}^{n} \log_2(1 + \frac{\gamma_r}{n}\varepsilon_k^2) \quad \text{(bits/second/Hz)}. \tag{4.7}$$

Note that the received signal-to-noise ratio $\gamma_r = \gamma$ at each receive antenna with maximal ratio combining is equal to the transmit power ($P_k = \gamma_r$) for normalization of noise power.

4.3 Spatial MIMO Channel Model

We assume a flat Rayleigh MIMO fading channel. The MIMO system using up to 4 antenna elements on either transmit or receive arrays, as shown in Figure 3.1. For the purpose of this study, we simplify the space-time MIMO channel model developed in Section 2.6 with the spatial MIMO channel model. For the pth transmit antenna at the mth receive antenna element, the spatial MIMO channel model for the downlink and uplink channels can be expressed by (2.31) and (2.43) by removing the temporal components of these two equations respectively. That is, the downlink spatial MIMO channel impulse response can be expressed as

$$h_{m,p}^{d} = \sum_{s=1}^{L_s} \frac{1}{\sqrt{L_s}} v_p^r(\theta_s^r) v_m^t(\theta_s^t) e^{j\phi_s}, \tag{4.8}$$

where L_s, ϕ_s, $v_p^r(\theta_s^r)$, and $v_m^t(\theta_s^t)$ are defined in Section 2.6. In this chapter, we assume a uniform distribution for θ_s^t and a truncated Gaussian distribution for θ_s^r. Similarly, the uplink spatial MIMO channel impulse response can be expressed as

$$h_{m,p}^{u} = \sum_{s=1}^{L_s} \frac{1}{\sqrt{L_s}} v_p^t(\theta_s^r) v_m^r(\theta_s^t) e^{j\psi_s} \tag{4.9}$$

where $v_p^t(\theta_s^t)$ and $v_m^r(\theta_s^r)$ are defined in Section 2.6. Note that $h_{m,p}^d$ and $h_{m,p}^u$ become a complex Gaussian random variables when L_s is large.

4.4 Simulation Methods and Validation

For practical considerations, an (4,4) MIMO system with a UCA and/or ULA antenna configurations at the mobile station and the base station is considered in this study. Due to symmetry between the uplink and downlink channels, the capacity results on one link can be easily translated to the other link by simply exchanging the transmitter and the receiver. We need only consider one link. so the uplink (transmitter at the mobile station and receiver at the base station) is chosen for this study. The uplink MIMO channel model developed in Section 4.3 is used to evaluate the channel capacity. We assume that channel varies at a rate slow enough that it can be regarded as essentially static for a given snap shot of data ($H_{m,p} = h^u_{m,p}$). The exact distribution of channel capacity for a general MIMO system with finite number of antenna elements is difficult to compute. Thus, we use Monte Carlo simulations to evaluate the channel capacity based on (4.7). We generate 800,000 instances of the channel for a given case study and calculate a histogram of channel capacity. For comparison purposes, the criteria of 10% outage channel capacity denoted as $C_{0.1}$ is used for various antenna configurations at both the mobile station and the base station. By 10% outage channel capacity we mean that the cumulative distribution of the channel capacity is 90%. There are four antenna configurations combinations that are considered (UCA,UCA), (UCA,ULA), (ULA,ULA), and (ULA,UCA). Note that "(UCA,ULA)" means that the transmitter uses a UCA and the receiver uses a ULA. Since we consider the uplink, "(UCA,ULA)" specifically means that the mobile station transmits with a UCA and the base station receives with a ULA.

To validate the simulation results, we set the same antenna configuration (ULA,ULA) and similar channel parameters to those used in [56][6]. We compare the simulated results on the basis of channel capacity with the aforementioned work. In Figure 4.2, we evaluate the 10% outage channel capacity for a statistical independent (4,4) MIMO Rayleigh flat fading channel and compare our simulation result (Tsai's result) with

Foschini's result given in [6]. The simulator is validated after both simulation results show a good agreement for various channel parameters.

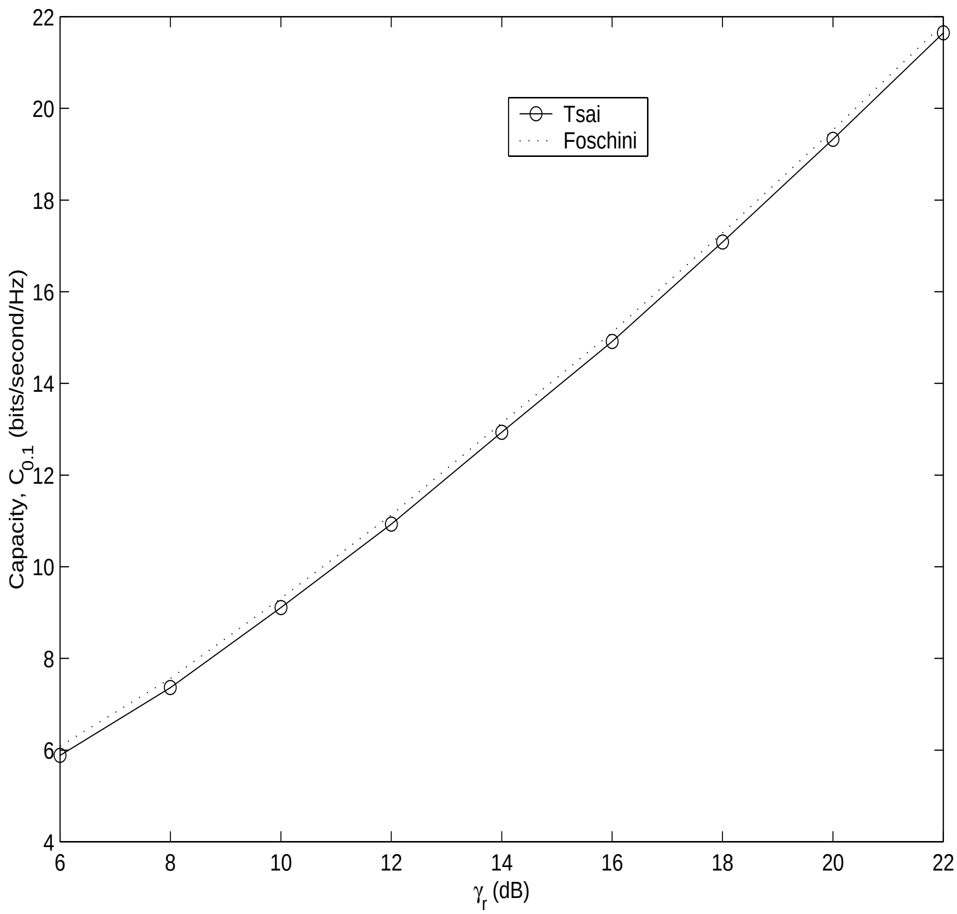

Figure 4.2: The 10% outage channel capacity for a statistical independent (4,4) MIMO Rayleigh flat fading channel.

4.5 Results on Channel Capacity

In this section, we evaluate the MIMO channel capacity based on the eigenvalues that obtained from $HH^{\dagger}$. It is noted that the results of the channel capacity presented here are based on the assumption of maximal-ratio combining at the receiver. The total antenna spacings for the base station and the mobile station are 10λ and 1.5λ. In addition, the channel capacity for Figure 4.3 to Figure 4.5 is averaged[1] over θ^r. Figure 4.3 compares channel capacities at $C_{0.1}$ for four antenna configurations in moderate angle spread mobile environment ($\sigma_a = 5°$). The result shows that the base station using a UCA yields a higher channel capacity than that obtained by using a ULA, regardless of whether a ULA or UCA is employed at the mobile station. This is because on average the spatial fading correlation of the UCA is lower than the ULA at the base station for small to moderate angle spread environments. However, at the mobile station both the ULA and the UCA experience essentially independent fading due to large assumed angle spread. This result also suggests that (ULA,UCA) may be the prefered choice of antenna configuration for an omni-cell system with small and moderate angle spread at the base station, since the ULA may be easily employed on a laptop PC computer rather than the UCA.

Figure 4.4 shows the complementary cumulative distribution function (c.c.d.f) of channel capacity of a (ULA,UCA) antenna configuration for various angle spreads at the base station. As expected, as angle spread σ_a increases, the channel capacity increases since the spatial fading correlation decreases . It is shown that with increasing angle spread the c.c.d.f curves approach the case of independent spatial fading. Figure 4.5 shows the effects of angle spread on channel capacity for both (ULA,UCA) and (ULA,ULA) antenna configurations for various angle spread at the base station. As shown, for angle spread $\sigma_a \leq 10°$, (ULA,UCA) results in significantly higher capacity than (ULA,ULA). As angle spread σ_a increases, the difference between these two antenna configuration decreases. That is, for large angle spread, the channel capacity of (ULA,UCA) is essentially no different from (ULA,ULA). Figure 4.6 shows the effects of user location (θ^r) on channel capacity for both (ULA,UCA) and (ULA,ULA) antenna configurations. The result shows that the (ULA,UCA) scheme experiences channel capacity which is non-monotonic in θ^r from $\theta^r = 0°$ to $90°$ while the (ULA,ULA) scheme shows monotonically

[1] Channel capacity varies with θ^r due to variable spatial correlation.

increasing capacity with θ^r. The ULA has a lower channel capacity at $\theta^r = 0^\circ$ (endfire) due to high spatial fading correlation and an increased channel capacity as θ^r approaches 90° (broadside) due to low spatial correlation.

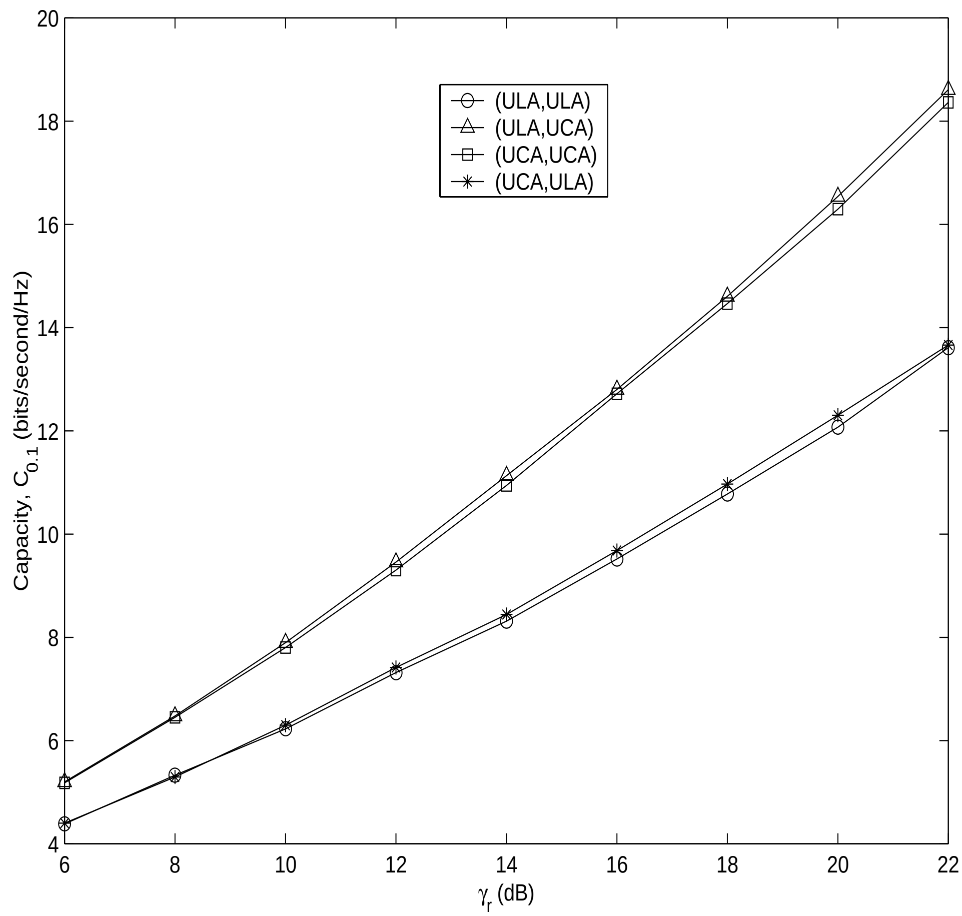

Figure 4.3: Comparisons of channel capacity for four antenna configurations, ($\sigma_a = 5^\circ$)

4.6 Summary

In this chapter, we presented an overview of the channel capacity for the MIMO wireless communications. We evaluated the information-theoretic channel capacity of a MIMO channel with both UCA and ULA antenna configurations for various angle spreads. The

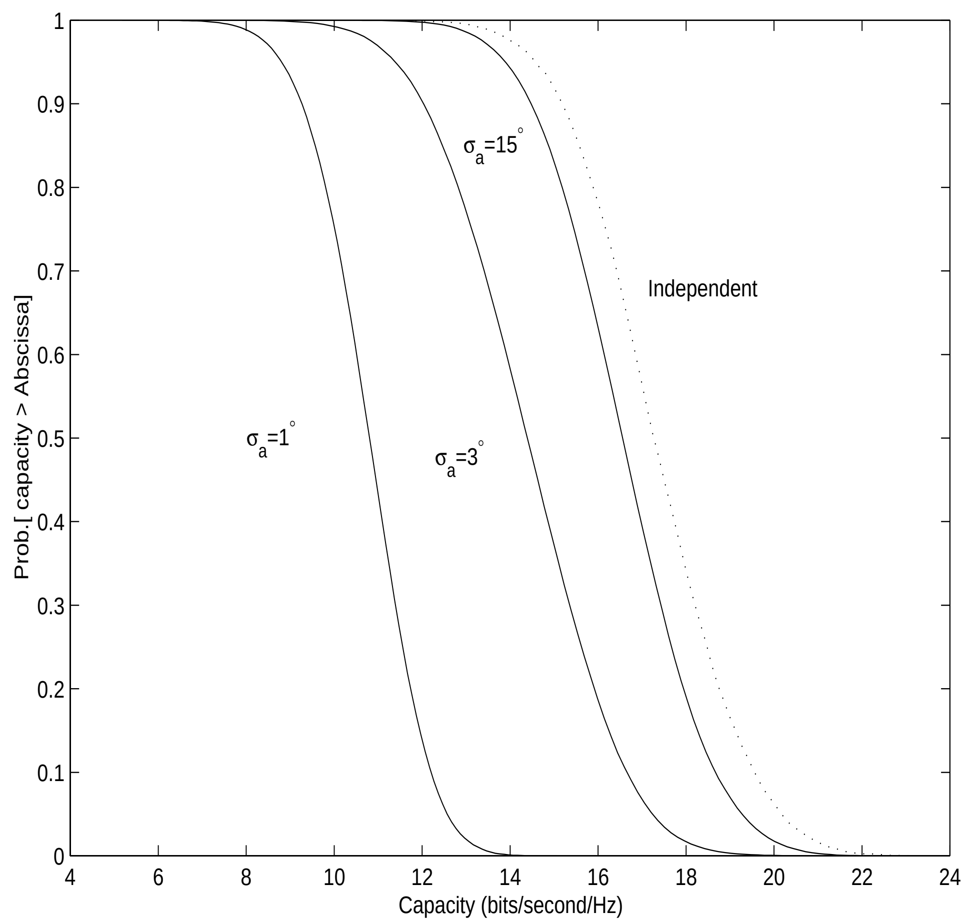

Figure 4.4: Complementary cumulative distribution function of channel capacity of (ULA,UCA) antenna configuration for various angle spreads (γ_r=16dB)

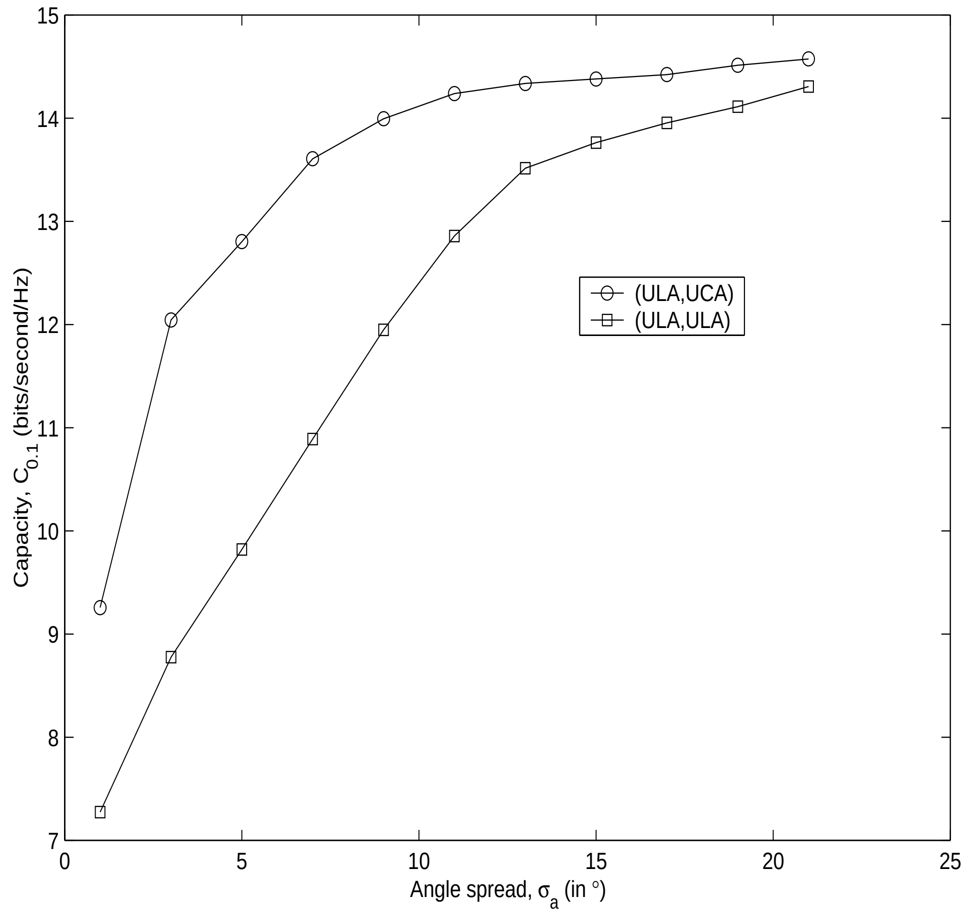

Figure 4.5: The effects of angle spread on channel capacity for both (ULA,UCA) and (ULA,ULA) antenna configurations (γ_r=16dB)

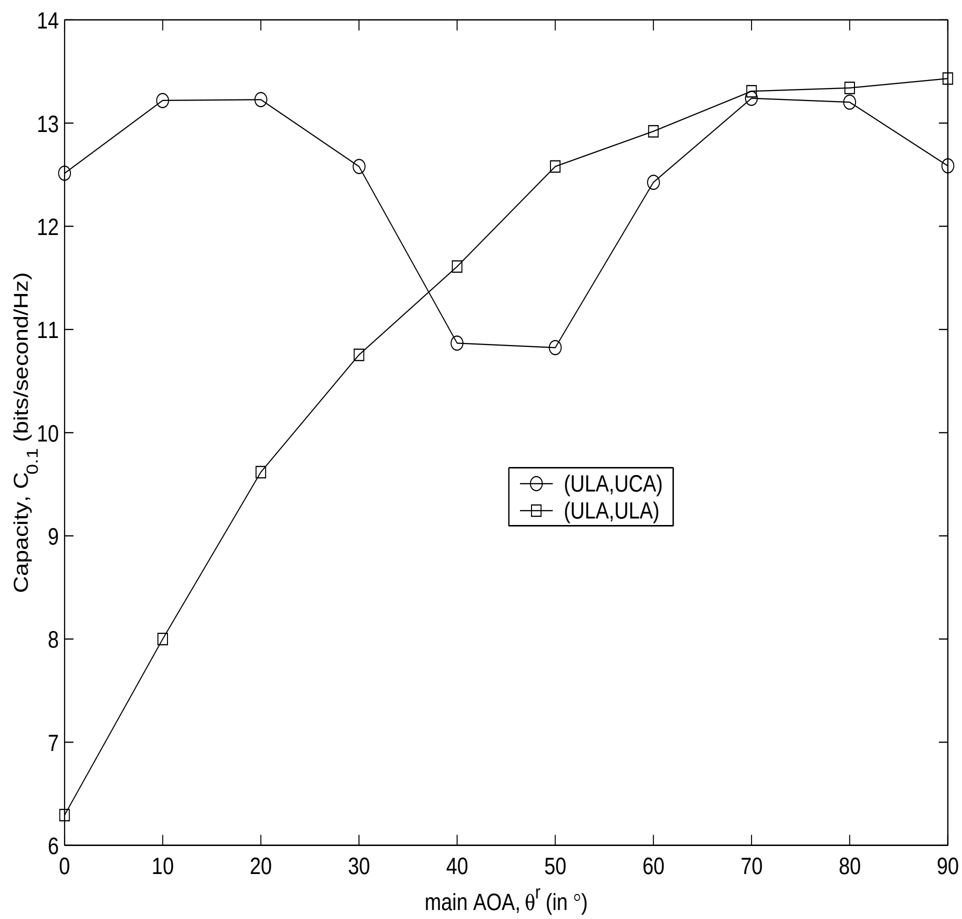

Figure 4.6: The effects of mobile location on channel capacity for both (ULA,UCA) and (ULA,ULA) antenna configurations ($\sigma_a = 3^\circ$ and γ_r=16dB)

results suggest that a (ULA,UCA) MIMO antenna configuration may be the prefered choice for higher channel capacity in mobile environments.

Chapter 5

Performance of Transmit Antenna Arrays

In this chapter, we examine two transmit antenna schemes for MIMO transmission systems over Rayleigh and Ricean fading channels: *open-loop transmit diversity* and *closed-loop transmit beamforming*. We show that closed-loop transmit beamforming is a well-suited transmission technique when the fading channel is Ricean or low Doppler spread (*i.e.,* low mobility), while open-loop transmit diversity method is better-suited when the fading channel is Rayleigh and high Doppler spread (*i.e.,* high mobility). In Section 5.1, we briefly describe the concepts of the open-loop transmit diversity and the closed-loop transmit beamforming for wireless communications. In Section 5.2, we present the system models for these two transmit antenna schemes. In Section 5.3, we analyze the performance of both open-loop transmit diversity and closed-loop transmit beamforming in mobile radio environments. In Section 5.4, we describe the statistical transmit vector channel model and review the transmit spatial fading correlation. The simulation procedure is presented in Section 5.5. Comparative BER results for both open-loop transmit diversity and closed-loop transmit beamforming over Rayleigh and

Ricean fading channels are presented in Section 5.6. Finally, a summary is given in Section 5.7. Note that we study the impact of the transmission on the system performance for MIMO systems. In the next chapter, on the other hand, we will examine the impact of the reception on the system performance for MIMO systems.

5.1 Open-Loop and Closed-Loop Transmit Antenna Arrays

Recently there is increasing interest in enhancing the downlink system capacity for the anticipated asymmetry in future data-dominated wireless systems. Two transmit antenna schemes have been proposed to improve downlink system capacity: open-loop transmit diversity and closed-loop transmit beamforming [59][5]. The difference between these two transmit antenna schemes is that the closed-loop scheme relies on the feedback of the transmit channel information based on mobile station measurements, while the open-loop scheme does not require any feedback. Figure 5.1 shows the system models for this two transmit antenna system. In principle, the open-loop scheme only provides the spatial diversity gain over the SISO system (*i.e.,* single input single output or no diversity system). The closed-loop scheme, on the other hand, provides not only spatial diversity, but the antenna aperture gain. Note that antenna aperture gain is increased by 3dB by doubling the number of antenna elements. However, from a system complexity point of view, the open-loop scheme is relatively simple.

The system performance of the closed-loop scheme is dominated by the reliability of the feedback channel information from the mobile station. In principle, the base station uses this feedback information to optimally weight the transmit signal to the mobile so as to achieve both diversity and aperture advantage. However, the usefulness of the scheme is limited by the feedback delay, feedback errors, and feedback quantization. It has been shown previously that feedback delay is particularly harmful in mobile radio

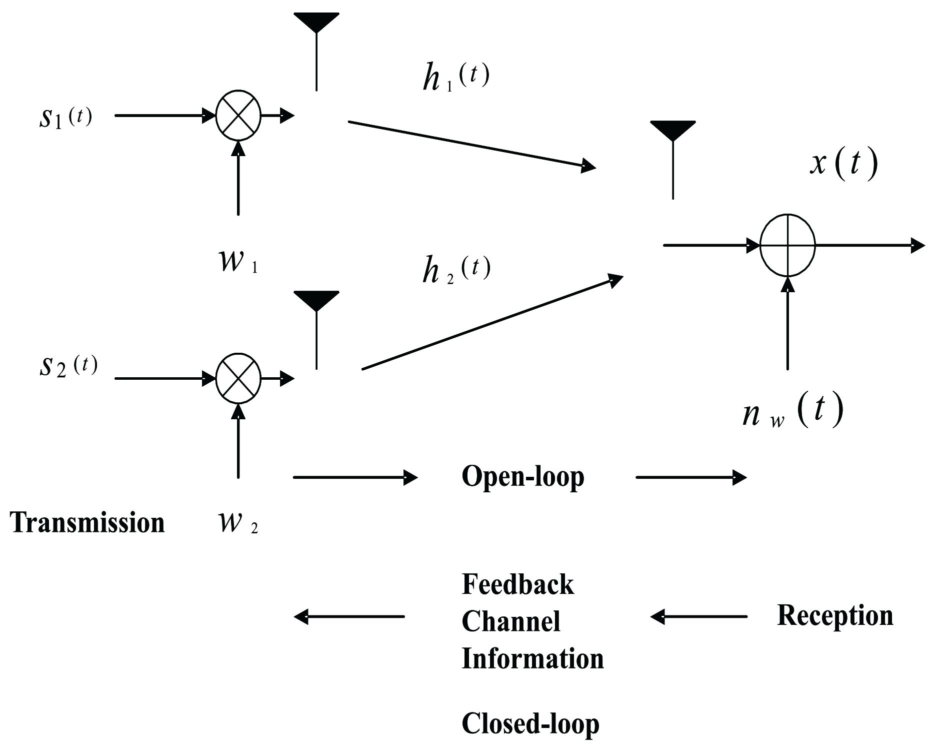

Figure 5.1: System models for open-loop transmit diversity and closed-loop transmit beamforming.

channels since the channel state (and thus the optimal weights) change faster than the mobiles ability to measure and feedback the information [60]. In Rayleigh fading channels this degradation is particularly harmful and can degrade the performance beyond that of a single antenna. In this study, we show that for Ricean channels, however, the performance is not nearly as sensitive to feedback delay nor to feedback quantization error. This is important since many operators report that Ricean fading dominates the channel distribution in CDMA cellular networks [61].

5.2 System Models for Transmit Antenna Systems

In this study we assume the use of two transmit antennas at the base station and one receive antenna at the mobile station, which corresponds to a practical application. The transmit signals from the two antennas are given by

$$s_1(t) = \sqrt{P}\, w_1\, d_1(t) + p_1(t) \tag{5.1}$$

and

$$s_2(t) = \sqrt{P}\, w_2\, d_2(t) + p_2(t) \tag{5.2}$$

where $d_1(t)$ and $d_2(t)$ are the data signals, which can be expressed as respectively

$$d_1(t) = \sum_{i=-\infty}^{\infty} d[i]\, O_1(t - iT_s), \tag{5.3}$$

$$d_2(t) = \sum_{i=-\infty}^{\infty} d[i]\, O_2(t - iT_s), \tag{5.4}$$

and where $d[i]$ is a QPSK modulated symbol, T_s is the symbol period. $O_1(t)$ and $O_2(t)$ are the orthogonal spreading codes to ensure the orthogonality between $s_1(t)$ and $s_2(t)$ in time. P is the transmit power. Further, there may be other signals code multiplexed onto the transmit signal, but they are irrelevant to the investigation. Each antenna also transmits a pilot $p_j(t)$ which is assumed to be code multiplexed onto the transmit signal. Further, the pilots $p_1(t)$ and $p_2(t)$ are assumed to be orthogonal in time. w_1 and w_2 are the transmit weights, with the transmit power constraint $|w_1|^2 + |w_2|^2 = 1$. For the open-loop transmit antenna scheme, the transmit weights are expressed as

$$w_1 = w_2 = \frac{1}{\sqrt{2}}. \tag{5.5}$$

For the closed-loop transmit antenna scheme, on the other hand, the transmit weights for w_1 and w_2 are based on the feedback information obtained from the mobile station. The transmit weights of w_1 and w_2 for the closed-loop antenna schema can be expressed as, respectively

$$w_1 = h_1^*(t - T_f), \tag{5.6}$$

$$w_2 = h_2^*(t - T_f), \tag{5.7}$$

where $h_j(t)$ is the normalized channel distortion experienced by the transmit signal coming from the jth antenna and T_f is the feedback delay. In a practical implementation, the closed-loop transmit beamforming with feedback of phase-information-only is prefered since the phase information dominates the performance of the closed-loop transmit beamforming [5]. The transmit weights of w_1 and w_2 for the closed-loop antenna scheme with the feedback of phase-information-only can be expressed as, respectively

$$w_1 = \frac{1}{\sqrt{2}}\, e^{j\theta_1}, \tag{5.8}$$

$$w_1 = \frac{1}{\sqrt{2}}\, e^{j\theta_2}, \tag{5.9}$$

where θ_1 and θ_2 are the phase of $h_1(t - T_f)$ and $h_2(t - T_f)$ respectively. The receive signal at the mobile station can be modeled as

$$x(t) = h_1(t)s_1(t) + h_2(t)s_2(t) + n_w(t), \tag{5.10}$$

where $n(t)$ is a complex Gaussian random process with autocorrelation $R_n n(\tau) = N_o\delta(\tau)$, N_o is the two-sided noise power spectral density, and $\delta(t)$ is unit impulse.

For the jth transmit antenna in open-loop antenna scheme, the received symbol after despreading for the ith symbol epoch can be expressed as

$$x_{op,j}[i] = \sqrt{\frac{P}{2}}\, h_j[i]\, d[i] + n_w[i], \tag{5.11}$$

where $n_w[i]$ is a white Gaussian noise sample with the variance $2\sigma^2 = N_o$ and $h_j[i]$ is the sampled version of $h_j(t)$. Note that the transmit signals $s_1(t)$ and $s_2(t)$ do not interfere with each other after orthogonal despreading at the receiver. For the closed-loop antenna scheme, the received symbol after despreading for the ith symbol can be expressed as

$$x_{cp}[i] = \sqrt{P}\, h_{eq}[i]\, d[i] + n_w[i], \tag{5.12}$$

where $h_{eq}[i]$ is the sampled version of $h_{eq}(t)$, which is given by

$$h_{eq}(t) = w_1\, h_1(t) + w_2\, h_2(t). \tag{5.13}$$

The receiver uses a pilot signal $p_j(t)$ to estimate the individual channels $h_j(t)$. It uses these along with assumed knowledge of w_j to calculate an estimate of $h_{eq}(t)$ which we denote $\widehat{h}_{eq}(t)$. Note that feedback error impacts knowledge of w_j and thus channel estimation.

5.3 Performance Analysis

In this section, we analyze the performance of both open-loop transmit diversity and closed-loop transmit beamforming in mobile radio environments. Clearly the performance of the system is dependent on the choice of w_j for the closed-loop transmit antenna scheme while for the open-loop transmit antenna scheme, the performance of the system is independent of the choice of w_j. If w_j is chosen to optimally combine (*i.e.,* maximal-ratio combining) the channels $h_1(t)$ and $h_2(t)$ for the closed-loop transmit antenna scheme, the system will experience a diversity advantage as well as a 3dB aperture advantage over the case of a single transmit antenna. However, if the value of w_j does not optimally combine the channels, the performance will degrade. This arrangement is commonly called closed-loop beamsteering since the transmitter cannot know the required value of w_j in advance and must rely on information from the receiver to choose w_j.

Typically, the receiver measures the pilots p_j and determines the value of w_j which optimally (maximizes SNR) combines the two channels. There are three sources of error in such a scheme: feedback delay, quantization error, and feedback error. The first is the most serious and arises due to the time-varying nature of the channels combined with the finite time required to measure, feedback and apply the necessary weight. The second error arises due to the limited feedback bandwidth and the third due to the unavoidable errors in the feedback path. These degradations have been examined extensively for Rayleigh fading channels and shown to be a serious impediment to system performance. In this study we examine the impact of these errors in Ricean fading channels. Ricean fading has commonly been reported to be the dominant fading distribution seen in cellular systems [61]. We show in this study that feedback delay, which is a serious problem in Rayleigh fading is not as detrimental in Ricean fading. To have a complete treatment on this subject, we present the BER results for both open-loop and closed-loop antenna schemes over both Rayleigh and Ricean channels.

With maximal ratio combining at the receiver, the estimated symbol for the open-loop antenna scheme at the ith symbol epoch can be expressed as

$$\widehat{d}[i] = \sum_{j=1}^{2} x_{op,j}[i]\, h_j^*[i]\, d[i] + n_w[i]\, h_j^*[i]. \tag{5.14}$$

Similarly, the estimated symbol for the closed-loop antenna scheme at the ith symbol epoch can be expressed as

$$\widehat{d}[i] = x_{cp}[i]\, h_{eq}^*[i]\, d[i] + n_w[i]\, h_{eq}^*[i]. \tag{5.15}$$

Note that $h_j[i]$ and $h_{eq}[i]$ are estimated from the pilot symbols. For non-ideal channel estimation, the channel estimation error ϵ for the open-loop antenna scheme can be modeled as

$$\widehat{h}_j[i] = (1-\epsilon)\, h_j[i], \tag{5.16}$$

where ϵ is the error between the known channel $h_j[i]$ and the estimated channel $\widehat{h}_j[i]$.

For the closed-loop antenna scheme, the channel estimation error ϵ can be modeled as

$$\widehat{h}_{eq}[i] = (1-\epsilon)\, h_{eq}[i], \tag{5.17}$$

where

$$\widehat{h}_{eq}[i] = \widehat{w}_1\, \widehat{h}_1[i] + \widehat{w}_2\, \widehat{h}_2[i], \tag{5.18}$$

where $\widehat{h}_j[i]$ can be obtained from (5.16) and $\widehat{w}_j$ is modeled as

$$\widehat{w}_j = (1-\epsilon)\, w_j. \tag{5.19}$$

As seen, the channel estimation error for the closed-loop scheme is comprised of $\widehat{w}_j\, \widehat{h}_j[i]$ while the channel estimation error for the open-loop is only dependent on $\widehat{h}_j[i]$. In the next section, we briefly discuss the transmit vector channel model $h_j(t)$ used in this study.

5.4 Transmit Vector Channel Model

Without loss of generality, we consider the case of a flat fading channel. Based on the vector channel model developed in Chapter 2, the channel impulse response for a Ricean fading channel at the jth transmit antenna can be expressed as

$$h_j(t) = \sqrt{\frac{K}{K+1}} + \sqrt{\frac{1}{K+1}} h_{j,sc}(t) \tag{5.20}$$

where $\sqrt{\frac{K}{K+1}}$ is the specular component, which is spatially deterministic from antenna to antenna due to a line-of-sight (LOS) propagation. $\sqrt{\frac{1}{K+1}}\, h_{j,sc}(t)$ is the scattered component, which is randomly varying from antenna to antenna due to multipath propagation paths. K is the power ratio of specular component to the scattered component. For the case of $K = 0$, $h_j(t)$ is a Rayleigh fading channel. For the case of $K = \infty$, $h_j(t)$ is an AWGN channel. $h_{j,sc}(t)$ can be expressed as a function of antenna spacing, Doppler frequency, and angle-of-departure (AOD). For the jth transmit antenna , $h_{j,sc}(t)$ for the downlink channel can be expressed by (2.31). We assume a truncated Gaussian distribution for AOD (θ_s), which reflects the fact that the energy is most likely to come from a central AOD. Figure 5.2 shows the channel model for downlink transmit Antenna arrays.

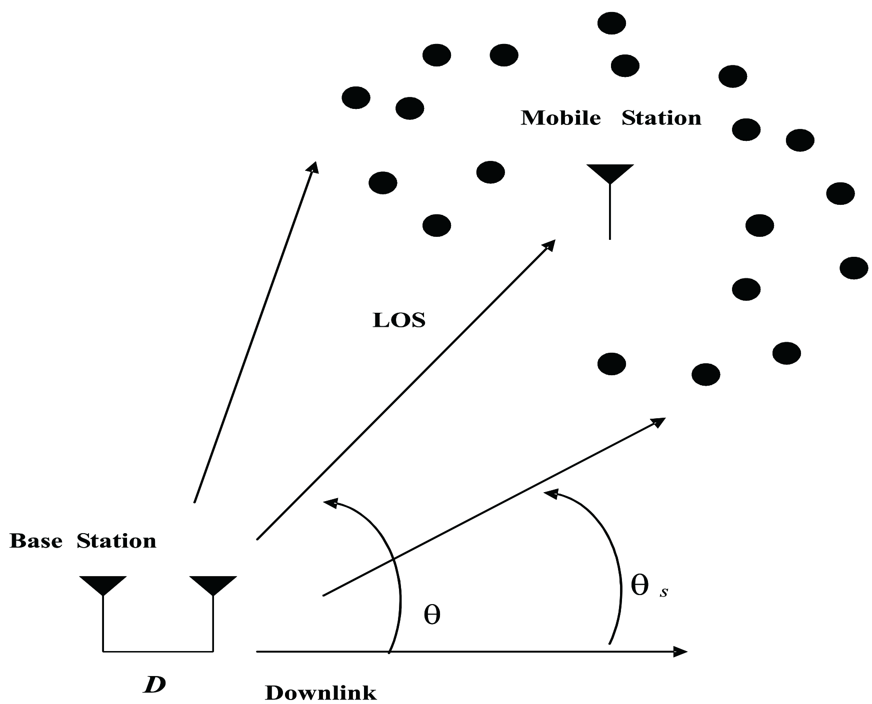

Figure 5.2: Channel model for downlink transmit Antenna arrays.

5.5 Simulation Validation

To validate the simulation results, the channel $h_j(t)$ is assumed known at the receiver. We first assume perfect feedback information for the closed-loop antenna scheme. Figure 5.3 show the BER performance of three transmit antenna schemes over a flat Rayleigh fading channel. Note that the legend "TD" denotes open-loop transmit diversity, "TB" denotes closed-loop transmit beamforming with optimal weights (the feedback of phase and amplitude), and "TP" denotes closed-loop transmit beamforming with the feedback of phase-information-only. For comparison purposes, we define γ_p as the ratio of the transmit signal power per bit to the receive noise power per bit and per receive antenna. It is seen that the simulated BER of the open-loop transmit diversity exhibits a good agreement with analytical BER results. In addition, the BER of closed-loop transmit beamforming has 3dB aperture gain over the open-loop transmit diversity. In this figure, it is also noted that the closed-loop transmit beamforming with the feedback of phase-only yields slightly worse performance than the case with the feedback of phase and amplitude. We also ran several simulation with similar channel parameters used in [59][5] and compared our simulated results with the aforementioned works. The simulator was validated as our simulation results show a good agreement with the published works.

5.6 Numerical Results

In this section, we present the simulated BER results of open-loop transmit diversity method and closed-loop transmit beamforming method with realistic system impairments.

In Figure 5.4, we plot the simulated results for the above transmit antenna schemes in a Rayleigh fading channel ($K = 0$). The two feedback methods are optimal weights (*i.e.,* MRC) and phase-only. No feedback error or quantization error or channel estimation error was assumed. The simulated BER is plotted versus the normalized feedback delay where normalization is with respect to the maximum Doppler shift of the channel. As seen, both closed-loop feedback methods experience performance degradation due to feedback delay when $F_d T_f \geq 0.02$, which means the feedback delay T_f must be smaller than the coherence time $\frac{1}{F_d}$. Note that the open-loop scheme is independent of the feedback delay. It is also seen that the closed-loop schemes outperforms the open-loop scheme when $F_d T_f \leq 0.1$. That is, the feedback rate $(\frac{1}{T_f})$ must be 10 times faster than the maximum Doppler frequency in order to yield a better BER performance than the

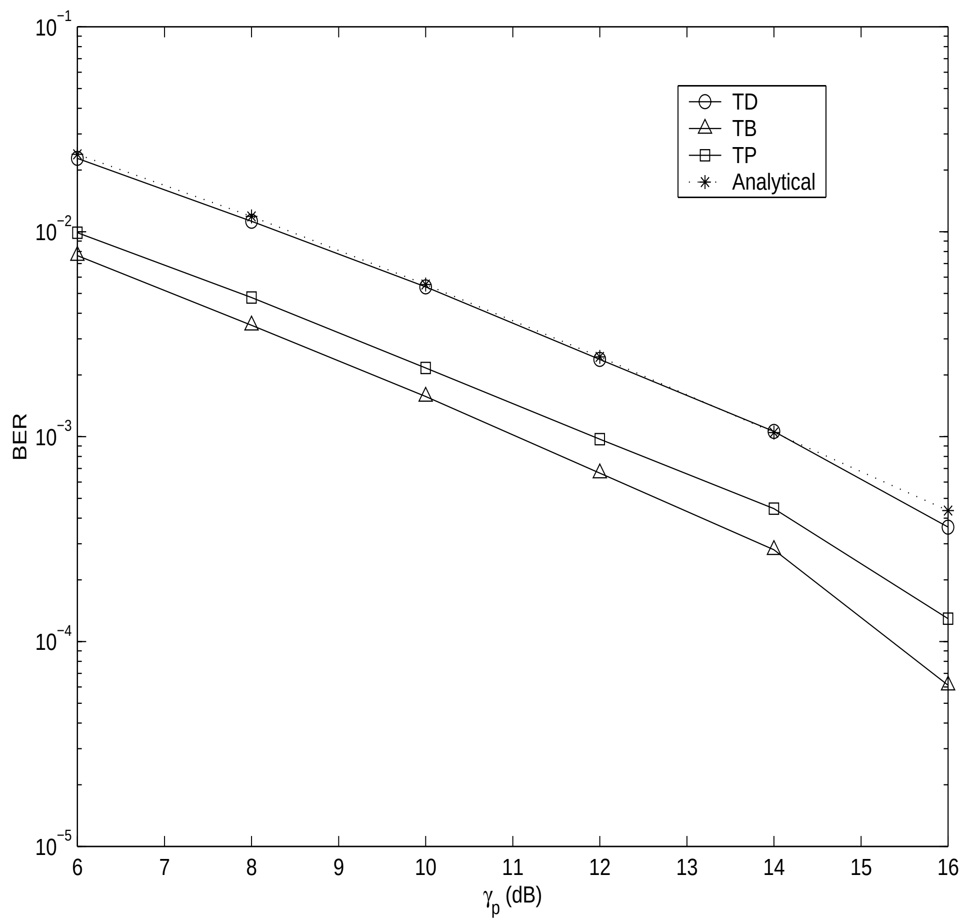

Figure 5.3: Comparative BER performance for transmit diversity and transmit beamforming ($\sigma_a = 20°$).

open-loop scheme. The above results apply to both small angle spread ($\sigma_a = 1°$) and large angle spread ($\sigma_a = 20°$).

Since TP (closed-loop scheme with the feedback of phase-only) is the prefered transmit beamforming scheme in a practical implementation, we consider the impact of quantization error for TP systems and compare their performance with transmit diversity schemes. Figure 5.5 shows the simulated BER for a TP system as function of Doppler frequency and the number of feedback bits for the feedback delay of $T_f = 1/1500$ second (similar to WCDMA system) in a Rayleigh fading. In this figure, no channel estimation error was assumed. The results show that quantization error has little impact on performance when the number of quantization bits is greater than two. The result also shows that performance degrades as Doppler frequency increases.

Figure 5.6 shows the impact of the channel estimation error for the above transmit antenna schemes in a Rayleigh fading channel. In this figure, no feedback error or quantization error was assumed. As seen, the closed-loop antenna scheme is much more sensitive to channel estimation error due to the fact that its channel estimation error is a composite of $\widehat{w}_j$ and $\widehat{h}_j[i]$.

In Figure 5.7, we plot simulated results for the above transmit antenna schemes in a Ricean fading channel. The two feedback methods are optimally weighting and phase-only. Again, no feedback error or quantization error or channel estimation error was assumed. Three Ricean fading channels are assumed: $K = 1$, $K = 5$, and $K = 10$. The simulated BER is plotted versus the normalized feedback delay where normalization is with respect to the maximum Doppler shift of the channel. Also plotted are the performance of open-loop transmit diversity [60]. Clearly, feedback delay is a major impediment to closed-loop beamforming in the case of $K = 1$ (close to Rayleigh fading). Performance degrades more for transmit diversity. However, in Ricean fading with large K, the feedback delay is not as serious with benefits being exhibited even when the feedback delay was equal to the maximum Doppler shift.

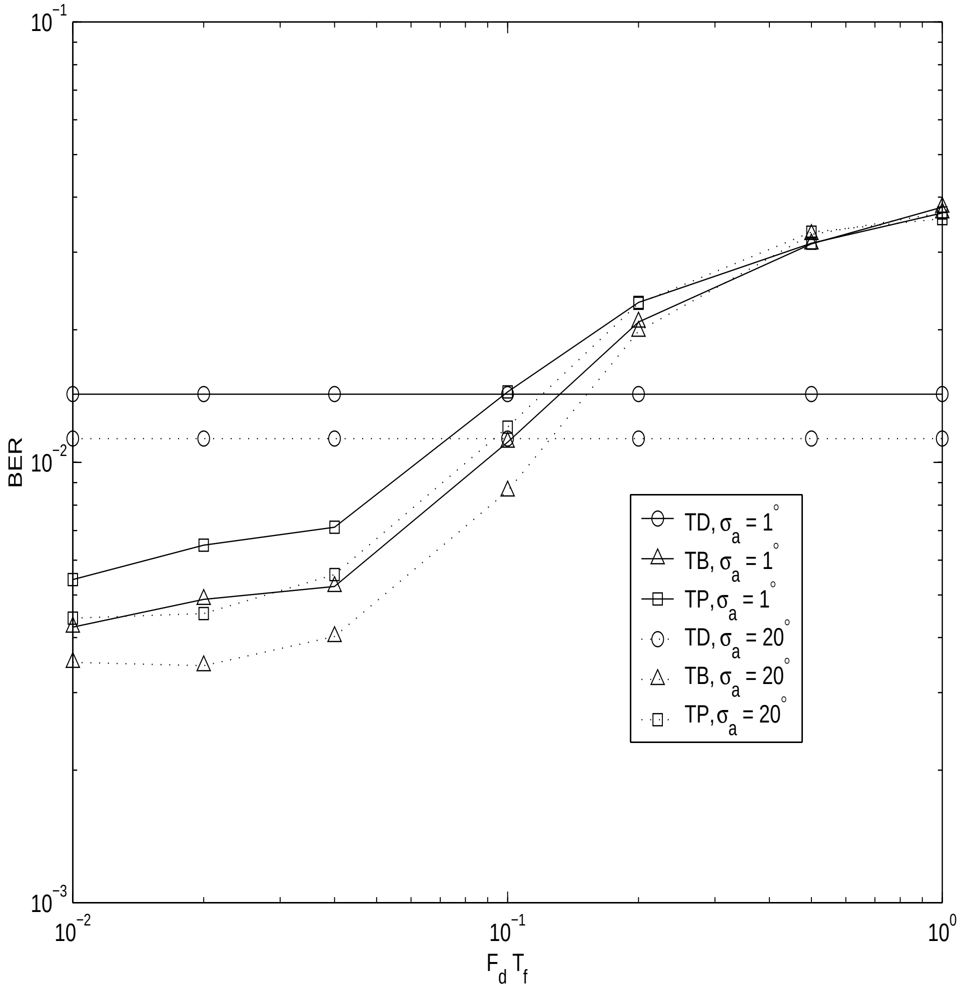

Figure 5.4: Comparative BER performance for transmit diversity and transmit beamforming (γ_p=8dB)

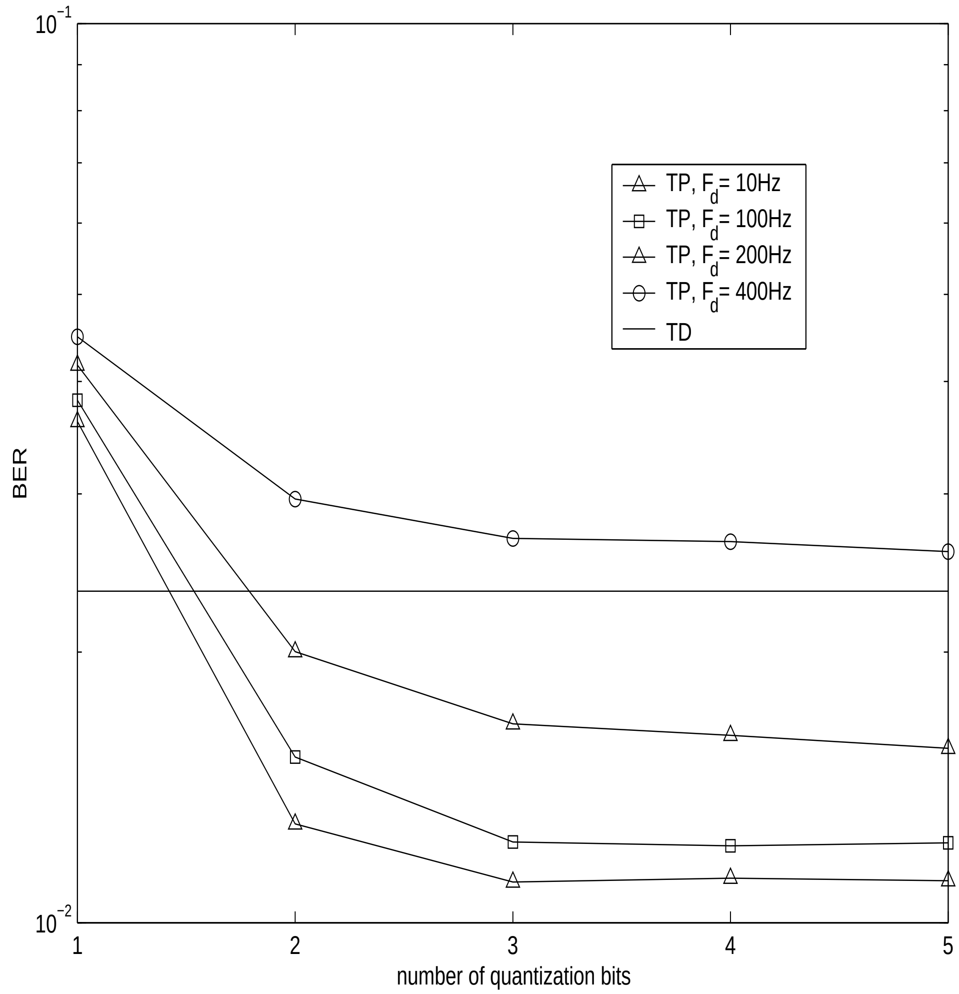

Figure 5.5: Impact of quantization error and feedback error on BER results for various Doppler frequencies F_d (γ_p=6dB, T_f=1/1500 seconds and $\sigma_a = 3°$).

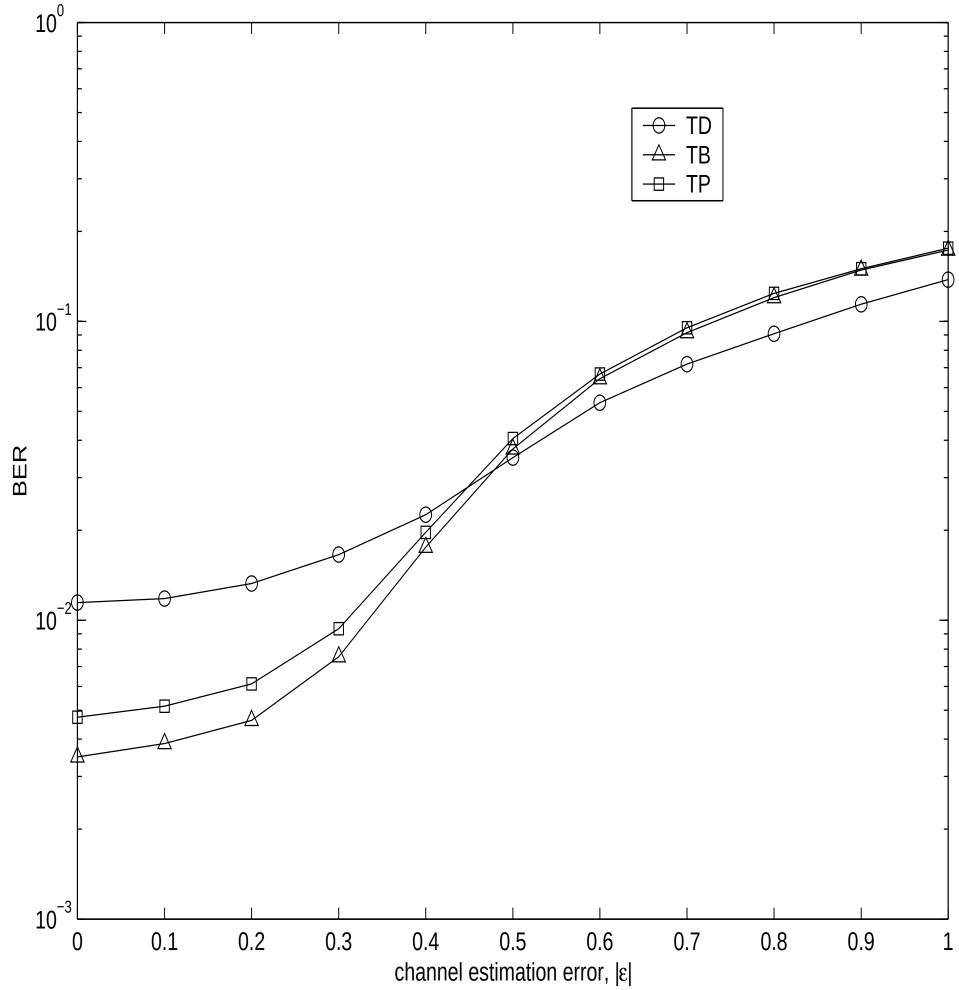

Figure 5.6: Impact of channel estimation on BER results for TD, TB, and TP transmit antenna schemes (γ_p=8dB and $\sigma_a = 20°$).

In Figure 5.8, we present the performance impact of quantization error for TP systems and compare its performance with transmit diversity schemes. No channel estimation error was assumed. Plotted are the simulated BER curves for the feedback schemes described above for Ricean fading (K=1 and K=10) versus the number of feedback bits for a delay of $T_f = 1/1500$ second and maximum Doppler shifts of 10Hz and 400Hz. The results show that quantization errors have little impact on performance when the number of quantization bits is greater than two. The result also shows that Doppler spread has little impact on performance for large K. This is because channel is dominated by a LOS component rather than scatter component.

Figure 5.8 shows the impact of channel estimation error for the above transmit antenna schemes in a Ricean fading channel. In this figure, no feedback error or quantization error was assumed. For the channel estimation error $|\epsilon| \geq 0.2$, the significant performance degradation is observed. As seen, the closed-loop antenna scheme is more sensitive to channel estimation error due to the fact that its channel estimation error is a composite of $\widehat{w}_j$ and $\widehat{h}_j[i]$.

5.7 Summary

In this chapter we examined two transmit antenna schemes for MIMO transmission systems over Rayleigh and Ricean fading channels. We found that the open-loop transmit scheme is prefered when the fading channel is Rayleigh and the Doppler spread is large (*i.e.,* high mobility), while the closed-loop is better-suited when the fading channel is Ricean or the Doppler spread is small. Furthermore, we examined the robustness of two-element transmit beamforming techniques. We showed that when the fading is Ricean, feedback methods are significantly more robust than when the fading is Rayleigh. This is significant since many cellular operators have measured Ricean fading in large portions of their cellular networks.

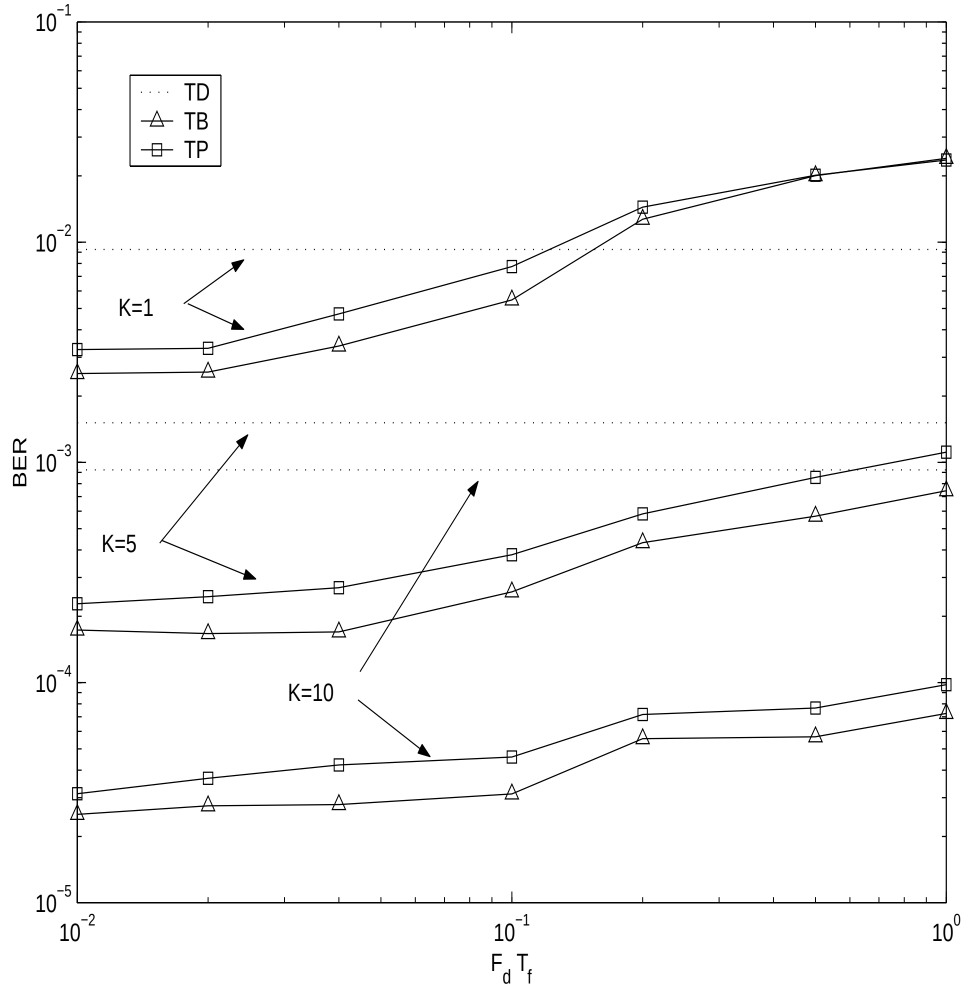

Figure 5.7: Comparative BER performance for transmit diversity and transmit beamforming (γ_p=8dB and $\sigma_a = 3°$).

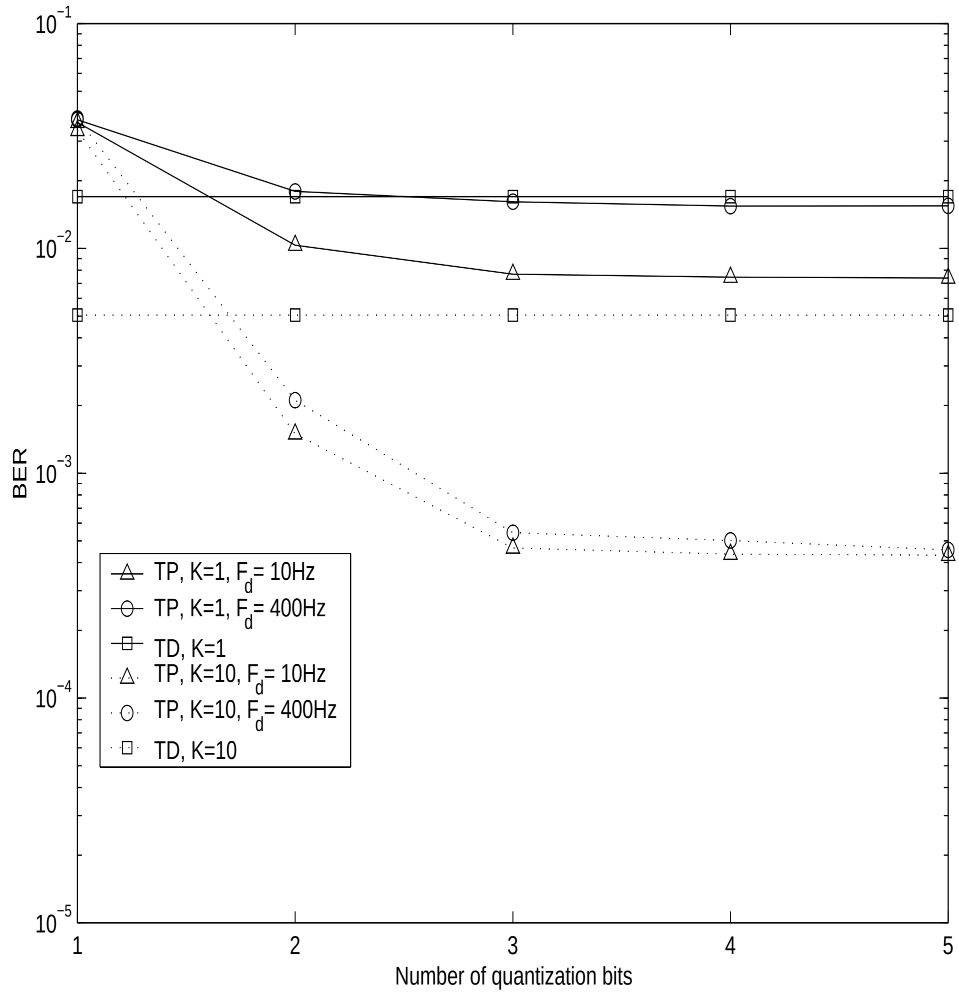

Figure 5.8: Impact of quantization error and feedback error on BER results for various Doppler frequencies F_d (γ_p=6dB, T_f=1/1500 seconds, and $\sigma_a = 3°$).

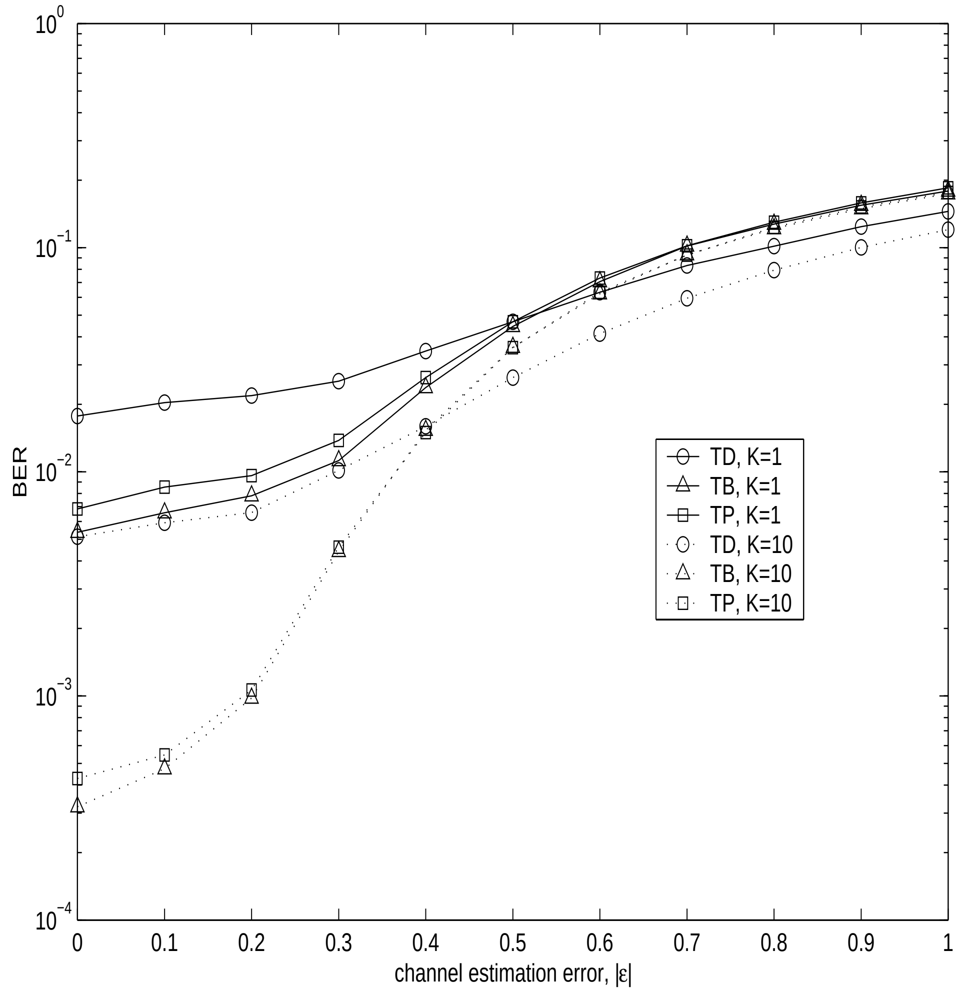

Figure 5.9: Impact of channel estimation on BER results for TD, TB, and TP transmit antenna schemes (γ_p=8dB and $\sigma_a = 20°$).

Chapter 6

Performance of Receive Antenna Arrays

In this chapter, we examine two receive antenna configurations for MIMO reception systems over a Rayleigh fading channel: a uniform circular array (UCA) and a uniform linear array (ULA). We present the comparative diversity performance of UCA and ULA using maximal-ratio-combining in mobile radio communications. Diversity performance is evaluated based on BER results. The analytical BER is derived as function of spatial fading antenna correlation for both types of antenna arrays. In Section 6.1, we describe the applications of various antenna configurations to wireless communications. In Section 6.2, we present the vector channel model for received antenna arrays in a mobile radio environment. The received signal model is given in Section 6.3. We analyze the BER performance of UCA and ULA in mobile radio channels in Section 6.4 and present their analytical and simulated BER results in Section 6.5. A summary is given in Section 6.6.

6.1 UCA and UCA Antenna Configurations

In mobile radio communications, multipath propagation causes signal strength fluctuation, thereby inducing signal fading and distortion. To mitigate these channel impairments, antenna arrays have been widely used in mobile radio communications to improve signal quality, thereby increasing system coverage, capacity, and link quality [1]. Among antenna array configurations, the uniform linear array is probably the most common form employed in cellular and PCS systems. Recently, there has been increased interest in using uniform circular arrays for military applications [41][42]. Thus, in this chapter, we evaluate the performance of the circular antenna array and compare the BER performance of the ULA and UCA in fading channels using diversity array combining.

6.2 Receive Vector Channel Model

Without loss of generality, we consider a 4-element antenna array for both UCA and ULA configurations. Figure 6.1 shows 4-element, uniformly spaced UCA and ULA receiver arrays for the mobile radio environment. For the purpose of this study, we assume a flat Rayleigh fading channel. We simplify the space-time channel model developed in Chapter 2 with the spatial channel model. For the mth receive antenna element, the spatial channel model for the uplink channels can be expressed by (2.43) by removing the temporal components of the equation. That is, the uplink spatial MIMO channel impulse response can be expressed as

$$h_m = \sum_{s=1}^{L_s} \frac{1}{\sqrt{L_s}} v_m(\theta_s) e^{j\psi_s} \tag{6.1}$$

where $v_m(\theta_s)$ is the mth element of the array response vector, and θ_s represents the angle-of-arrival for the sth scattered path. Based on limited field measurement data, the distribution of the AOA at the received base station antenna array is assumed to be a truncated Gaussian AOA distribution, as described in Chapter 2. Note that h_m

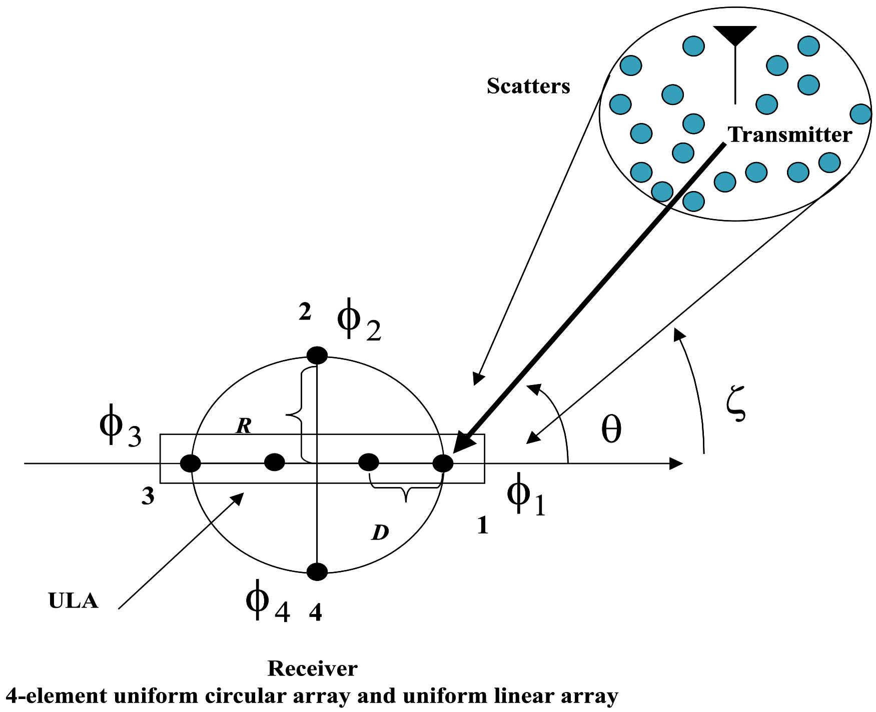

Figure 6.1: 4-element UCA and ULA in mobile radio communications.

become a complex Gaussian random variables when L_s is large. $v_m(\theta_s)$ is a function of antenna element spacing. We define D is the antenna element spacing for a ULA and R is the circular radius of the antenna array for a UCA. Note that $R = 1.5D$ for 4-element UCA-ULA antenna configurations, as shown in Figure 6.1

6.3 Received Signal Model

We consider a single user communicating with a base station over a flat Rayleigh fading channel. The received signal after matched filtering is sampled at the symbol rate $(\frac{1}{T_s})$ at each antenna element. The baseband equivalent received signal on the mth antenna element during the ith symbol at the base station can be expressed as

$$x_m[i] = \sqrt{P_r}\, d[i]\, h_m[i] + n_m[i], \tag{6.2}$$

where $d[i]$ is a QPSK modulated symbol at the ith symbol epoch, P_r is the received power at the antenna, $n_m[i]$ is additive Gaussian noise with variance $2\,\sigma^2$ and $h_m[i]$ is the discrete channel gain resulting from filtering at the symbol rate. The vector form of the complex discrete received signal at the ith epoch thus can be expressed as

$$\mathbf{x}[i] = \sqrt{P_r}\,\mathbf{h}[i]\,d[i] + \mathbf{n}[i], \tag{6.3}$$

where $\mathbf{x}[i]$, $\mathbf{h}[i]$ and $\mathbf{n}[i]$ are $M \times 1$ column vectors. Note that boldface type is used to represent vector quantities. The decision metric for QPSK using MRC combining is

$$y[i] = \mathbf{w}[i]^{\dagger}\mathbf{x}[i], \tag{6.4}$$

where $\mathbf{w}[i]$ is the vector of complex optimum weights and the superscript $\dagger$ denotes the transpose and conjugate. It can be shown that for MRC combining with perfect channel estimation $\mathbf{w}[i]$ is given by [62]

$$\mathbf{w}[i] = \mathbf{h}[i]. \tag{6.5}$$

6.4 BER Analysis for Receive Antenna Arrays

Since the BER of QPSK with gray codings is the same as the BER of BPSK, we only need to consider the in-phased component of the decision statistics. The signal components of $y[i]$ can be treated as M jointly complex Gaussian random variables and is shown as function of a spatial correlation matrix in [63]. In Appendix F, we show that the BER of D-element MRC antenna combining for BPSK can be expressed as function of the eigenvalues of the spatial correlation matrix. Therefore, for the case of $M = D$, the BER can be expressed as

$$P_e = \frac{1}{2}\sum_{\substack{m=1\\ m\neq k}}^{M} \frac{\lambda_m^{M-1}}{\prod_{m\neq k}(\lambda_m - \lambda_k)}\left(1 - \sqrt{\frac{\lambda_m}{1+\lambda_m}}\right), \tag{6.6}$$

where λ_m are the eigenvalues of the spatial correlation matrix $\mathbf{R}_{\mathrm{aa}}$, which can be defined as

$$\mathbf{R}_{\mathrm{aa}} = \gamma_c \mathbf{R}_s, \tag{6.7}$$

where γ_c is the received signal-to-noise ratio per bit, per antenna and $\mathbf{R}_s$ is defined as

$$\mathbf{R}_s = E\{\mathbf{v}(\zeta)\mathbf{v}(\zeta)^\dagger\}, \tag{6.8}$$

The array spatial correlation between the mth and nth antenna element can then be expressed as

$$\begin{aligned} \mathbf{R}_s(m,n) &= E\{v_m(\zeta)v_n(\zeta)^*\} \\ &= \int_\zeta v_m(\zeta)v_n(\zeta)^* f(\zeta)d\zeta, \end{aligned} \tag{6.9}$$

where $f(\zeta)$ is the probability density function of the AOA. In Appendix B, it is shown that for a truncated Gaussian AOA distribution, the real and imaginary parts of $\mathbf{R}_s(m,n)$ for a UCA are expressed by (3.19) and (3.20) respectively. In Appendix D, it is shown that the real and imaginary parts of $\mathbf{R}_{\mathsf{aa}}(m,n)$ for a ULA are expressed by (3.25) and (3.26) respectively.

6.5 Analytical and Simulation Results

Figure 6.2 shows the analytical BER performance of UCA and ULA for various values of angle spread, σ_a, with a radius of $R = 5\lambda$ and for the UCA, and θ is assumed uniformly distributed over $[0,\, 2\pi]$. Note that for a 4-element antenna array the element spacing is $D = \frac{2}{3}R$. As the angle spread σ_a increases, the spatial fading correlation decreases, thus the BER performance improves. It is also seen that the UCA outperforms the ULA *on average* for small and moderate σ_a. The performance is nearly identical for large angle spread.

For verification purposes, simulations were carried out and compared to the analytical BER results in Figure 6.3. The figure shows both analytical and simulation BER performance of the UCA and the ULA for angle spread $\sigma_a = 5°$. It is shown that simulation results provide good agreement with the analytical results. Note that we have presented

BER results averaged over all values of central AOA (θ) since correlation and BER vary with AOA.

Figure 6.4 shows the analytical BER performance of the UCA and the ULA as function of θ (AOA). As shown, the UCA significantly outperforms the ULA at endfire ($\theta = 0°$). However, at central AOA values within 30 degrees of 0 (*i.e.,* broadside of the linear array), the linear array performs similarly to or even better than the UCA. This effect is more pronounced at moderate angle spreads ($\sigma_a = 5°$) where the UCA outperforms the ULA by over an order of magnitude at endfire while the ULA provides an order of magnitude improvement over the UCA at broadside. This variability is due to the fact that the correlation between elements is very large for the ULA when the central angle-of-arrival is near endfire, unless angle spread is very large. This variation correlation has been previously reported in [1][54].

6.6 Summary

In this chapter, we compared the diversity performance of a uniform circular array and a uniform linear array using maximal ratio combining in a mobile radio environment. Diversity performance is evaluated based on BER results. The analytical BER is derived as function antenna correlation for both types of antenna arrays. Results show that for similar aperture size the UCA outperforms the ULA when considering all angles-of-arrival. This is most pronounced for small and moderate angle spread. For angles-of-arrival concentrated near the broadside of the linear array, the ULA typically performs as well as or better than the UCA. A truncated Gaussian angle-of-arrival (AOA) distribution and flat Rayleigh fading were assumed in this chapter. Simulations were carried out to verify the analytical BER results.

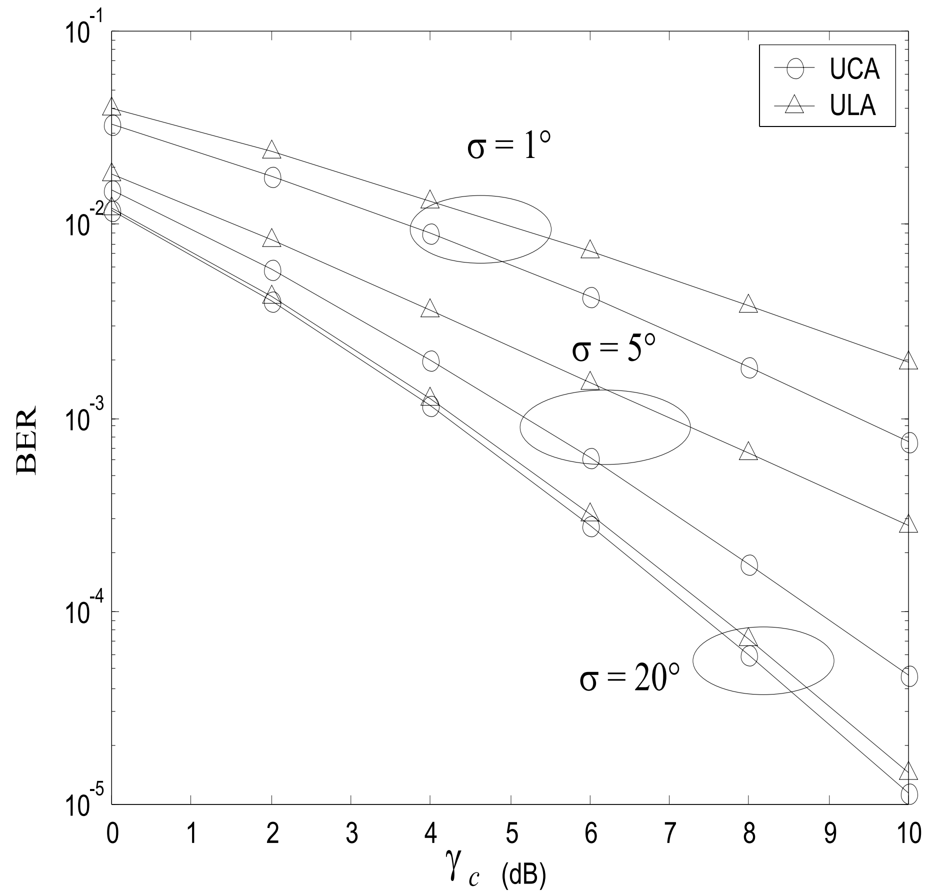

Figure 6.2: Analytical BER performance of UCA and ULA for various angle spread variance σ=σ_a with the circle of radius of $R = 5\lambda$. Note that θ is assumed uniformly distributed over $[0,\, 2\pi]$.

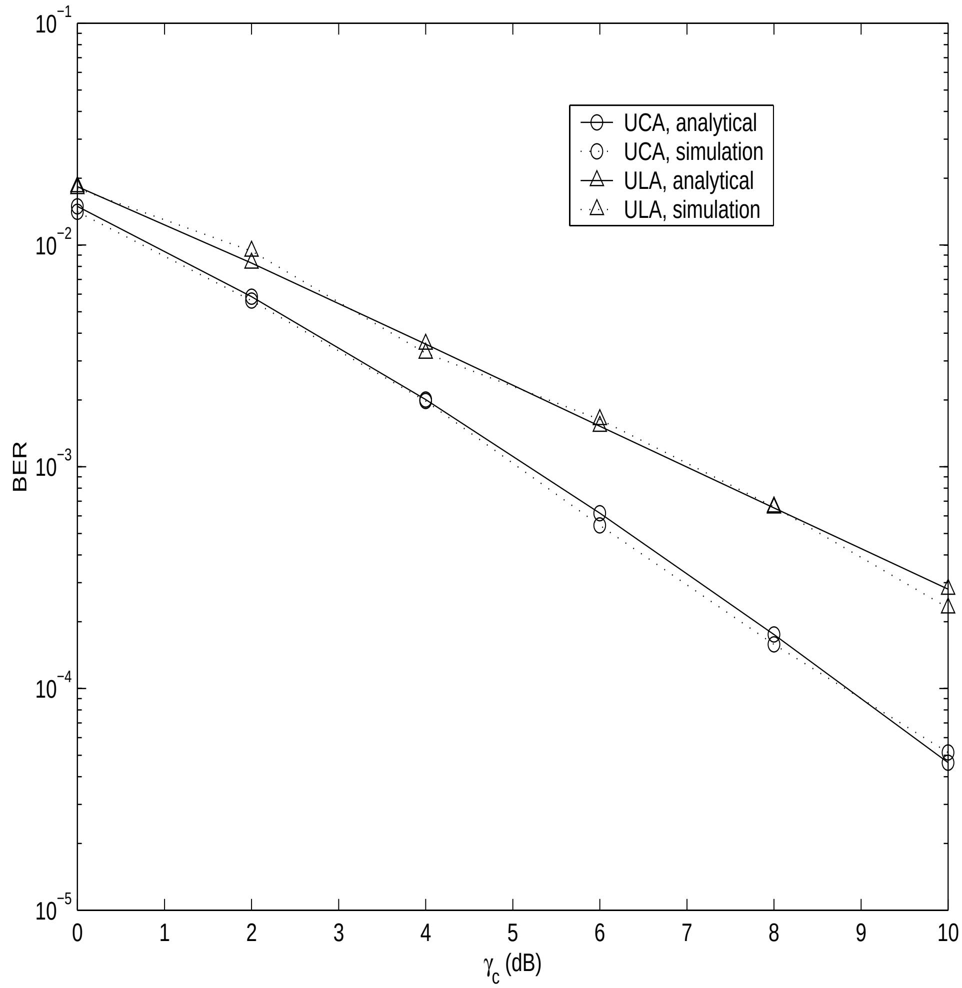

Figure 6.3: Analytical and simulated BER performance of UCA and ULA for angle spread variance $\sigma_a = 5^{\circ}$. Note that θ is assumed uniformly distributed over $[0,\, 2\pi]$.

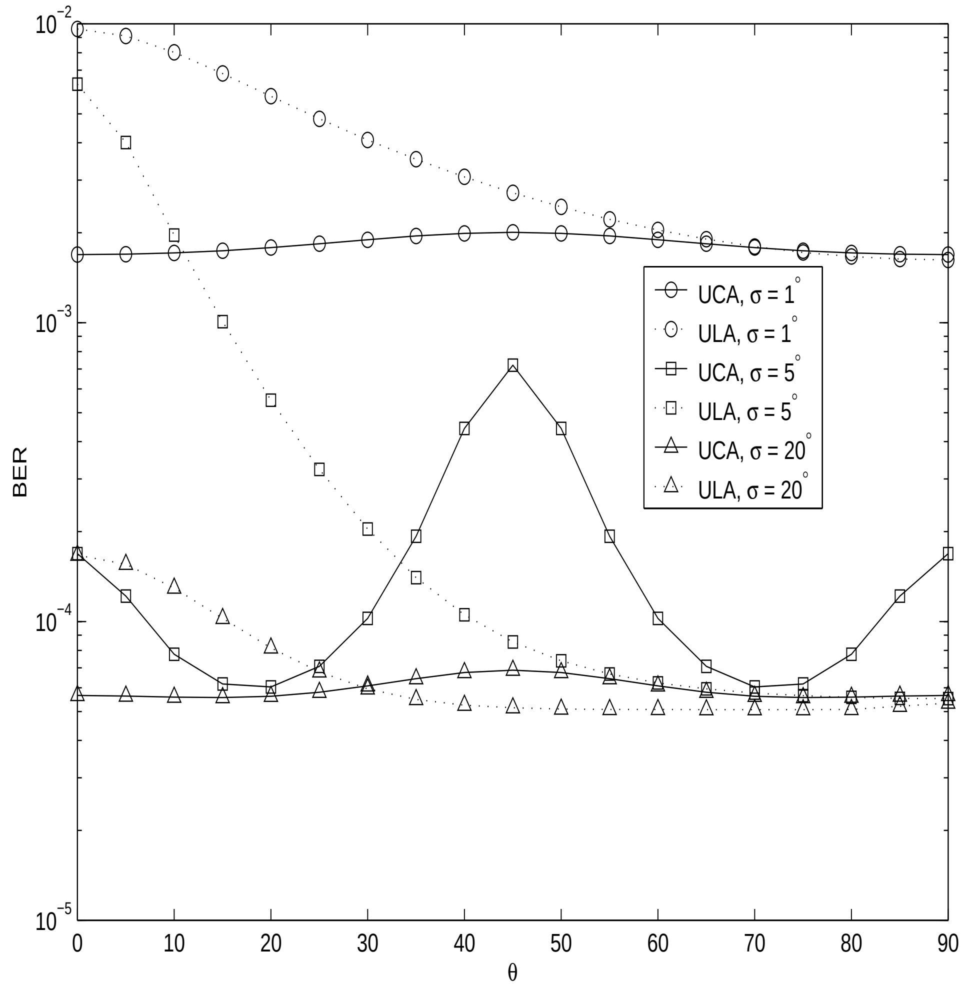

Figure 6.4: Analytical BER performance of UCA and ULA as function of AOA θ.

Chapter 7

Performance of Orthogonal Transmit Waveforms in MIMO Channels

In this chapter, we evaluate the performance of a simple orthogonal transmit waveform that exploits space-time diversity (OTW-STD) in a CDMA cellular environment. The performance of the OTW-STD waveform in a MIMO system is evaluated based on the bit-error-rate (BER) performance for both uplink and downlink communications in a flat Rayleigh fading channel. This chapter is organized as follows. In Section 7.1, we briefly describes the applications of MIMO antenna arrays systems to wireless communications. In Section 7.2, we discuss the principle of the proposed OTW-STD waveform for CDMA systems. In Section 7.3, we present the signal model and transmitter model for the OTW-STD system. We introduce our notation and describe the signal models for both a baseline system and the proposed OTW-STD system. In Section 7.4, we present a statistical MIMO channel model for a mobile radio environment. In Section 7.5, we describe the receiver structure of the proposed OTW-STD system. The BER performance analysis of OTW-STD system is described in Section 7.6. The analytical and simulated BER results of OTW-STD waveform are compared with the baseline system (no diversity) in Section 7.7. The application of OTW-STD waveform to a conventional cellular CDMA scenario is also evaluated as a special case of MIMO systems in Section 7.8. Conclusion remarks are given in Section 7.9.

7.1 Motivation for MIMO Systems

There is much interest in improving the system capacity performance of current cellular and PCS systems. The idea of using multiple transmit and receive antenna systems has been considered as a viable approach to enhance the system capacity. MIMO channels have been shown to provide significant capacity improvement from an information-theoretic perspective [6]. Multiple-transmit-antenna diversity schemes like open-loop transmit diversity and closed-loop transmit beamforming methods have been proposed to enhance the system performance [3][5]. In conjuction with the above transmit diversity schemes, space-time codes have been proposed and examined for practical communication applications [4]. However, as shown in Chapter 5, the closed-loop schemes suffer severely in a high mobility environments. This is particularly pronounced for a Rayleigh fading channel. However, the open loop schemes, while providing less potential gain, are much robust in the presence of high speed fading channels. In [3][59], the open-loop space-time spreading (STS) technique is shown significant performance improvement over closed-loop schemes. However, the above open-loop STS methods provide little gain over the baseline (no diversity) systems in absence of spatial diversity (*i.e.,* small angle spread environment). In [64], we proposed a simple open-loop based orthogonal transmit waveform that exploits both space and time diversity for CDMA downlink systems in small angle spread environment. The result showed that the proposed orthogonal transmit waveform can provide the advantage of temporal diversity over the STS scheme when spatial diversity is not avaliable. In this chapter, we extend our previous work to the case where MIMO channels are considered. We derive an analytical BER formula for evaluating the performance of the OTW-STD scheme in MIMO channels. The BER formula is expressed as function of the eigenvalues of the space-time channel covariance matrix. The analytical space-time channel covariance matrix is derived as a function of channel parameters such as Doppler spread, angle spread, and antenna spacing. We evaluate the BER performance of the OTW-STD scheme in MIMO channels for both uplink and downlink communications in a Rayleigh fading channel.

7.2 Orthogonal Transmit Waveform for MIMO Systems

In this section, we present a simple orthogonal transmit waveform that exploits space-time diversity (OTW-STD) in a CDMA cellular environment. The main idea behind the proposed OTW-STD scheme is to split an original information bit stream into multiple substreams (or branches), where the processing gain of a symbol on each split OTW-STD branch is increased by multiple times over the case without splitting, provided that the spectral efficiency is the same for both cases. We can view the larger processing gain as allowing a data symbol to be repeated multiple times in the time domain. This allows the data symbol to be transmitted on multiple antennas (exploiting spatial diversity) and multiple time slots (exploiting temporal diversity). With proper design of an orthogonal spreading code for each split OTW-STD branch, multiple symbols from different OTW-STD branches can be simultaneously transmitted over a channel without interfering with one another, due to the orthogonality of the spreading codes. Without loss of generality, we consider the number of branches in OTW-STD system to be two and each branch uses QPSK modulation. As shown in Figure 7.1, the information bit stream with the rate of R_b can be split into multiple QPSK branches, where each branch is further split and modulated by an orthogonal spreading code. For a flat fading channel and a single user system, the orthogonal code can be designed such that the number of chips per modulated symbol is equal to the number of transmit branches to ensure orthogonality between transmit branches. For a frequency-selective fading channel and a multiuser system, an orthogonal spreading code needs to covered by a Gold-like scrambling code and the processing gain of a modulated symbol needs to be increased to suppress the multipath interference and multiple access interference (MAI). For comparison purposes, the transmit power, data rate, and system bandwidth for the OTW-STD systems are kept the same as the baseline system.

We consider a single-user DS-CDMA system transmitting over a MIMO Rayleigh flat fading channel. For comparison purposes, the baseline system (no diversity) is assumed to be a single transmit antenna and a single receive antenna for both downlink and uplink communications. For the proposed OTW-STD system, two transmitting antennas and two receiving antennas are employed for both uplink and downlink communications. For a 2×2 MIMO antenna array system, we assume a uniform linear antenna array is used with total antenna spacing of 5 λ at the base station and 1.5 λ at the mobile station, as shown in Figure 7.2. For the OTW-STD systems, since the number of transmit branches of the OTW-STD systems is two, the processing gain for the QPSK symbol on each OTW-STD branch is doubled ($2N_p$) over that of the baseline QPSK symbol. For a given OTW-STD branch, we divide one QPSK symbol with PG $= 2N_p$ into two repeated QPSK symbols with each repeated QPSK symbol having PG $= N_p$. As stated earlier, for a single user and flat fading channel, N_p is equivalent to the number of transmitting branches in order to provide orthogonality between transmitting branches (N_p=2).

7.3 Transmitter Model for OTW-STD Systems

The baseband complex equivalent tranmitted signal for the baseline system can be represented as

$$S_{\mathsf{Base}}(t) = \sum_{i=-\infty}^{\infty} \sqrt{P_t}\, d[i]\, C(t - iT_s), \tag{7.1}$$

where $d[i]$ is a QPSK modulated symbol, T_s is the symbol period, P_t is the transmitted power, and $C(t)$ is the spreading code that can be expressed as

$$C(t) = \sum_{n=-\infty}^{\infty} c_{\mathsf{I}}[n]\, G(t-nT_c) + j \sum_{n=-\infty}^{\infty} c_{\mathsf{Q}}[n]\, G(t-nT_c), \tag{7.2}$$

where $c_{\mathsf{I}}[n]$ is the in-phase component of the spreading sequence, $c_{\mathsf{Q}}[n]$ is the quadrature component of the spreading sequence, $N_p = T_s/T_c$ is the processing gain (PG), T_c is the chip period, and $G(t)$ is the rectangular chip waveform. For the OTW-STD systems, the two repeated QPSK symbols are spread by an orthogonal spreading code and then scrambled by a Gold-like scrambling code, as shown in Figure 7.1. Note that the proposed OTW-STD systems require two orthogonal code per user. For the upper branch transmit signal denoted as $d_A[i]$, the first repeated QPSK symbol is transmitted on antenna A and the second repeated QPSK symbol is transmitted with a delay of N_s symbols on antenna B. Similarly, for the lower branch transmit signal denoted as $d_B[i]$, the first repeated QPSK symbol is transmitted on antenna B and the second repeated QPSK symbol is transmitted with the delay of $N_s/2$ symbols on antenna A. In our analysis, $N_s/2$ can range from 1 to several WCDMA time slot periods, where the time slot period for WCDMA is 2560 chips long. That is, $N_s = N_d\,(2560/N_p)$ and N_d is the number of time slots. For notational clarity, the signal for the OTW system is generated block-by-block. For a given block with a length of N_s symbols long, the complex baseband equivalent tranmitted signals for antenna A and antenna B can be expressed as, respectively

$$S_{\mathsf{A}}(t) = \sum_{i=0}^{N_s/2-1} \sqrt{\frac{P_t}{2}} d_A[i] U_{\mathsf{A,a}}(t-iT_s) + \sum_{i=N_s/2}^{N_s-1} \sqrt{\frac{P_t}{2}} d_B[i-N_s] U_{\mathsf{B,\,b}}(t-(i+\frac{N_s}{2})T_s), \tag{7.3}$$

$$S_{\mathsf{B}}(t) = \sum_{i=0}^{N_s/2-1} \sqrt{\frac{P_t}{2}} d_B[i] U_{\mathsf{B,a}}(t-iT_s) + \sum_{i=N_s/2}^{N_s-1} \sqrt{\frac{P_t}{2}} d_A[i-N_s/2] U_{\mathsf{A,\,b}}(t-(i+\frac{N_s}{2})T_s), \tag{7.4}$$

where

$$U_{\mathsf{A,a}}(t) = U_{\mathsf{A,b}}(t) = O_1(t)C(t), \tag{7.5}$$

$$U_{\mathsf{B,a}}(t) = U_{\mathsf{B,b}}(t) = O_2(t)C(t). \tag{7.6}$$

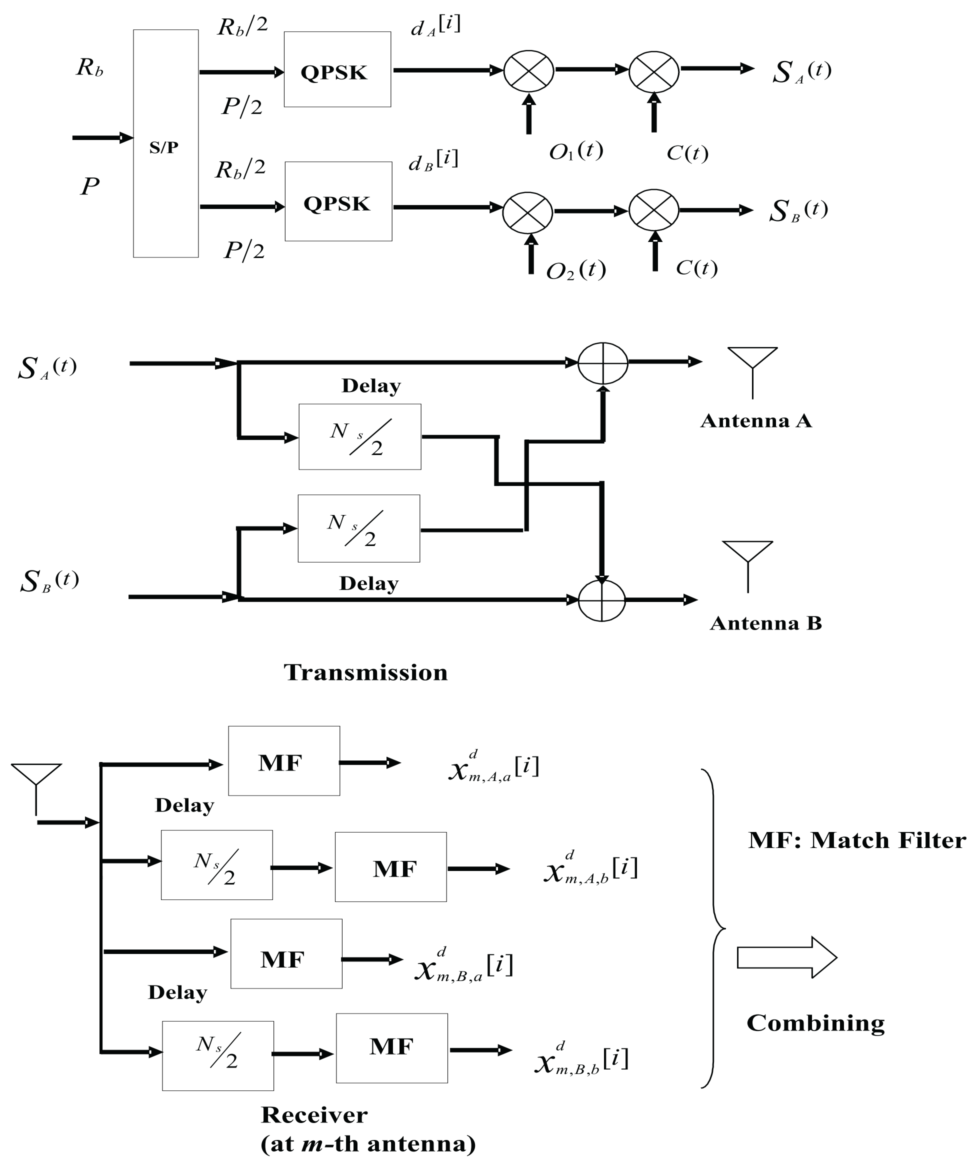

Figure 7.1: System model for the OTW-STD transmission and reception systems.

The subscript a denotes the signal transmitted without delay and the subscript b denotes the signal transmitted with the delay $N_s/2$. $O_1(t)$, $O_2(t)$ are orthogonal spreading codes. They can be expressed as, respectively

$$O_1(t) = \sum_{n=0}^{N_p-1} o_1[n]\mathrm{rect}_T(t - nT_c) + j \sum_{n=0}^{N_p-1} o_1[n]\mathrm{rect}_T(t - nT_c), \tag{7.7}$$

$$O_2(t) = \sum_{n=0}^{N_p-1} o_2[n]\mathrm{rect}_T(t - nT_c) + j \sum_{n=0}^{N_p-1} o_2[n]\mathrm{rect}_T(t - nT_c). \tag{7.8}$$

where $\mathrm{rect}_T(\cdot)$ is the rectangular waveform.

7.4 Statistical MIMO Channel Model

For practical applications, we assume a 2-element transmit and 2-element receive (denoted as 2×2) MIMO antenna array system, as shown in Figure 7.2. Based on the

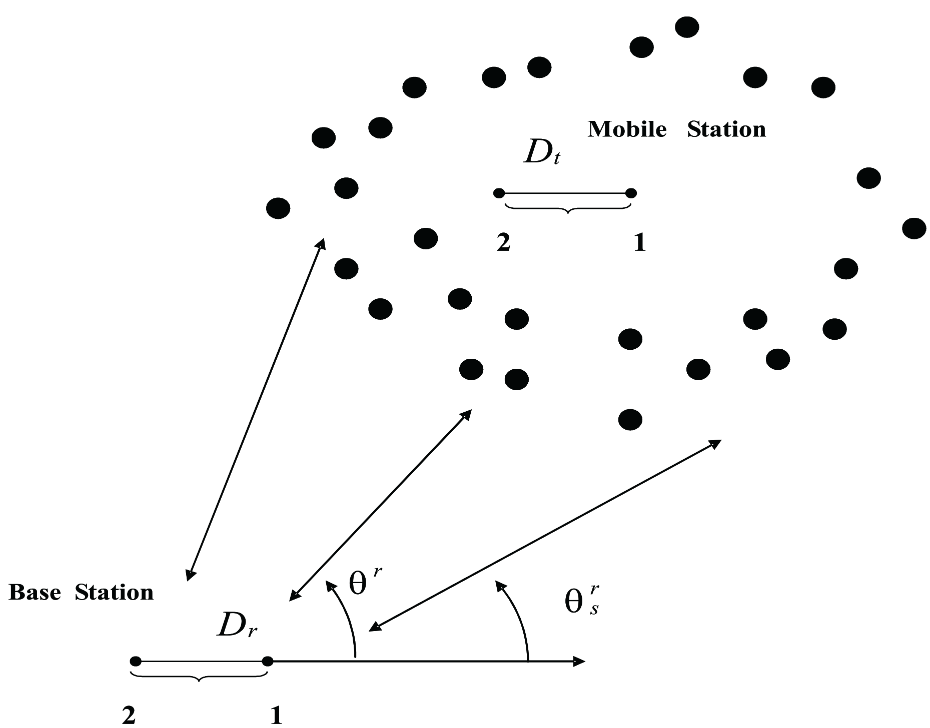

Figure 7.2: Channel model for a 2×2 MIMO system in mobile radio communications.

MIMO channel model developed in Section 2.6, the multipath channel impulse response for the pth transmit antenna at the mth receive antenna element for both downlink and uplink communications can be expressed as, respectively

$$h^d_{m,p}(t;\tau) = \sum_{l=1}^{L} \sqrt{\Gamma_l} h^d_{l,m,p} \delta(t - \tau_l), \tag{7.9}$$

and

$$h^u_{m,p}(t;\tau) = \sum_{l=1}^{L} \sqrt{\Gamma_l} h^u_{l,m,p} \delta(t - \tau_l), \tag{7.10}$$

where the superscript d and u denote the downlink and uplink respectively, and Γ_l is the relative average received power for lth resolvable path. $h^d_{l,m,p}$ and $h^u_{l,m,p}$ are function of antenna element spacing, Doppler frequency, and angle-of-arrival (AOA). They can be expressed as (2.31) and (2.43) respectively. In this chapter, we assume a uniform AOA distribution at the mobile station and a truncated Gaussian AOD distribution at the base station for the downlink channel. For simplicity, we consider the case of a flat fading channel here. Later in this chapter, a frequency-selective fading channel is considered when the application of the OTW-STD systems to a conventional cellular system is evaluated.

7.5 Receiver Model for OTW-STD Systems

For downlink communications, the total received signal with additive white Gaussian noise for the baseline system can be expressed as

$$x^d_{\mathsf{Base}}(t) = S_{\mathsf{Base}}(t)\, h^d_{1,1}(t) + n_w(t), \tag{7.11}$$

where $n_w(t)$ is AWGN with zero mean and two-sided power spectral density given by $N_o/2$. For simplicity, we consider a MIMO Rayleigh flat fading channel. The received signal for the OTW-STD system at the mth received antenna in the downlink can be expressed as

$$x^d_{m,\mathsf{OTW\text{-}STD}}(t) = S_{\mathsf{A}}(t)\, h^d_{m,1}(t) + S_{\mathsf{B}}(t)\, h^d_{m,2}(t) + n_w(t), \tag{7.12}$$

where $h^d_{m,p}(t)$ is the downlink time-varying channel response, as defined in Section 2.6. For the baseline system, the downlink discrete-time form of the received signal after chip matched filter at the ith symbol

$$x^d_{\mathsf{Base}}[i] = \sqrt{P_r}\, h^d_{1,1}[i]\, d[i] + n_w[i]. \tag{7.13}$$

It should be noted that the channels $h^d_{m,p}(t)$ is normalized to unity for the sake of simplicity. P_r is the received power and is equivalent to the transmitted power P_t for a normalized channel. $n_w[i]$ is the white Gaussian noise sample with variance $2\,\sigma^2$. For the OTW system, the reverse operation of transmission system is implemented at the receiver, as shown in Figure 7.1. The discrete-time form of the received signal for the ith symbol at the mth received antenna can be written as

$$x^d_{m,\mathsf{A,a}}[i] = \sqrt{\frac{P_r}{2}}\, h^d_{m,1}[i]\, d_A[i] + n_w[i], \tag{7.14}$$

$$x^d_{m,\mathsf{A,b}}[i] = \sqrt{\frac{P_r}{2}}\, h^d_{m,2}[i + N_s/2]\, d_A[i] + n_w[i], \tag{7.15}$$

$$x^d_{m,\mathsf{B,a}}[i] = \sqrt{\frac{P_r}{2}}\, h^d_{m,2}[i]\, d_B[i] + n_w[i], \tag{7.16}$$

$$x^d_{m,\mathsf{B,b}}[i] = \sqrt{\frac{P_r}{2}}\, h^d_{m,1}[i + N_s/2]\, d_B[i] + n_w[i], \tag{7.17}$$

where $h^d_{m,p}[i]$ is obtained from sampling $h^d_{m,p}(t)$ at the ith symbol period. $x^d_{\mathsf{A,a}}[i]$ and $x^d_{\mathsf{A,b}}[i]$ correspond to the despread received signal for the transmit signal $S_{\mathsf{A}}(t)$ at transmit time a (without delay) and b (with delay $N_s/2$) respectively. Note that due to the channel reciprocity between downlink and uplink channels, the system performance for both links are equivalent for 2×2 MIMO systems. Thus, from this point we only evaluate the BER performance of OTW-STD downlink systems, but similar results can be applied to uplink systems.

7.6 BER Analysis for OTW-STD systems

For BER analysis, we assume the channel information is known to the receiver and a maximal-ratio combining (MRC) scheme is employed for diversity combining. For the baseline system, the decision statistics of the estimated symbol $\widehat{d}[i]$ at the ith symbol for the downlink can be expressed as follow, respectively

$$\widehat{d}[i] = Z^d = x_{\mathsf{Base}}[i]\,(h_1^d[i])^* \tag{7.18}$$

Since the decision statistics of $d_A[i]$ are equivalent to $d_B[i]$ for the OTW system, only the decision statistics of $d_A[i]$ are presented here. The decision statistics of the estimated symbols $\widehat{d_A}[i]$ for the OTW-STD system at the ith symbol can be expressed as

$$Z^d_{\mathsf{A,\ OTW\text{-}STD}} = \sum_{m=1}^{M} x^d_{m,\mathsf{A,a}}[i]\,(h^d_{m,1}[i])^* + x^d_{m,\mathsf{A,b}}[i]\,(h^d_{m,2}[i+N_s/2])^* \tag{7.19}$$

Note that $M = 2$ for 2×2 MIMO systems. With the substitution of (7.14) and (7.15) into (7.19), $Z^d_{\mathsf{A,\ OTW\text{-}STD}}$ can be further expressed as

$$Z^d_{\mathsf{A,\ OTW\text{-}STD}} = \sum_{m=1}^{M} \sqrt{\frac{P_r}{2}} \left\{(h^d_{m,1}[i])^2 + (h^d_{m,2}[i+N_s/2])^2\right\} d_A[i] + N_z[i], \tag{7.20}$$

where $N_z[i]$ is the weighted white noise sample given by

$$N_z[i] = n_w[i] \left\{(h^d_{m,1}[i])^* + (h^d_{m,2}[i+N_s/2])^*\right\}. \tag{7.21}$$

For a flat fading channel, the signal components of $Z^d_{\mathsf{A,\ OTW\text{-}STD}}$ is the combination of $2M$ Gaussian radom variables. Based on [63], it is shown in Appendix F that the BER of D-branch MRC combining for QPSK with gray coding can be expressed as function of the eigenvalues of the space-time covariance matrix. That is,

$$P_e = \frac{1}{2} \sum_{d=1}^{D} \frac{\lambda_d^{D-1}}{\prod_{k \neq d}(\lambda_d - \lambda_k)} \left(1 - \sqrt{\frac{\lambda_d}{1+\lambda_d}}\right) \tag{7.22}$$

where $D = 2M$, and λ_d is the eigenvalue of the space-time covariance matrix $\mathbf{R}_{\mathsf{st,MIMO}}$, which can be defined as

$$\mathbf{R}_{\mathsf{st,MIMO}} = \gamma_c \widetilde{\mathbf{R}}_{\mathsf{st,MIMO}} \tag{7.23}$$

where γ_c is the received signal to noise ratio per bit, per antenna. $\widetilde{\mathbf{R}}_{\mathsf{st,MIMO}}$ is normalization of $\mathbf{R}_{\mathsf{st,MIMO}}$, which can be expressed as

$$\widetilde{\mathbf{R}}_{\mathsf{st,MIMO}} = E\{\mathbf{h}_{\mathsf{MIMO}}(t)\mathbf{h}^{\dagger}_{\mathsf{MIMO}}(t+\nu)\}, \tag{7.24}$$

where $\dagger$ denotes the operation of complex conjugate and transpose, and $\mathbf{h}_{\mathsf{MIMO}}(t)$ is the channel vector, which can be expressed as

$$\mathbf{h}_{\mathsf{MIMO}}(t) = [h_{1,1}(t)\, h_{1,2}(t) \cdots h_{m,1}(t)\, h_{m,2}(t) \cdots h_{M,2}(t)]^T, \tag{7.25}$$

where $(.)^T$ denotes transpose operation, the size of $\widetilde{\mathbf{R}}_{\mathsf{st,MIMO}}$ is $2M \times 2M$. Note that the entry of $\widetilde{\mathbf{R}}_{\mathsf{st,MIMO}}$ can be evaluated analytically, as shown in Chapter 3.

7.7 Analytical and Simulation Results

In this section, we present the BER results of OTW-STD for a MIMO Rayleigh channel. The CDMA system uses the Walsh codes as orthogonal codes and a Gold code as a spreading code $C(t)$. The processing gain N_p is 2 for a flat fading channel. For comparison, we define γ_p as the ratio of the average transmitted power per bit over the average receiver noise power per bit and per received antenna, so that

$$\gamma_p = \frac{P_r}{2\sigma^2} = \frac{P_t}{2\sigma^2}. \tag{7.26}$$

Note that $\gamma_p = \gamma_c$ with MRC combining in a flat fading channel. Figure 7.3 shows comparative BER results of OTW systems and the baseline (no diversity) system for various angle spread environments. As shown, the analytical BER has good agreement with the simulation BER for OTW systems. It is also observed that the OTW system significantly outperforms the system with no diversity as angle spread σ_a increases. Figure 7.4 shows the comparative BER results for OTW-STD systems and the baseline system in a small angle spread environment (*i.e.,* in the absence of transmit spatial diversity). It is shown that the analytical BER shows a good agreement with the simulated BER for OTW systems, and that the OTW system can provide additional temporal diversity improvement over the baseline system as Doppler spread increases. Figure 7.5 shows the effects of AOA and antenna spacing at a base station on the BER performance of the OTW systems. As shown, BER performance improves as antenna spacing D_r increases for a fixed AOA (θ_r). It is also observed that the BER result occuring at $\theta_r = 90°$ (broadside) is better than the result for the case of $\theta_r = 0°$ (endfire). Figure 7.6 shows the effect of delay on the BER performance of temporal diversity. When the Doppler spread is low, temporal diversity can be obtained as the delay time N_d increases. It is also seen that the BER results improve as N_d increases for a fixed Doppler frequency.

7.8 Application of OTW-STD

In this section, we consider the application of a OTW-STD waveform to a conventional cellular CDMA scenario as a special case of MIMO OTW-STD systems. For a cellular scenario, two antennas are employed at the base station and one antenna employed at the mobile station for transmission and reception. Both downlink and uplink communications are evaluated. We consider two transmit antennas and one receive antenna on the downlink and one transmit antenna and two receive antennas on the uplink. Since there are two transmit antennas on the downlink, the size of $\widetilde{\mathbf{R}}_{\mathsf{st,MIMO}}$ is reduced to 2×2. The two eigenvalues of $\mathbf{R}_{\mathsf{st,MIMO}}$ on the downlink can further be expressed as

$$\lambda_1 = \gamma_c(1 + |\rho_{st}(\nu, 11, 12)|), \tag{7.27}$$

$$\lambda_2 = \gamma_c(1 - |\rho_{st}(\nu, 11, 12)|), \tag{7.28}$$

where $\rho_{st}(\nu, 11, 12)$ can be evaluated analytically, as shown in Chapter 3. Similarly, since there are two receive antenna on the uplink, the two eigenvalues of $\mathbf{R}_{\mathsf{st,MIMO}}$ at the uplink can be further expressed as

$$\lambda_1 = \gamma_c(1 + |\rho_{st}(\nu, 11, 21)|), \tag{7.29}$$

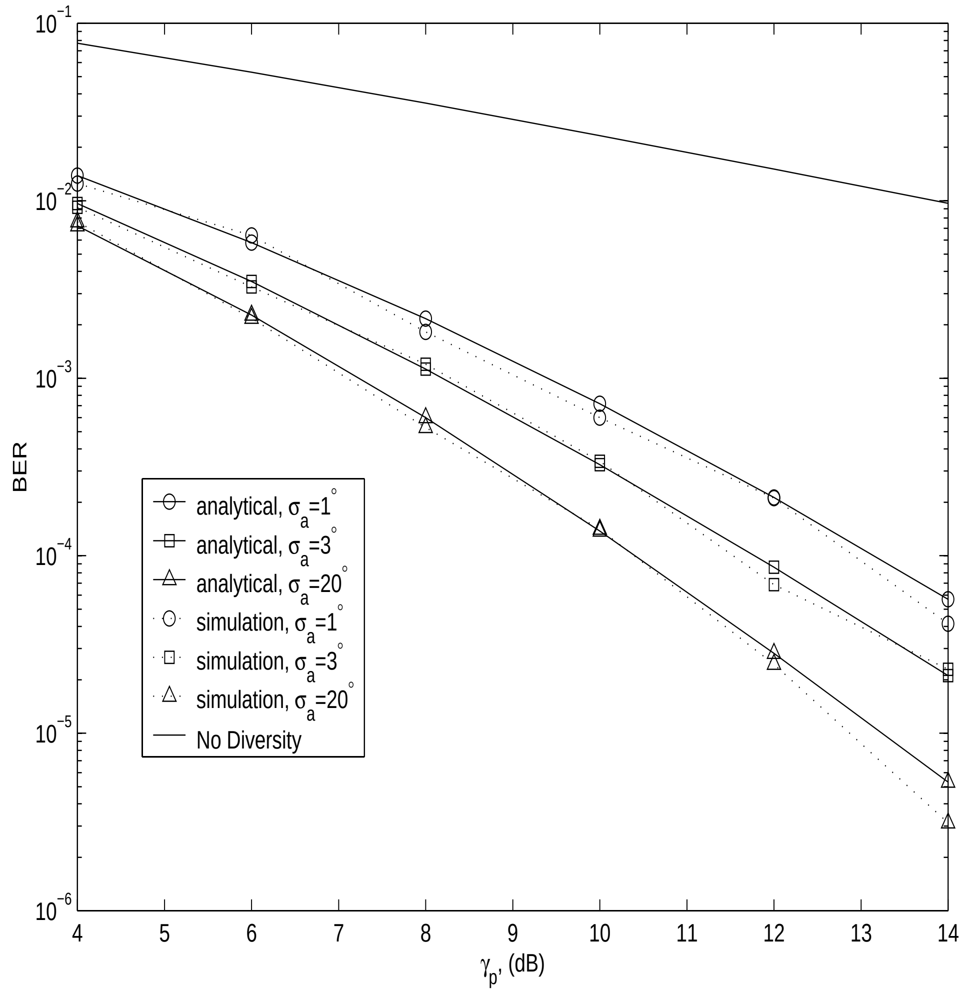

Figure 7.3: Comparative BER results of OTW (2×2) systems and the baseline (no diversity) system for various angle spread environments $(F_d = 100Hz)$.

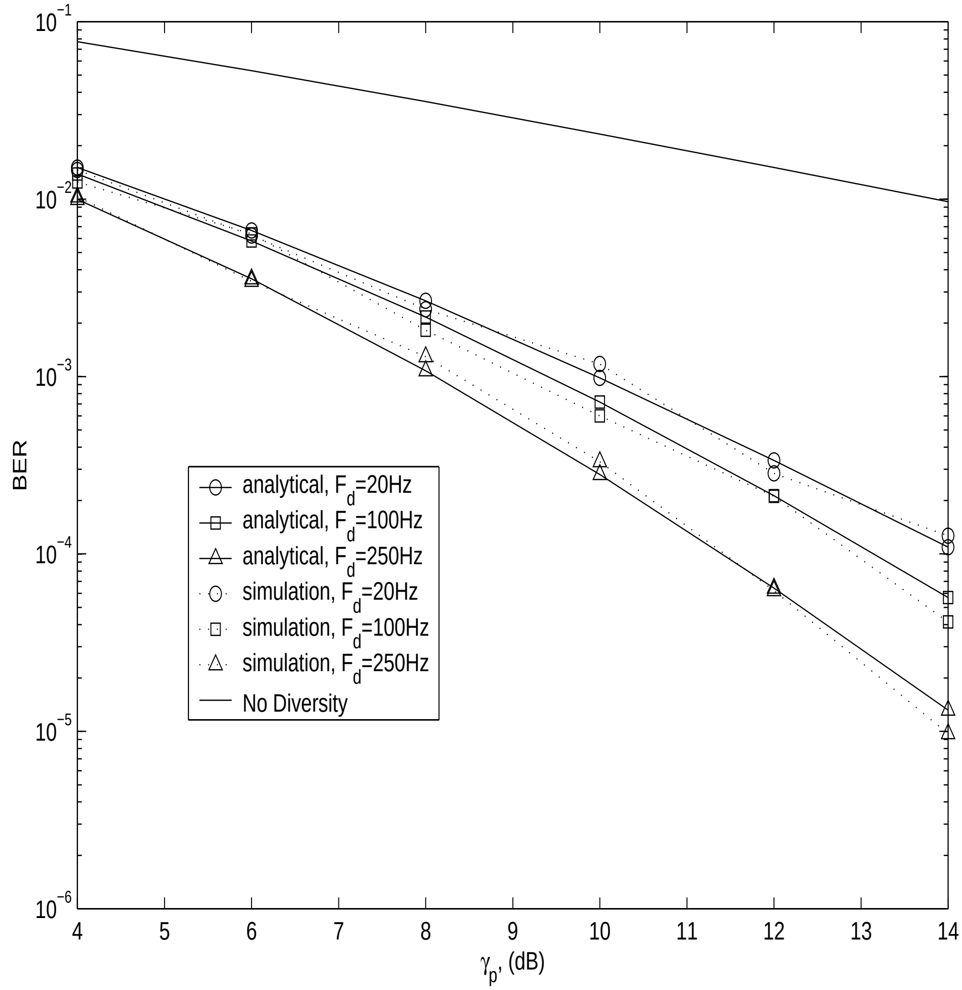

Figure 7.4: Comparative BER results of OTW (2×2) systems and the baseline (no diversity) system in a small angle spread environment ($\sigma_a = 1°$)

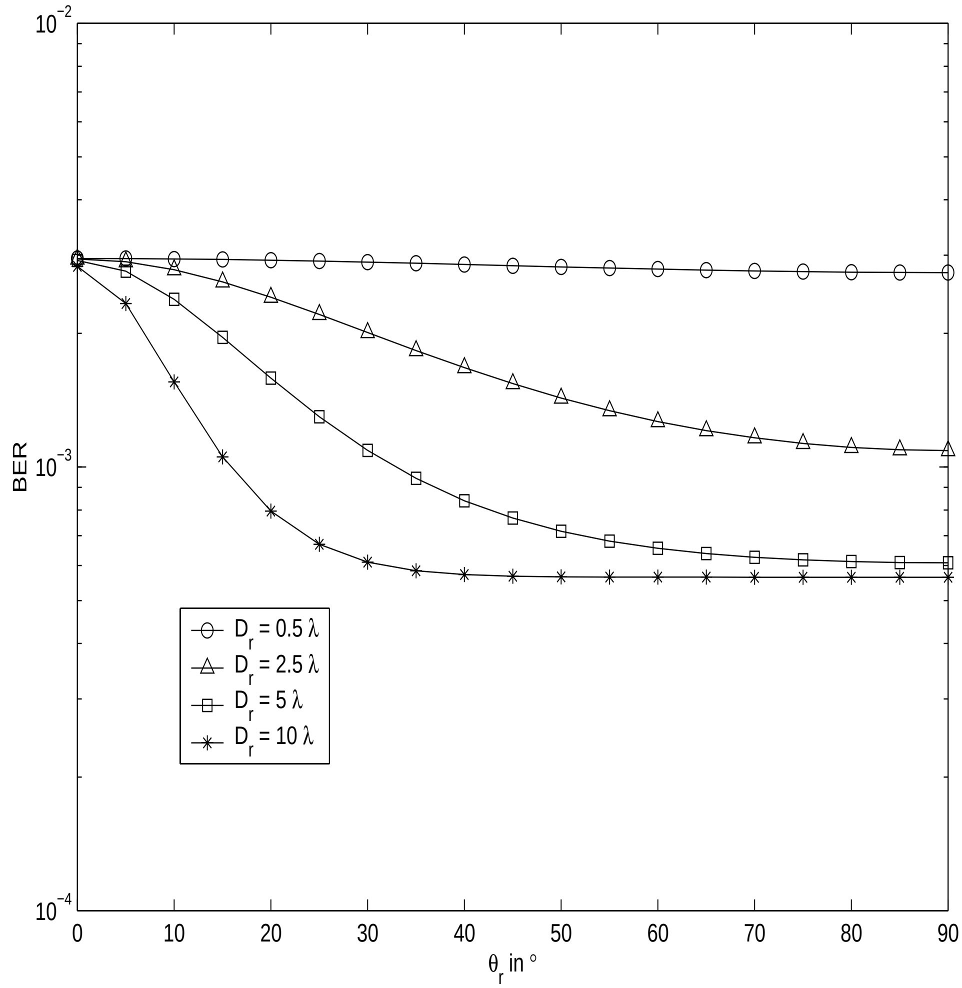

Figure 7.5: The effects of AOA and antenna spacing at a base station on the BER performance of the OTW (2×2) systems ($\sigma_a = 3°$ and $F_d = 100Hz$)

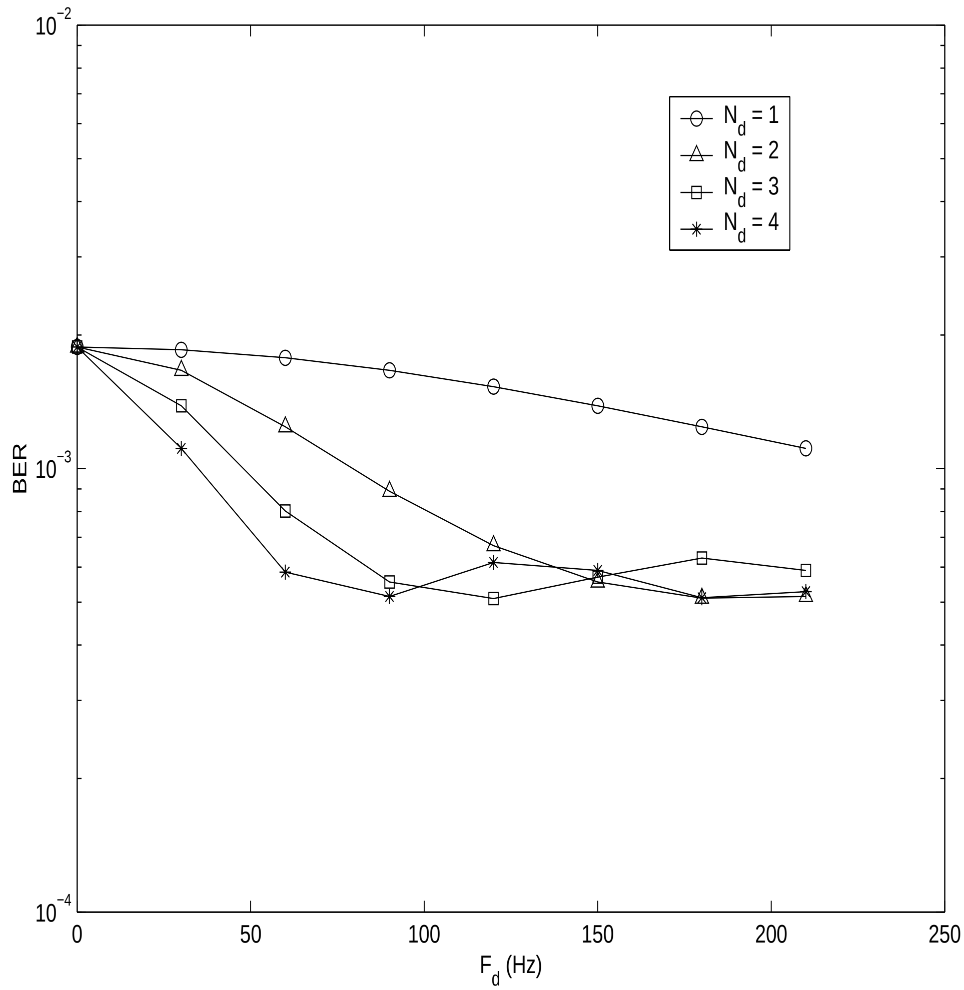

Figure 7.6: The effects of delay time on the BER results of the OTW (2×2) systems system in a small angle spread environment. Note that N_d is the number of delay slots. ($\sigma_a = 1°$).

$$\lambda_2 = \gamma_c(1 - |\rho_{st}(\nu, 11, 21)|). \tag{7.30}$$

Figure 7.7 shows the downlink analytical and simulated BER results of the baseline and OTW systems for angle spread $\sigma_a = 20°$ and Doppler spread $F_d = 120Hz$. As shown, for the case of flat fading ($L = 1$), the analytical BER has a good agreement with the simulation BER for both the baseline and OTW systems. It is also observed that the OTW system outperforms the baseline system for both the case of frequency-selective fading ($L = 2$) and the base of flat fading ($L = 1$) due to the transmit spatial diversity. In a small angle spread and a high mobility cellular environment (*i.e.,* lack of transmit spatial diversity, but significant temporal diversity), Figure 7.8 shows that the OTW system can provide a temporal diversity improvement over both the baseline (no diversity) system, and the BER improves as the Doppler frequency increases. It is also shown that in absence of transmit spatial diversity, the proposed OTW-STD outperform STS systems. For uplink communications, Figure 7.9 shows that the OTW system using two received antenna elements ($M = 2$) exhibits improved BER over the baseline system using four received antenna elements ($M = 4$) in a small angle spread and high mobility cellular environment. Note that the total antenna spacing is equivalent for both cases of $M = 2$ and $M = 4$ (*i.e.,* 5λ corresponding to a fixed physical dimension for the antenna system).

7.9 Summary

In this chapter, we derived an analytical BER formula for evaluating the performance of a proposed OTW-STD system in a MIMO Rayleigh fading channel. The analytical BER formula for the OTW-STD waveform is derived as a function of the eigenvalues of the space-time channel covariance matrix. The space-time channel correlation is function of angle spread and Doppler frequency for a mobile radio channel. The results show that the OTW system can fully exploit the spatial and temporal diversity of mobile radio channels and provide significant performance improvement over systems

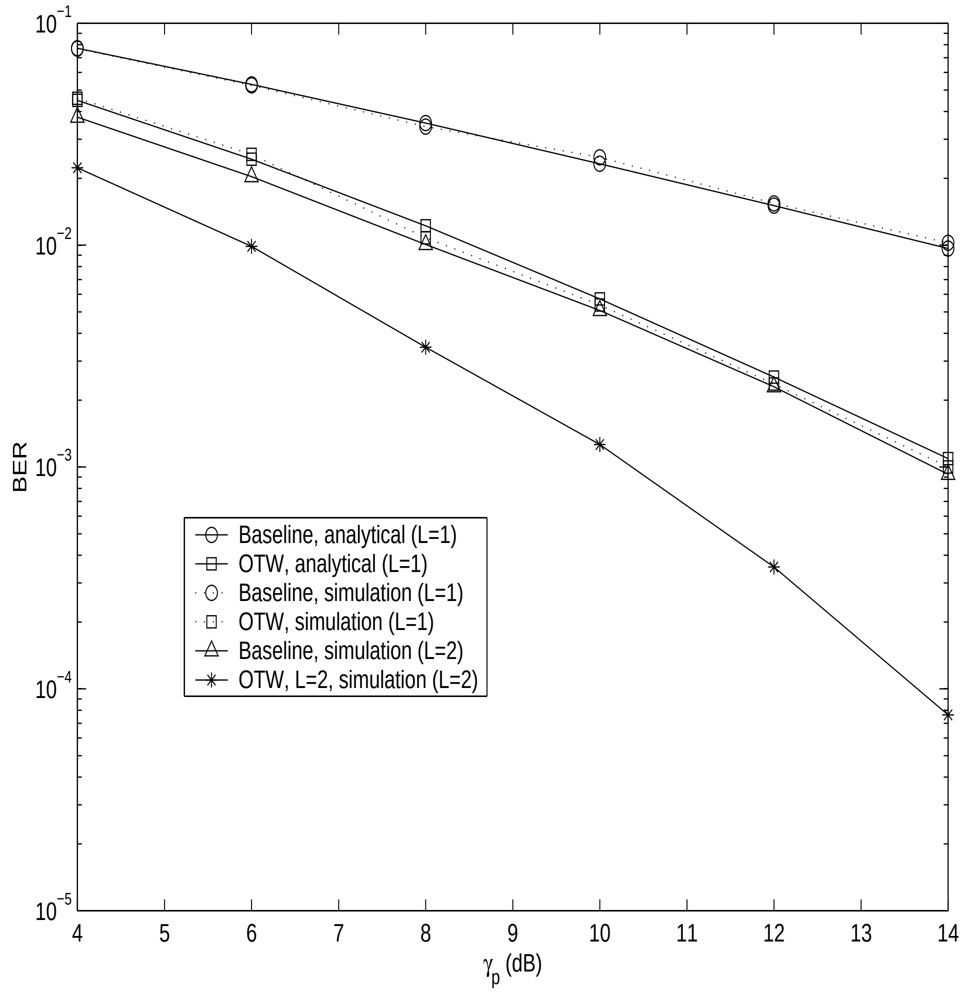

Figure 7.7: Comparative BER results of the baseline and OTW (2TX-1RX) systems for $\sigma_a = 20^\circ$ ($N_d = 1$).

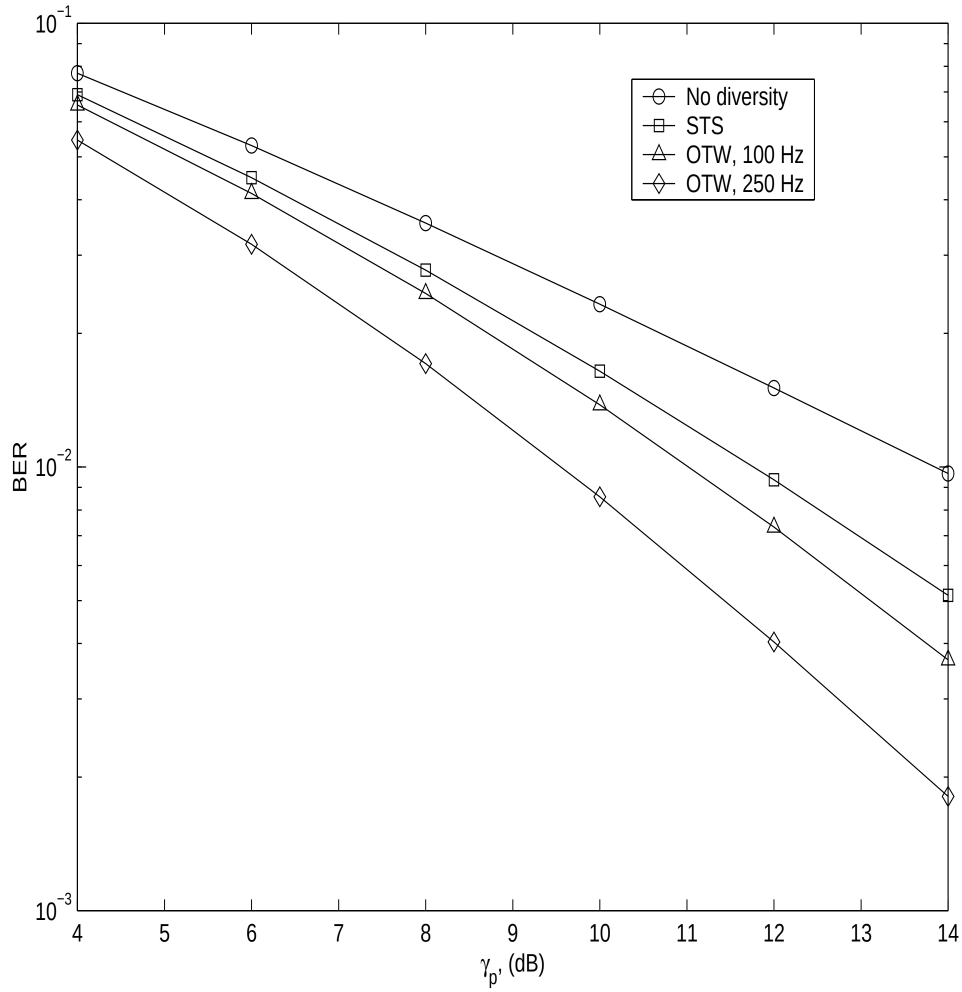

Figure 7.8: Analytical BER results of the OTW (2TX-1RX) system for various Doppler frequencies ($F_d = 100Hz$, $\sigma_a = 1^\circ$ and $N_d = 1$).

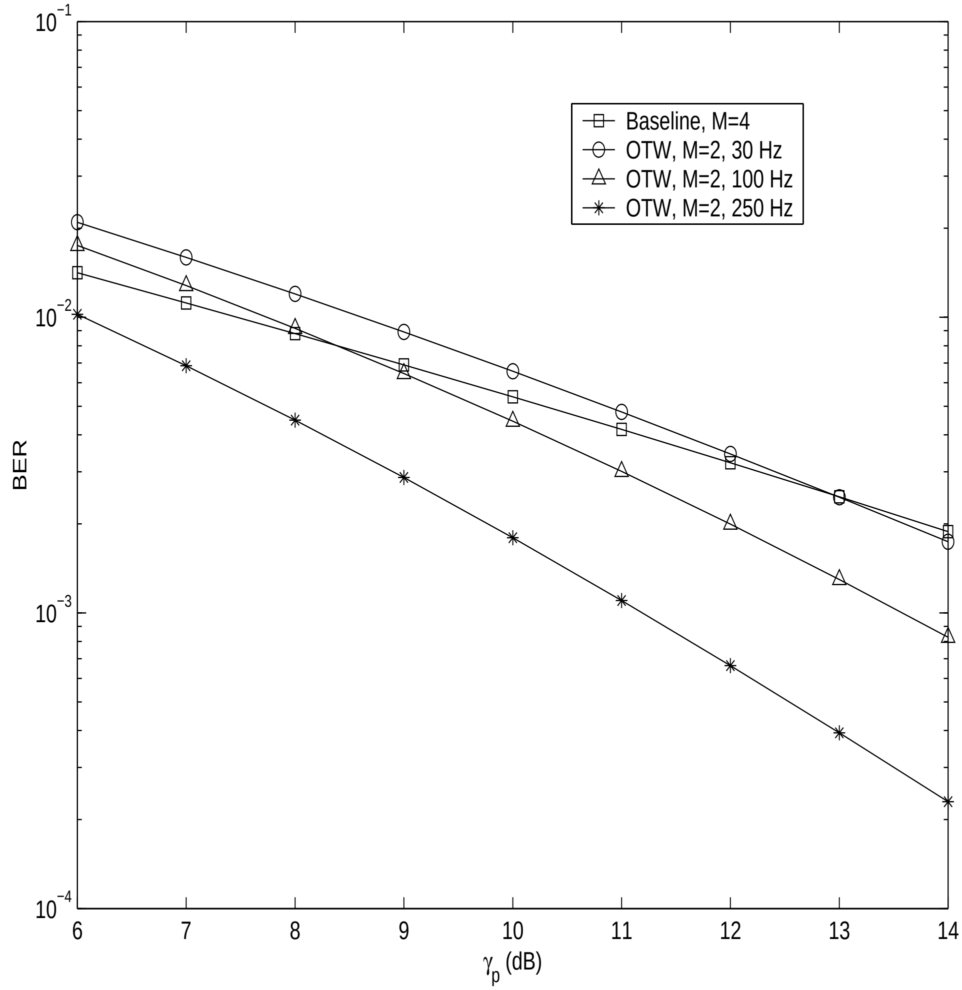

Figure 7.9: Comparative analytical BER results of the OTW (1TX-2RX) systems for various Doppler spread. Note that the baseline is 1TX-4RX system. ($F_d = 100Hz$, $\sigma_a = 1^\circ$ and $N_d = 1$).

without diversity. In addition, it is shown that the effects of system parameters such as AOA, antenna spacing, delay time have a great impact on the BER performance of the proposed OTW-STD system. Finally, the application of OTW-STD waveform to a conventional cellular CDMA scenario is considered. It is shown that in absence of transmit spatial diversity, the proposed OTW-STD outperform STS systems. The result suggests that the OTW-STD waveform is better-suited for high mobility and small angle spread environment.

Chapter 8

Survey of Multiuser Receiver and Adaptive Antenna Arrays

In this chapter, we survey two active ongoing research areas on signal processing techniques in wireless communications, namely multiuser detection systems and smart antenna systems (or adaptive antenna array systems). We begin with the principles and fundamentals of signal detection techniques for multiuser detection systems. We discuss the features of both optimum multiuser receivers and various suboptimum multiuser receivers. Later, we investigate various optimization criterion for adaptive antenna array combining techniques. The practical issues on the implementation of adaptive antenna array combining algorithms are discussed.

8.1 Multiuser Receivers

A communication receiver generally can be divided into two major classes. The first is the conventional single-user receiver. The other is the multiuser receiver. The fundamental difference between these two types of receivers is that multiuser receivers not only exploit the decision statistics of the desired user, but also those of the interfering signals. To utilize the additional information of the interfering signals at the receiver, the concept of multiuser detection is introduced. The basic idea of multiuser detection is first to demodulate all of the active users in the system, and then try to make use of the interference information to reduce the effects of the interference from other users. This can be accomplished by joint detection techniques, adaptive interference suppression techniques, or subtractive interference cancelation techniques [31][32][33]. Although in principle multiuser detection can be applied to both CDMA (wideband signal) systems as well as TDMA (narrowband signal) systems, most of work in the past decade focus wireless CDMA systems. This is because wireless CDMA capacity significantly suffers from the near-far problem due to imperfect power control, and multiuser detection techniques can provide near-far resistance to enhance system capacity. Hence, we will primarily review the multiuser detection techniques that have developed for wireless CDMA systems. For the readers interested in applying multiuser detection to TDMA systems, references [65][66][67] provide a comprehensive description on this area.

8.2 System Model for a Multiuser Receiver

To facilitate the discussion of the multiuser receiver structure presented here, we provide a mathematical model of the CDMA system under consideration. We consider a DS-CDMA wireless communication system with K asynchronous users. The baseband complex equivalent transmitted signal of user k can be represented as

$$S_k(t) = \sum_{i=-\infty}^{\infty} \sqrt{P_k} e^{j\Phi_{0,k}} d_k[i] C_k(t - iT_s - \mu_k), \tag{8.1}$$

where $d_k[i]$ is a modulated symbol, T_s is the symbol period, P_k is the transmitted power, μ_k is the random delay due to asynchronous transmission, $\Phi_{0,k}$ is a uniformly distributed random phase angle on $[0, 2\pi]$, and $C_k(t)$ is the spreading code for user k. $C_k(t)$ can be expressed as

$$C_k(t) = \sum_{n=-\infty}^{\infty} c_{\mathsf{I},k}[n] G_r(t - nT_c) + j \sum_{n=-\infty}^{\infty} c_{\mathsf{Q},k}[n] G_r(t - nT_c), \tag{8.2}$$

where $c_{\mathsf{I},k}[n]$ is in-phase component of the spreading sequence, $c_{\mathsf{Q},k}[n]$ is quadrature component of the spreading sequence, $N_p = T_s/T_c$ is the processing gain, T_c is the chip period, and $G_r(t)$ is the chip waveform and can be expressed as

$$G_r(t) = \mathrm{rect}_T(t) = \begin{cases} 1 & : \quad 0 \le t \le T_c \\ 0 & : \quad \text{otherwise} \end{cases} \tag{8.3}$$

where $\mathrm{rect}_T(\cdot)$ is the rectangular waveform. The total received signal is the superposition of the signal from K users plus the additive white noise. The baseband equivalent received signal can be expressed as

$$x(t) = \sum_{k=1}^{K} S_k(t) \star h_k(t;\tau) + N_w(t), \tag{8.4}$$

where the symbol $\star$ represents the convolution operation and the channel impulse response $h_k(t;\tau)$ is normalized to unity for ease of analysis. For the sake of discussion, we assume an AWGN channel (*i.e.*, $h_k(t;\tau) = \delta(t)$). Thus the received signal can be simply expressed as

$$x(t) = \sum_{k=1}^{K} S_k(t) + N_w(t), \tag{8.5}$$

where $N_w(t)$ is AWGN with zero mean and two-sided power spectral density given by $N_0/2$. Often it is desirable to represent the baseband received signal after despreading. After a filter matched to the kth user's spreading waveform over a period of symbol T_s, the despread output at ith symbol interval can be represented as

$$x_k[i] = \int_{(i-1)T_s+\mu_k}^{iT_s+\mu_k} x(t) C_k(t - iT_s - \mu_k)\, dt. \tag{8.6}$$

Figure 8.1 shows a block diagram of a generic multiuser receiver. For the purposes of analysis, a vector representation of the matched filter outputs at ith symbol interval can be expressed as

$$\mathbf{x}[i] = \mathbf{R}_c(-1)\mathbf{W}_{p,i-1}\mathbf{d}_{i-1} + \mathbf{R}_c(0)\mathbf{W}_{p,i}\mathbf{d}_i + \mathbf{R}_c(1)\mathbf{W}_{p,i+1}\mathbf{d}_{i+1} + \mathbf{N}_{w,i} \tag{8.7}$$

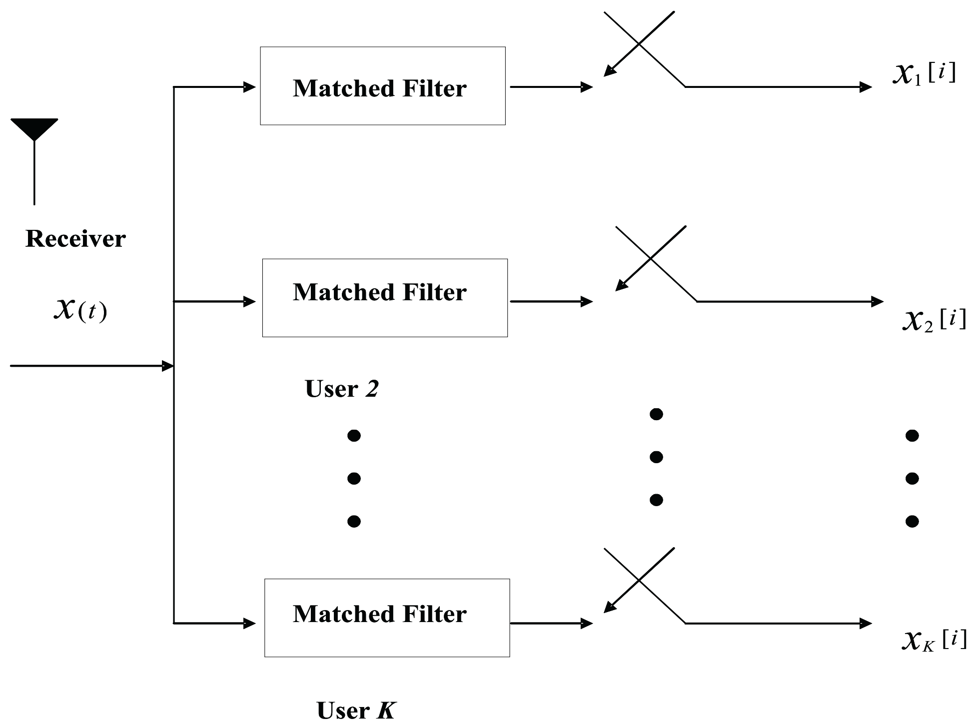

Figure 8.1: A block diagram of multiuser receivers

where

$$\mathbf{x}[i] = \Big[x_1[i], x_2[i], \cdots, x_K[i]\Big]^T \tag{8.8}$$

and $\mathbf{R}_c(i)$ is a K x K matrix which represents the partial correlation between users over the ith relative symbol interval. The elements of $\mathbf{R}_c(i)$ at the jth row and the kth column is given as

$$\mathbf{R}_{c,j,k} = \int_{\mu_j}^{T_s+\mu_j} C_j(t-\mu_j)C_k(t-iT_s-\mu_k)\,dt, \tag{8.9}$$

$\mathbf{W}_{p,i} = \mathbf{W}_p[i]$ is the a diagonal matrix with diagonal elements $\sqrt{w_{p,i,1}}$, $\sqrt{w_{p,i,2}}$, $\cdots$, $\sqrt{w_{p,i,K}}$. $\sqrt{w_{p,i,k}}$ can be expressed as

$$\sqrt{w_{p,i,k}} = \sqrt{P_{i,k}}T_s \tag{8.10}$$

$\mathbf{d}[i]$ and $\mathbf{N}_{w,i}$ can be expressed as follows, respectively

$$\mathbf{d}[i] = \Big[d_1[i], d_2[i], \cdots, d_K[i]\Big]^T, \tag{8.11}$$

$$\mathbf{N}_w[i] = \Big[n_{w,1}[i], n_{w,2}[i], \cdots, n_{w,K}[i]\Big]^T, \tag{8.12}$$

where T denotes the transpose operation. If a sequence of N_b data symbols is observed from each of K users, the observed sequence of the matched filter outputs can be represented by

$$\mathbf{x} = \mathcal{R}_c \mathcal{W}_p \mathbf{d} + \mathbf{N}_w, \tag{8.13}$$

where $\mathbf{x}$, $\mathbf{d}$, and $\mathbf{N}_w$ can be represented as follows, respectively.

$$\mathbf{x} = \Big[\mathbf{x}[1], \mathbf{x}[2], \cdots, \mathbf{x}[N_b]\Big]^T, \tag{8.14}$$

$$\mathbf{d} = \Big[\mathbf{d}[1], \mathbf{d}[2], \cdots, \mathbf{d}[N_b]\Big]^T, \tag{8.15}$$

$$\mathbf{N}_w = \Big[\mathbf{N}_w[1], \mathbf{N}_w[2], \cdots, \mathbf{N}_w[N_b]\Big]^T, \tag{8.16}$$

$\mathcal{W}_p$ is a KN_b x KN_b diagonal matrix with the diagonal elements $\mathbf{W}_p[1]$,$\mathbf{W}_p[2]$, $\cdots$,$\mathbf{W}_p[N_b]$ and $\mathcal{R}_c$ can be expressed as

$$\begin{pmatrix} \mathbf{R}_c(0) & \mathbf{R}_c(-1) & 0 & \cdots & \cdots & 0 \\ \mathbf{R}_c(1) & \mathbf{R}_c(0) & \mathbf{R}_c(-1) & \cdots & \cdots & 0 \\ 0 & \mathbf{R}_c(1) & \mathbf{R}_c(0) & \cdots & \cdots & 0 \\ \vdots & & \ddots & \ddots & & \vdots \\ 0 & \cdots & & & & \mathbf{R}_c(-1) \\ 0 & \cdots & & & \mathbf{R}_c(-1) & \mathbf{R}_c(0) \end{pmatrix} \tag{8.17}$$

Based on the system model developed in this section, we will discuss various multiuser receiver structures that have significant impact on CDMA system performance in the following sections. To put various multiuser receivers into perspective, Figure 8.2 lists a summary of CDMA receivers. As shown, multiuser receivers can be divided into two major classes: *optimal multiuser receivers* and *sub-optimal multiuser receivers*. The principle of optimal multiuser receivers is based on the maximum likelihood sequence estimation while the idea of sub-optimal multiuser receivers is based on interference suppression or interference subtraction. In general, the sub-optimal multiuser receivers with interference suppression is known as linear multiuser receivers. On the other hand, the sub-optimal multiuser receivers with interference subtraction is known as non-linear sub-optimal multiuser receivers. Based on the optimization criterion, the linear multiuser receivers can be further divided into two types of multiuser receivers: *decorrelators* and MMSE multiuser receivers. Based on the interference cancelation process, the non-linear sub-optimal multiuser receivers, on the other hand, can be divided into two types of multiuser receivers:*parallel interference cancelation receivers (PIC)* and *successive interference cancelation receivers (SIC)*. In the next sections, we discuss each of the major classes of multiuser receivers shown in the figure.

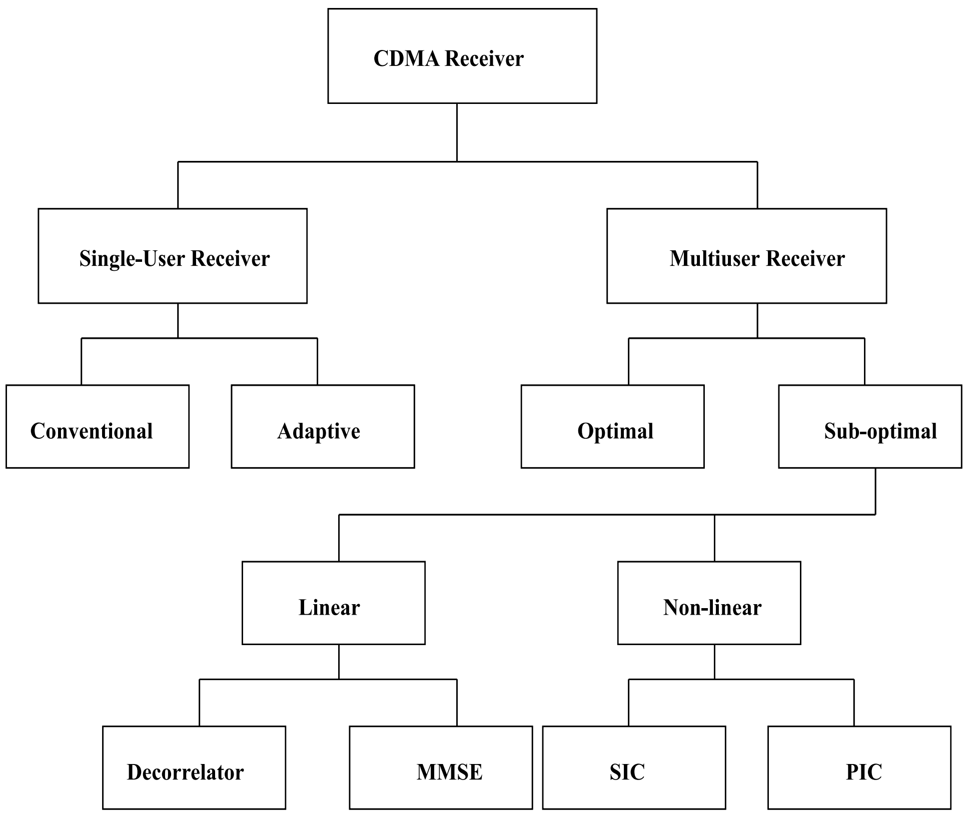

Figure 8.2: Summary of CDMA receivers

8.3 Optimum Multiuser Receivers

For the sake of discussion, the result developed in the following is based on AWGN channel conditions. However, it can be extended into the fading channels as well. Based on the works in [68][31], Verdu developed a more comprehensive mathematical model for multiuser detection with the importance case of the asynchronous channel [32]. The optimal multiuser receiver developed in [32][31] is based on the maximum likelihood sequence detection criteria. The joint posteriori probability we desire to maximize for maximum likelihood sequence detection is expressed as

$$P[\mathbf{d}|x(t)]. \tag{8.18}$$

where $x(t)$ and $\mathbf{d}$ are defined in (8.4) and (8.11), respectively. With the assumption of all input symbols being equally likely, this is equivalent to maximizing

$$P[x(t)|\mathbf{d}]. \tag{8.19}$$

The desired data vector $\mathbf{d}$ based on this maximization can be obtained by

$$\mathbf{d} = \text{argmax}\Big[\exp(\Omega(\mathbf{d})/2\sigma^2)\Big], \tag{8.20}$$

where $\Omega(\mathbf{d})$ is given by

$$\Omega(\mathbf{d}) = 2\int_{-\infty}^{\infty} S(\mathbf{d})x(t)\,dt - \int_{-\infty}^{\infty} S^2(\mathbf{d})\,dt, \tag{8.21}$$

where $S(\mathbf{d})$ is the matrix of all K user's transmitted signals. With the decomposition in (8.20), we can treat the estimation of $\mathbf{d}$ as a maximum likelihood decoding problem for a single user. The estimation of $\mathbf{d}$ in (8.20) using maximum likelihood criterion can be implemented by the Viterbi algorithm. Figure 8.3 shows the optimal receiver structure for CDMA systems. One important consideration in multiuser detection is the computational complexity. Although the optimal multiuser receiver provides significant performance enhancement and near-far resistance, it has the drawback of exponential complexity in terms of the number of users. This limits its userfulness for practical

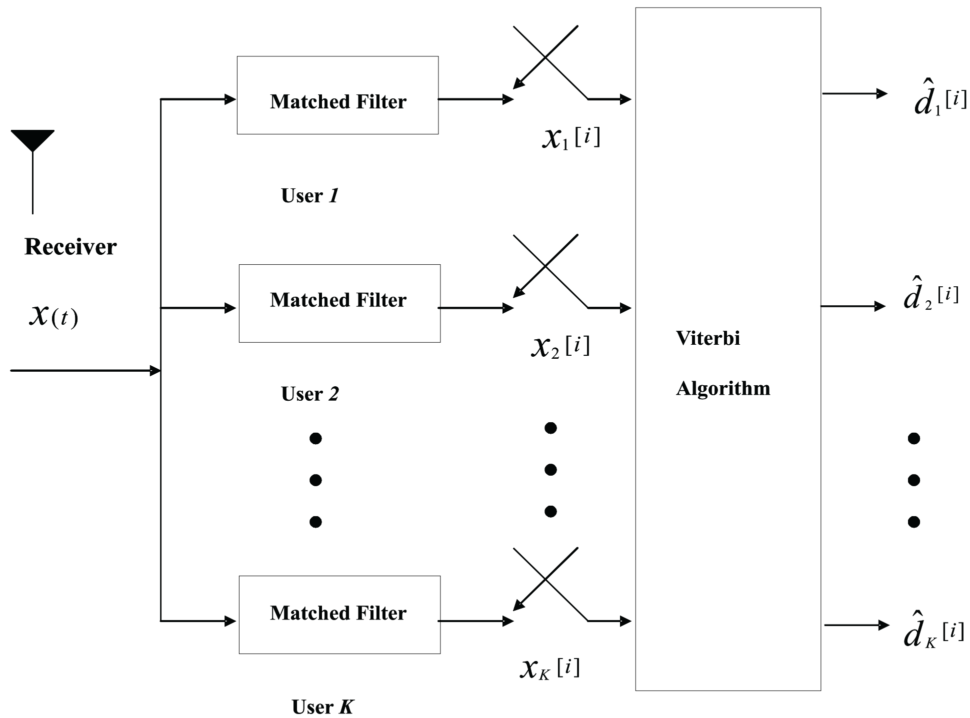

Figure 8.3: CDMA optimum receivers

applications. Extensive work on reducing the computational complexity of optimum multiuser receivers was presented in [69][70]. The theory of combining optimum multiuser detection with channel decoding techniques has been developed in [71][72][73]. To reduce the complexity of the optimum multiuser receiver, several sub-optimal solutions have been proposed in the past decade [74][75]. These sub-optimal receivers in general substantially improve the system performance over conventional single-user receiver with a reasonable increas in complexity.

8.4 Sub-optimum Multiuser Receivers

There are two main classes of sub-optimal multiuser receivers, linear sub-optimal multiuser receivers, and non-linear sub-optimal multiuser receivers. Based on the optimization criterion, the linear multiuser receivers can be divided into two types of linear multiuser receivers: *decorrelators* and *MMSE receivers* [76][75][77]. The non-linear multiuser receivers are also known as decision-oriented multiuser receivers. The principle of the non-linear multiuser receivers are to subtract the interference from the received signal such that the residual signal is essentially free of interference. This type of multiuser receiver is also known as subtractive interference cancelation receivers. There are two main approaches to subtractive interference cancelation receivers: *successive interference cancelation (SIC)* and *parallel interference cancelation (PIC)* [78][79][80]. From an interference reduction point of view, the principle of the linear multiuser receivers is to suppress the interference from the received signal based on the optimization criterion while the principle of the non-linear multiuser receivers is to directly cancel the undesired interference from the received signal. In the following sections, we review these four sub-optimal multiuser receivers.

8.4.1 Decorrelators

The decorrelator was first developed by Lupas in [74][76] for both synchronous and asynchronous channels. We consider the asynchronous case here. Figure 8.4 shows a block diagram of the decorrelating receiver. As shown, the estimate of data vector $\widehat{\mathbf{d}}$ can be obtained by the linear transformation of the set of decision statistics given in (8.13). That is,

$$\widehat{\mathbf{d}} = \mathbf{T}\mathbf{x}, \tag{8.22}$$

where the linear operator $\mathbf{T}$ can be shown as

$$\mathbf{T} = \mathcal{R}_c^{-1}. \tag{8.23}$$

By substituting $\mathbf{x}$ defined in (8.13) and $\mathbf{T}$ defined in (8.23) into (8.22), $\widehat{\mathbf{d}}$ can be rewritten as

$$\widehat{\mathbf{d}} = \mathcal{W}_p\mathbf{d} + \mathcal{R}_c^{-1}\mathbf{N}_w. \tag{8.24}$$

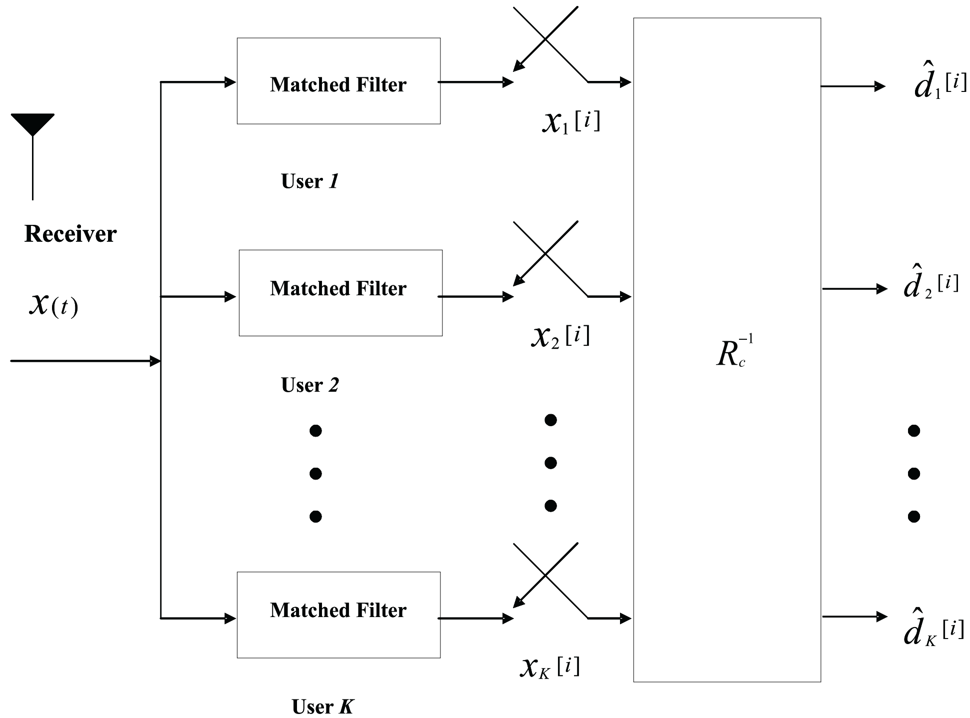

Figure 8.4: CDMA Decorrelator receivers

By observing (8.24), it is seen that the solution of estimating **d** requires to calculate the inverse matrix of $\mathcal{R}_c$ and to estimate the timing of each user along with knowledge of spreading waveforms. However, it does not require the knowledge of the users' received signal energies; thus inherently it provides near-far resistance [76]. Extensive work on this type of multiuser receivers on various fading channel conditions has been done, as reported in [81][82][83]. In addition, work considering noncoherent modulation is given in [84][85]. There are, however, two main disadvantages of this receiver. The first is the need to calculate the inverse matrix of $\mathcal{R}_c$. This is generally quite computationally intensive when the number of users is large. The second is the noise enhancement problem. As seen in (8.22), the noise component $\mathbf{N}_w$ can be enhanced by $\mathcal{R}_c^{-1}$ when signal-to-noise ratio (SNR) is low. This is similar to the situation in channel equalization when zero-forcing algorithm is employed for the ISI channel [34].

8.4.2 MMSE Multiuser Receivers

As mentioned in the previous section, the decorrelator in principle is very similar to the zero-forcing equalizer. Ideally, the optimization criterion of the decorrelator leads to complete elimination of all of the interference. However, since the received SNR for CDMA systems is generally very low at receivers, the decorrelator can result in noise enhancement problem on signal detection. To remedy this problem, the optimization criterion based on the MMSE was proposed [86][75][87]. The MMSE optimization criterion can be formulated as follows

$$\min_{\mathsf{T}} J = E\{(\widehat{\mathbf{d}} - \mathbf{d})^*(\widehat{\mathbf{d}} - \mathbf{d})\}, \tag{8.25}$$

where $\widehat{\mathbf{d}} = \mathbf{Tx}$, as defined in (8.22). For the MMSE criteria, the linear transformation $\mathbf{T}$ can be shown as [75]

$$\mathbf{T} = \left(\mathcal{R}_c + \frac{N_o}{2\mathcal{W}_p^2}\right)^{-1}. \tag{8.26}$$

Thus, the estimate of $\mathbf{d}$ is given by

$$\widehat{\mathbf{d}} = \left(\mathcal{R}_c + \frac{N_o}{2\mathcal{W}_p^2}\right)^{-1}\mathbf{x}. \tag{8.27}$$

It is shown that the performance of this receiver is upper-bounded by the decorrelator [34]. As seen in (8.26), the linear transformation $\mathbf{T}$ reduces to $\mathcal{R}_c^{-1}$ as in the case of a decorrelating receiver, when $N_o \simeq 0$. That is, the performance of MMSE receivers is identical to the decorrelating receivers when SNR is high. On the other hand, when N_o is extremely large, the linear transformation $\mathbf{T}$ becomes a diagonal matrix with each diagonal element corresponding to each user's SNR, then MMSE receivers reduce to the conventional receiver. Based on the above discussion, the operation of the MMSE receivers can be viewed as striking a balance between interference suppression and noise enhancement. Figure 8.5 shows a block diagram of the CDMA MMSE receivers. Like the decorrelator, the MMSE receiver achieves optimal near-far resistance, but requires the knowledge of the users' received signal energies. From an implementation point of view, the MMSE receiver lends itself well to adaptive implementation. The BER

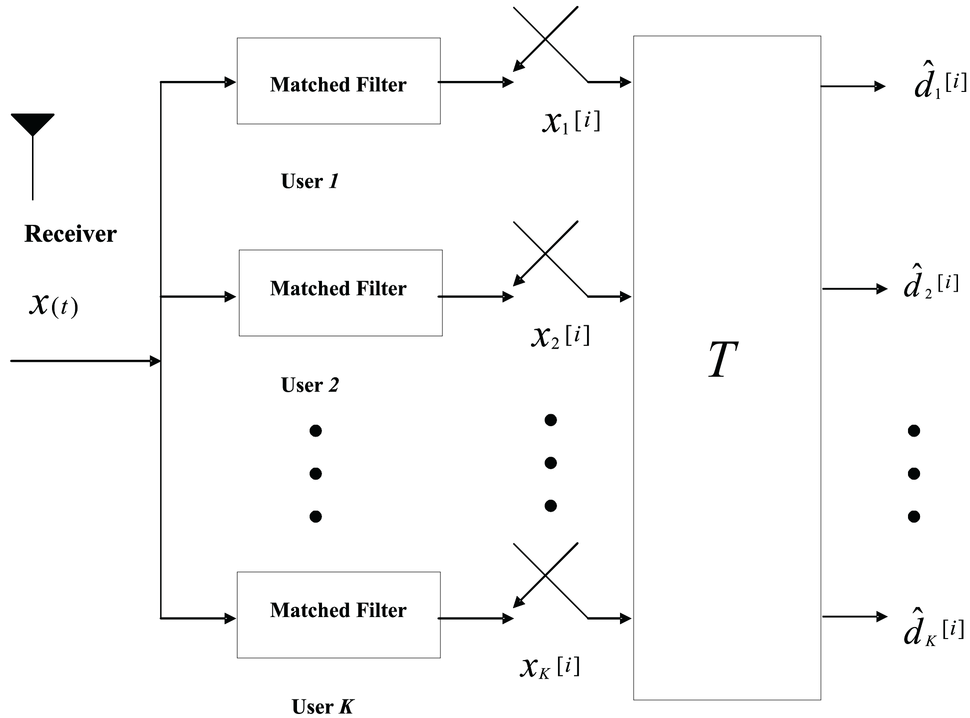

Figure 8.5: CDMA MMSE receivers

expression for the MMSE multiuser receiver is analyzed in [88]. The performance of the MMSE multiuser receivers in conjuction with a power control scheme was evaluated in [89]. Some elaborate solutions have been proposed to deal with the fading channels [90][91][92].

8.4.3 Successive Interference Cancelation Receivers

The successive interference cancelation receiver was first proposed by Viterbi [93]. The idea of the successive interference cancelation approach is that if the decision of a strong user's symbol has been made, then the strong user's signal can be regenerated at the receiver and subtracted from the received signal $x(t)$. After the subtraction process is completed, the residual signal would contain less interference, and this subtraction process can be repeated with the other users until the weakest user has been detected.

The key to ensure the success of the repeated subtraction process is the power variation among all the users. It is suggested that some degree of power variation is quite beneficial for this type of receivers [80]. However, if the dynamic range of power variation level is quite large, the weak users may not be able to estimate its symbol properly due the noise and the residue interference. A block diagram of successive interference cancelation receivers is shown in Figure 8.6. The BER analysis for successive interference cancelation

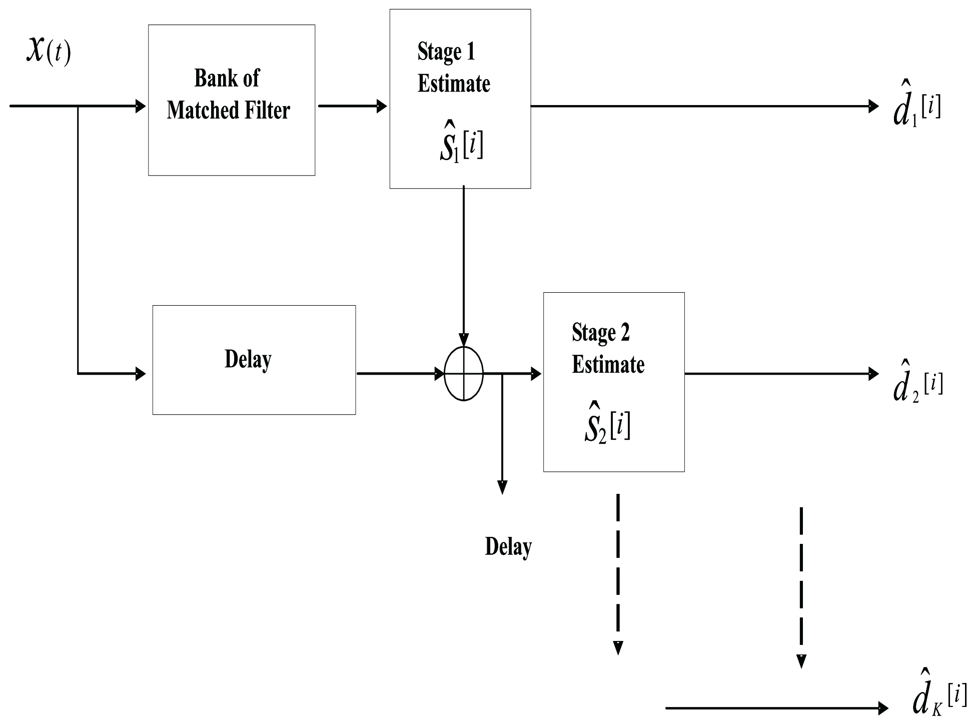

Figure 8.6: CDMA SIC receivers

receivers was developed by Patel and Holtzman [80]. The analysis of successive interference cancelation was extended in [94][95] by dealing with practical implementation issues as well as multipath fading. In general, the performance of successive interference cancelation is dominated by the estimates of the received signal energies of each user.

Several features of successive interference cancelation receivers are listed as follows.

- Successive interference cancelation can be applied to any multiple access channel where the received signal is the superposition of the transmitted signals.

- Successive interference cancelation works effectively when power variation between each step of cancelation is about 6 to 10 dB.
- Successive interference cancelation inherently possess a latency problem as the number of users in the system increases.
- Successive interference cancelation requires the knowledge of the received signal energies. Any error decision made in the current subtraction process translate into the residue interference for the following detection process.

In this research, we have exploited the above features of successive interference cancelation by jointly combining with adaptive antenna array techniques for an overloaded arrays environment.

8.4.4 Parallel Interference Cancelation Receivers

A similar approach to successive interference cancelation discussed above is called parallel interference cancelation. The difference between these two types of interference cancelation is two fold. First, the decisions made on the initial matched filter outputs are tentative for parallel interference cancelation, but are final for successive interference cancelation. Secondly, the users' symbols are estimated in a parallel manner for parallel interference cancelation, but in a successive manner for successive interference cancelation. Parallel interference cancelation receivers are also known as *multistage receivers*. The BER analysis for parallel interference cancelation receivers using correlator was developed by Varanasi and Azahang [78]. An extensive work based on [78] was presented in [96]. An adaptive filtering based approach was presented in [97]. The analysis of parallel interference cancelation was extended in [98][99] by dealing with practical implementation issues as well as multipath fading.

In parallel interference cancelation, there are situations where the cancelation of specific users does not enhance the performance, but actually degrades the performance. This is due to the poor cancellation of the weak users. In fact, it is shown that the higher the interference power level, the better the estimates of its data symbol, signal energies, and timing. This results in negligible interference contribution to other users [100]. It is observed that parallel interference cancelation is somewhat sensitive to the estimation of the data symbols, the users' signal energies, delay, and timing mismatch [101][102].

It should be noted that the reliability of the initial stage estimates for parallel interference cancelation is extremely critical. The unreliable estimates can introduce additional interference and hence actually degrade performance. It is suggested that the use of coding techniques can significantly improve the reliability of the estimates [103].

One of the key issues is the decision bias problem. The bias is introduced in the decision statistics due to the composite effects of imperfect estimation and high users' cross-correlation. This problem can be mitigated by partial parallel interference approach [104].

Finally, it is important to note that generally parallel interference cancelation perform well for the situation where the users' received power levels are relatively uniform, while the successive interference cancelation work more effectively for the situation where the users' received power levels vary greatly. The combining adaptive antenna and multiuser receivers have been shown that the significant performance gain can be achieved at the expense of increased complexity [36][37][38][105][106]. We will discuss the adaptive antenna array system in the following section.

8.5 Background on Adaptive Antenna Arrays

As compared to the multiuser detection which is a temporal-domain signal processing approach, adaptive antenna array combining, on the other hand, can be viewed as spatial-domain signal processing approach. In wireless communications, the adaptive antenna array system can be used to suppress cochannel interference, to provide signal diversity or a combination of both [107][28][29][108].

Depending on the channel conditions, the application of adaptive antenna array systems can be divided into two main classes: phased arrays and diversity arrays. The use of phased arrays is generally based on the following assumptions [109].

- The incoming signals are plane waves.
- The antenna array has an equal interelement spacing less than one-half wavelength.
- The antenna array is composed of identical elements.

However, in mobile wireless communications, the channel suffers from multipath fading as discussed in Chapter 2. This requires diversity arrays. The use of diversity arrays relies on the fact that the above assumptions are violated to provide diversity against fading. In the following section, we present a system model of adaptive antenna array systems, then discuss various optimization criterion for both phased arrays and diversity arrays.

8.6 System Model for Adaptive Antenna Arrays

We consider a wireless communication system where K asynchronous users' signals are received at a receiver employing an M-element antenna array, as shown in Figure 8.7. The total received signal is the superposition of the signal from K users plus the additive white noise. The baseband complex equivalent received signal $\mathbf{x}(t)$ for the desired user (User 1) at the antenna array can be expressed as

$$\mathbf{x}(t) = S_1(t) \star \mathbf{h}_1(t;\tau) + \sum_{k=2}^{K} S_k(t) \star \mathbf{h}_k(t;\tau) + \mathbf{N}_w(t), \tag{8.28}$$

where K is the number of users in the system, and $\mathbf{N}_w(t)$ is modeled as a complex Gaussian white noise vector with zero mean and covariance

$$E\{\mathbf{N}_w(t)\mathbf{N}_w(t)^\dagger\} = \sigma_n^2\mathbf{I}, \tag{8.29}$$

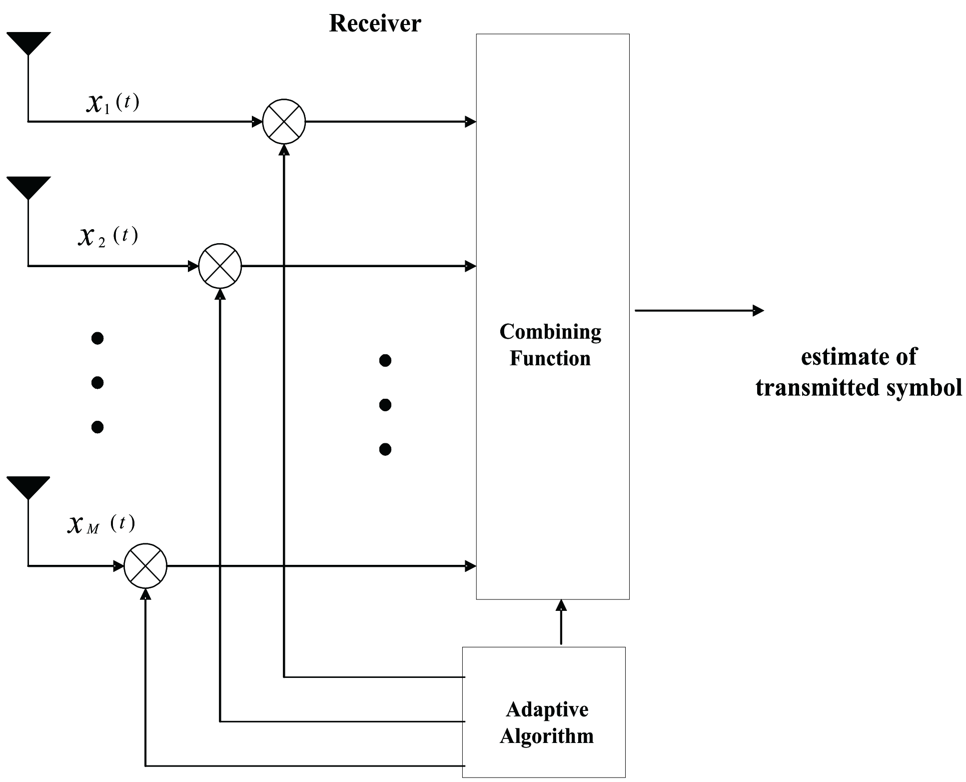

Figure 8.7: System model of adaptive antenna arrays

where $\mathbf{I}$ is the M x M identity matrix and $\sigma_n^2 = N_o/2$ is the antenna noise variance. The symbol † denotes the Hermitian transpose operation. $S_k(t)$ and $\mathbf{h}_k(t;\tau)$ are the transmit signal and the vector channel response for the kth user, respectively. For TDMA systems, $S_k(t)$ can be expressed as

$$S_k(t) = \sum_{i=-\infty}^{\infty} \sqrt{P_k} e^{j\Phi_{0,k}} d_k[i] G(t - iT_s - \mu_k), \tag{8.30}$$

where T_S is the symbol period, $G(t)$ is the square-root raised-cosine waveform, and $d_k[i]$ represents the discrete time modulated signal sequence for the kth user. μ_k is the random delay due to asynchronous transmission and $\Phi_{0,k}$ is a uniformly distributed phase angle between $[0,\ 2\pi]$. For CDMA systems, $S_k(t)$ can be expressed as

$$S_k(t) = \sum_{i=-\infty}^{\infty} \sqrt{P_k} e^{j\Phi_{0,k}} d_k[i] C_k(t - iT_s - \mu_k), \tag{8.31}$$

where $C_k(t)$ is the spreading code for user k. $C_k(t)$ can be expressed as

$$C_k(t) = \sum_{n=-\infty}^{\infty} c_{\mathsf{I},k}[n] G(t - nT_c) + j \sum_{n=-\infty}^{\infty} c_{\mathsf{Q},k}[n] G_r(t - nT_c), \tag{8.32}$$

where $c_{\mathsf{I},k}[n]$ is the in-phase component of the spreading sequence, $c_{\mathsf{Q},k}[n]$ is the quadrature component of the spreading sequence, $N_p = T_s/T_c$ is the processing gain, and T_c is the chip period. $S_1(t)$ is the desired transmit signal. $\mathbf{h}_k(t;\tau)$ is time-varying and is given by

$$\mathbf{h}_k(t;\tau) = \sum_{l=1}^{L} \mathbf{h}_{l,k}(t)\delta(t - \tau_l), \tag{8.33}$$

where L is the number of multipath, $\mathbf{h}_{l,k}(t)$ is the baseband complex equivalent channel gain for the lth path. By substituting (8.33) into (8.28), the receiver signal can be rewritten as

$$\mathbf{x}(t) = \sum_{l=1}^{L} S_1(t)\mathbf{h}_{l,1}(t) + \sum_{l=1}^{L}\sum_{k=2}^{K} S_k(t)\mathbf{h}_{l,k}(t) + \mathbf{N}_w(t). \tag{8.34}$$

For simplicity, we consider $L = 1$, That is, $\mathbf{h}_k(t;\tau) = \mathbf{h}_k\delta(\tau)$. Thus (8.34) can be rewritten as

$$\mathbf{x}(t) = S_1(t)\mathbf{h}_1(t) + \sum_{k=2}^{K} S_k(t)\mathbf{h}_k(t) + \mathbf{N}_w(t). \tag{8.35}$$

As discussed in Chapter 2, if the propagation wavefront is assumed a plane wave impinging upon the array or the angle spread is near zero, the vector channel response $\mathbf{h}_k(t)$ for the kth user can be expressed as

$$\mathbf{h}_k(t) = \beta_k(t)\mathbf{v}(\theta_k), \tag{8.36}$$

where $\mathbf{v}(\theta_k)$ and θ_k are the array response vector and the angle of arrival for kth user, respectively. For an AWGN channel, $\beta_k(t)$ is modeled as unity and θ_k is a constant. For a Rayleigh fading channel, $\beta_k(t)$ can be expressed by the multipath scalar channel as defined in Chapter 2. That is,

$$\beta_k(t) = \alpha_k(t)e^{j\Theta_k(t)}, \tag{8.37}$$

where $\alpha_k(t)$ is Rayleigh distributed and $\Theta_k(t)$ is a uniformly distributed on $[0,\ 2\pi]$. On the other hand, if the angle spread is relatively large, $\mathbf{h}_k(t)$ for the kth user can be expressed by the multipath vector channel response as defined in Chapter 2. That is,

$$\mathbf{h}_k(t) = [h_{1,k}(t), h_{2,k}(t), \cdots, h_{M,k}(t)]^T, \tag{8.38}$$

where

$$\begin{aligned} h_{m,k}(t) &= \alpha_{m,k}(t)e^{j\Theta_{m,k}(t)} \\ &= \beta_{m,k}(t). \end{aligned} \tag{8.39}$$

Using the discussion in Chapter 2, we can express $e^{j\Theta_{m,k}(t)}$ as a function of angle of arrival. That is

$$e^{j\Theta_{m,k}(t)} = \sum_{s=1}^{L_s} e^{j2\pi[F_d \cos(\Psi_{m,k,s})t + \phi_{m,k,s}]} v_m(\theta_{s,k}), \tag{8.40}$$

where L_s, $\phi_{m,k,s}$, $\Psi_{m,k,s}$, and F_d are the channel parameters defined in Chapter 2. $\theta_{s,k}$ is a uniform random variable with mean $= \theta_k$. Note that $\alpha_{m,k}(t)$ is Rayleigh distributed and $\Theta_{m,k}(t)$ is a uniformly distributed on $[0,\ 2\pi]$.

8.7 Optimization Criterion for Adaptive Antenna Array

The goal of an adaptive antenna array is to linearly combine each weighted antenna output to form a scalar estimate of the desired transmitted signal $y(t)$

$$y(t) = \mathbf{w}^{\dagger}\mathbf{x}(\mathbf{t}), \tag{8.41}$$

where $\mathbf{w}$ denotes the complex adaptive weight vector, and $\mathbf{x}(\mathbf{t})$ is the received signal vector. The adaptive weights are derived based on the optimization criterion. The optimization criterion for phased arrays and diversity arrays are classified as follows. For clarity, it is noted that phased arrays with adaptive combining are known as adaptive beamforming arrays while diversity arrays with adaptive combining are known as adaptive optimal combining arrays. Specific combining techniques are:

- Phased Arrays (Adaptive beamforming)
  - Maximum likelihood (ML)
  - Maximum signal-to-noise ratio (MSNR, also known as beam-steering)
  - Maximum signal-to-interference plus noise ratio (MSINR)
  - Minimum mean square error (MMSE)
  - Minimum variance distortionless response (MVDR)
- Diversity Arrays (Optimal combining)
  - Maximum likelihood (ML)
  - Maximum signal-to-noise ratio (known as MRC i.e., maximal ratio combining)
  - Maximum signal-to-interference plus noise ratio (MSINR)
  - Minimum mean square error (MMSE)

– Minimum variance distortionless response (MVDR)

It is seen that the optimization criterion of the adaptive beamforming are very similar to those for adaptive optimal combining. Thus, we will present the solutions of the optimization criterion for both adaptive beamforming and adaptive optimal combining in the following discussion. To facilitate the discussion, we rewrite (8.35) as

$$\begin{aligned}\mathbf{x}(t) &= S_1(t)\mathbf{h}_1(t) + \sum_{k=2}^{K} S_k(t)\mathbf{h}_k(t) + \mathbf{N}_w(t), \\ &= S_1(t)\mathbf{h}_1(t) + \mathbf{I}_c(t) + \mathbf{N}_w(t),\end{aligned} \tag{8.42}$$

where

$$\mathbf{I}_c(t) = \sum_{k=2}^{K} S_k(t)\mathbf{h}_k(t), \tag{8.43}$$

and let the undesired signals be written as

$$\mathbf{u}(t) = \mathbf{I}_c(t) + \mathbf{N}_w(t). \tag{8.44}$$

We define the array covariance matrix $\mathbf{R}_{xx}$ and $\mathbf{R}_{uu}$:

$$\mathbf{R}_{xx} = E\{\mathbf{x}(t)\mathbf{x}(t)^*\}. \tag{8.45}$$

$$\mathbf{R}_{uu} = E\{\mathbf{u}(t)\mathbf{u}(t)^*\}. \tag{8.46}$$

A brief review of the aforementioned criterion are described as follows. The adaptive weights based on certain optimization criterion can be obtained through the use of the reference signals. The reference signals are generally pilot symbols or a training sequence. Adaptive algorithms with the aid of reference signal are considered *data-aided algorithms*, while adaptive algorithms that don not need the reference signals are known as *blind algorithms*. In this section, we first discuss the adaptive data-aided algorithms based on the above optimization criterion. In the next section, we will discuss adaptive blind algorithms for some optimization criterion.

8.7.1 Maximum likelihood (ML)

Conventionally, the maximum likelihood criterion is derived for a single-user antenna arrays receiver and it requires the assumption that the composite interference $\mathbf{I}_c(t)$ is Gaussian so that the undesired signals appear to have multivariate Gaussian distribution [46]. We define the likelihood function of the received signal $\mathbf{x}(t)$ as

$$\mathcal{L}(\mathbf{x}(t)) = \frac{1}{\pi \mathbf{R}_{uu}} e^{[\mathsf{x}(t) - S_1(t)\mathsf{h}_1(t)]^\dagger \mathsf{R}_{uu}^{-1} [\mathsf{x}(t) - S_1(t)\mathsf{h}_1(t)]}. \tag{8.47}$$

The estimate of $S_1(t)$ can be obtained by maximizing the likelihood function of the received signal $\mathcal{L}(\mathbf{x}(t))$.

$$y(t) = \mathbf{w}_{\mathsf{ML}}^\dagger \mathbf{x}(t). \tag{8.48}$$

The maximum likelihood adaptive weight vector $\mathbf{w}_{\mathsf{ML}}$ based on $\mathcal{L}(\mathbf{x}(t))$ in (8.47) can be shown to have the form [110][48]

$$\mathbf{w}_{\mathsf{ML}} = \frac{\mathbf{R}_{uu}^{-1}\mathbf{h}_1}{\mathbf{h}_1^\dagger \mathbf{R}_{uu}^{-1}\mathbf{h}_1}. \tag{8.49}$$

For adaptive beamforming, the maximum likelihood adaptive weight vector $\mathbf{w}_{\mathsf{ML}}$ in (8.49) can be further expressed as a function of array response vector using (8.36)

$$\mathbf{w}_{\mathsf{ML}} = \frac{\mathbf{R}_{uu}^{-1}\mathbf{v}(\theta_1)}{\mathbf{v}^\dagger(\theta_1)\mathbf{R}_{uu}^{-1}\mathbf{v}(\theta_1)}. \tag{8.50}$$

For adaptive optimal combining, the maximum likelihood adaptive weight vector $\mathbf{w}_{\mathsf{ML}}$ in (8.49) can be obtained by the substitution of $\mathbf{h}_1$ with (8.38) and (8.39) for the case of $k = 1$.

Recently, the maximum likelihood criterion has extended for a multiuser antenna arrays receiver. The proposed scheme reformulates the single-user Maximum Likelihood Sequence Estimation (MLSE) in temporal domain into the multi-user Maximum Likelihood Sequence Search in spatial domain. The techniques called Spatially Reduced Search Joint Detection (SRSJD) have been applied in an overloaded array environment for airborne communication applications [41][42]. The detail of SRSJD is beyond the scope of this research. For the readers interested in SRSJD techniques, [111] provides a comprehensive study on this area.

8.7.2 Maximum Signal-to-Noise Ratio (MSNR)

The derivation of the MSNR adaptive weight vector $\mathbf{w}_{\text{MSNR}}$ can be obtained by solving the MSNR optimization problem. The MSNR optimization problem can be formulated as follows

$$\max_{\mathrm{W}_{\text{MSNR}}} J = \frac{\sigma_s^2 E\{|\mathbf{W}_{\text{MSNR}}\mathbf{h}_1|^2\}}{E\{\mathbf{N}_w \mathbf{N}_w^\dagger\}} \tag{8.51}$$

where $\sigma_s^2 = E\{S_1(t)S_1^*(t)\}$. It can be shown that the MSNR adaptive weight vector $\mathbf{w}_{\text{MSNR}}$ has the form [48]

$$\mathbf{w}_{\text{MSNR}} = \mathbf{h}_1. \tag{8.52}$$

For adaptive beamforming, the adaptive weight vector $\mathbf{w}_{\text{MSNR}}$ with the substitution of (8.36) can be expressed as

$$\mathbf{w}_{\text{MSNR}} = \beta_1 \mathbf{v}(\theta_1). \tag{8.53}$$

For adaptive optimal combining, the adaptive weight vector $\mathbf{w}_{\text{MSNR}}$ can be obtained by the substitution of $\mathbf{h}_1$ with (8.38) and (8.39) for the case of $k = 1$. In the literature, the adaptive optimal combining with MSNR optimization criterion is typically referred as maximal ratio combining (MRC).

The estimate of $S_1(t)$ can be obtained by linearly combining the weighted received signal

$$y(t) = \mathbf{w}_{\text{MSNR}}^\dagger \mathbf{x}(t). \tag{8.54}$$

It is important to note that the MSNR performance is optimum if

$$\mathbf{x}(t) = S_1(t)\mathbf{h}_1(t) + \mathbf{N}_w(t), \tag{8.55}$$

or $\mathbf{u}(t)$ is temporally and spatially white [112]. In fact, the MSNR adaptive antenna arrays can be thought of a spatially matched filter where the spatially adaptive weights are matched to the spatial vector channel.

8.7.3 Maximum Signal-to-Interference plus Noise Ratio (MSINR)

The adaptive weight vector can be optimized by maximizing the signal-to-interference plus noise ratio (SINR) at the combining output. The maximizing SINR problem can be formulated as follows:

$$\max_{\mathrm{W}_{\mathsf{MSINR}}} J = \frac{\sigma_s^2 E\{|\mathbf{W}_{\mathsf{MISNR}}\mathbf{h}_1|^2\}}{E\{\mathbf{u}\mathbf{u}^\dagger\}}. \tag{8.56}$$

The MSINR adaptive weight vector $\mathbf{w}_{\mathsf{MSINR}}$ can be shown to have the form [48][113]

$$\mathbf{w}_{\mathsf{MSINR}} = \zeta \mathbf{R}_{uu}^{-1}\mathbf{h}_1, \tag{8.57}$$

where ζ is any nonzero complex constant, and $\mathbf{h}_1 = \beta_1 \mathbf{v}(\theta_1)$ for adaptive beamforming. For adaptive optimal combining, $\mathbf{h}_1$ can be expressed by (8.38) and (8.39) with the case of $k = 1$.

8.7.4 Minimum Mean Square Error (MMSE)

The adaptive weight vector can be obtained by minimizing the mean square error (MSE) between the desired signal and the post-combining output. That is,

$$e(t) = S_1(t) - \mathbf{w}_{\mathsf{MMSE}}^\dagger \mathbf{x}(t). \tag{8.58}$$

The minimization MSE problem can be formulated as follows:

$$\min_{\mathrm{W}_{\mathsf{MMSE}}} J = E\{|e(t)|^2\} = E\{[S_1(t) - \mathbf{w}_{\mathsf{MMSE}}^\dagger \mathbf{x}(t)][S_1(t) - \mathbf{w}_{\mathsf{MMSE}}^\dagger \mathbf{x}(t)]^\dagger\}. \tag{8.59}$$

The MMSE adaptive weights $\mathbf{w}_{\mathsf{MMSE}}$ can be shown as [113][114]

$$\mathbf{w}_{\mathsf{MMSE}} = \mathbf{R}_{xx}^{-1}\mathbf{r}_{xd}, \tag{8.60}$$

where

$$\mathbf{r}_{xd} = E\{\mathbf{x}(t)d_1(t)^*\}, \tag{8.61}$$

where $d_1(t)$ the training sequence of the desired user. $\mathbf{w}_{\text{MMSE}}$ in (8.60) is often referred as Wiener-Hopf solution. With the assumption that the signals $S_1(t), S_2(t), \cdots, S_K(t)$ are uncorrelated, the $\mathbf{r}_{xd}$ can be shown as [110]

$$\mathbf{r}_{xd} = \sigma_s^2 \mathbf{h}_1. \tag{8.62}$$

Note that $\sigma_s^2 = 1$ if the channel gain and the transmitted power are assumed unity. Thus

$$\mathbf{r}_{xd} = \mathbf{h}_1, \tag{8.63}$$

where $\mathbf{h}_1$ for both adaptive beamforming and adaptive optimal combining is the same as the case of MSINR criterion.

8.7.5 Minimum Variance Distortionless Response (MVDR)

The MVDR adaptive weights is known as the solution of the constrained version of the linear Wiener optimization problem. The goal is to minimize the variance at the output of antenna combining subject to the constraint that the desired signal remains unaffected. The MVDR criterion can be considered as the special case of the linearly constrained minimum variance (LCMV) criterion with the constraint that the output of antenna combining maintains distortionless for the desired signal. The minimizing problem can be formulated as follows:

$$\min_{\mathbf{w}_{\text{MVDR}}} J = \mathbf{w}_{\text{MVDR}}^\dagger \mathbf{R}_{xx} \mathbf{w}_{\text{MVDR}}, \tag{8.64}$$

subject to the constraint

$$\mathbf{w}_{\text{MVDR}}^\dagger \mathbf{h}_1 = 1. \tag{8.65}$$

The MVDR adaptive weights, which also maximize the output of antenna combining is derived through the method of Lagrange multipliers. The solution can be shown as [114]

$$\mathbf{w}_{\text{MVDR}} = \frac{\mathbf{R}_{xx}^{-1} \mathbf{h}_1}{\mathbf{h}_1^\dagger \mathbf{R}_{xx} \mathbf{h}_1}. \tag{8.66}$$

Similarly, $\mathbf{h}_1$ for both adaptive beamforming and adaptive optimal combining are the same as the case of MSINR criterion.

8.8 Adaptive Blind Algorithms

In this section, we review two major blind adaptive algorithms for wireless communication applications: *constant modulus algorithm* and *dominant eigen-mode searching.*

8.8.1 Constant Modulus Algorithm (CMA)

The Constant modulus algorithm is based on the principle that attempts to restore the signal properties at the output of antenna combining and thus inherently suppress interference [115]. For digital wireless communications, CMA is used to restore to the signal property of PSK, FSK, and QAM signals on the basis of low modulus variations. This can be achieved by choosing the adaptive weight vector $\mathbf{w}_{\mathsf{CMA}}$ to minimize the cost function $J(\widehat{S}_1(t))$ that provides a measure of the envelope variation [116][117]. The minimizing problem can be formulated as follow

$$\min_{\mathsf{W}_{\mathsf{CMA}}} J = E\{|\widehat{S}_1(t)|^2 - 1\}, \tag{8.67}$$

where

$$\widehat{S}_1(t) = \mathbf{w}^{\dagger}_{\mathsf{CMA}}\mathbf{x}(t). \tag{8.68}$$

The CMA adaptive weight vector $\mathbf{w}_{\mathsf{CMA}}$ can be obtained adaptively according to [116]

$$\mathbf{w}_{\mathsf{CMA}}[i+1] = \mathbf{w}_{\mathsf{CMA}}[i] - \mu_s(|\widehat{S}_1[i]|^2 - 1)\mathbf{x}[i], \tag{8.69}$$

where $[i]$ denote the adaption period indexed at ith symbol period.

8.8.2 Dominant Eigen-Mode Searching (DEMS)

The second adaptive blind algorithm is based on estimating the second-order statistics of the interference -plus noise subspace and the received signal subspace. The estimation of the subspaces problems can be accomplished by the method of dominant eigen-mode searching [118][30]. A common criterion for dominant eigen-mode searching is to maximize the post-combining SINR at the output of antenna combining. To maximize the SINR, the adaptive weight vector can be obtained by solving the following problem

$$\max_{\mathrm{W} \neq 0} J = \frac{\mathbf{w}^{\dagger}\mathbf{R}_{xx}\mathbf{w}}{\mathbf{w}^{\dagger}\mathbf{R}_{uu}\mathbf{w}}, \tag{8.70}$$

where $\mathbf{R}_{xx}$ and $\mathbf{R}_{uu}$ are correlation matrix as defined in Section (8.7). Since $\mathbf{R}_{xx}$ and $\mathbf{R}_{uu}$ are Hermitian matrix, thus are positive definite, for any vector $\mathbf{w} \neq 0$, we have

$$\lambda_{max} \geq \frac{\mathbf{w}^{\dagger}\mathbf{R}_{xx}\mathbf{w}}{\mathbf{w}^{\dagger}\mathbf{R}_{uu}\mathbf{w}} \geq \lambda_{min}, \tag{8.71}$$

where $\lambda_{max} \geq \lambda_{max} \geq, \cdots, \geq \lambda_{min} > 0$ are the ordered generalized eigenvalues of matrix pair $(\mathbf{R}_{xx}, \mathbf{R}_{uu})$. The maximum SINR criterion is then satisfied when the weight vector equals the dominant eigenvector of the above pair [119][120], that is

$$\mathbf{R}_{xx}\mathbf{w} = \lambda_{max}\mathbf{R}_{uu}\mathbf{w}. \tag{8.72}$$

8.9 Comments on Adaptive Algorithms

In Sections 8.7 and 8.8, we described various adaptive algorithms that can be applied to adaptive antenna arrays system. From the practical application point of view, MMSE-based adaptive combining is considered one of the best approaches for wireless applications. Many adaptive antenna arrays systems based on MMSE algorithm have been implemented for current cellular and PCS systems [121][122]. As compared to ML algorithm, MMSE algorithm provides a similar capability for interference suppression with reduced complexity. With the assumption that the signals $S_1(t), S_2(t), \cdots, S_K(t)$ are uncorrelated, it can be shown that MMSE, MSINR, and MVDR algorithms indeed lead to the similar adaptive weights; thus achieve the same performance [48]. However, MMSE algorithm lends itself to adaptive implementation, which is prefered approach from the real implementation point of view. As compared to the MSNR algorithm, the MMSE algorithm significantly outperform the MSNR algorithm when the interference $\mathbf{I}_c(t)$ is dominant and appears to be a color noise. As compared to blind-based adaptive algorithms, the MMSE algorithm is relatively robust on parameter estimation errors and numerical errors [114]. Thus, in this research we focus on the MMSE algorithm for the study of adaptive antenna combining. Since wireless channel is time-varying, it is needed to develop the adaptive tracking algorithm for real implementation. In the following section, we review some adaptive tracking algorithms for wireless communications, based the on MMSE criterion

8.10 MMSE Adaptive Tracking Algorithms

Three main classes of adaptive tracking algorithms for wireless communications were developed, based on MMSE criterion: *direct matrix inversion* (DMI), *least mean square* (LMS), and *recursive lease square* (RLS) [114][112]. For simplifying the following discussion, we rewrite (8.60) in a discrete form. That is,

$$\mathbf{w}_{\mathsf{MMSE}}[i] = \mathbf{R}_{xx}^{-1}[i]\mathbf{r}_{xd}[i], \tag{8.73}$$

where

$$\mathbf{R}_{xx}[i] = E\{\mathbf{x}[i]\mathbf{x}^{\dagger}[i]\}, \tag{8.74}$$

$$\mathbf{r}_{xd}[i] = E\{\mathbf{x}[i]d_1[i]^*\}. \tag{8.75}$$

8.10.1 Direct Matrix Inversion

The algorithm to obtain the MMSE adaptive weight vector $\mathbf{w}_{\mathsf{MMSE}}[i]$ by directly calculating the inverse of the covariance matrix in (8.73) is referred as Direct Matrix Inversion algorithm. In DMI implementation, the covariance matrix $\mathbf{R}_{xx}[i]$ is generally estimated on symbol-by-symbol basis. Thus, the estimated covariance matrix $\widehat{\mathbf{R}}_{xx}[i]$ can be expressed as

$$\widehat{\mathbf{R}}_{xx}[i] = \frac{1}{N_a}\sum_{n=0}^{N_a-1}\mathbf{x}[i-N_a+n]\mathbf{x}^{\dagger}[i-N_a+n], \tag{8.76}$$

where N_a is the number of symbols (samples) used in the estimate, also known as the fixed average window. Ideally, N_a should be related to the coherent time of the time-variant channel. However, since the coherent time of the channel is not known *apriori*, a value of N_a must choose which gives the best performance over a range of channel coherent times. Note that the coherent time of the channel is inversely proportional to the maximum Doppler frequency.

To save memory the fixed window can also be implemented as a single pole filter:

$$\widehat{\mathbf{R}}_{xx}[i+1] = \alpha_f \widehat{\mathbf{R}}_{xx}[i] + (1-\alpha_f)\mathbf{x}[i]\mathbf{x}^{\dagger}[i], \tag{8.77}$$

where α_f determine the time constant of the update, also know as a forgetting factor. For a slowly varying channel and consequently long coherence time, a large α_f can be used to reduce the effects of the thermal noise on estimation. However, as the coherence time approaches the symbol duration, α_f must be reduced to track the channel variation [121].

Similar to the covariance matrix, the correlation vector $\mathbf{r}_{xd}[i]$ can be estimated as

$$\widehat{\mathbf{r}}_{xd}[i+1] = \alpha_f \widehat{\mathbf{r}}_{xd}[i] + (1-\alpha_f)\mathbf{x}[i]d_1^*[i]. \tag{8.78}$$

Thus, in real time DMI implementation the estimated MMSE adaptive weight vector $\widehat{\mathbf{w}}_{\mathsf{MMSE}}[i]$ can be obtained adaptively by [123]

$$\widehat{\mathbf{w}}_{\mathsf{MMSE}}[i] = \widehat{\mathbf{R}}_{xx}^{-1}[i]\widehat{\mathbf{r}}_{xd}[i]. \tag{8.79}$$

8.10.2 Least Mean Square (LMS)

An alternative approach to calculate the adaptive weight vector $\mathbf{w}_{\mathsf{MMSE}}[i]$ is based on *stochastic gradient search* algorithms [112]. A significant feature of a stochastic gradient search algorithm is its recursive implementations. A common algorithm based on the stochastic gradient search is the LMS algorithm. The estimated MMSE adaptive weight vector $\widehat{\mathbf{w}}_{\mathsf{MMSE}}[i]$ based on LMS algorithm can be calculated iteratively as

$$\widehat{\mathbf{w}}_{\mathsf{MMSE}}[i+1] = \widehat{\mathbf{w}}_{\mathsf{MMSE}}[i] + \mu_s \mathbf{x}[i]\{d_1^*[i] - \mathbf{x}^\dagger[i]\widehat{\mathbf{w}}_{\mathsf{MMSE}}[i]\}, \tag{8.80}$$

where μ_s is the step-size parameters, which must satisfy the condition

$$0 \leq \mu_s \leq \frac{2}{\lambda_{max}}, \tag{8.81}$$

where λ_{max} is the largest eigenvalue of the covariance matrix $\mathbf{R}_{xx}$. The practical importance of the LMS algorithm is largely due to its simplicity of implementation. The computational complexity of the LMS algorithm is $O(M)$. The standard form of the LMS algorithm experiences the *gradient noise amplification* problem when $\mathbf{x}[i]$ is large. The improved version of the LMS algorithm known as the normalized LMS algorithm can be used to overcome this difficulty [124]. The main limitation of the LMS algorithm is its relatively slow rate of convergence. A detail discussion of the convergence behavior of the LMS algorithm is given [112].

8.10.3 Recursive Lease Square (RLS)

An alternative recursive algorithm known as RLS algorithm can be used to improve the slow convergence rate of the LMS algorithm. The convergence rate of the RLS algorithm is typically an order of magnitude faster than the simple LMS algorithm. This performance improvement, however, is achieved at the expense of increase in computational complexity. It should be emphasized that the improvement in the rate of convergence of RLS algorithm over the LMS algorithm holds only when signal-to-noise ratio is high. The RLS algorithm is summarized as follows [114].

- Initialize the algorithm by setting $\mathbf{P}[0] = \delta^{-1}\mathbf{I}$ and $\widehat{\mathbf{w}}_{\mathsf{MMSE}}[0] = 0$
- For each instant of time, $i = 1, 2, \cdots$, compute

  1. $\mathbf{k}[i] = \frac{\lambda^{-1}\mathsf{P}[i-1]\mathsf{x}[i]}{1+\lambda^{-1}\mathsf{x}^\dagger[i]\mathsf{P}[i-1]\mathsf{x}^\dagger[i]}$

2. $\xi[i] = S_1[i] - \widehat{\mathbf{w}}_{\mathsf{MMSE}}[i-1]\mathbf{x}^{\dagger}[i]$
3. $\widehat{\mathbf{w}}_{\mathsf{MMSE}}[i] = \widehat{\mathbf{w}}_{\mathsf{MMSE}}[i-1] + \mathbf{k}[i]\xi^{*}[i]$
4. $\mathbf{P}[i] = \lambda^{-1}\mathbf{P}[i-1] - \lambda^{-1}\mathbf{k}[i]\mathbf{x}^{\dagger}[i]\mathbf{P}[i-1]$

One of the problem encountered in applying the RLS algorithm is that of numerical instability. The square-root based RLS algorithms known as $QR - RLS$ algorithm were proposed to mitigate this problem. The QR-RLS algorithm, or more specifically, the *QR decomposition-based RLS* algorithm is accomplished by working directly with the received data matrix (formed by $\mathbf{x}[i]$) via QR decomposition rather than working the time-average covariance matrix $\mathbf{R}_{xx}$. Accordingly, the QR-RLS algorithm is numerically more stable than the standard RLS algorithm Several extended versions of the QR-RLS algorithm were proposed to facilitate the practical implementation [125][126].

8.11 Summary

We have reviewed two active ongoing research areas on signal processing techniques in wireless communications: multiuser detection systems and adaptive antenna array system. We described the principles and fundamentals of signal detection techniques for multiuser detection systems and discuss the features of both optimum multiuser receivers and various suboptimum multiuser receivers. We examine various optimization criterion for adaptive antenna array combining techniques and review the practical issues on the implementation of adaptive antenna array combining algorithms. The performance of adaptive antenna arrays for WCDMA and OFDM systems is presented in Chapter 9. The topic of joint multiuser detection and adaptive antenna arrays for an overloaded array environment is discussed in Chapter 10.

Chapter 9

Performance of Adaptive Beamforming for WCDMA and OFDM

In this chapter, we evaluate the performance of adaptive beamforming for WCDMA (wideband CDMA) and OFDM systems in ground-based communications. The adaptive beamforming performance is evaluated based on bit-error-rate (BER) simulations. Two adaptive beamforming algorithms are considered: *Maximum SNR and Minimum Mean Square Error* (MMSE). We evaluate the BER performance of beamforming algorithms for OFDM systems in the presence of strong wideband interference while we evaluate the beamforming performance for WCDMA in presence of multiple access interference (MAI). The strength of the strong wideband interference generally ranges from 0dB to 30dB above the desired user's power while the strength of MAI is assumed equal to the desired user's power (*i.e.,* ideal power control scenario). The effect of a finite number of samples for estimating the appropriate statistics is also considered. We further evaluate the impacts of angle spread and the user location on the BER performance of these beamforming algorithms.

This chapter is organized as follows. In Section 9.1, we briefly describes the applications of OFDM and WCDMA systems to the future wireless systems. In Section 9.2, we present the transmitter model for the OFDM system. In Section 9.3, we review the statistical vector channel model used in this study. In Section 9.4, we describe the receiver model for the OFDM system. The adaptive beamforming algorithms are described in Section 9.5. Simulation validation is described in Section 9.6. The simulated BER results of beamforming algorithms for OFDM systems are evaluated in Section 9.7. In Section 9.8.1, we present the transmitter model and receiver model for WCDMA systems. The simulated BER results of beamforming algorithms for WCDMA systems are evaluated in Section 9.9. Concluding remarks are given in Section 9.10. Note that in this chapter we consider the number of interferers to be less than or equal to the number of antenna elements. In the next chapter, we will consider the case where the number of interferers is greater than the number of antenna elements.

9.1 Introduction

There is increasing interest in using OFDM for ground-based mobile radio communications [22]. It has been adopted as a modulation scheme for the European terrestrial digital broadcasting systems [17][18]. The significance of OFDM is its capability to mitigate the distortion due to multipath propagation in ground-based wireless communications [19][20][21]. Recent research efforts have focus on investigating the application of OFDM systems to future wireless local area network (wireless LAN). Another promising technique for the future wireless systems is based on DS-CDMA technologies, known as Wideband CDMA. For moderate processing gain and good power control DS-CDMA systems generally can provide significant interference suppression capability for multipath resistance and multiple access interference reduction. Further, the wide bandwidth can be used to mitigate the effects of fading channels.

In this study, our focus is on the performance of a multiple antenna system which uses adaptive beamforming for OFDM modulation in the presence of wideband interference and for WCDMA systems in the presence of multiple access interference. Multiple receiver antenna arrays have been widely used in mobile radio communications to improve signal quality, thereby increasing system coverage, capacity, and link quality [1]. In typical ground-based mobile radio communications, the wave propagates through a physical medium that results in a line-of-sight (LOS) propagation, non-LOS propagation, or combined LOS and non-LOS propagation, depending on the richness of scattering environment. For LOS-only propagation, the wireless channel can be considered an AWGN channel while a non-LOS propagation is generally modeled as a fading channel. Non-LOS reflected propagation paths (known as multipath propagation) causes signal strength fluctuation, thereby inducing signal fading and distortion.

Two beamforming algorithms are considered for OFDM and WCDMA systems: Maximum SNR and MMSE. For OFDM systems, we evaluate the BER performance for the beamforming algorithms under AWGN and Rayleigh fading channels. The impacts of angle spread and the user location on the BER performance of these beamforming algorithms are also considered. For WCDMA systems, we evaluate the BER performance of the beamforming algorithms in a Rayleigh fading channel. The tradeoff between processing gain (*i.e.,* temporal processing gain) and interference suppression gain (*i.e.,* spatial processing gain) using MMSE beamforming is investigated for small and large angle spread environments.

In the next several sections, we examine the performance of adaptive beamforming for OFDM systems. Later in this chapter, we investigate the performance of adaptive beamforming for WCDMA systems.

9.2 Transmitter Model for OFDM

We consider an OFDM user communicating with a base station in the presence of a strong unknown jammer. Figure 9.1 shows the uplink system model (from a mobile to a base station) for a OFDM user. The complex baseband equivalent transmitted signal for the desired user after IFFT modulation for an OFDM block can be written as

$$S(t) = \sum_{n=0}^{N_c} s_n e^{j2\pi f_n t}, \quad t \in [0, T], \tag{9.1}$$

where N_c is the total number of subcarriers for an OFDM block, $T = N_c T_s$ is the OFDM symbol period, and T_s is the QPSK symbol period. s_n is the transmit signal on the nth subcarrier, which can be expressed as

$$s_n = \sqrt{P_t}\, d[n] \ , \tag{9.2}$$

where $d[n]$ is the nth QPSK modulated symbol and P_t is the signal transmit power. Note that T is chosen such that a channel is quasi-static during an OFDM symbol. The unknown jammer is modeled as either temporally white and spatially colored Gaussian noise or a Cosine Waveform (CW).

9.3 Channel Model

In this study, we consider both AWGN and Rayleigh fading channels. For the purpose of this study, we are primarily interested in the BER performance of various beamforming algorithms, thus we consider a frequency-flat channel (*i.e.,* non-time-dispersive channel) and the channel is quai-static over the adaption period. In addition, we consider a 4-element uniform linear array (ULA) employed at the base station. For an AWGN chanel, the propagation wavefront is a plane wave impinging upon the array. Therefore, the vector channel response for the kth user can be expressed as

$$\mathbf{h}_k = \mathbf{v}(\theta_k), \tag{9.3}$$

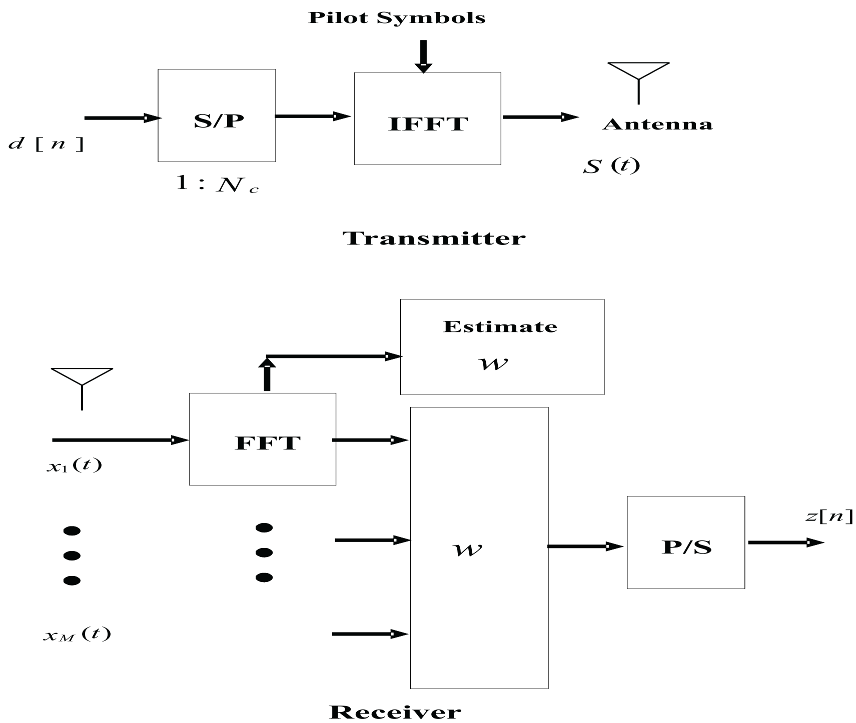

Figure 9.1: Transmitter and receiver models for OFDM systems.

where

$$\mathbf{h}_k = [h_{1,k}\, h_{2,k}, \cdots h_{M,k}]^T, \tag{9.4}$$

where $\mathbf{v}(\theta_k)$ is the array response of ULA for the kth user and is defined in Chapter 2. Without loss of generality, we consider $k = 1$ as a desired user and $k = 2$ as a jammer. For a Rayleigh flat fading channel, the vector channel impulse response can be expressed by (2.43). Based on limited field measurement data, the distribution of the AOA at the received base station antenna array is assumed to be a truncated Gaussian AOA distribution, as described in Chapter 2. Figure 9.2 shows spatial vector channel model for ULA in a AWGN channel and a Rayleigh channel.

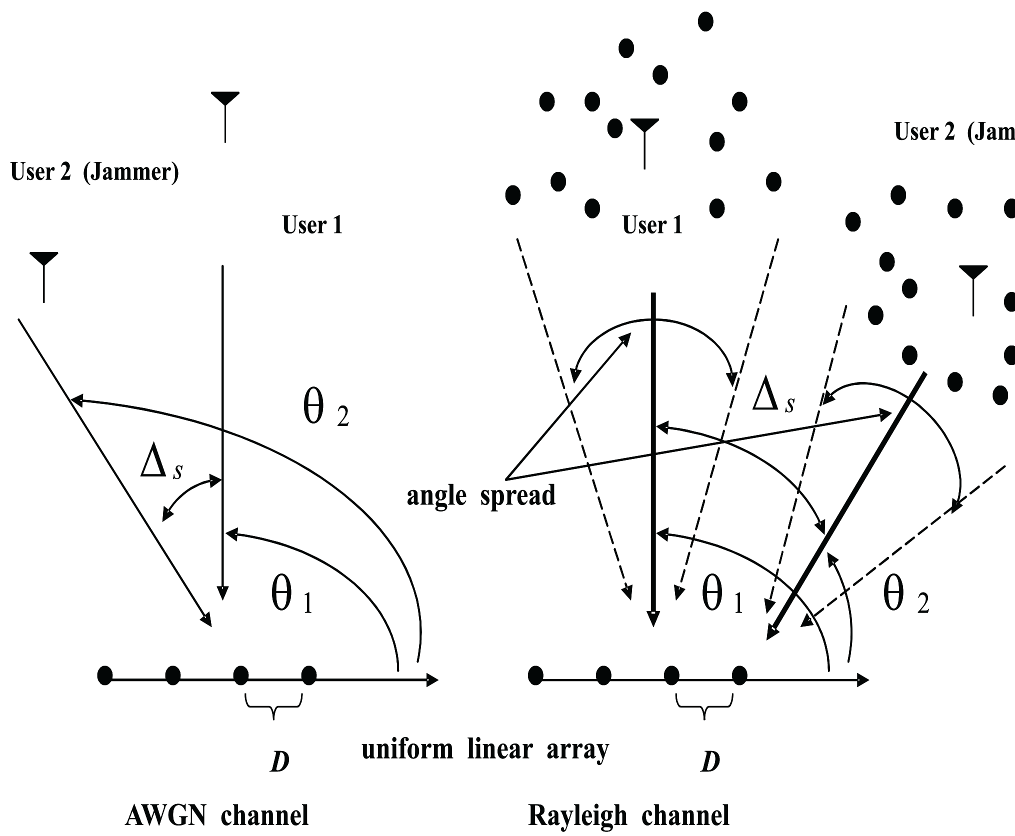

Figure 9.2: Spatial vector channel model for ULA in a AWGN channel and a Rayleigh channel

9.4 Receiver Model for OFDM

Figure 9.1 shows the receiver model for an OFDM base station. The total received signal is the superposition of the desired signal, the jammer's signal, and additive white noise. After FFT demodulation, the received signal of the desired user for the mth antenna element at the nth subcarrier is expressed as

$$x_m[n] = H_{m,1}[n]s_n + u_m[n], \tag{9.5}$$

where $u_m[n]$ is the undesired signal component and is expressed as

$$u_m[n] = I_t[n] + n_w[n], \tag{9.6}$$

where $n_w[n]$ is the white Gaussian noise sample with the variance $2\sigma^2$. $I_t[n]$ is the interference from a wideband jammer. $H_{m,1}[n]$ is the frequency response of channel for the desired user at the mth antenna element. Since we consider the frequency-flat channel, $H_{m,k}[n]$ is independent of subcarriers and can be expressed as

$$H_{m,k} = h_{m,k}. \tag{9.7}$$

Note that for a quai-static channel, $h_{m,k}$ is constant over an OFDM symbol. The vector forms of (9.5) and (9.6) can be expressed as, respectively

$$\mathbf{x}[n] = [x_1[n] \cdots x_m[n] \cdots x_M[n]]^T, \tag{9.8}$$

$$\mathbf{u}[n] = [u_1[n] \cdots u_m[n] \cdots u_M[n]]^T. \tag{9.9}$$

9.5 Beamforming Algorithms

In this study, we consider three beamforming algorithms: Maximum SNR and MMSE. The decision statistics of the estimated symbol after beamforming can be expressed as

$$z[n] = \widehat{d}_1[n] = \mathbf{w}^\dagger \mathbf{x}[n], \tag{9.10}$$

where $\mathbf{w}$ is the vector of complex adaptive weights and the superscript $\dagger$ denotes transpose and conjugate. $\mathbf{w}$ can be calculated as described below.

9.5.1 Maximum SNR

For Maximum SNR combining, $\mathbf{w}[n]$ is equivalent to the channel response of the desired user. That is

$$\mathbf{w} = \mathbf{h}_1. \tag{9.11}$$

9.5.2 MMSE

For MMSE combining, $\mathbf{w}$ can be shown to be [114]

$$\mathbf{w} = \mathbf{R}_{xx}^{-1}\mathbf{r}_{xd}, \tag{9.12}$$

where $\mathbf{R}_{xx} = E\left\{\mathbf{x}\mathbf{x}^{\dagger}\right\}$ is the covariance matrix of the received signal with the size $M \times M$. In a practical implementation, $\mathbf{R}_{xx}$ is estimated from pilot symbols and is expressed as

$$\widehat{\mathbf{R}}_{xx} = \frac{1}{N}\sum_{q=1}^{N}\mathbf{x}[q]\mathbf{x}^{\dagger}[q], \tag{9.13}$$

where N is the number of pilot symbols. $\mathbf{r}_{xd} = E\left\{\mathbf{x}d^{*}\right\}$ is the correlation between the received signal and the desired signal. $\mathbf{r}_{xd}$ is also estimated from pilot symbols and is expressed as

$$\widehat{\mathbf{r}}_{xd} = \frac{1}{N}\sum_{q=1}^{N}\mathbf{x}[q]d_1^{*}[q]. \tag{9.14}$$

9.6 Simulation Validation

We consider the scenario where one OFDM user and one strong wideband jammer are present in the system. We define the spatial separation between the desired OFDM user and the jammer as

$$\Delta_s = \theta_1 - \theta_2, \tag{9.15}$$

where $\theta_1 = 90°$ is the AOA of the desired user and θ_2 is the AOA of the jammer. The power ratio of the jammer over the desired user is defined as

$$\chi = \frac{P_I}{P_r}, \tag{9.16}$$

where P_I is the jammer's receive power and P_r is the receiver power for the desired user. The received signal-to-noise ratio per bit and per receive antenna for $z[n]$ is denoted as γ_c. To validate the simulation results, we first calibrate the channel effects of the simulator. Figure 9.3 show the analytical and simulated BER results for AWGN and Rayleigh channels. It is shown that the simulated BER results exhibit a good agreement with the analytical BER results. Secondly, we validate the algorithms performance for the simulator. Figure 9.4 show the comparative BER results for the estimated MMSE weights and the ideal MMSE weights in a AWGN channel. The results shows the performance of the estimated MMSE weights is bounded by the ideal case. Figure 9.5 illustrate the beamforming pattern using MMSE algorithm. As shown, the jammer is nulled out with MMSE beamforming.

9.7 Simulation Results for OFDM

In this section, we present the BER performance of the beamforming algorithms. The number of subcarriers for an OFDM symbol is 128 ($N_c = 128$). The QPSK symbol rate is 384,000 symbols per second ($1/T_s$). The antenna spacing D is equal to one half wavelength (0.5 λ).

9.7.1 AWGN

Figure 9.6 shows the BER performance of MMSE beamforming as function of the number of pilots used to estimate $\widehat{\mathbf{R}}_{xx}$ and $\widehat{\mathbf{r}}_{xd}$ for various separation Δ_s values in an AWGN channel. In this figure, the jammer is assumed to transmit Gaussian noise with χ=20dB.

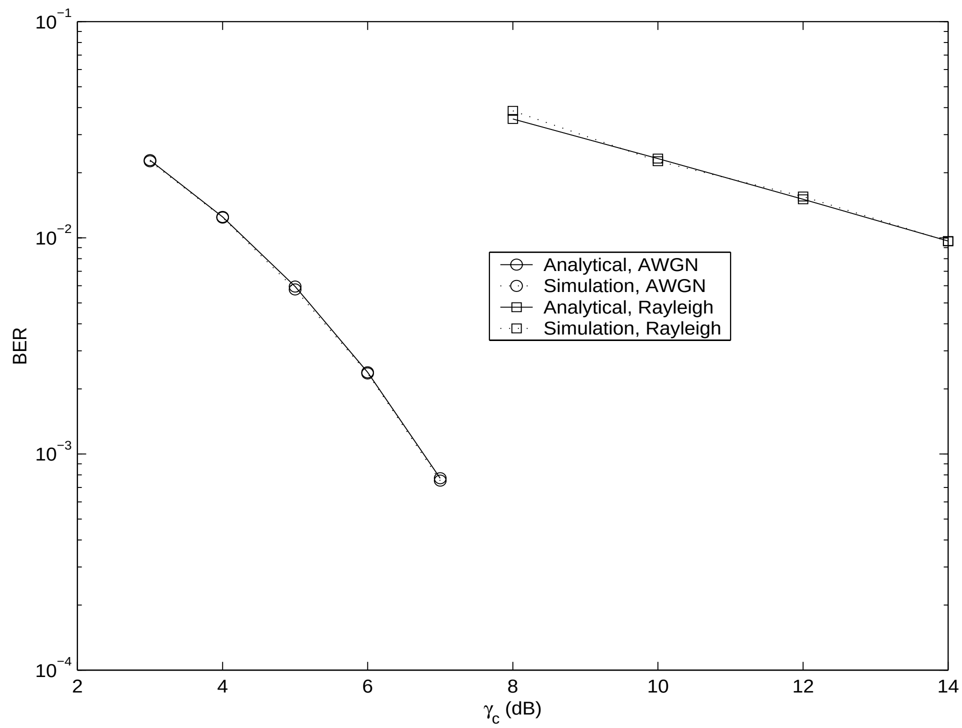

Figure 9.3: Analytical and simulated BER results for AWGN and Rayleigh channels.

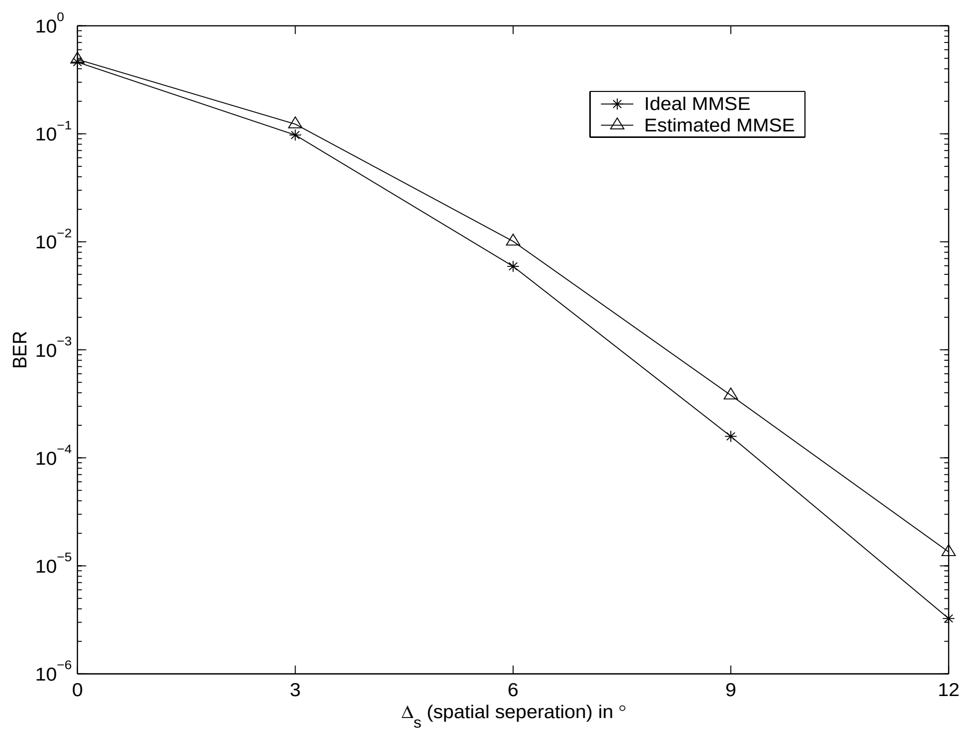

Figure 9.4: BER results for the estimated beamforming weights and the ideal beamforming weights (γ_c=8dB).

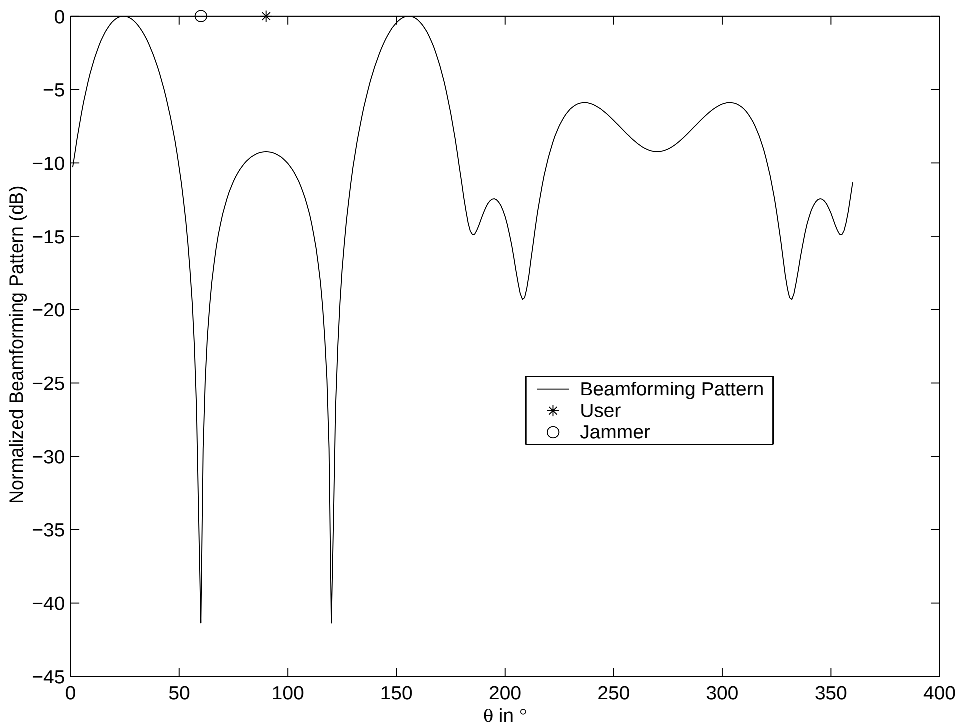

Figure 9.5: MMSE beamforming pattern (γ_c=8dB).

It is seen that the number of pilots greater than 25 would provide the sufficient accuracy for estimating $\widehat{\mathbf{R}}_{xx}$ and $\widehat{\mathbf{r}}_{xd}$. Figure 9.7 shows the BER performance of MMSE beamforming as function of space separation Δ_s for various power ratio χ in an AWGN channel. It is shown that the BER performance improves as the spatial separation Δ_s increases. This is because the spatial signature of the desired user is more distinguishable from the jammer as Δ_s increases. In this figure, the jammer is consider as temporally white and spatially colored Gaussian noise or Cosine Waveform with variable power ratio χ. It is observed that the BER performance is independent of the jammer's temporal characteristics.

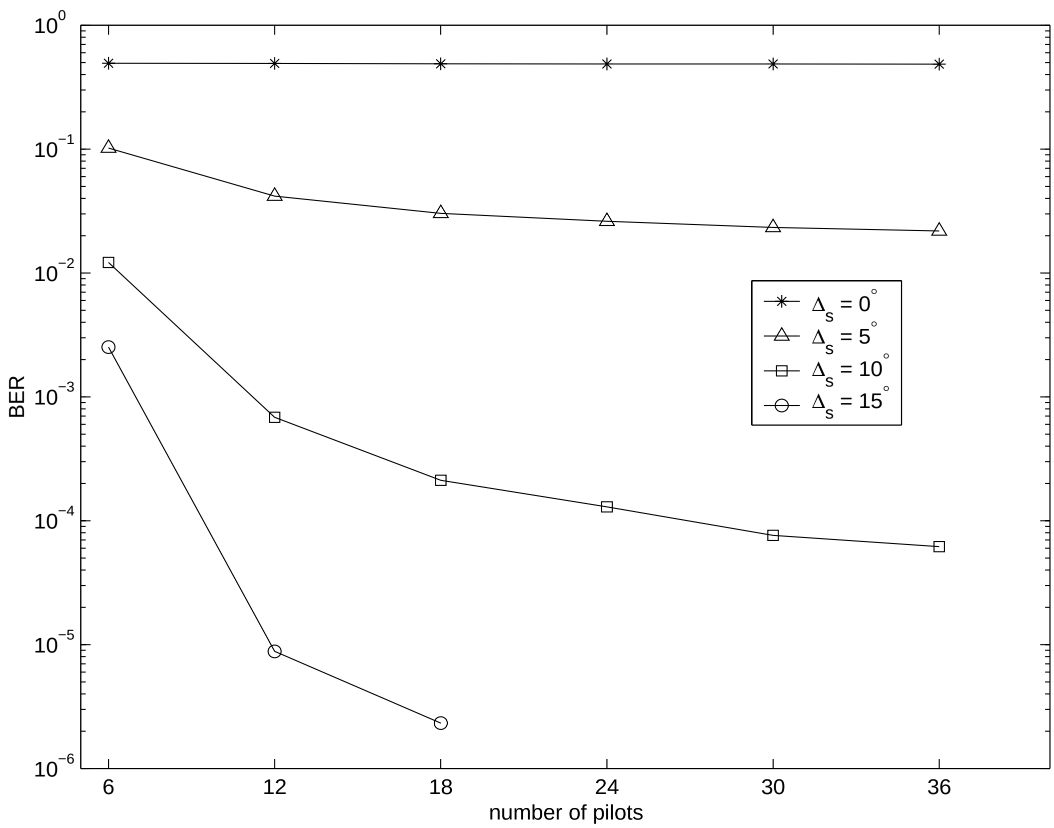

Figure 9.6: BER performance as function of the number of pilots used to estimate covariance matrix for various spatial separation Δ_s in AWGN channel (χ=20dB and γ_c=8dB).

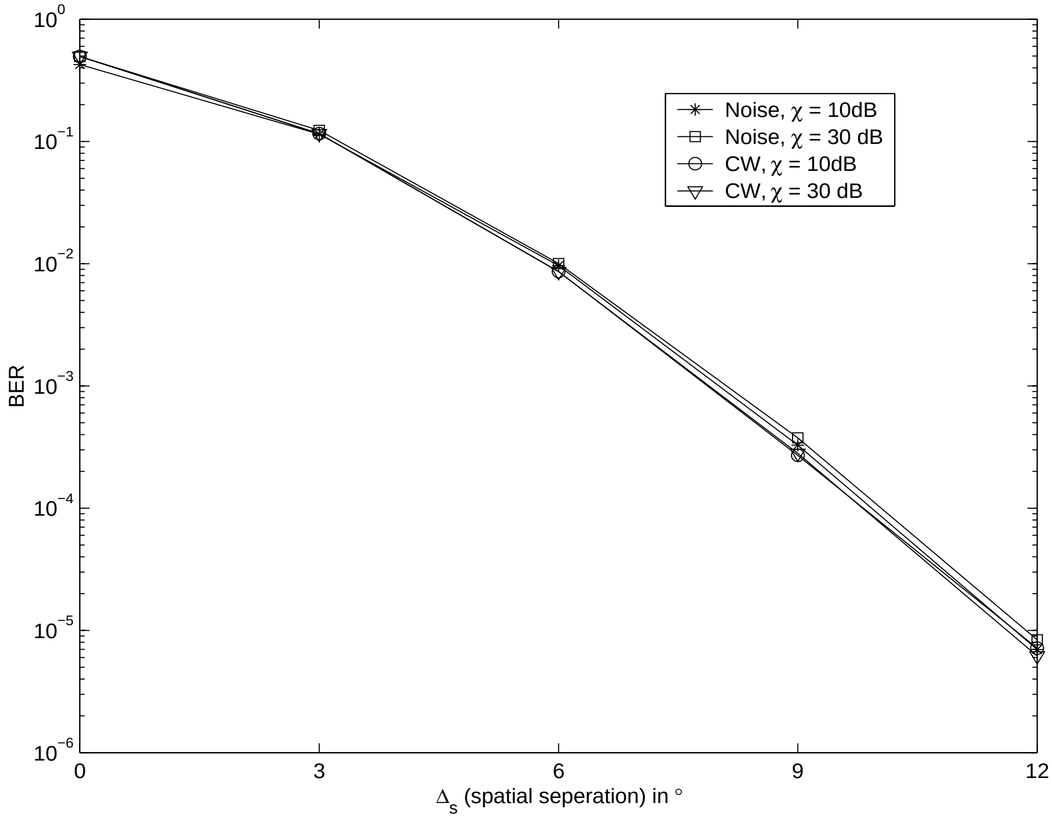

Figure 9.7: BER performance of MMSE beamforming as function of spatial separation Δ_s for various power ratio χ in AWGN channel (N=25 and γ_c=8dB).

9.7.2 Rayleigh Fading

Figure 9.8 shows the BER performance of MMSE beamforming as function of spatial separation Δ_s for various values of angle spread in a Rayleigh fading channel. It is shown that the BER performance is a function of spatial separation Δ_s for small angle spread, but it is independent of Δ_s for large angle spread. This is because the antenna array performs as phased array for small angle spread and acts as a diversity array for large angle spread. Figure 9.9 shows the BER performance of MMSE vs. Maximum SNR (*i.e.,* MRC) as function of γ_c for various χ in a Rayleigh fading channel. In this figure, the angle spread (σ_a) is assumed $1°$ (*i.e.,* small angle spread) and the performance of MRC without interference provides a lower bound on performance. As seen, MMSE outperforms Maximum SNR significantly as χ increases. In addition, MMSE almost achieves the lower bound performance within 1dB. Figure 9.10 shows the BER performance of MMSE vs. Maximum SNR as function of γ_c for various χ in a Rayleigh fading channel, assuming $\sigma_a = 20°$ (*i.e.,* large angle spread). Again, MMSE outperforms Maximum SNR significantly and is within approximately 2dB of the lower bound on performance. In contrast, the performance of MMSE in large angle spread channels yields better performance than the case of small angle spread because the large angle spread can provide more spatial diversity gain than the small angle spread. However, as compared to their lower bound performance, the small angle spread is much closer to its lower bound performance than the large angle spread.

9.8 System Model for WCDMA

In the following sections, we present the transmitter model and receiver model for WCDMA systems.

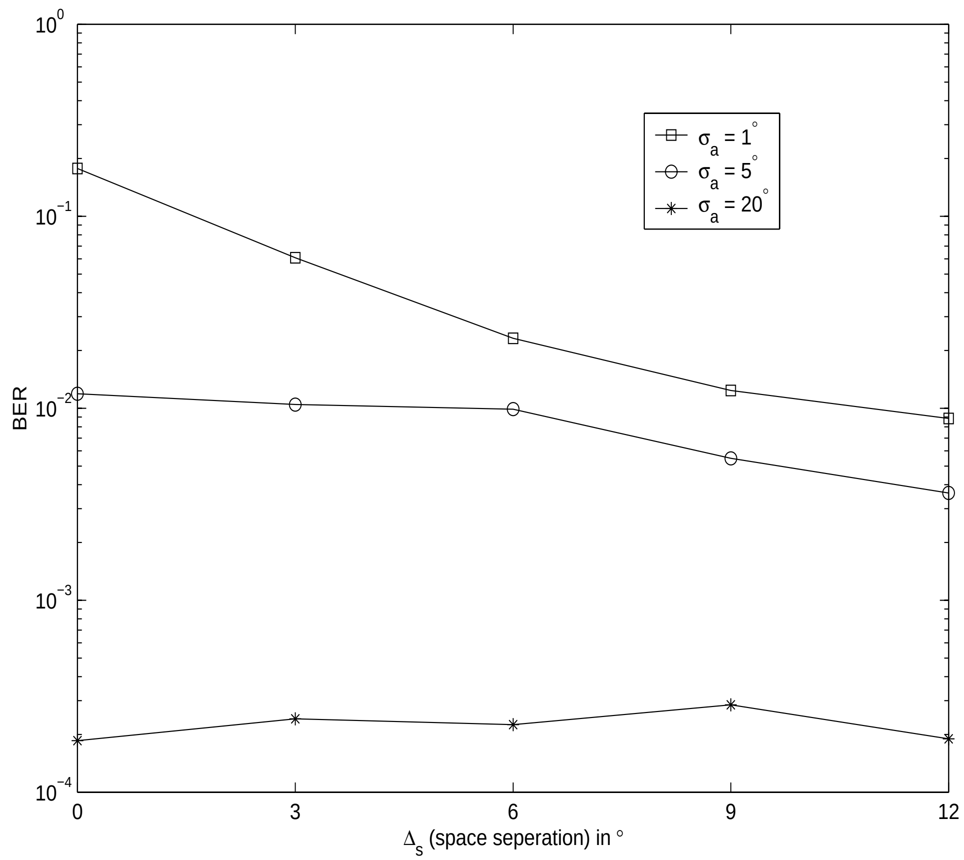

Figure 9.8: BER performance of MMSE beamforming as function of spatial separation Δ_s for various angle spread in Rayleigh fading channel (N=25, χ=20dB and γ_c=10dB).

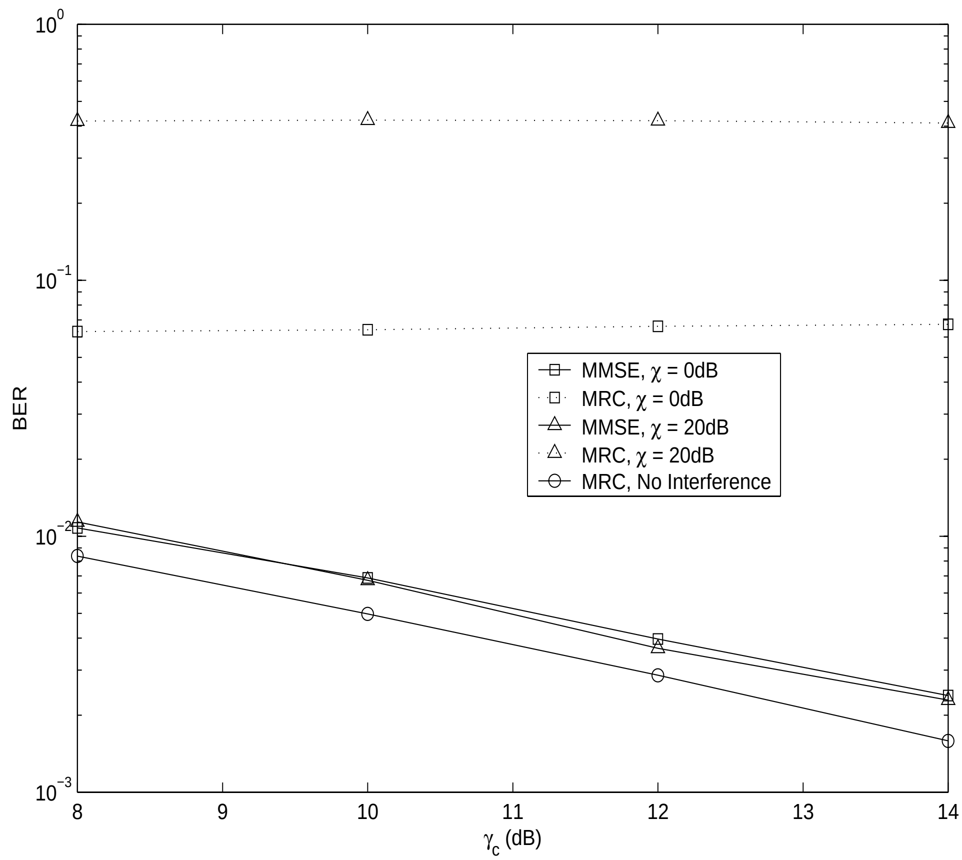

Figure 9.9: BER performance of MMSE vs. Maximum SNR as function of γ_c for various χ in Rayleigh fading channel (N=25 and $\sigma_a = 1°$).

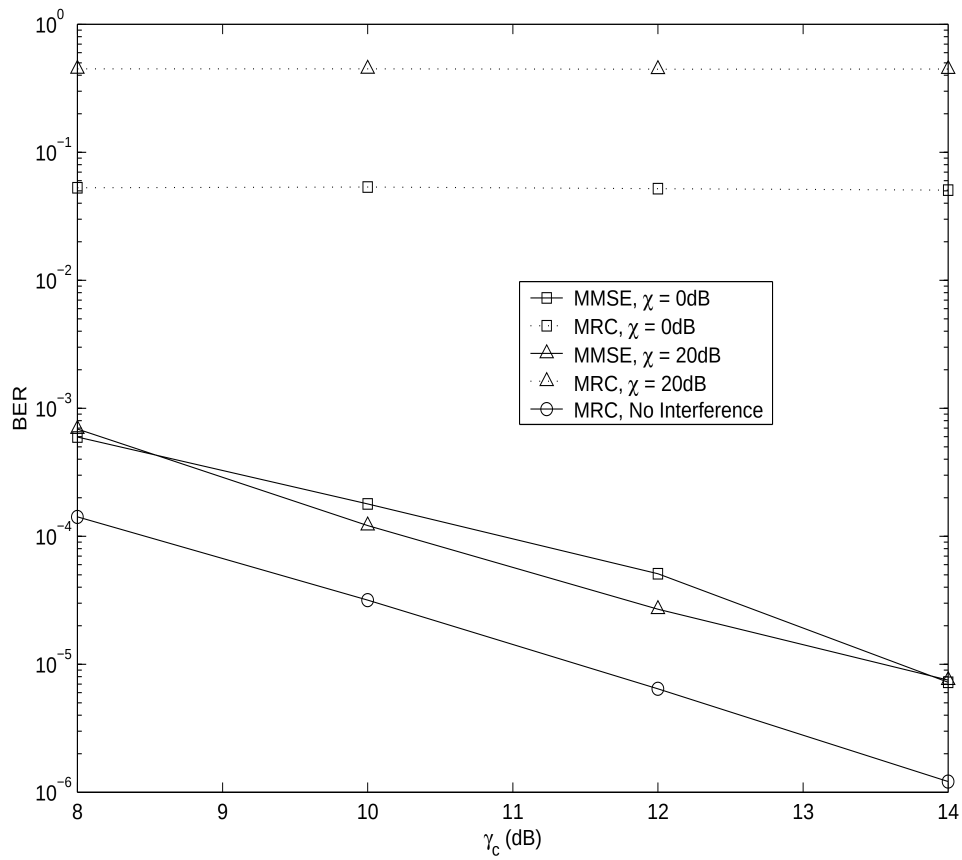

Figure 9.10: BER performance of MMSE vs. Maximum SNR as function of γ_c for various χ in Rayleigh fading channel (N=25 and $\sigma_a = 20°$).

9.8.1 Transmitter Model for WCDMA

We consider a uplink wireless communication system, where a base station with M antennas receives DS-CDMA signals from K mobile users with asynchronous multiple access transmission. The baseband complex equivalent tranmitted signal of the kth employing QPSK modulation can be represented as

$$S_k(t) = \sum_{i=-\infty}^{\infty} \sqrt{P_k} e^{j\Phi_{0,k}} d_k[i] C_k(t - iT_s - \mu_k), \tag{9.17}$$

where $d_k[i]$ is a QPSK modulated symbol, T_s is the symbol period, P_k is the transmitted power, μ_k is the random delay due to the asynchronous transmission, and $\Phi_{0,k}$ is a uniformly distributed phase angle between $[0,\, 2\pi]$. $C_k(t)$ is the spreading code for user k and can be expressed as

$$C_k(t) = \sum_{n=-\infty}^{\infty} c_{\mathrm{I},k}[n] G(t - nT_c) + j \sum_{n=-\infty}^{\infty} c_{\mathrm{Q},k}[n] G(t - nT_c), \tag{9.18}$$

where $c_{\mathrm{I},k}[n]$ is the in-phase component of the spreading sequence, $c_{\mathrm{Q},k}[n]$ is the quadrature component of the spreading sequence, $N_p = T_s/T_c$ is the processing gain (PG), T_c is the chip period, and $G(t)$ is the raised-cosine chip waveform. Note that the spreading code $C_k(t)$ assigned for each user a Gold code.

9.8.2 Receiver Model for WCDMA

Without loss of generality, we consider a flat Rayleigh fading channel in this study. Figure 9.11 shows a K-user wireless communication system employing an 4-element uniform circular antenna array. The total received signal is the superposition of the signal from K users plus the additive white noise. The baseband equivalent received signal for the mth antenna element can be expressed as

$$x_m(t) = \sum_{k=1}^{K} S_k(t)\, h_{m,k}(t) + n_w(t), \tag{9.19}$$

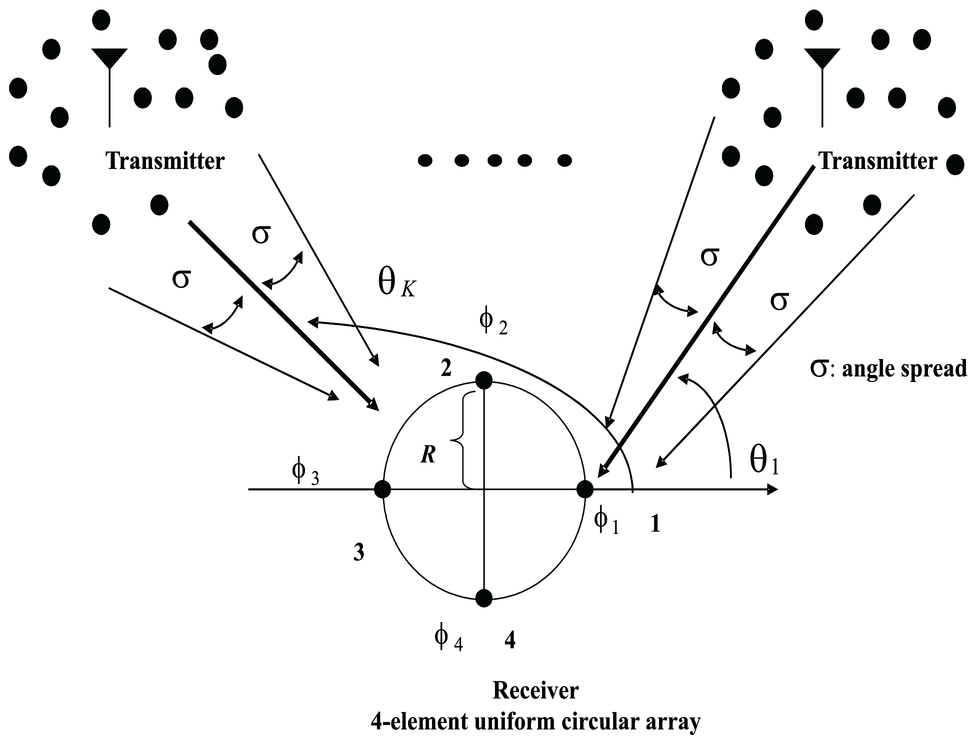

Figure 9.11: Spatial vector channel model for UCA in wireless channel

where $h_{m,k}(t)$ is defined in Section 9.3 with the substitution of $v_m(\theta_{s,k})$ by

$$\mathbf{v}(\theta_{s,k}) = \begin{bmatrix} v_1(\theta_{s,k}) \\ v_2(\theta_{s,k}) \\ \vdots \\ v_M(\theta_{s,k}) \end{bmatrix} = \begin{bmatrix} e^{-j2\pi\frac{R}{\lambda}cos(\theta_{s,k}-\phi_1)} \\ e^{-j2\pi\frac{R}{\lambda}cos(\theta_{s,k}-\phi_2)} \\ \vdots \\ e^{-j2\pi\frac{R}{\lambda}cos(\theta_{s,k}-\phi_M)} \end{bmatrix}, \tag{9.20}$$

where $\theta_{s,k}$, R, and ϕ_m are defined in Chapter 2. The antenna spacing R is equal to one half wavelength (0.5 λ) in this study. $n_w(t)$ is Gaussian noise with zero mean and two-sided power spectral density given by $No/2$. Note that path loss and shadowing are normalized to unity for K users. Thus the receiver power for the kth user is equal to P_k. We assume k=1 is the index of the desired user.

The discrete-time received signal after a chip-matched filter for the mth antenna element during the ith symbol epoch can be written as

$$x_m[i] = \sqrt{P_1}h_{m,1}d_1[i] + \sum_{k=2}^{K} h_{m,k}\, S_k^r[i] + n_w[i], \tag{9.21}$$

where $S_k^r[i]$ is the sampled version of $S_k^r(t)$, which can be expressed as

$$S_k^r(t) = \sum_{n=0}^{N_p-1} \int_0^{T_c} S_k(t - nT_c - \zeta)C_1(\zeta - nT_c)^* d\zeta, \tag{9.22}$$

The vector forms of (9.21) can be expressed as

$$\mathbf{x}[i] = [x_1[i] \quad \cdots x_M[i]]^T. \tag{9.23}$$

The decision statistics of the estimated symbol after beamforming can be expressed as

$$y[i] = \widehat{d}_1[i] = \mathbf{w}^\dagger \mathbf{x}[i], \tag{9.24}$$

where $\mathbf{w}$ is the vector of complex adaptive weights obtained from Section 9.5.

9.9 Simulation Results for WCDMA

We first consider the scenario where there is one WCDMA user and one strong multiple access interferer in the system. The power ratio of the strong interference over the desired user is defined as

$$\chi = \frac{P_2}{P_1}, \tag{9.25}$$

where P_1 and P_2 are the receive powers for the desired user and the strong interference. Figure 9.12 shows the BER performance of MMSE vs. Maximum SNR (MRC) as function of χ for various processing gain (N_p) in a Rayleigh fading channel. In this figure, the angle spread (σ_a) is assumed 1°. As seen, MMSE with $N_p = 4$ can still outperform MRC with large N_p as χ increases. This means that we can achieve the interference suppression gain by using beamforming (spatial domain processing) instead of ineffectively suppressing the interference with large processing gain (temporal domain processing). Figure 9.13 shows the BER performance of MMSE vs. Maximum SNR (MRC) as function of χ for various processing gain (N_p) in a Rayleigh fading channel, assuming the angle spread $\sigma_a = 20°$. Again, MMSE with N_p=4 outperforms MRC with large N_p as χ increases. Next, we consider the scenario where there are multiple access WCDMA users in the system. We define the spatial separation between the desired WCDMA user and other multiple access WCDMA users as

$$\Delta_{s,j} = \theta_1 - \theta_j, \quad j \geq 2, \tag{9.26}$$

where θ_1 is the AOA of the desired user and θ_j is the AOA of the jth WCDMA user. In this study, we assume $\Delta_{s,j}$ is 15°. We further assume ideal power control scenario where the receiver powers $P_1 = P_2 = \cdots = P_K$. Figure 9.14 shows the BER performance of MMSE as function of angle spread σ_a and the number of multiple access users K in a Rayleigh fading channel. As seen, for the case of $K = 1$ (no interference), the impact of angle spread on the BER performance is significant because the performance is dominated by the signal fading. As the number of users (K) increases, the impact of angle spread become less significant. This is because the performance is dominated by both signal fading and multiple access interference. It is anticipated that the four curves in this figure would be close together for large K.

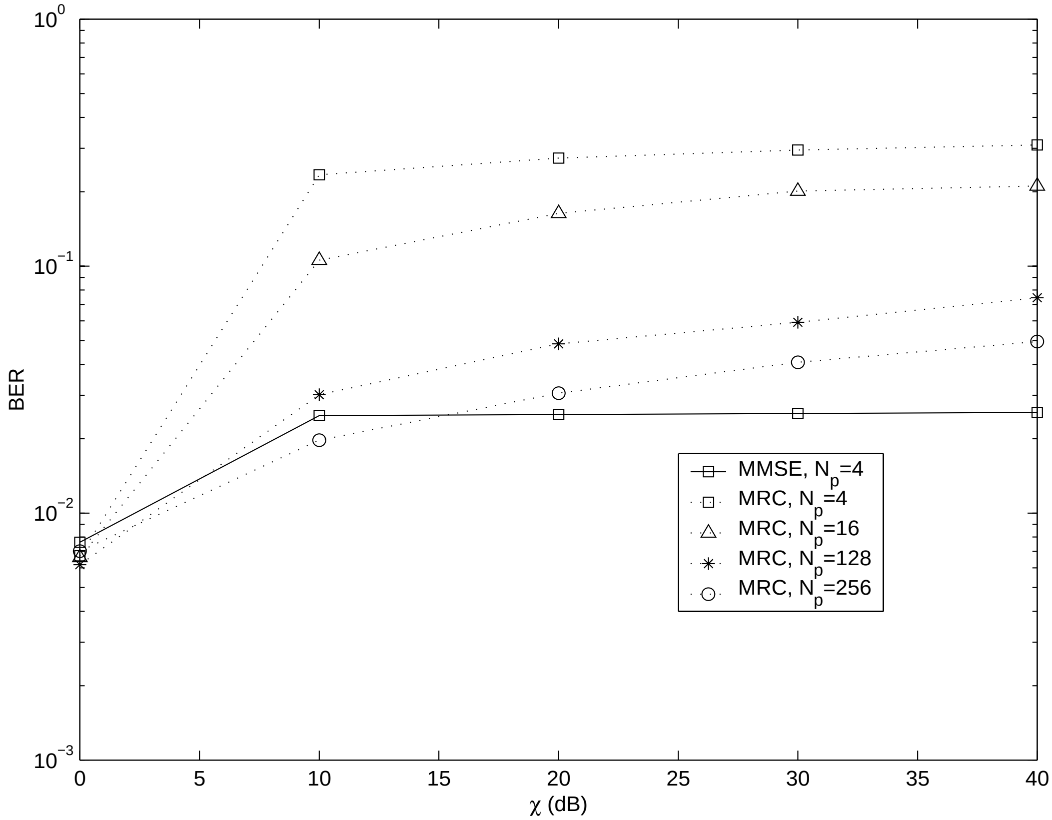

Figure 9.12: BER performance of MMSE vs. Maximum SNR (MRC) as function of χ for various processing gain (N_p) in a Rayleigh fading channel (N=25, $\sigma_a = 1°$, and γ_c=10dB).

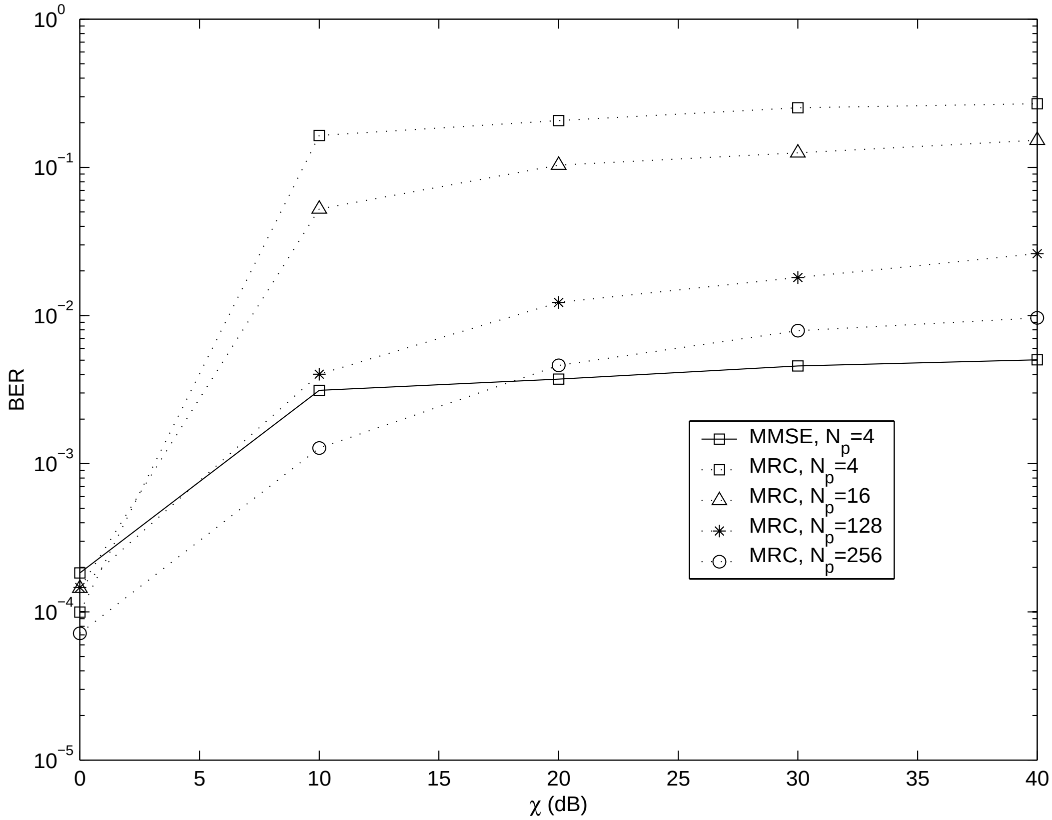

Figure 9.13: BER performance of MMSE vs. Maximum SNR (MRC) as function of χ for various processing gain (N_p) in a Rayleigh fading channel (N=25, $\sigma_a = 20°$, and γ_c=10dB).

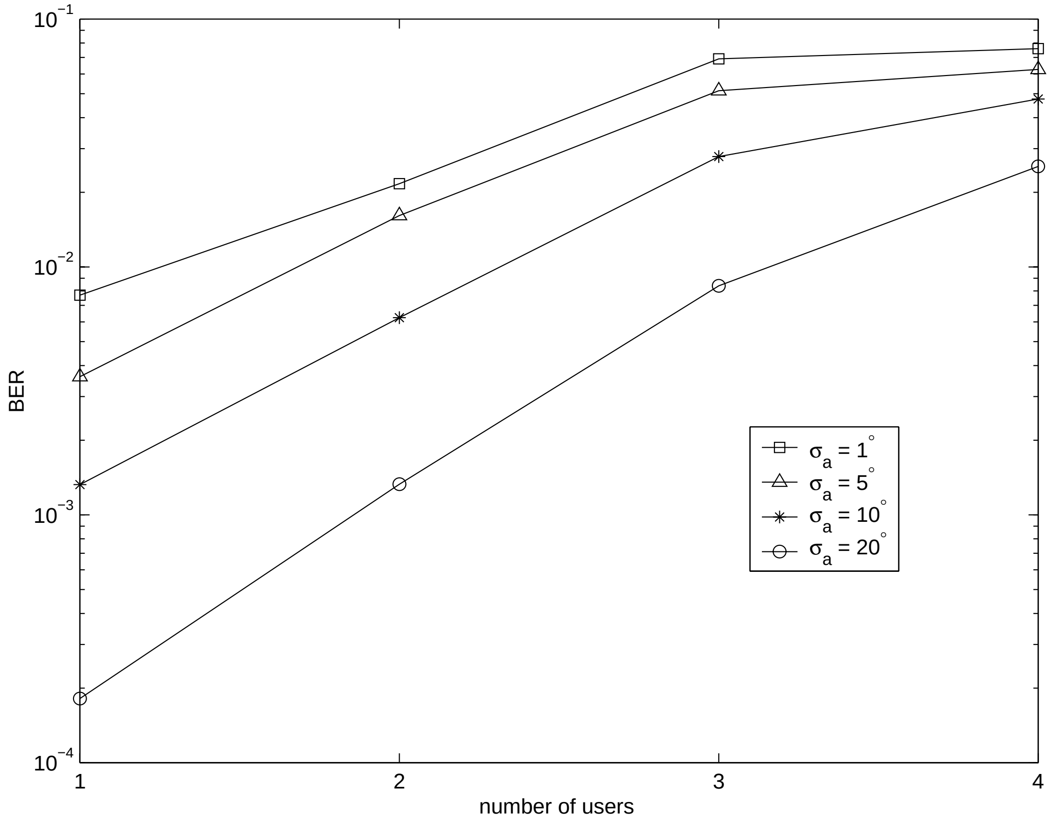

Figure 9.14: BER performance of MMSE as function of angle spread σ_a and the number of multiple access users K in a Rayleigh fading channel (N=25, γ_c=10dB, and $N_p = 4$).

9.10 Summary

In this study, we have presented the BER performance of MMSE beamforming for OFDM and WCDMA system in ground-based radio communications. For OFDM systems, results show that a number of pilots greater than 25 would provide the sufficient accuracy for estimating covariance matrix. This result is similar to those found in non-OFDM systems. It is also shown that the BER performance of MMSE beamforming improve as the space separation Δ_s increases in an AWGN channel. It is observed that the BER performance of MMSE beamforming is independent of the jammer's temporal characteristics. In a Rayleigh fading channel, the results show that the BER performance is function of space separation Δ_s for small angle spread, but is independent of Δ_s for large angle spread. For WCDMA systems, results show that the interference suppression gain can be achieved effectively by using beamforming (spatial domain processing) instead of ineffectively suppressing the interference with large processing gain (temporal domain processing).

Chapter 10

Performance of MMSE-SIC for Overloaded Array Systems

In this chapter, we propose a new signal extraction method that combines MMSE beamforming with successive interference cancelation (SIC) for an overloaded antenna array. By an overloaded array system, we mean that the number of desired signals exceeds the number of distinct antenna elements, often by a significant amount. We evaluate the performance of the proposed signal extraction method through the use of BER simulation. These simulations show that the new signal extraction method can increase the number of users that can be supported in an overloaded array environment.

This chapter is organized as follows. In Section 10.1, we start with the introduction of the overloaded array problem. In Section 10.2, we describe the system models for both synchronous and asynchronous overloaded array systems. In Section 10.3, the proposed signal extraction method and the block diagram of the proposed system architecture are presented. We describe the adaptive beamforming algorithm, the error correction decoding algorithm, and the implementation of the SIC technique. In Section 10.4, we describe the simulation validation and simulation methods used in this study. In Section 10.5, we present the BER results of the proposed signal extraction method with various directional antenna elements in an overloaded environment. We compare the performance the proposed signal extraction method with that of the conventional linear beamformer without successive interference cancelation. Finally, some concluding remarks are given in Section 10.6.

10.1 Introduction

The increase of system capacity and transmission rate has been a major goal for wireless communications research. The use of multiple antennas at the receiver has been an attractive option for increasing the capacity of cellular and PCS systems by suppressing or rejecting interference adaptively in the spatial domain. This technique is commonly referred as adaptive beamforming. In general, adaptive beamforming with M antenna elements can effectively suppress up to $M-1$ interferer [49]. That is, standard adaptive beamforming can work properly in the environment where the number of interferes is less than the number of antenna elements. However, for airborne cellular communication applications, such as airborne repeaters, the number of co-channel interferes seen at the receiver is greater than the number of antenna elements. This results in an overloaded environment. With such an environment, a conventional beamforming approach would fail to extract the desired signal from received signals.

To tackle such a problem, there have been few contributions geared specifically towards signal extraction in an overloaded array environment. Hicks and Bayram proposed the Spatially Reduced Search Joint Detection (SRSJD) technique in an overloaded array environment for airborne communication applications. Their proposed scheme reformulates the single-user Maximum Likelihood Sequence Estimation (MLSE) in temporal domain into the multi-user Maximum Likelihood Sequence Search in spatial domain. They demonstrate that SRSJD signal extraction method can successfully demodulate the number of users twice as many as the number of antenna element in an overloaded array system [41][42]. The example given in [41][42] assumes that the total number of users in a system is 16 with equal received power and the number of antenna element is 8 with uniform circular array.

Despite its effectiveness in signal extraction capability, SRSJD suffers from several drawbacks. First, in order for SRSJD to be implemented with a regular trellis structure, the geometry of the antenna array must be symmetric and the interferer locations have to be equally spaced. This may limit its application to a narrow range of wireless communication systems. Second, the computation cost of SRSJD is exponential complexity in terms of the number of users.

In this chapter, we propose the new signal extraction method that combines MMSE beamformer with successive interference cancelation technique for an overloaded antenna array system. As compared to the complexity of SRSJD, the computation cost of the proposed signal extraction method is significantly reduced due to the fact that the computation complexity for both adaptive beamformer and SIC are relatively moderate. The adaptive beamformer is based on the MMSE criteria, implemented via Direct Matrix Inversion (DMI). The antenna configuration is an 8-element circular array. Direction antenna elements may be employed within the circular array. In the proposed SIC scheme, the order of cancelation for signals is based on their BER performance rather than their received power level as with the standard SIC technique [79][94]. That is to say, a user with BER below a certain threshold is canceled first. As an example, the proposed signal extraction method is applied to a waveform modeled on the IS-136 standard.

10.2 System Model

The signal model is based on the TDMA-IS136 signal format and an AWGN channel is assumed to be a satisfactory model for ground-to-aircraft propagation. Both synchronous and asynchronous systems are considered in this study. The received signal after matched filter is sampled at symbol rate at each antenna element. For synchronous system, the baseband equivalent received signal with K synchronous users on mth antenna element during ith symbol is expressed as

$$x_m^{syn}[i] = \sum_{k=1}^{K} h_{m,k}[i] d_k[i] + N_m[i], \tag{10.1}$$

where $h_{m,k}[i]$ is the channel gain for the kth user on mth antenna element. The discrete time sequence $d_k[i]$ represents the $\pi/4$ DQPSK modulated signal for the kth user and $N_m[i]$ is an additive white Gaussian noise sample. For asynchronous systems, the baseband equivalent received signal after matched filter for the kth users on mth antenna element during ith symbol is expressed as

$$x_{m,k}^{asyn}[i] = h_{m,k}[i] d_k[i] + \sum_{n=1, n\neq k}^{K} h_{m,n}[i] d_n[i]^r + N_m^r[i], \tag{10.2}$$

where

$$d_n[i]^r = \int_0^{T_s} S_n(t-\zeta) S_k(\zeta) d\zeta, \tag{10.3}$$

$$N_m[i]^r = \int_0^{T_s} N_m(t-\zeta) S_k(\zeta) d\zeta, \tag{10.4}$$

and

$$S_k(t) = \sum_{i=-\infty}^{\infty} \sqrt{P} d_k[i] G(t - iT_s), \tag{10.5}$$

where T_s is the symbol period and $G(t)$ is the square-root raised-cosine waveform.

The vector form of the complex discrete received signal for synchronous systems at ith epoch thus can be expressed as

$$\mathbf{x}^{syn}[i] = \sum_{k=1}^{K} \mathbf{h}_k[i] d_k[i] + \mathbf{N}[i], \tag{10.6}$$

where $\mathbf{x}^{syn}[i]$, $\mathbf{h}_k[i]$ and $\mathbf{N}[i]$ are $M \times 1$ column vectors. M is the number of antenna elements. We can further rewrite (10.6) as

$$\mathbf{x}^{syn}[i] = \mathbf{H}\mathbf{s} + \mathbf{N} \tag{10.7}$$

where

$$\mathbf{H} = \left[\mathbf{h}_1[i] \quad \cdots \mathbf{h}_K[i]\right], \tag{10.8}$$

and

$$\mathbf{s} = \left[d_1[i] \quad \cdots d_K[i]\right] \tag{10.9}$$

Note that boldface type is used to represent vector quantities. Similarly, for asynchronous system, the vector form of the complex discrete received signal for kth user at ith epoch can be expressed as

$$\mathbf{x}_k^{asyn}[i] = \mathbf{h}_k[i]d_k[i] + \sum_{n=1,n\neq k}^{K} \mathbf{h}_n[i]d_n[i]^r + \mathbf{N}^r[i], \tag{10.10}$$

where $\mathbf{x}^{asyn}[i]$ and $\mathbf{N}^r[i]$ are $M \times 1$ column vectors. As recalled in Chapter 2, the vector channel of the kth user for a uniform circular array in AWGN chanel can be expressed as

$$\mathbf{h}(\theta) = \begin{bmatrix} \exp^{-j2\pi\frac{R}{\lambda}\sin(\varsigma)cos(\theta-\phi_1)} \\ \exp^{-j2\pi\frac{R}{\lambda}\sin(\varsigma)cos(\theta-\phi_2)} \\ \vdots \\ \exp^{-j2\pi\frac{R}{\lambda}\sin(\varsigma)cos(\theta-\phi_M)} \end{bmatrix}, \tag{10.11}$$

where R the circular radius of the antenna array, θ is the angle of arrival (AOA) and ϕ_m is the phase excitation of mth element in azimuth plane. It is important to note that we consider an encoded system based on IS-136 standard in our simulation. That is, the signal is convolutionally encoded before $\pi/4$ DQPSK modulation.

10.3 Proposed Signal Extraction Methods

Figure 10.1 shows the block diagram of the proposed signal extraction system structure. As shown, the received signal is first processed by MMSE beamformer. The outputs of MMSE beamformer are the estimated modulated symbols for all the users. After the demodulation process, the estimated encoded bits can be obtained. The estimated encoded bits are then fed into Viterbi decoder. Based on the output performance of the Viterbi decoder, the BER for all the users are estimated. The modulated symbols of the users with no bit error or very small bit error are regenerated and removed from the received signal in the process of successive interference cancelation. The overall process can be performed iteratively until the final user's information bits are detected.

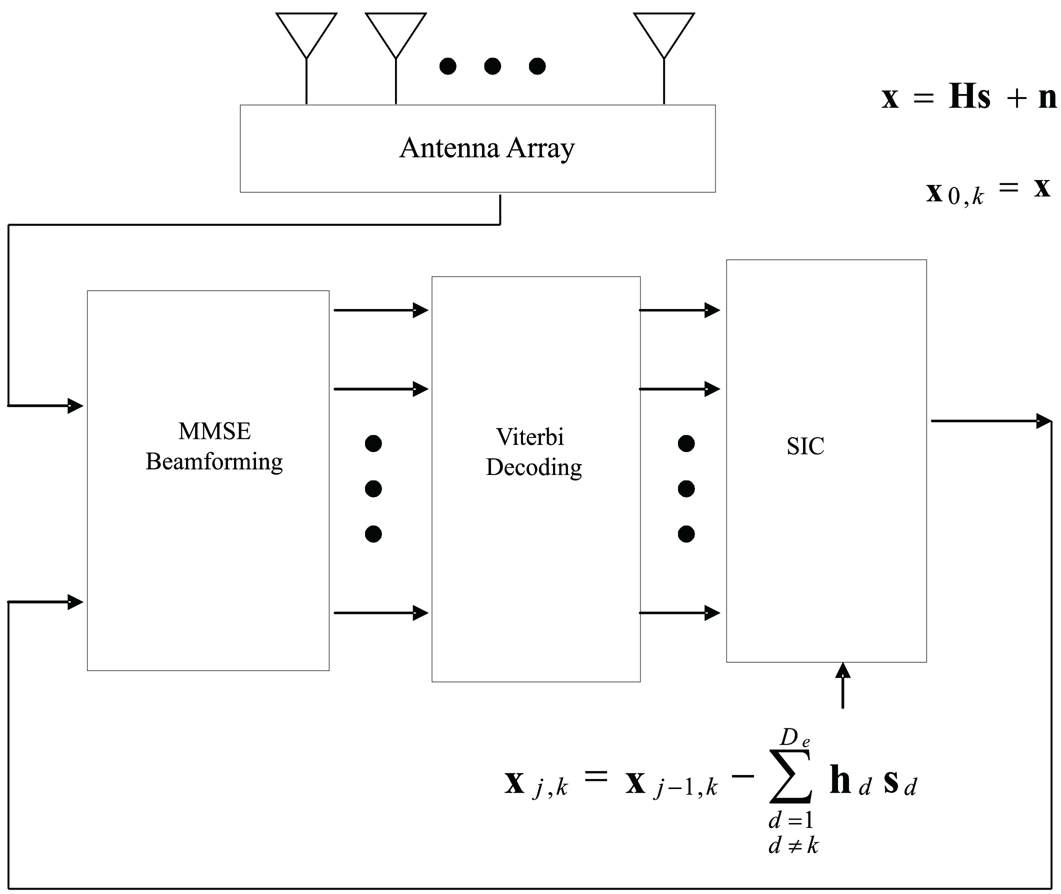

Figure 10.1: Block diagram of the proposed signal extraction method for an overloaded array system

10.3.1 MMSE Beamforming

We start with the description of the MMSE beamforming of the proposed signal extraction methods. The outputs of MMSE beamformer are the weighted sum of the element outputs and are equivalent to the estimated modulated symbols. The estimated modulated symbol at the ith epoch for kth user in synchronous systems can be expressed as

$$y_k[i] = \mathbf{w}_k^\dagger[i]\mathbf{x}^{syn}[i], \tag{10.12}$$

where $\mathbf{w}_k$ is the vector of complex adaptive weights for kth user and the superscript $\dagger$ denotes transpose and conjugate. Similarly, for asynchronous systems, the estimated modulated symbol at the ith epoch for kth user can be expressed as

$$y_k[i] = \mathbf{w}_k^\dagger[i]\mathbf{x}_k^{asyn}[i], \tag{10.13}$$

The adaptive weights are calculated based on the MMSE criterion also known as the Wiener-Hopf solution. The weights can be shown to be [114]

$$\mathbf{w}[i] = \mathbf{R}_{xx}^{-1}[i]\mathbf{r}_{xd}[i], \tag{10.14}$$

where $\mathbf{R}_{xx} = E\{\mathbf{x}[i]\mathbf{x}^\dagger[i]\}$ is the covariance matrix of the received signal and $\mathbf{r}_{xd} = E\{\mathbf{x}[i]d_k^\dagger[i]\}$ is the correlation between the received signal and the desired signal. Both the covariance matrix $\mathbf{R}_{xx}[i]$ and $\mathbf{r}_{xd}[i]$ are estimated from training sequence at the beginning of each time slot. Since an AWGN channel is assumed, the adaptive weights are calculated and updated once per time slot within the simulation, rather than once per symbol. Although from an implementation viewpoint these weight can be obtained adaptively from LMS, RLS, or DMI (Direct Matrix Inversion) algorithms, we consider DMI beamforming algorithm only in this study. In DMI implementation, the estimated covariance matrix $\widehat{\mathbf{R}}_{xx}[i]$ and $\hat{\mathbf{r}}_{xd}[i]$ can be expressed as follows, respectively

$$\widehat{\mathbf{R}}_{xx}[i] = \frac{1}{N_a}\sum_{n=0}^{N_a-1}\mathbf{x}[i-N_a+n]\mathbf{x}^\dagger[i-N_a+n], \tag{10.15}$$

$$\hat{\mathbf{r}}_{xd}[i] = \frac{1}{N_a} \sum_{n=0}^{N_a-1} \mathbf{x}[i - N_a + n] d_k^*[i - N_a + n], \tag{10.16}$$

where N_a is the number of symbols in the training sequence.

The differential demodulation is performed after the MMSE beamformer. The demodulated symbols for kth user are

$$\hat{d}_{k,\mathsf{I}}[i] = \mathrm{sgn}[\mathrm{Re}\{y_k[i]^* y_k[i-1]\}], \tag{10.17}$$

$$\hat{d}_{k,\mathsf{Q}}[i] = \mathrm{sgn}[\mathrm{Im}\{y_k[i]^* y_k[i-1]\}], \tag{10.18}$$

where $\hat{d}_{k,\mathsf{I}}[i]$ and $\hat{d}_{k,\mathsf{Q}}[i]$ are the estimated encoded bits for I and Q channel, respectively. The estimated encoded bits following the output of $\pi/4$ DQPSK demodulator are used as the input data sequence to a channel decoder. The Viterbi decoding algorithm is then performed in the channel decoder and the estimated information bits are obtained from the output of the decoder. The coded BER performance then can be determined by comparing the estimated information bits with the pre-decoded information bits.

10.3.2 Successive Interference Cancelation (SIC)

In general, an adaptive beamformer can provide acceptable BER performance for the case where the number of antennas exceeds the number of interferes. However, for an overloaded environment ($M < K$), a conventional adaptive beamformer would fail to provide acceptable performance due to the lack of capability for rejecting interference. To overcome this problem, the proposed signal extraction method combines the MMSE beamformer with SIC to further enhance the system performance in an overloaded antenna array system.

SIC has been extensively studied in the area of multiuser detection for CDMA systems [80]. The idea of SIC is that if a reliable decision has been make about an strong user's bit, then that strong signal can be regenerated at the receiver and subtracted from the received signal first. Once the subtraction process is completed, the resulting signal contains less interference and the process can be repeated with the next strongest user until all the users are demodulated.

In order to fully exploit the SIC technique, it is suggested that some variation in received power levels among users is beneficial for a SIC receiver [79][80]. This allows stronger users to be correctly detected; therefor their signals can be effectively canceled from the received signal. Thus the weak users would have a chance to be successfully detected after the strong interference is removed from their received signals. To create such power variation in received signal, we use a directional pattern at each antenna element in the simulated circular array.

It is important to note that the order of cancelation in SIC technique in the proposed approach is based on their BER performance. That is to say, a user with BER below certain predetermined BER threshold is canceled first. The BER performance can be determined from the output of the Viterbi algorithm. At each cancelation stage, there may be several users with good BER performance can be canceled from the received signal.

Suppose that D_e users with BER below a certain predetermined BER threshold are selected to be canceled at jth successive interference stage, the residual signal for kth user in synchronous and asynchronous systems then can be expressed as follows, respectively

$$\mathbf{x}_{j,k}^{syn}[i] = \mathbf{x}_{j-1,k}^{syn}[i] - \sum_{u=1}^{D_e} \mathbf{h}_u[i] d_u[i] \tag{10.19}$$

$$\mathbf{x}_{j,k}^{asyn}[i] = \mathbf{x}_{j-1,k}^{asyn}[i] - \sum_{u=1}^{D_e} \mathbf{h}_u[i] d_u^r[i]. \tag{10.20}$$

The initial values of $\mathbf{x}_{0,k}^{syn}[i]$ and $\mathbf{x}_{0,k}^{asyn}[i]$ are given by

$$\mathbf{x}_{0,k}^{syn}[i] = \mathbf{x}^{syn}[i], \tag{10.21}$$

$$\mathbf{x}_{0,k}^{asyn}[i] = \mathbf{x}_{k}^{asyn}[i], \tag{10.22}$$

As shown in Figure 10.1, the residual signals of $\mathbf{x}_{j,k}^{syn}[i]$ and $\mathbf{x}_{j,k}^{asyn}[i]$ are fed back to MMSE beamformer again for detecting the rest of the users. This signal extraction process is performed iteratively until the last (weakest) user is detected.

10.4 Simulation Methods and Validation

We use Monte Carlo simulations to evaluate the BER performance of the proposed MMSE-SIC techniques. Each BER data point is averaged over 2500 frame data, corresponding 50 seconds of data. Each frame is convolutionally encoded with data rate approximately 48,000 symbols per second. We assume that the users have equal received power at antenna array. The antenna array scheme is assumed to 8-element uniform circular array with the antenna element spacing $R = 5\lambda$. Each antenna element pattern is either a omnidirectional or a directional pattern. The directional patterns of each antenna used in simulation are shown in Figure 10.2. It is noted that the users' locations are evenly spaced over $[0,2\pi]$. That is, the angle of arrival θ is evenly distributed.

To validate the simulation results, we first verify $\pi/4$ DQPSK modulator and convolutional encoder used in the simulation by comparing their performance with the similar results presented in [62]. The simulator is validated after both simulation results have a good agreement. We slightly modify the verified MMSE beamforming algorithm used in Chapter 9 and adopted it for this study. We also run several simulation with similar channel parameters used in [95] to verify the SIC simulation. The simulator is validated after both simulation results have a good agreement.

10.5 Simulation Results

In this section, we present BER simulation results of the proposed signal extraction method in an overloaded antenna array system. The practical issues such as channel

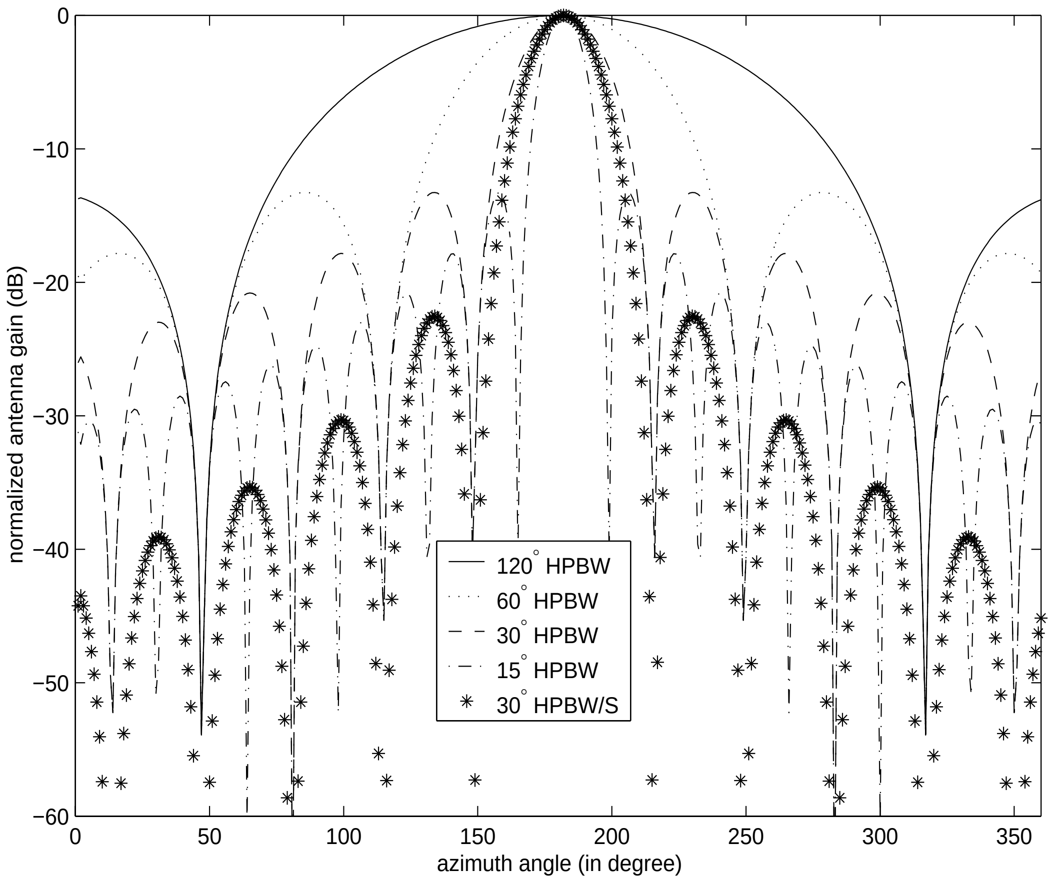

Figure 10.2: Directional antenna patterns used in simulation

estimation are also considered. We describe the channel estimation issues on the following.

10.5.1 Pilot-Symbol Based Channel Estimation

We consider the problem of channel estimation for the SIC technique used in the proposed signal extraction method. The approach we take to channel parameter estimation is based on the known pilot symbols embedded into data sequence. Such pilot symbols are present in the IS-136 standard. Note that because we are operating in the heavy multiple access interference environment of the overloaded antenna, the pilot symbols must potentially be extracted in the presence of heavy multiple access interference. Hence, we assume orthogonal sequences are used as pilot symbol sequences for synchronous channels while the maximum-length PN (pseudo-noise) sequences are used for asynchronous channels. The estimated channel vector for kth user in synchronous channels can be obtained by correlated the received signal with known orthogonal pilot sequence:

$$\widehat{\mathbf{h}}_k = E\{\mathbf{x}^{syn}[i] d_k^{\dagger}[i]\}, \tag{10.23}$$

where $d_k^{\dagger}[i]$ is the pilot symbol sequence for kth user and is orthogonal to the others. Similarly, for the asynchronous channels, the estimated channel vector for kth user is given by

$$\widehat{\mathbf{h}}_k = E\{\mathbf{x}_k^{asyn}[i] d_k^{\dagger}[i]\}, \tag{10.24}$$

where $d_k^{\dagger}[i]$ is the pilot symbol sequence for kth user and is the maximum-length PN sequence. Note that the length of pilot symbol sequence is assumed 32 and 31 for synchronous and asynchronous channels, respectively. In addition, the number of possible pilot sequences that can be generated is based on the length of the pilot symbols. In simulation, $\widehat{\mathbf{h}}_k$ is implemented as

$$\widehat{\mathbf{h}}_k[i] = \frac{1}{N_a} \sum_{n=0}^{N_a-1} \mathbf{x}[i - N_a + n] d_k^{*}[i - N_a + n], \tag{10.25}$$

where N_a is assumed 32 and 31 for synchronous and asynchronous channels, respectively.

10.5.2 Simulation Results for Synchronous Systems

With the proposed signal extraction method, it is expected that the BER performance among users would vary quite significantly. This is due to the use of SIC scheme in the signal extraction process. In order to predict the number of users that can be supported in an overloaded environment, we only to show the BER performance of the worst users.

Figure 10.3 shows the BER result of the worst user in an overloaded antenna array system. The legend 'MMSE/Omni' means that MMSE beamformer is employed without SIC and omni-directional pattern is used at each antenna element. 'MMSE/SIC/Omni' and 'MMSE/SIC/X' mean that joint MMSE beamformer with SIC are employed with omni-directional antenna and X° half power beam-width antenna (HPBW), respectively. We show the BER of the worst user in order to calculate the maximum possible number of users that can be supported in a system. For voice applications within an IS-136 system, a target bit error rate in the range of 10^{-2} to 10^{-3} should assure acceptable performance. Note that we assume the channel is known to the receiver in this figure.

It is seen that by using the proposed signal extraction method the number of users that achieve the target BER increase as the antenna beamwidth of a directional pattern gets narrower. This is because a narrower beamwidth of a directional antenna pattern can create a larger variance in the received power levels and result in a significant distinction between strong users and weak users. As a result, the received power scenario is beneficial for SIC receivers. However, when the antenna beamwidth is too narrow, this results in a huge power distinction between the strong and weak users. Therefore, the residual interference from the previous stage of successive interference cancelation process would still present a quite amount of interference to weak users. As shown in Figure 10.3, the performance of the proposed signal extraction method starts to degrade for a narrower beamwidth of 15° HPBW. We found that a 60° HPBW of a directional pattern can support up 16 users (twice as many as number of antenna element) and a 30° HPBW of a directional pattern with lower sidelobe can support up 24 users (three times as many as number of antenna element).

In Figure 10.4, we vary Eb/No from 5 to 15 dB and show the BER result for two cases. Note that γ_c is the received signal-to-noise ratio per bit (E_b/N_o) at a received antenna element. Case one consists of a 60° HPBW directional pattern and 16 supported users. Case two consists of a 30° HPBW directional pattern with lower sidelobes and 24 supported users. As expected, BER decreases as Eb/No increase. Note that both the known channel and pilot symbol based channel estimation are considered in this figure. As expected, the case with channel estimation suffer performance degradation as compared to the case of the known channel.

Figure 10.5 shows the BER performance of the total 16 users that is supported by using the proposed signal extraction methods with a 60° HPBW of a directional pattern. It is observed that the strong users (at antenna mainlobe) experience better BER performance that the weaker users. It is also observed that the performance experience some degree of degradation as compared to the case of the known channel.

Figure 10.6 shows the BER performance of the total 24 users that is supported by using the proposed signal extraction methods with a 30° HPBW of a directional pattern with lower sidelobe. The same performance trend is observed as in Figure 10.5.

10.5.3 Simulation Results for Asynchronous Systems

For asynchronous systems, it is found that the proposed signal extraction methods with known channel can support 26 user, 28 users, and 32 users for using a 120° HPBW, a 60° HPBW, and a 30° HPBW, respectively.

Figure 10.7 shows the BER performance of the 26 users using the proposed signal extraction methods with a 120° HPBW of a directional pattern. It is expected that the strong users (located at the antenna mainlobe) experience better BER performance that the

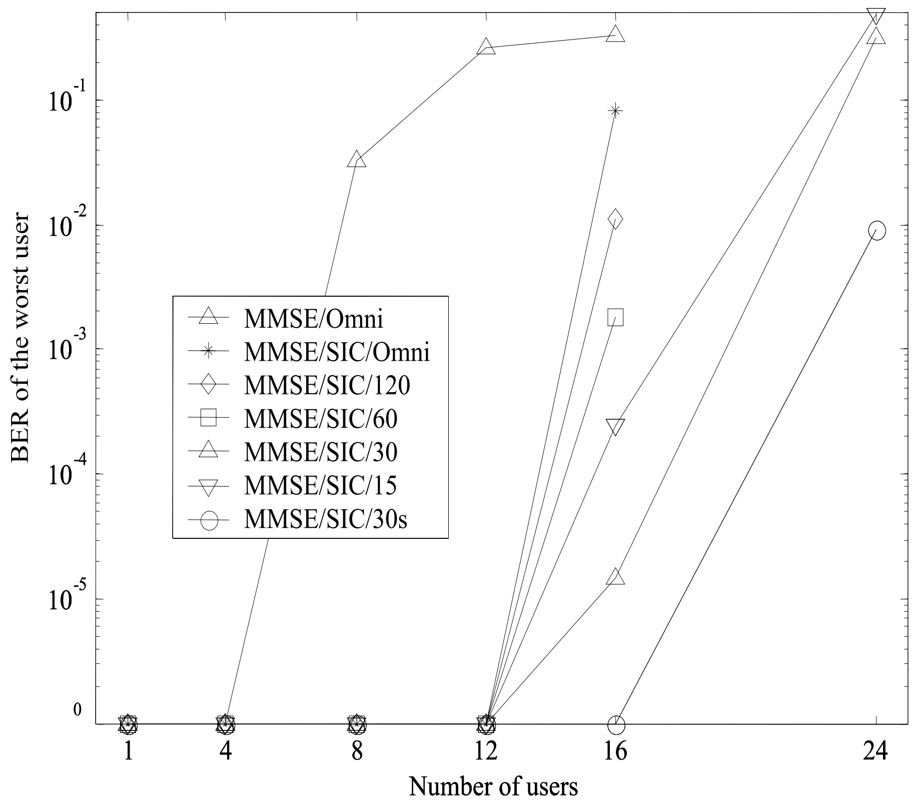

Figure 10.3: BER of the worst user with MMSE beamformer and joint MMSE beamformer/SIC with various directional antenna patterns (Eb/No=15 dB, $\pi/4$ DQPSK, Rate =1/2, Convolutional code with constraint length =5).

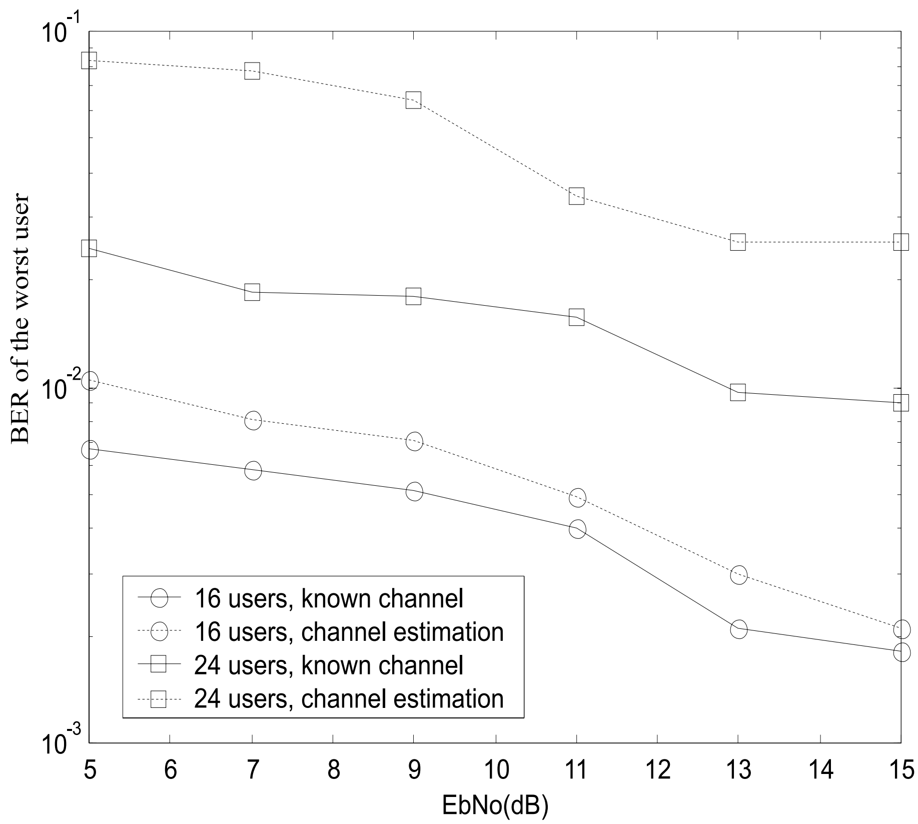

Figure 10.4: BER of the worst user for two cases using the proposed signal extraction method, case one: 16 users and 60° HPBW. case two: 24 users and 30°HPBW with lower sidelobe ($\pi/4$ DQPSK, Rate =1/2, Convolutional code with constraint length =5).

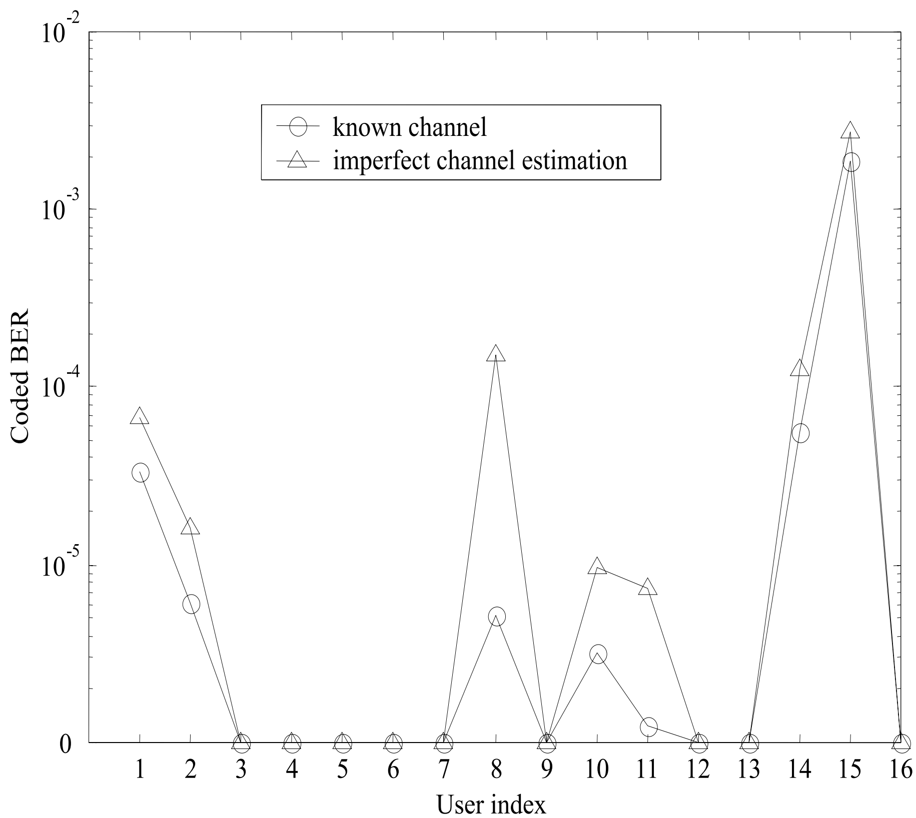

Figure 10.5: BER performance of the total 16 users that is supported by using the proposed signal extraction methods with a 60° HPBW of a directional pattern

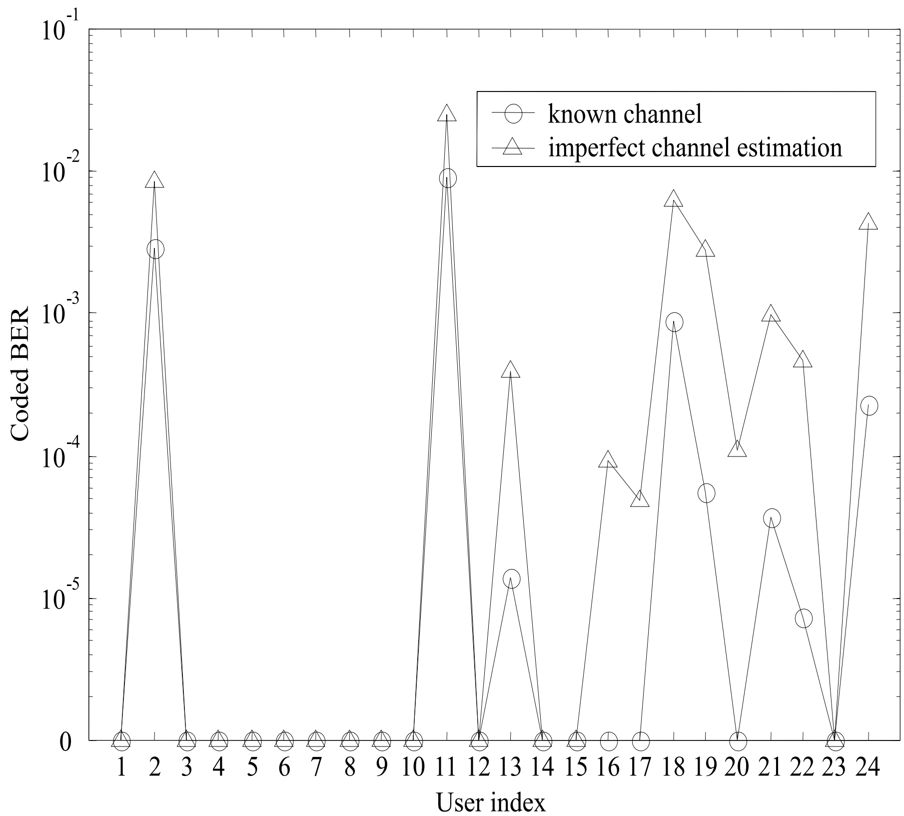

Figure 10.6: BER performance of the total 24 users that is supported by using the proposed signal extraction methods with a 30° HPBW of a directional pattern with lower sidelobe

weaker users (located at the antenna sidelobe). It is also seen that the case with channel estimation experience performance degradation as compared to the case of known channel.

Figure 10.8 shows the BER performance of the 28 users using the proposed signal extraction methods with a 60° HPBW of a directional pattern. The same performance trend is observed as in Figure 10.7. It is also suggested that the SIC technique is generally sensitive to the channel estimation errors.

Figure 10.9 shows the BER performance of the 32 users using the proposed signal extraction methods with a 30° HPBW of a directional pattern. The performance with channel estimation degrades significantly. This is because the number of PN code sequences (31) that can be generated based on the length of pilot symbol sequence is less than the number of users supported in the systems.

10.6 Summary

The simulation results show that the proposed signal extraction method that combines MMSE beamformer with a SIC technique generally outperforms a conventional beamformer and can significantly increase the number of users that can be supported in an overloaded array environment. As compared to Spatially Reduced Search Joint Detection (SRSJD) technique in [41][42], the complexity of the proposed signal extraction is relatively moderate. For synchronous systems, we found that the proposed signal extraction method with a 60° HPBW of a directional pattern can support up 16 users (twice as many as number of antenna element) and a 30° HPBW of a directional pattern with lower sidelobe can support up 24 users (three times as many as number of antenna element). For asynchronous systems, it is found that the proposed signal extraction methods with known channel can support 26 users, 28 users, and 32 users for using a 120° HPBW, a 60° HPBW, and a 30° HPBW, respectively. It is also seen that the

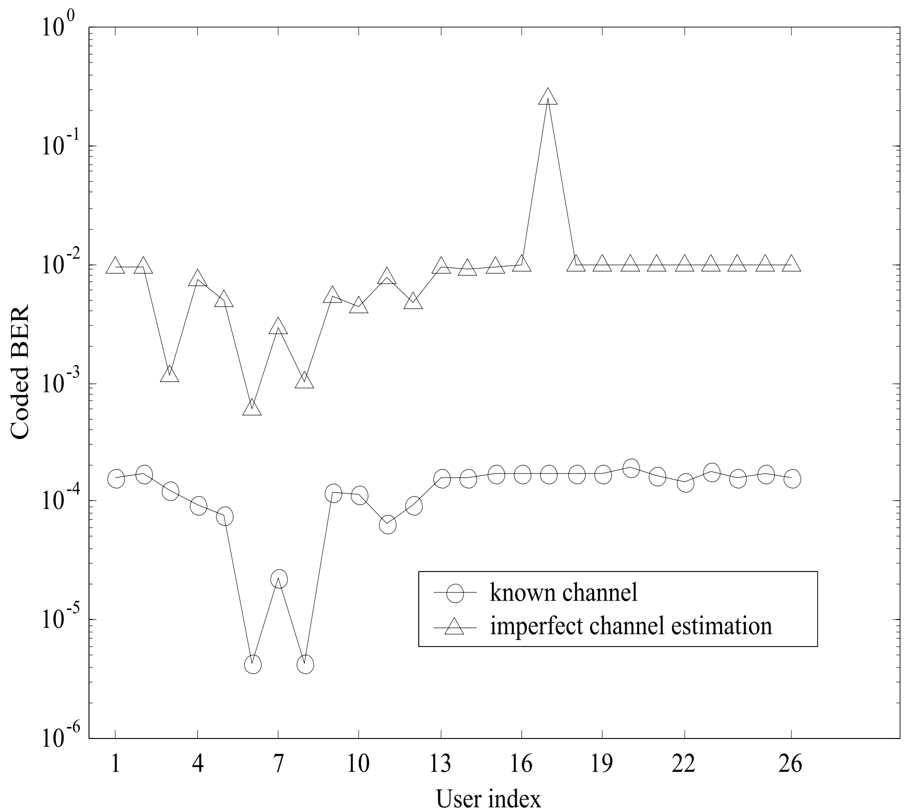

Figure 10.7: BER performance of the total 26 users that is supported by using the proposed signal extraction methods with a 120° HPBW of a directional pattern

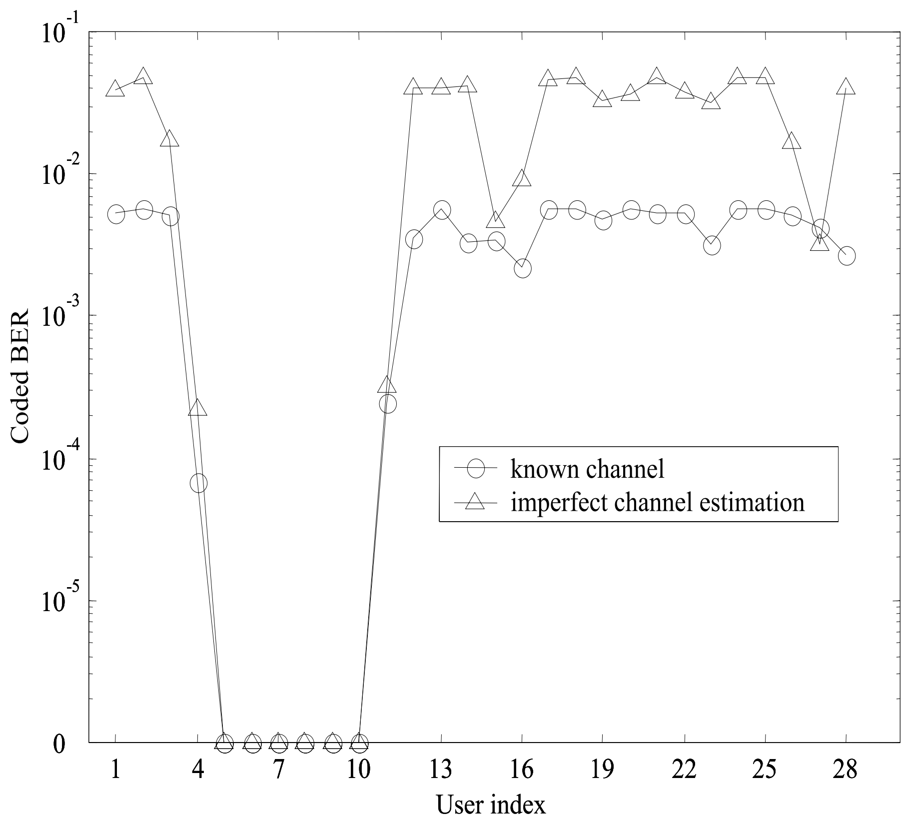

Figure 10.8: BER performance of the total 28 users that is supported by using the proposed signal extraction methods with a 60° HPBW of a directional pattern

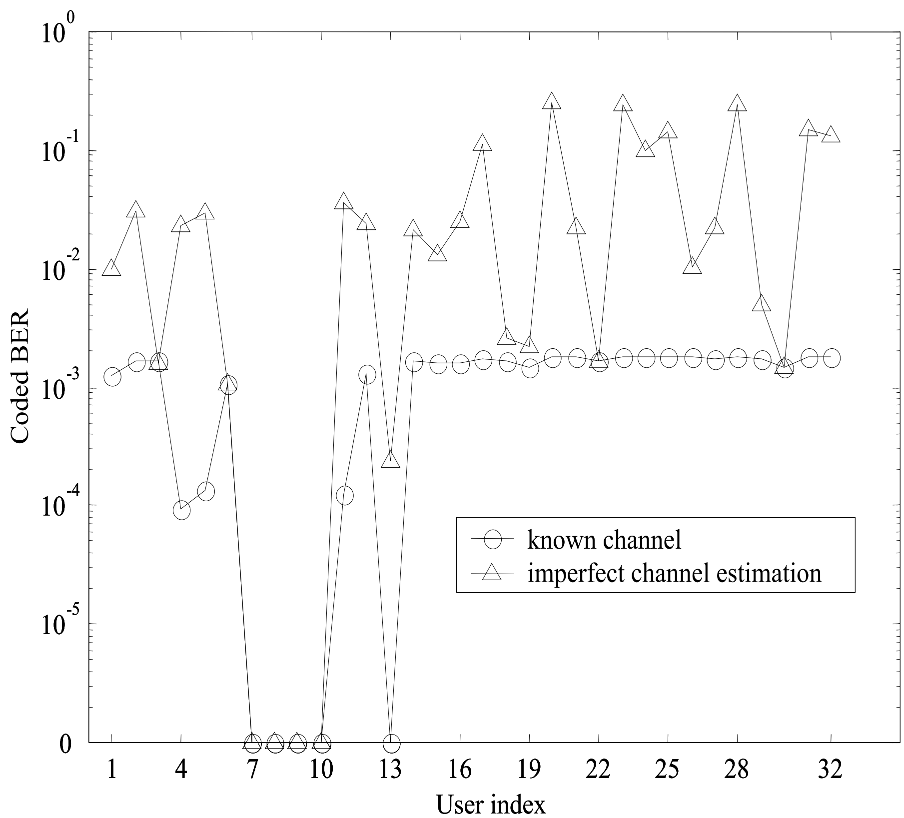

Figure 10.9: BER performance of the total 32 users that is supported by using the proposed signal extraction methods with a 30° HPBW of a directional pattern

performance experienced degradation in the presence of imperfect channel estimation.

Chapter 11

Summary and Future Work

This dissertation examined the system performance of MIMO antenna systems for wireless communications. We summarize the results from this work in Section 11.1. Future work is described in Section 11.2 and concluding remarks are given in Section 11.3.

11.1 Summary

This work has studied the use of multiple transmit and multiple receive antenna arrays in wireless communications. The motivation for using multiple transmit and multiple receive antenna arrays for wireless communications was thoroughly discussed in Chapter 1. The benefit of space-time diversity provided by combining MIMO systems with orthogonal transmit waveforms for future wireless communications was also discussed. A space-time MIMO channel model for mobile radio environments was developed and examined in Chapter 2. We found that a parameter-based statistical MIMO channel model is a better-suited model for our study of mobile radio communications. The statistical MIMO channel is modeled as a function of statistical channel parameters such as angle spread, Doppler spread, and delay spread.

In Chapter 3, we derived an analytical expression for the MIMO channel space-time fading correlation for a uniform circular array and a uniform linear array in a mobile radio environment. The MIMO channel space-time fading correlation was evaluated for both uplink and downlink communication. The MIMO space-time fading correlation is composed of a temporal fading correlation and a spatial fading correlation. The temporal fading correlation is a function of the Doppler spread and time delay, while the spatial fading correlation is a function of the angle spread and distance between elements. Results showed that the temporal fading correlation decreases as the Doppler spread and/or time delay increase, and the spatial fading correlation decreases as the antenna spacing and/or angle spread increases. Three AOA distributions were considered: uniform, truncated Gaussian, and truncated Laplacian. Results show that the three AOA distributions give similar spatial fading correlation for the same angle spread suggesting that the variance of the distribution is more important than the actual distribution. Computer simulations are carried out to verify the analytical results.

In Chapter 4, we evaluated the information-theoretic channel capacity of a MIMO channel with both UCA and ULA antenna configurations. The information-theoretic channel capacity was evaluated as function of the spatial fading correlation due to both the transmit array and the receive array. The results suggested that a (ULA,UCA) MIMO antenna configuration may be the prefered choice for higher channel capacity in mobile radio communications.

In Chapter 5, we examined the transmit side of MIMO systems. We evaluated the BER performance of the open-loop transmit diversity and the closed-loop transmit beamforming over Rayleigh and Ricean fading channels. We showed that closed-loop transmit beamforming is beneficial when the fading channel is Ricean or has low Doppler spread (low mobility) while the open-loop transmit diversity method is a better-suited transmission technique when the fading channel is Rayleigh and the Doppler spread is high (high mobility).

In Chapter 6, we examined the receive side of MIMO systems. We presented the BER performance of a uniform circular array and a uniform linear array in mobile radio communications. The analytical BER was derived as a function of spatial fading antenna correlation for both types of antenna arrays. Results show that for similar aperture size, the UCA outperforms the ULA when considering all angles-of-arrival. This is most pronounced for small and moderate angle spread. For angles-of-arrival concentrated near the broadside of the linear array, the ULA typically performs as well as or better than the UCA. A truncated Gaussian angle-of-arrival (AOA) distribution and flat Rayleigh fading were assumed. Simulations were carried out to verify the analytical BER results.

In Chapter 7, we designed and evaluated the performance of a simple space-time orthogonal transmit waveform in a MIMO cellular environment. We derived an analytical BER formula for evaluating the performance of the proposed OTW-STD system in a MIMO Rayleigh fading channel. The analytical BER formula for the OTW-STD waveform was derived as a function of the eigenvalues of the space-time channel covariance matrix. The space-time channel correlation is a function of angle spread and Doppler frequency for a mobile radio channel. The results show that the OTW system can fully exploit the spatial and temporal diversity of mobile radio channels and provide significant performance improvement over systems without diversity. We applied the ST-OTW waveform to a conventional cellular systems where two antennas are employed at the base station and one antenna is employed at the mobile station. We derived an analytical BER expression for the OTW-STD waveform and compared with its BER performance with the baseline system (no diversity) and STS system. BER analysis were carried for both downlink and uplink communications. It is shown that in absence of transmit spatial diversity, the OTW-STD outperforms the STS system. The result suggests that the OTW-STD waveform is better-suited for high mobility and small angle spread environments.

In Chapter 8, we reviewed two active signal processing techniques for interference cancelation in wireless communications: multiuser detection systems and adaptive antenna array system. We describe the principles and fundamentals of signal detection techniques for multiuser detection systems and discuss the features of both optimum multiuser receivers and various suboptimum multiuser receivers. We examine various optimization criterion for adaptive antenna array combining techniques and review the practical issues on the implementation of adaptive antenna array combining algorithms.

In Chapter 9, we evaluated the performance of MMSE beamforming for both DS-CDMA and OFDM systems in AWGN and Rayleigh fading channels. The performance of MMSE beamforming was evaluated based on BER simulations. The effects of angle spread and the user location as well as practical implementation issues were considered. The comparative BER performance of MMSE beamforming and MRC beamforming were also evaluated. Results showed that the number of pilot symbols should be greater than 25 to provide the sufficient accuracy for estimating covariance matrix. This result is similar to those found in others systems. Results also showed that the BER performance of MMSE beamforming improves as the spatial separation increases in an AWGN channel. In a Rayleigh fading channel, the results show that the BER performance is a function of spatial separation for small angle spread, but it is independent of spatial separation for large angle spread.

In Chapter 10, we proposed a signal extraction method that combines MMSE beamforming with successive interference cancelation or parallel interference cancelation for an overloaded antenna array system. The combined MMSE beamforming with successive interference cancelation (MMSE-SIC) was proposed for overloaded airborne communications using narrowband TDMA signal formats. The simulation results showed that the proposed signal extraction method that combines a MMSE beamformer with a SIC technique generally outperforms a conventional beamformer and can significantly increase the number of users that can be supported in an overloaded array environment. As compared to the Spatially Reduced Search Joint Detection (SRSJD) technique, the complexity of the proposed signal extraction approach is relatively moderate.

11.2 Future Work

The research described in this dissertation leads naturally to several extensions. These extensions include:

- In the area of channel modeling, we have developed the statistical-based multipath MIMO channel model based on limited measurement data. The statistical distribution of the channel parameters used in the study such as angle spread and delay spread need to be verified by more measurement data.

- In the area of the OTW-STD waveform, we have evaluated the performance of the OTW-STD waveform in a single-user and uncoded system. The impact of coding on the OTW-STD system needs to be investigated further. In addition, the performance of the OTW-STD waveform in a multiuser system needs to be evaluated.

- In the area of adaptive beamforming, we have extensively investigated the performance of MMSE beamforming in non-frequency-selective channel. The work of MMSE beamforming can be expanded to frequency-selective channel. In addition, comparison between MMSE beamforming and other adaptive algorithms such as maximum SINR are also very interesting.

- In the area of overloaded array processing, we have proposed the MMSE-SIC techniques to an overloaded array system. We have evaluated the performance of MMSE-SIC based on perfect channel estimation. The impact of practical channel estimation on SIC techniques needs to be further investigated. In addition, comparisons between MMSE-SIC receivers and a single-user space-time adaptive receiver would also be very interesting.

11.3 Conclusions

This research has shown how the channel capacity and system performance can be enhanced by using MIMO systems for wireless communications. This work also extensively examined the system performance of various transmit antenna schemes and various receive antenna configurations for MIMO systems. This research proposed a space-time orthogonal transmit waveform for wireless commutations. In conjunction with MIMO systems, the proposed space-time orthogonal transmit waveform can fully provide space-time diversity unlike the baseline systems. It was also shown that the proposed waveform can outperform the existing STS system in the absence of transmit spatial diversity. Finally, this dissertation investigates a number of interference cancelation techniques for multiple-receive antenna systems. When the number of receive antennas is greater than or equal to the number of users in the system, we examined the MMSE beamforming techniques for interference suppression. For the case when the number of users exceeds the number of receive antennas (known as the overloaded array system), we proposed a joint approach that combines MMSE beamforming with multiuser detection for both interference cancelation and suppression.

Appendix A

Derivation of Spatial Correlation for UCA with Uniform Distributions

Using the equation (3.14), the transmit spatial correlation between the pth and p'th antenna element for a UCA with a uniform AOD distribution can be expressed as

$$\begin{aligned} \mathrm{R}_s(p,p')^d &= \int_{\zeta^r} v_p^r(\zeta^r) v_{p'}^{r,*}(\zeta^r) f(\zeta^r) d\,\zeta^r \\ &= \frac{1}{2\Delta}\int_{-\Delta+\theta^r}^{\Delta+\theta^r} e^{-j2\pi\frac{R_r}{\lambda}\{[cos\phi_p - \cos\phi'_p]\cos(\zeta^r)+[sin\phi_p - \sin\phi'_p]\sin(\zeta^r)\}} d\zeta^r \end{aligned} \tag{A.1}$$

Let

$$K_{1,r} = 2\pi\frac{R_r}{\lambda}[cos(\phi_p) - \cos(\phi'_p)], \tag{A.2}$$

$$K_{2,r} = 2\pi\frac{R_r}{\lambda}[sin(\phi_p) - \sin(\phi'_p)], \tag{A.3}$$

$$\sin(\alpha^r) = \frac{K_{1,r}}{\sqrt{K_{1,r}^2 + K_{2,r}^2}}, \tag{A.4}$$

$$\cos(\alpha^r) = \frac{K_{2,r}}{\sqrt{K_{1,2}^2 + K_{2,r}^2}}, \tag{A.5}$$

$$Z_c^r = \sqrt{K_{1,r}^2 + K_{2,r}^2}. \tag{A.6}$$

Using the definitions of (A.6), (A.2), (A.3), (A.4), and (A.5), we can rewrite (A.1) as

$$\mathrm{R}_s(p,p')^d = \frac{1}{2\Delta}\int_{-\Delta+\theta^r}^{\Delta+\theta^r} e^{-jZ_c^r\{\sin(\alpha^r+\zeta^r)\}}\,d\zeta^r. \tag{A.7}$$

Let $x = \zeta^r + \alpha^r$, we can rewrite the real and imaginary parts of (A.7) as follows

$$\mathrm{Re}\{\mathrm{R}_s(p,p')^d\} = \frac{1}{2\Delta}\int_{-\Delta+\theta^r+\alpha^r}^{\Delta+\theta^r+\alpha^r} \cos[Z_c^r\sin(x)]\,dx, \tag{A.8}$$

$$\mathrm{Im}\{\mathrm{R}_s(p,p')^d\} = \frac{1}{2\Delta}\int_{-\Delta+\theta^r+\alpha^r}^{\Delta+\theta^r+\alpha^r} \sin[Z_c^r\sin(x)]\,dx. \tag{A.9}$$

By making use of the well-known series, $\cos[Z_c^r\sin(\varphi)]$ and $\sin[Z_c^r\sin(\varphi)]$ can be further represented as, respectively

$$\cos[Z_c^r\sin(\varphi)] = J_0(Z_c^r) + 2\sum_{k=1}^{\infty} J_{2k}(Z_c^r)\cos(2k\varphi), \tag{A.10}$$

$$\sin[Z_c^r\sin(\varphi)] = 2\sum_{k=0}^{\infty} J_{2k+1}(Z_c^r)\sin((2k+1)\varphi). \tag{A.11}$$

By integrating (A.8) and (A.9) with the substitution of (A.10) and (A.11) respectively, we can obtain (3.16) nad (3.17).

Appendix B

Derivation of Spatial Correlation for UCA with Gaussian Distributions

Using the equation (3.14), the transmit spatial correlation between the pth and p'th antenna element for a UCA with a truncated Gaussian AOD distribution can be expressed as

$$\begin{aligned}
\mathrm{R}_s(p,p')^d &= \int_{\zeta^r} v_p^r(\zeta^r) v_{p'}^{r,*}(\zeta^r) f(\zeta^r) d\,\zeta^r \\
&= \int_{-\pi+\theta^r}^{\pi+\theta^r} e^{-j2\pi\frac{R_r}{\lambda}\{[cos\phi_p - \cos\phi'_p]\cos(\zeta^r)+[sin\phi_p - \sin\phi'_p]\sin(\zeta^r)\}} C_g e^{-\frac{(\zeta^r-\theta^r)^2}{2\sigma_a}}\,d\zeta^r.
\end{aligned} \tag{B.1}$$

Using the definitions of (A.6), (A.2), (A.3), A.4), and (A.5), we can rewrite (B.1) as

$$\mathrm{R}_s(p,p')^d = C_g \int_{-\pi+\theta^r}^{\pi+\theta^r} e^{-jZ_c^r\{\sin(\alpha^r+\zeta^r)\}} e^{-\frac{(\zeta^r-\theta^r)^2}{2\sigma_a}}\,d\zeta^r. \tag{B.2}$$

Let $x = \zeta^r - \theta^r$, we can rewrite the real and imaginary parts of (B.2) as follows

$$\mathrm{Re}\{\mathrm{R}_s(p,p')^d\} = C_g \int_{-\pi}^{\pi} \cos[Z_c^r \sin(\alpha^r+\theta^r+x)] e^{-\frac{x^2}{2\sigma_a}}\,dx, \tag{B.3}$$

$$\mathrm{Im}\{\mathrm{R}_s(p,p')^d\} = C_g \int_{-\pi}^{\pi} \sin[Z_c^r \sin(\alpha^r+\theta^r+x)] e^{-\frac{x^2}{2\sigma_a}}\,dx. \tag{B.4}$$

By integrating (B.3) and (B.4) with the substitution of (A.10) and (A.11) respectively, we can obtain

$$\mathrm{Re}\{\mathrm{R}_s(p,p')^d\} = J_0(Z_c^r) + 2\sqrt{2\pi}C_g\sigma_a \sum_{k=1}^{\infty} e^{-2k^2\sigma_a^2} J_{2k}(Z_c^r)\cos[2k(\theta^r + \alpha^r)], \tag{B.5}$$

$$\mathrm{Im}\{\mathrm{R}_s(p,p')^d\} = 2\sqrt{2\pi}C_g\sigma_a \sum_{k=0}^{\infty} e^{\frac{-(2k+1)^2\sigma_a^2}{2}} J_{2k+1}(Z_c^r)\sin[(2k+1)(\theta^r + \alpha^r)]. \tag{B.6}$$

Appendix C

Derivation of Spatial Correlation for UCA with Laplacian Distributions

Using the equation (3.14), the transmit spatial correlation between the pth and p'th antenna element for a UCA with a truncated Laplacian AOD distribution can be expressed as

$$\begin{aligned}
\mathrm{R}_s(p,p')^d &= \int_{\zeta^r} v_p^r(\zeta^r) v_{p'}^{r,*}(\zeta^r) f(\zeta^r) d\,\zeta^r \\
&= \int_{-\pi+\theta^r}^{\pi+\theta^r} e^{-j2\pi \frac{R_r}{\lambda}\{[cos\phi_p - \cos\phi_p'] \cos(\zeta^r) + [sin\phi_p - \sin\phi_p'] \sin(\zeta^r)\}} C_l e^{-a|\zeta^r - \theta^r|}\, d\zeta^r.
\end{aligned} \tag{C.1}$$

Using the definitions of (A.6), (A.2), (A.3), A.4), and (A.5), we can rewrite (C.1) as

$$\mathrm{R}_s(p,p')^d = C_l \int_{-\pi+\theta^r}^{\pi+\theta^r} e^{-jZ_c^r\{\sin(\alpha^r+\zeta^r)\}} e^{-a|\zeta^r-\theta^r|}\, d\zeta^r. \tag{C.2}$$

Let $x = \zeta^r - \theta^r$, we can rewrite the real and imaginary parts of (C.2) as follows

$$\mathrm{Re}\{\mathrm{R}_s(p,p')^d\} = 2C_l \int_0^{\pi} \cos[Z_c^r \sin(\alpha^r + \theta^r + x)] e^{-ax}\, dx, \tag{C.3}$$

$$\mathrm{Im}\{\mathrm{R}_s(p,p')^d\} = 2C_l \int_0^{\pi} \sin[Z_c^r \sin(\alpha^r + \theta^r + x)] e^{-ax}\, dx. \tag{C.4}$$

By integrating (C.3) and (C.4) with the substitution of (A.10) and (A.11) respectively, we can obtain

$$\mathrm{Re}\{\mathrm{R}_s(p,p')^d\} = J_0(Z_c^r) + 4C_l \sum_{k=1}^{\infty} \frac{a^2(1-e^{-a\pi})}{a^2+4k^2} J_{2k}(Z_c^r)\cos[2k(\theta^r+\alpha^r)], \tag{C.5}$$

$$\mathrm{Im}\{\mathrm{R}_s(p,p')^d\} = 4C_l \sum_{k=0}^{\infty} \frac{a(1+e^{-a\pi})}{a^2+(2k+1)^2} J_{2k+1}(Z_c^r)\sin[(2k+1)(\theta^r+\alpha^r)], \tag{C.6}$$

Appendix D

Derivation of Spatial Correlation for ULA with Gaussian Distributions

Using the equation (3.14), the transmit spatial correlation between the pth and p'th antenna element for a ULA with a truncated Gaussian AOD distribution can be expressed as

$$\begin{aligned} \mathrm{R}_s(p,p')^d &= \int_{\zeta^r} v_p^r(\zeta^r) v_{p'}^{r,*}(\zeta^r) f(\zeta^r) d\,\zeta^r \\ &= \int_{-\pi+\theta^r}^{\pi+\theta^r} C_g e^{-jZ_l^r \sin(\zeta^r)} e^{-\frac{(\zeta^r-\theta^r)^2}{2\sigma_a}} d\,\zeta^r, \end{aligned} \tag{D.1}$$

where $Z_l^r = 2\pi \frac{(p-p')D_r}{\lambda}$. Let $x = \zeta^r - \theta^r$, we can rewrite the real and imaginary parts of (D.1) as follows

$$\mathrm{Re}\{\mathrm{R}_s(p,p')^d\} = C_g \int_{-\pi}^{\pi} \cos[Z_l^r \sin(\theta^r + x)] e^{-\frac{x^2}{2\sigma_a}}\, dx, \tag{D.2}$$

$$\mathrm{Im}\{\mathrm{R}_s(p,p')^d\} = C_g \int_{-\pi}^{\pi} \sin[Z_l^r \sin(\theta^r + x)] e^{-\frac{x^2}{2\sigma_a}}\, dx. \tag{D.3}$$

By making use of the well-known series, $\cos[Z_l \sin(\varphi)]$ and $\sin[Z_l \sin(\varphi)]$ can be further represented as, respectively

$$\cos[Z_l \sin(\varphi)] = J_0(Z_l) + 2\sum_{k=1}^{\infty} J_{2k}(Z_l)\cos(2k\varphi), \tag{D.4}$$

$$\sin[Z_l \sin(\varphi)] = 2\sum_{k=0}^{\infty} J_{2k+1}(Z_l)\sin((2k+1)\varphi). \tag{D.5}$$

By integrating (D.2) and (D.3) with the substitution of (D.4) and (D.5) respectively, we can obtain (3.25) and (3.26).

Appendix E

Derivation of Spatial Correlation for ULA with Laplacian Distributions

Using the equation (3.14), the transmit spatial correlation between the pth and p'th antenna element for a ULA with a truncated Laplacian AOD distribution can be expressed as

$$\begin{aligned} \mathrm{R}_s(p,p')^d &= \int_{\zeta^r} v_p^r(\zeta^r) v_{p'}^{r,*}(\zeta^r) f(\zeta^r) d\,\zeta^r \\ &= \int_{-\pi+\theta^r}^{\pi+\theta^r} C_l e^{-jZ_l^r \sin(\zeta^r)} e^{-a|\zeta^r-\theta^r|} d\,\zeta^r, \end{aligned} \tag{E.1}$$

Let $x = \zeta^r - \theta^r$, we can rewrite the real and imaginary parts of (D.1) as follows

$$\mathrm{Re}\{\mathrm{R}_s(p,p')^d\} = 2C_l \int_0^{\pi} \cos[Z_l^r \sin(\theta^r + x)] e^{-ax}\, dx, \tag{E.2}$$

$$\mathrm{Im}\{\mathrm{R}_s(p,p')^d\} = 2C_l \int_0^{\pi} \sin[Z_l^r \sin(\theta^r + x)] e^{-ax}\, dx. \tag{E.3}$$

By integrating (E.2) and (E.3) with the substitution of (D.4) and (D.5) respectively, we can obtain

$$\mathrm{Re}\{\mathrm{R}_s(p,p')^d\} = J_0(Z_l^r) + 4C_l \sum_{k=1}^{\infty} \frac{a^2(1-e^{-a\pi})}{a^2+4k^2} J_{2k}(Z_l^r) \cos[2k(\theta^r)], \tag{E.4}$$

$$\mathrm{Im}\{\mathrm{R}_s(p,p')^d\} = 4C_l \sum_{k=0}^{\infty} \frac{a(1+e^{-a\pi})}{a^2+(2k+1)^2} J_{2k+1}(Z_l^r) \sin[(2k+1)(\theta^r)], \tag{E.5}$$

Appendix F

Derivation of Analytical BER for D Correlated Rayleigh Branch Combining

The decision statistic given in (7.20) is the sum of jointly complex Gaussian random variables [63]. Since the BER of QPSK with gray coding is the same as the BER of BPSK, the probability of error given $\{\alpha_d\}$ can be expressed as

$$P(e|\alpha_d) = Q\left(\sqrt{2\gamma}\right), \tag{F.1}$$

where the γ is the received signal to noise ratio and is expressed as

$$\gamma = \frac{E_b}{N_o}\sum_{d=1}^{D}\alpha_d^2 = \gamma_c\sum_{d=1}^{D}\alpha_d^2, \tag{F.2}$$

where $\gamma_c = \frac{E_b}{N_o}$ is the received signal-to-noise ratio per bit, per antenna. $N_o = 2\sigma^2$ is the power spectral density of the white noise. The distribution function of γ is shown as

$$p(\gamma) = \frac{1}{j2\pi}\oint_{c-j\infty}^{c+j\infty}\frac{1}{\prod_{d=1}^{D}(1+s\lambda_d)}e^{s\gamma}ds, \tag{F.3}$$

where λ_d are the eigenvalues of $\mathbf{R}_{\text{st,MIMO}}$. Now, averaging over all γ_c the probability of error is

$$P_e = \int_0^\infty Q\left(\sqrt{2\gamma}\right) p(\gamma) d\gamma. \tag{F.4}$$

Now using the theory of residues, the probability density function becomes

$$\begin{aligned} p(\gamma) &= \frac{1}{j2\pi} \int_{c-j\infty}^{c+j\infty} e^{s\gamma} \sum_{d=1}^{D} \left[\frac{\lambda_d^{D-2}}{\prod_{k \neq d}(\lambda_d - \lambda_k)} \frac{1}{s + 1/\lambda_d} \right] \\ &= \sum_{d=1}^{D} \text{Residue} \left\{ \frac{e^{s\gamma} \lambda_d^{D-2}}{\prod_{k \neq d}(\lambda_d - \lambda_k)}, -\frac{1}{\lambda_d} \right\} \\ &= \sum_{d=1}^{D} e^{-\gamma/\lambda_d} \frac{\lambda_d^{D-2}}{\prod_{k \neq d}(\lambda_d - \lambda_k)}. \end{aligned} \tag{F.5}$$

Inserting (F.5) into (F.4) we obtain the probability of error for D branch diversity in the presence of Rayleigh fading as

$$P_e = \frac{1}{2} \sum_{d=1}^{D} \frac{\lambda_d^{D-1}}{\prod_{k \neq d}(\lambda_d - \lambda_k)} \left(1 - \sqrt{\frac{\lambda_d}{1 + \lambda_d}} \right). \tag{F.6}$$

Bibliography

[1] W.C. Jakes, *Microwave Mobile Communications.* Wiley, 1st ed., 1974.

[2] J.R. Pierce and S. Stein, "Multiple diversity with nonindependent fading," *Proc. IRE*, vol. 48, pp. 89–104, Nov. 1960.

[3] R.A. Soni, R.M. Buehrer, and Jiann-An Tsai, "Open-loop transmit diversity in IS-2000 systems," in *The Thirty-Third Asilomar Conference*, pp. 654–658, 1999.

[4] S. Alamouti, "A simple transmit diversity technique for wireless communications," *IEEE Journal on Selected Ares in Communications*, vol. 16, pp. 1451–1458, Oct. 1998.

[5] Jyri Hamalainen and R. Wichman, "Close-loop transmit diversity for FDD WCDMA systems," in *The 34th Asilomar Conference*, Nov 2000.

[6] G.J. Foschini and M.J. Gans, "On limits of wireless communications in a fading environment when using multiple antennas," in *In Proc. Wireless Personal Communications*, p. 311, March 1998.

[7] E. I. Telatar and D. Tse, "Capacity and mutual information of broadband multipath fading channel," in *Proc. IEEE Int. Symp. Information Theory*, p. 188, 1998.

[8] V. Tarokh, N. Seshadri, and A.R. Calderbank, "Space-time codes for high data rates wireless communications: Performance criterion and code construction," *IEEE Transactions on Information Theory*, vol. 44, pp. 744–765, March 1998.

[9] A.F. Naguib, V. Tarokh, N. Seshadri, and A.R. Calderbank, "A space-time coding modem for high data rate wireless communications," *IEEE Journal on Selected Areas in Communications*, vol. 16, pp. 1459–1478, Oct. 1998.

[10] R.L. Pickholtz, D.L. Schilling, and L.B. Milstein, "Theory of spread spectrum communications-A tutorial," *IEEE Transactions on Communications*, pp. 855–884, May 1982.

[11] R.C. Dixon, *Spread Spectrum Systems.* Wiley, 1st ed., 1984.

[12] R.A. Scholtz, "The origins of spread spectrum communications," *IEEE Transactions on Communications*, vol. 30, pp. 882–854, May 1982.

[13] K.S. Gilhousen and et. al., "On the capacity of a CDMA system," *IEEE Transactions on Vehicular Technolgy*, vol. 40, pp. 303–312, May 1991.

[14] R.L. Pickholtz, L.B. Milstein, and D.L. Schilling, "Spread spectrum for mobile communications," *IEEE Transactions on Vehicular Technolgy*, pp. 313–322, May 1991.

[15] W.C. Lee, "Overview of celluar CDMA," *IEEE Transactions on Vehicular Technolgy*, pp. 291–302, May 1991.

[16] D.L. Schilling, *et al.*, "Broadband CDMA for personal communication systems," *IEEE Communications Mag.*, vol. 29, pp. 86–93, Nov. 1991.

[17] T. O'Leary, "Terrestrial digital audio broadcast in europe," in *EBU Technical Review*, pp. 19–26, 1993.

[18] R. Monnier, J.B. Rault, and T. Couasnon, "Digital television broadcasting with high spectral efficiency in europe," in *ICB Technical Report*, pp. 380–384, 1992.

[19] L.J. Cimini, Jr., "Analysis and simulation of a digital mobile channel using orthogonal frequency division multiplexing," *IEEE Transactions on Communications*, vol. 33, pp. 665–675, July 1985.

[20] J.A.C Bingham, "Multicarrier modulation for data transmission: An idea whose time has come," *IEEE Communications Magazine*, pp. 5–14, May 1990.

[21] Ye Li and L.J. Cimini, Jr., "Bound on the interchannel interference of OFDM in time-varying impairments," *IEEE Transactions on Communications*, vol. 49, pp. 401–404, Mar. 2001.

[22] R. Van Nee and R. Prasad, *OFDM for wireless multimedia communications.* Artech House Publishers, 2000.

[23] S. Hara and R. Prasad, "Overview of multicarrier CDMA," *IEEE Communications Magazine*, vol. 35, pp. 126–133, Dec. 1997.

[24] L. Vandendorpe, "Multitone spread spectrum multiple access communications system in a multipath ricean fading channel," *IEEE Transactions on Vehicular Technologies*, vol. 44, pp. 327–337, May 1995.

[25] E.A. Sourour and M. Nakagawa, "Performance of orthogonal multicarrier CDMA in a multipath fading channel," *IEEE Transactions on Communications*, vol. 44, pp. 119–129, Mar. 1996.

[26] Stefan Kaiser, "OFDM-CDMA versus DS-CDMA: performance evaluation for fading channels," in *ICC*, pp. 1722–1726, Jan. 1995.

[27] L.L. Chong and L.B. Milstein, "Comparing DS-CDMA and multicarrier CDMA with imperfect channel estimation," in *11th IEEE Signal Processing Workshop*, pp. 385–388, Nov 2001.

[28] J.H. Winters, "Optimum combining in mobile radio with cochannel interference," *IEEE Transactions Vehicular Technology*, vol. 33, pp. 144–155, Aug. 1984.

[29] J.H. Winters, "On the capacity of radio communication systems with diversity in a rayleigh fading environment," *IEEE Journal on Selected Ares in Communications*, vol. 5, pp. 871–878, June 1987.

[30] A.F. Naguib, *Adaptive Antenna for CDMA Wireless Network*. PhD thesis, Standford University, Palo Alto, CA, August 1996.

[31] S. Verdu, "Optimum sequence detection of asynchronous multiple access communications," in *IEEE Int. Symp. on Information Theory*, p. 80, Sep. 1983.

[32] S. Verdu, "Minimum probability of error for asynchronous gaussian multiple-access channels," *IEEE Transactions on Information Theory*, vol. 32, pp. 85–96, Jan. 1986.

[33] S. Verdu, "Optimum multiuser asymptotic efficiency," *IEEE Transactions on Communications*, vol. 34, pp. 890–897, Sep. 1986.

[34] S. Verdu, *Multiuser Detection*. Cambridge Unversity Press, 1st ed., 1998.

[35] M.L. Honig and M.K. Tsatsanis, "Adaptive techniques for multiuser CDMA receivers," *IEEE Signal Processing Mag.*, pp. 49–61, May 2000.

[36] S. Kapoor, *et al.*, "Adaptive multiuser detection and beamforming for interference suppression in CDMA mobile radio system," *IEEE Transactions on Vehicular Technolgy*, pp. 1341–1354, Sep. 1999.

[37] J. Blanz, A. Klein, M. Nssshan, and A. Steil, "Performance of a hybrid c/tdma mobile radio system applying joint detection and coherent receiver and antenna diversity," *IEEE Journal On Selected Ares in Communications*, vol. 12, pp. 568–579, May 1994.

[38] V. Moghadam and M. Kaveh, “Interference cancellation using antenna arrays,” in *PIMRC*, July 1995.

[39] Jiann-An Tsai, J. Hicks, and B.D. Woerner, “Joint MMSE beamforming with SIC for an overloaded array system,” in *MILCOM*, pp. 1261–1265, Oct. 2001.

[40] Jiann-An Tsai and B.D. Woerner, “Performance of orthogonal transmit waveforms for CDMA uplink systems in MIMO rayleigh channels,” in *WCNC*, pp. 206–209, March 2002.

[41] S. Bayram, J. Hicks, J.H. Reed, and B. Boyle, “Joint ML approach in overloaded array processing,” in *Vehicular Technology Conference*, (Boston, MA), pp. 394–400, September 2000.

[42] S. Bayram, J. Hicks, J.H. Reed, and B. Boyle, “Overloaded array processing in wireless airborne communication systems,” in *MILCOM*, (Los Angles, CA), pp. 1151–1158, October 2000.

[43] T.S. Rappaport, *Wireless Communication: Principles and Practice*. Prentice Hall Publishing Company, 1rd ed., 1996.

[44] W.C. Lee, *Mobile Communications Design Fundamentals*. Wiley, 2nd ed., 1993.

[45] R.S. Kennedy, *Fading Dispersive Communication Channels*. John Wiley and Sons, 1969.

[46] A. Papoulis, *Probability, Random Variables, and Stochastic Processes*. McGraw Hill, 3rd ed., 1991.

[47] W.L. Stutzman and G.A. Thiele, *Antenna Theory and Design*. John Wieley & Son, 1st ed., 1981.

[48] R.A. Monzingo and T.W. Miller, *Introduction to Adaptive Arrays*. John Wiley and Sons, 1980.

[49] D.H. Johnson and D.E. Dudgeon, *Array Signal Processing.* Prentice Hall Publishing Company, 1993.

[50] R.B. Ertel, *Antenna Array Systems: Propagation and Performance.* PhD thesis, Virginia Polytechnic Institute and State University, Blacksburg, VA, July 1999.

[51] R.H. Clarke, "A statistical theory of mobile radio reception," *Bell Labs Technical Journal*, vol. 47, pp. 957–1000, Sep. 1968.

[52] M.J. Gans, "A power spectral theory of propagation in mobile radio environment," *IEEE Transactions on Vehicular Technology*, vol. 21, pp. 27–38, Feb. 1972.

[53] P Petrus, *Novel Adaptive Array Algorithms and Their impact on Cellular System Capacity.* PhD thesis, Virginia Polytechnic Institute and State University, Blacksburg, VA, 1997.

[54] J. Salz and J.H. Winters, "Effect of fading correlation on adaptive arrays in digital mobile radio," *IEEE Transactions on Vehicular Technologies*, vol. 43, pp. 1049–1057, Nov. 1994.

[55] Jiann-An Tsai and B.D. Woerner, "The fading correlation function of a circular antenna array in mobile radio environment," in *GLOBECOM*, pp. 3232–3236, Nov. 2001.

[56] D.-H. Shiu , *et al.*, "Fading correlation and its effects on the capacity of multielement antenna systems," *IEEE Transactions on Communications*, vol. 48, pp. 502–512, March 2000.

[57] T.M. Cover and J.A. Thomas, *Element of Information Theory.* Wiley, 1991.

[58] G.J. Foschini, "Layered space-time architecture for wireless communication in a fading environment when using multi-element antennas," *Bell LAb. Technical Journal*, vol. 4, no. 2, pp. 160–169, 1996.

[59] B. Hochwald, T. L. Marzetta, and C. B. Papadias, "A transnmit diversity scheme for wideband CDMA systems based on space-time spreading," *IEEE Journal On Selected Ares in Communications*, vol. 19, pp. 48–60, Jan. 2001.

[60] TR45.5, *Physical Layer Standard for cdma2000 Spread Spectrum Systems.* TIA/EIA/IS-2000.2, 1999. (Ballot Version).

[61] R. Walton, M. Wallace, and S. Howard, "CDMA downlink performance issues," in *IEEE International Symposium on Personal, Indoor and Mobile Radio Communications*, pp. 308–312, Oct 1998.

[62] J.G. Proakis, *Digital Communications.* McGraw-Hill, 3st ed., 1995.

[63] D. Brennan, "Linear diversity combining techniques," *Proceeding of IRE*, vol. 47, pp. 1075–1102, 1959.

[64] Jiann-An Tsai and B.D. Woerner, "A new orthogonal transmit waveform with space-time diversity for wireless CDMA downlink systems," in *35th Asilomar Conference*, pp. 241–245, Nov. 2001.

[65] G. Caire, G. Taricco, J.V. Travest, and E. Biglieri, "A multiuser approach to narrowband cellular communications," *IEEE Transactions on Information Theory*, vol. 43, pp. 1503–1517, Sep. 1997.

[66] S.W. Wales, "Technique for cochannel interference suppression in TDMA mobile radio systems," *IEE Proc. on Communications*, vol. 142, pp. 106–114, Apr. 1995.

[67] P. Ranta, Z. Honkasalo, and J. Tapaninen, "TDMA celullar network application of an interference cancellation technique," in *Vehicular Technology Conference*, pp. 296–300, July 1995.

[68] S. Verdu, *Optimum Multi-User Signal Detection.* PhD thesis, University of Illinois, Urbana-Champaign, 1984.

[69] L. Wei, L. Rasmussen, and R. Wyrwas, “Near optimum tree-search detection-schemes for bit-synchronous multiuser CDMA system over gaussian and two-path rayleigh fading channels,” *Proc. IEE*, vol. 45, pp. 691–700, June 1997.

[70] Z. Xie, C. Rushforth, and R. Short, “Multiuser signal detection using sequential decoding,” *IEEE Transactions on Communications*, vol. 38, pp. 578–583, Sep. 1990.

[71] T. Giallorenzi and S. Wilson, “Multiuser ML sequence estimator for convolutionally coded asynchronous DS-CDMA systems,” *IEEE Transactions on Communications*, vol. 44, pp. 997–1008, Aug. 1996.

[72] U. abd B. Aazhang, “A multiuser receiver for code-division multiple-access systems with trellis-based modulation,” *IEEE Journal On Selected Ares in Communications*, vol. 14, no. 8, pp. 1602–1609, 1996.

[73] T. Giallorenzi and S. Wilson, “Trellis-based multiuser receiver for convolutionally coded CDMA systems,” in *31st Allerton Conf. for Communications, Control, and Computing*, pp. 839–848, October 1993.

[74] R. Lupas, *Near-Far Resistant Linear Multiuser Detection*. PhD thesis, Princeton University, Princeton, NJ, 1989.

[75] U. Madhow and M.L. Honig, “MMSE interference suppression for direct-sequence spread-spectrum CDMA,” *IEEE Transactions on Communications*, vol. 42, pp. 1339–1343, Dec. 1994.

[76] R. Lupas and S. Verdu, “Linear multiuser detectors for synchronous code-division multiple-access channels,” *IEEE Transactions on Information Theory*, vol. 35, pp. 123–136, Jan 1989.

[77] R. Lupas and S. Verdu, “Near-far resistance of multiuser detection in asynchronous channels,” *IEEE Transactions on Communications*, pp. 496–508, Apr. 1990.

[78] M.K. Varanasi and B. Aazhang, "Multistage detection in asyncronous code-division multi-access communications," *IEEE Transactions on Communications*, vol. 38, pp. 509–519, Apr. 1990.

[79] R.M. Buehrer, *The Application of Multiuser Detection to Cellular CDMA*. PhD thesis, Virginia Polytechnic Institute and State University, Blacksburg, VA, June 1996.

[80] P. Patel and J. Holtzman, "Analysis of a simple successive interference cancellation scheme in a DS-CDMA system," *IEEE Journal on Selected Areas in Commnications*, pp. 796–807, June 1994.

[81] Z. Zvoner and D. Brady, "Multiuser detection in single-path fading channels," *IEEE Transactions on Communications*, vol. 42, pp. 1729–1739, March 1994.

[82] Z. Zvoner and D. Brady, "Adaptive multiuser receiver with diversity reception for nonselective rayleigh fading asynchronous CDMA channels," in *MILCOM*, pp. 982–985, Oct 1994.

[83] Z. Zvoner and D. Brady, "Suboptimum multiuser detector for synchronous cdma frequency-selective rayleigh channels," in *GLOBECOM*, pp. 82–86, Dec. 1992.

[84] M.K. Varanasi, "On multiuser detection in noncoherent cdma channels," in *GLOBECOM*, pp. 846–850, Dec. 1991.

[85] M.K. Varanasi and B. Aazhang, "Optimally near-far resistant multiuser detection in differentially coherent synchronous channels," *IEEE Transactions on Information Theory*, vol. 37, pp. 1006–1018, July 1991.

[86] S. Miller, M.L. Honig, M. Shensa, and L. Milstein, "MMSE reception of DS-CDMA for frequency-selective fading channels," in *IEEE Int. Symp. on Information Theory*, p. 51, July 1997.

[87] S.L. Miller, "An adaptive direct-sequence code-division multiplt-access receiver for multiuser interference rejection," *IEEE Transactions on Communications*, vol. 43, pp. 1746–1755, Dec. 1995.

[88] H.V. Poor and S. Verdu, "Probability of error in MMSE multiuser detection," *IEEE Transactions on Information Theory*, vol. 43, pp. 858–871, May 1997.

[89] P.S. Kumar and J. Holtzman, "Power control for a spread spectrum system with multiuser receivers," in *PIMRC*, July 1995.

[90] H. Huang, *Combined Multipath Processing, Array Processing, and Multiuser Detection for CDMA Channels.* PhD thesis, Princeton University, Princeton, NJ, 1996.

[91] H. Huang and S. Verdu, "Linear differentially coherent multiuser detection for multipath channels," in *Wireless Personal Communications*, pp. 113–136, Jan. 1998.

[92] H. Huang and S. Schwartz, "A comparative analysisof linear multiuser detector for multipath fading channels," in *GLOBECOM*, pp. 11–21, Dec. 1994.

[93] A.J. Viterbi, "Very low rate convolutional codes for maximum theoretical performance of spread-spectrum multiple-access channels," *IEEE Journal on Selected Areas in Communications*, vol. 30, pp. 641–649, May 1990.

[94] J.M. Holtzman, "Successive interference cancellation for direct sequence code division multiple access," in *MILCOM*, pp. 997–1001, Nov. 1994.

[95] P. Patel and J. Holtzman, "Performance comparison of a DS/CDMA systems using a successive interference cancellation (IC) scheme and a parallel (IC) scheme under fading," in *ICC*, pp. 510–514, May 1994.

[96] R.M. Buehrer and B.D. Woerner, "Analysis of multistage interference cancellation for CDMA using improved gausssian approximation," *IEEE Transactions on Communications*, vol. 44, pp. 1308–1321, Oct. 1996.

[97] R. abd H. Imai, M. Hatori, and S. Pasupathy, "An adaptive cancellation of cochannel interference for spread-spectrum multiple-access communication networks in a power line," *IEEE Journal On Selected Ares in Communications*, vol. 8, pp. 691–699, 1990.

[98] R.M. Buehrer and B.D. Woerner, "A simulation comparison of multiuser receivers for cellular CDMA," *IEEE Transactions on Vehicular Technolgy*, pp. 1065–1085, July 2000.

[99] S.D. Gray, M. Kocic, and D. Brady, "Multiuser detection in mismatched multiplt access channels," *IEEE Transactions on Communications*, vol. 43, pp. 3080–3089, Dec. 1995.

[100] A. Kaul and B.D. Woerner, "Analytical limits on the performance of adaptive multistage interference cancellation for CDMA," *IEE Electronic Letters*, pp. 2093–2094, Dec. 1995.

[101] R.M. Buehrer and B.D. Woerner, "Analysis of multistage interference cancellation for CDMA with phase and timing errors," *IEEE Journal On Selected Ares in Communications*, vol. 14, pp. 1522–1535, Oct. 1996.

[102] S. Kubota, S. Kato, and K. Feher, "Inter-channel interference cancellation techniques for CDMA mobile and personal communication systems," in *PIMRC*, July 1992.

[103] A. Saifuddin, R. Kohno, and H. Imai, "Cascaded combination of cancellation cochannel interference and decoding of error-correcting codes for CDMA," in *Proc. of 3rd Intl. Symp. on Spread Spectrum System, Technique, and Application*, pp. 171–175, 1994.

[104] R.M. Buehrer and S.P. Nicoloso, “Comments on partial parallel interference cancellation CDMA,” *IEEE Transactions on Communications*, vol. 47, pp. 658–661, May 1999.

[105] P. Jung and J. Blanz, “Joint detection with coherent receiver antenna diversity in CDMA mobile radio systems,” *IEEE Transactions on Vehicular Technology*, vol. 44, pp. 76–88, Jan. 1995.

[106] R. Kohno, N. Ishi, and M. Nagatsuka, “A spatially and temporally optimal multiuser receiver using an antenna array for DS-CDMA,” in *PIMRC*, July 1995.

[107] P. Balaban and J. Salz, “Optimum diversity combining and equalization in digital data transmission with application to cellular mobile radio,” *IEEE Transactions on Vehicular Technolgy*, vol. 40, pp. 342–354, May 1991.

[108] A.F. Naguib, A. Paulraj, and T. Kailath, “Capacity improvement with base station antenna arrays in cellular CDMA,” *IEEE Transactions on Vehicular Technology*, vol. 43, pp. 691–698, Nov. 1994.

[109] R.M. Buehrer, A.G. Kogiantis, S.C. Liu, Jiann-An Tsai, and D. Uptegrove, “Intelligent antenna for wireless communications:uplink,” *Bell Labs Technical Journal*, vol. 4, pp. 73–103, Sep. 1999.

[110] H.L. Van Trees, *Detection, Estimation, and Modulation*. John Wiley and Sons, 1969.

[111] J. Hicks, “Overloaded array processing with spatially reduced search joint detection,” Master’s thesis, Virginia Polytechnic Institute and State University, Blacksburg, VA, May 2000.

[112] B. Widrow and S. Stern, *Adaptive Signal Processing*. Prentice Hall Publishing Company, 1985.

[113] S. Haykin, *Array Signal Processing.* Prentice Hall Publishing Company, 2nd ed., 1984.

[114] S. Haykin, *Array Filter Theory.* Prentice Hall Publishing Company, 3rd ed., 1996.

[115] B.G. Agee, "Blind seperation and capture of communications signal using multi-target constant modulus beamforming," in *MILCOM*, pp. 340–346, 1989.

[116] R. Gooch and J. Lundell, "The CMA array: An adaptive beamforming for constant modulus signals," in *In Proc. ICASSP*, pp. 2523–2526, April 1986.

[117] J.J. Shynk and R.P. Gooch, "The constant modulus array for cochannel signal copy and direction finding," *IEEE Transactions on Signal Processing*, vol. 44, pp. 652–660, March 1996.

[118] S.C. Liu, *New Sapce-Time Processing Techniques for Spread-Spectrum Wireless Networks.* PhD thesis, University of Maryland, 1998.

[119] G.H. Golub and C.F. Loan, *Matrix Computations.* The John Hopkins University Press, 1989.

[120] G. Stewart and J.G. Sun, *Matrix Perturbation Theory.* Academic Press Inc., 1990.

[121] Jiann-An Tsai and R.M. Buehrer, "Frequency reuse reduction for IS-136 using a four-element adaptive array," in *Proc. 8th Virginia Tech. Symp. on Wireless Personal Communications*, pp. 11–22, June 1998.

[122] Jiann-An Tsai, R.M. Buehrer, and D. Uptegrove, "Performance comparisons of adaptive antenna arrays with fixed multibeam systems for IS-136," in *Vehicular Technology Conference*, pp. 1079–1083, May 1999.

[123] J.H. Winters, "Signal acquisition and tracking with adaptive arrays in digital mobile radio system IS-54 with flat fading," *IEEE Transactions Vehicular Technologies*, vol. 42, pp. 377–384, Nov. 1993.

[124] T.C. Hsia, "Convergence analysis of LMS and NLMS adaptive algorithm," in *ICASSP*, pp. 667–670, May 1983.

[125] W.M. Gentlemean, "Least square computations by givens transformation without square roots," in *J. Inst. Math. Its Application*, pp. 329–336, April 1973.

[126] S.Y. Kung, *VLSI Array Processor.* Prentice Hall Publishing Company, 1988.

Vita

Jiann-An Tsai was born in Taiwan, on August 4, 1968. He received his B.S. degree on Electrical Engineering in 1991 from National Taiwan Institute of Technology in Taipei, Taiwan. In December, 1994, he obtained his MSEE from Virginia Polytechnic Institute and State University where his research focused on mobile radio communication systems. From 1995 to 2000 he was a member of technical staff in the Wireless Base Station and Radio Technology Department of Lucent's Wireless Networks Group in Whippany, New Jersey. He was responsible for evaluating the performance of adaptive antenna arrays for TDMA and CDMA wireless communication systems and developing computer simulation tools for analyzing advanced signal processing techniques. His primary research interests are adaptive beamforming, multiuser detection, and space-time signal processing in multiple-antenna wireless systems.